Technical Report EL-94-5
May 1994

US Army Corps
of Engineers
Waterways Experiment
Station

Hydrodynamics and Eutrophication Model Study of Indian River and Rehoboth Bay, Delaware

by Carl F. Cerco, Barry Bunch,
Mary A. Cialone, Harry Wang

Prepared for U.S. Environmental Protection Agency
Delaware Department of Natural Resources and Environmental Control
and U.S. Army Engineer District, Philadelphia

Technical Report EL-94-5
May 1994

Hydrodynamics and Eutrophication Model Study of Indian River and Rehoboth Bay, Delaware

by Carl F. Cerco, Barry Bunch,
Mary A. Cialone, Harry Wang

U.S. Army Corps of Engineers
Waterways Experiment Station
3909 Halls Ferry Road
Vicksburg, MS 39180-6199

Final Report

Approved for public release; distribution is unlimited

Prepared for U.S. Environmental Protection Agency, Region III
Philadelphia, PA 19107

Delaware Department of Natural Resources and Environmental Control
Dover, DE 19903

and U.S. Army Engineer District, Philadelphia
Philadelphia, PA 19106-2991

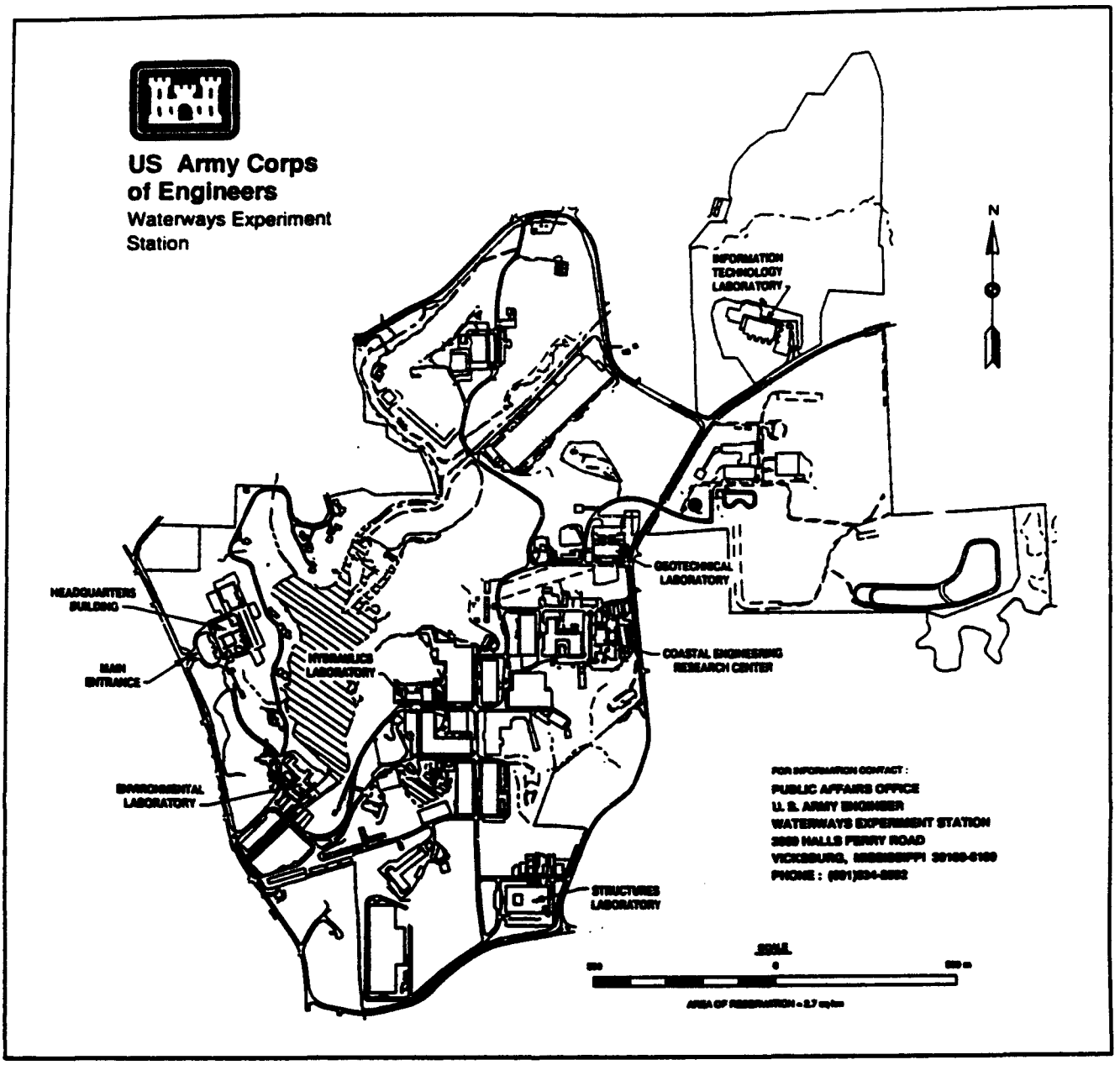

Waterways Experiment Station Cataloging-in-Publication Data

Hydrodynamics and eutrophication model study of Indian River and Rehoboth Bay, Delaware / by Carl F. Cerco ... [et al.] ; prepared for U.S. Environmental Protection Agency, Region III, Delaware Department of Natural Resources and Environmental Control and U.S. Army Engineer District, Philadelphia.

262 p. : ill. ; 28 cm. — (Technical report ; EL-94-5)

Includes bibliographic references.

1. Eutrophication — Delaware —Rehoboth Bay. 2. Hydrodynamics — Mathematical models. I. Cerco, Carl F. II. United States. Army. Corps of Engineers. Philadelphia District. III. United States. Environmental Protection Agency. Region III. IV. Delaware. Dept. of Natural Resources and Environmental Control. V. U.S. Army Engineer Waterways Experiment Station. VI. Series: Technical report (U.S. Army Engineer Waterways Experiment Station) ; EL-94-5.

TA7 W34 no.EL-94-5

Contents

Preface

The Hydrodynamic-Eutrophication Model Study of the Delaware Inland Bays was sponsored by the U.S. Environmental Protection Agency, Region III (USEPA), the Delaware Department of Natural Resources and Environmental Control (DNREC), and the U.S. Army Engineer District, Philadelphia (CENAP). Project monitors were Messrs. Charles App and Robert Runowski, USEPA, Mr. John Schneider, DNREC, and Mr. Jeff Gebert, CENAP.

The eutrophication modeling was conducted by Drs. Carl F. Cerco and Barry Bunch, Water Quality and Contaminant Modeling Branch (WQCMB), Environmental Laboratory (EL), U.S. Army Engineer Waterways Experiment Station (WES). Supervision of the eutrophication model activities was provided by Dr. Mark Dortch, Chief, WQCMB.

The hydrodynamic modeling was conducted by Ms. Mary Cialone, Coastal Processes Branch (CPB), and Dr. Harry Wang, Coastal Oceanography Branch (COB), Coastal Engineering Research Center (CERC), WES. Supervision of the hydrodynamic model activities was provided by Mr. Bruce Ebersole, Chief, CPB, and Dr. Martin Miller, Chief, COB.

Project management was provided by Mr. Donald Robey, Chief, Environmental Processes and Effects Division, EL, and Mr. H. Lee Butler, Chief, Research Division, CERC. Overall supervision was provided by Dr. John Harrison, Director, EL, and Dr. James Houston, Director, CERC.

At the time of publication of this report, WES Director was Dr. Robert W. Whalin. Commander was COL Bruce K. Howard, EN.

This report should be cited as follows:

> Cerco, C. F., Bunch, B., Cialone, M. A., and Wang, H. (1994). "Hydrodynamic and eutrophication model study of Indian River and Rehoboth Bay, Delaware," Technical Report EL-94-5, U.S. Army Engineer Waterways Experiment Station, Vicksburg, MS.

Chapter I: Introduction

The Study System

Indian River and Rehoboth Bay (Figure 1-1) are two water bodies that form part of the interlocked Delaware Inland Bays system. Rehoboth Bay is connected to Delaware Bay to the north via a canal and to Indian River Bay to the south. Indian River Bay is connected to the Atlantic Ocean on the east via an inlet and to Little Assawoman Bay via a canal to the south. The western portion of Indian River Bay, referred to as Indian River, terminates at the Millsboro dam. Drainage area of the system is 55647 hectares (Ritter 1986) of which 14339 hectares is upstream of the impoundment at Millsboro. The basin contains one long-term stream gauging station (USGS 01484500) on Stockley Branch. Mean flow for the period of record (43 years) is 0.196 m^3 sec^{-1} or 1.44 x 10^{-4} m^3 sec^{-1} $hectare^{-1}$. Employing the runoff at Stockley to characterize the remainder of the basin indicates a long-term basin mean flow of 8.03 m^3 sec^{-1}.

Surface area and volume of the system are 7.31 x 10^7 m^2 and 1.21 x 10^8 m^3 respectively. Mean depth is 1.66 m which characterizes most of the system except near the inlet in which local mean depth exceeds ten meters. Mean tide range at the inlet is 1.25 m (Smullen 1992). The tidal prism is 51 x 10^6 m^3 (Smullen 1992). The system is well-mixed from surface to bottom and is saline virtually throughout its extent. Median salinity is 22.7 ppt and 95% of observations exceed 4.3 ppt. Lowest salinities occur immediately downstream of the Millsboro dam during periods of high runoff. Residence time of the system, determined as volume divided by freshwater flow rate is lengthy: 174 days. An alternate estimate of residence time, volume divided by tidal prism over the tidal period, is much less: 1.2 days. Except near headwaters and in constricted areas in which the tide is dampened, tidal flushing is more effective than runoff in the determination of volumetric flows and mass transport throughout the system.

Objectives

The primary objective of this study is to provide a hydrodynamic/water quality model package of the Indian River - Rehoboth Bay system. The

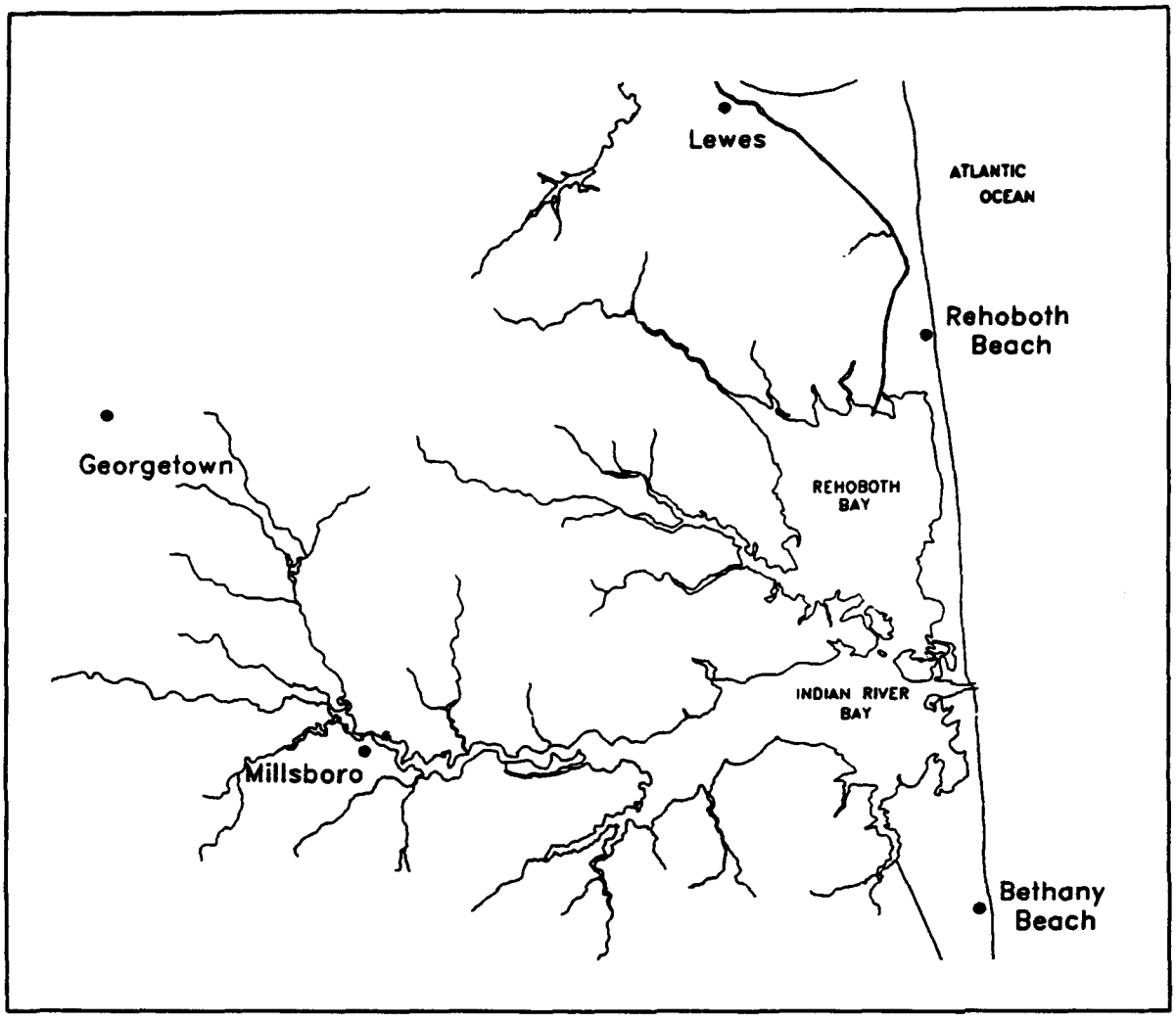

Figure 1-1. Indian River and Rehoboth Bay

package is to be suitable for development of total maximum daily loads, point-source waste load allocations, and nonpoint-source load allocations of nutrients and organic substances. Additional requirements are that the model package operate in a continuous multi-year mode and provide information on diurnal dissolved oxygen variations. The model package is also to provide an organized framework for collection and employment of additional observations in the study system. The period covered by the study extends from January 1988 to December 1990.

Chapter II: Data Bases

Hydrographic Data Bases

Bathymetry

A hydrographic survey of the dual bay and inlet system was performed in 1988 by the U.S. Army Engineer District, Philadelphia. The survey was referenced to State Plane coordinates and all soundings were referenced to National Geographic Vertical Datum (NGVD). These data were used to determine the depth in each cell of the Indian River-Rehoboth Bay grid by applying a 3-point linear interpolation scheme to the data. In addition, the data were converted from State Plane coordinates to map inches for consistency between the grid reference system and bathymetric reference system.

Tide gages

Tide data referenced to NGVD were collected by the United States Geologic Survey at five locations (Figure 2-1). These data (Table 2-1) were used to specify the inlet boundary condition and for calibration purposes. Tide records at the inlet were not complete for the three-year model application period, 1988-1990. Missing data were obtained by transformation of tide records at Lewes, Delaware. The transformation was accomplished by comparing the inlet and Lewes gages for the time period when data were available at both gages and establishing a relationship between the two gages.

Current meters

Velocity data employed in the model calibration were collected at four locations near Middle Island from 30 June to 1 July 1988 (Figure 2-1 and Table 2-2).

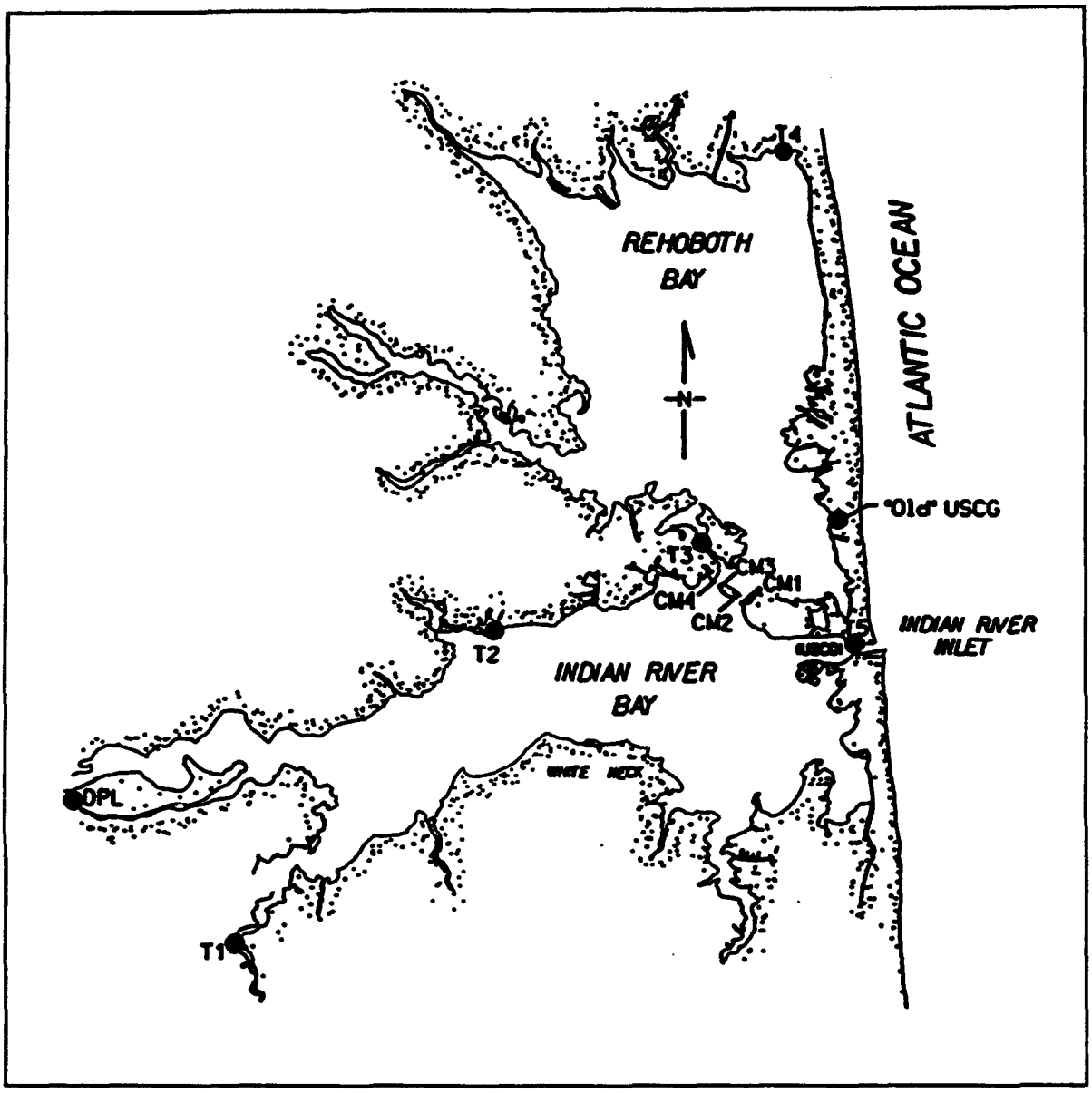

Figure 2-1. Gauge locations for model calibration

Wind Data

Three sources of wind data were available. The State of Delaware, Division of Soil and Water Conservation, provided data from an anemometer mounted above the dune line at the "old" United States Coast Guard (USCG) station (Figure 2-1). The Delmarva Power and Light (DPL) Company provided wind data at the power plant (Figure 2-1). Weather data from the Dover

Table 2-1
Tide Gauge Data

Location	Gauge Number	Northing	Easting	Time Periods
Vines (T1)	01484549	202070	560870	06–29–88 to 07–05–88 10–01–88 to 09–30–89 10–01–89 to 10–13–89 07–06–90 to 09–30–90
Potnets (T2)	01484605	222270	576670	06–29–88 to 09–30–88 10–01–88 to 09–07–89 09–25–89 to 09–30–89 10–01–89 to 07–17–90
Massey (T3)	01484680	227670	590800	06–29–88 to 08–15–88 08–17–88 to 09–30–88 10–01–88 to 09–30–89 10–01–89 to 07–17–90
Dewey (T4)	01484670	253070	594750	06–29–88 to 07–05–88 10–01–88 to 09–30–89 10–01–89 to 09–30–90 10–01–90 to 11–04–91
Inlet (USCG) (T5)	01484683	222170	599600	06–29–88 to 09–30 88 10–01–88 to 10–09–88 10–13–88 to 06–19–89

Table 2-2
Current Meter Data

Location	Northing	Easting	Time Periods
east of Middle Island (east gauge) (CM1)	224610	592800	06–30–88 to 07–01–88
east of Middle Island (west gauge) (CM2)	224900	592470	06–30–88 to 07–01–88
west of Middle Island (east gauge) (CM3)	225600	591330	06–30–88 to 07–01–88
west of Middle Island (west gauge) (CM4)	225730	591200	06–30–88 to 07–01–88

Delaware Air Force Base provided the third source of wind data. For the 1988 calibration, data from the DPL anemometer were used because this local data source was most complete. For the 1989 and 1990 simulations, weather data from Dover was the most complete data source and was therefore utilized.

Water Quality Data

STORET

Data from over 60 stations within the Indian River - Rehoboth Bay watershed was retrieved from the STORET data base. Stations were plotted on topographic maps according to reported longitude and latitude. In many cases, reported longitude and latitude were not consistent with landmarks in the station descriptions. Longitude and latitude were then revised to conform to station descriptions. Some stations could not be accurately located and were dropped as were stations that contained no water quality constituents of interest. The STORET data was divided into two data sets, "Upland" data from freeflowing streams and "Water" data collected in the tidal portions of Indian River and Rehoboth Bay. "Upland" data was used to compute distributed loads to the system and to characterize boundary conditions in the freeflowing streams. "Upland" data was available for 35 stations and was collected in the years 1970 - 1991. All months of the year were represented in the "Upland" data set. "Water" observations were employed to calibrate and verify the water quality model. "Water" data was available for 18 stations (Figure 2-2) and was restricted to the years within the study period, 1988-1990. Virtually all (97.6%) of the "Water" data was collected in the months April - September. The number of observations at each station ranged from 2 to 18 and varied according to constituent. STORET data employed in this study is summarized in Table 2-3.

University of Delaware

Additional data for calibration and verification of the model was provided by Dr. William Ullman of the College of Marine Studies (CMS), University of Delaware. Protocol in the CMS study called for sample collection at consistent salinity concentrations rather than consistent physical locations. As a consequence each observation was generally collected in a unique location. Surveys were conducted in October 1989 (Figure 2-3) and in March, May, July, August, and September 1990 (Figure 2-4). The CMS data set is also summarized in Table 2-3.

Sediment-Water Fluxes

Observations of sediment-water fluxes of dissolved oxygen, ammonium, phosphate, and nitrate were provided by Dr. Sybil Seitzinger of the Academy of Natural Sciences. Observations were collected at four stations (Figure 2-5) during May and August 1992.

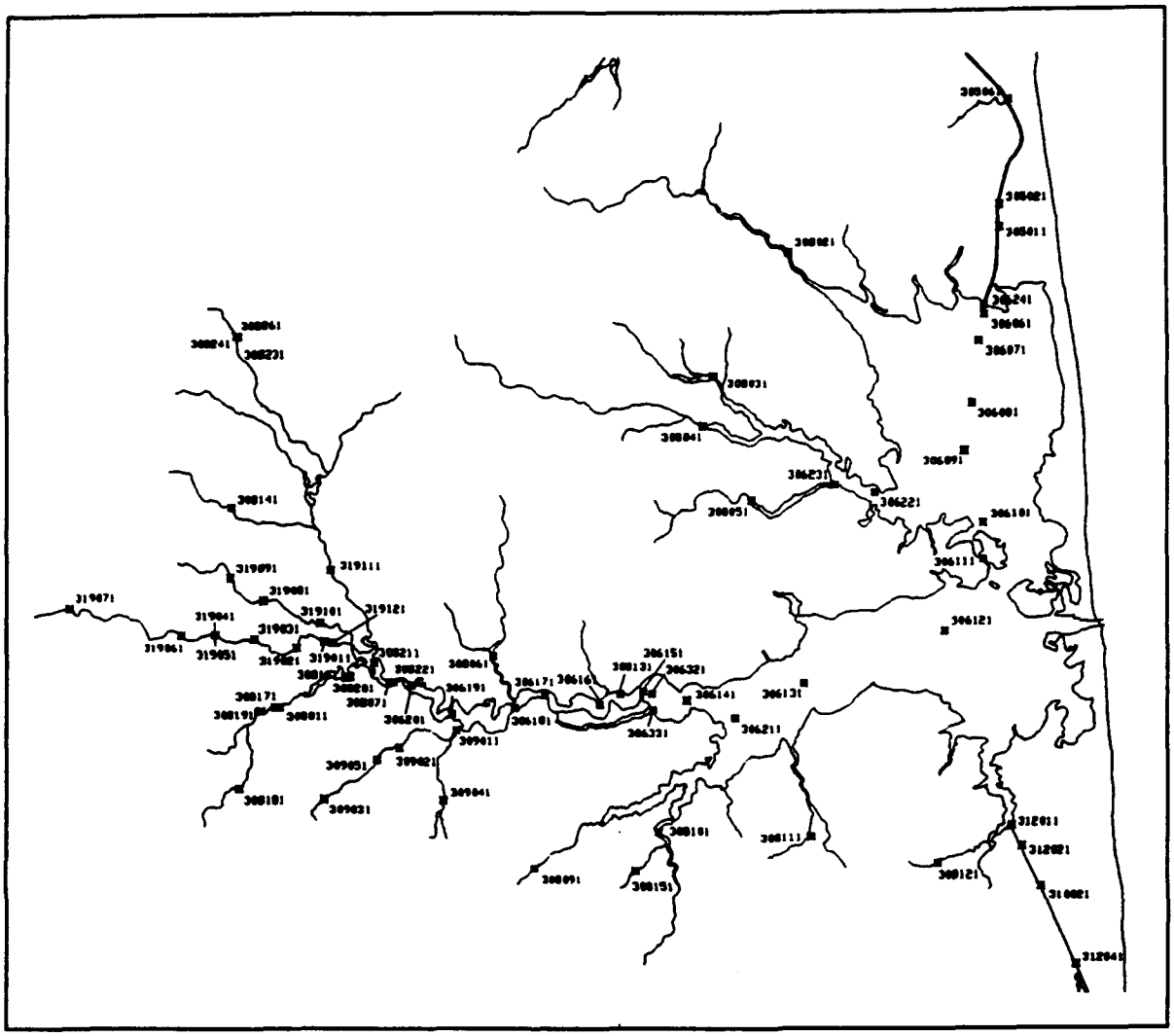

Figure 2-2. STORET Data Locations

Light Extinction Data

Observations of disk visibility (secchi depth) and chlorophyll collected at nine stations (Figure 2-6) during 1985 and 1986 were obtained from an Academy of Natural Sciences Report (Academy of Natural Sciences, 1988). These observations were combined with disk visibility and chlorophyll data collected at numerous locations by the College of Marine Studies from July 1990 through October 1992. The combined data base was employed in the computation of light extinction.

Table 2-3
Observations in Major Data Sets

Source	STORET "Water"	University of Delaware	STORET "Upland"
Period	March 1988 - December 1990	October 1989 - September 1990	1970 - 1991
Stations	18	185	35
Temperature	205	185	641
Salinity	205	148	617
Ammonium	205	185	623
Total Kjeldahl Nitrogen	182	0	604
Nitrate	126	185	629
Phosphate	78	185	271
Total Phosphorus	173	0	477
Dissolved Oxygen	205	0	631
BOD5	51	0	481
Chlorophyll 'a'	81	184	9

Diurnal Dissolved Oxygen Surveys

Diurnal dissolved oxygen data were obtained from two sources. The Department of Natural Resources and Environmental Control provided data collected at four locations (Figure 2-7) in July 1991. Observations of temperature, salinity and dissolved oxygen were conducted at fifteen-minute intervals for 24 hours. Diurnal data collected at five stations (Figure 2-7) in August 1983 were obtained from a University of Delaware report (Biggs, 1984). Hourly measures of dissolved oxygen conducted for 24 hours were supplemented with less frequent measures of nitrogen, phosphorus, and chlorophyll.

Offshore Water Quality

Water quality observations collected offshore of the Indian River inlet were provided by the Region III U.S. Environmental Protection Agency. Data were from May - November, 1988 - 1990, and were collected as part of the EPA Coastal Eutrophication Surveys. The observations were employed in the specification of oceanic boundary conditions for temperature, salinity, ammonium, nitrate, phosphate, chlorophyll, and dissolved oxygen.

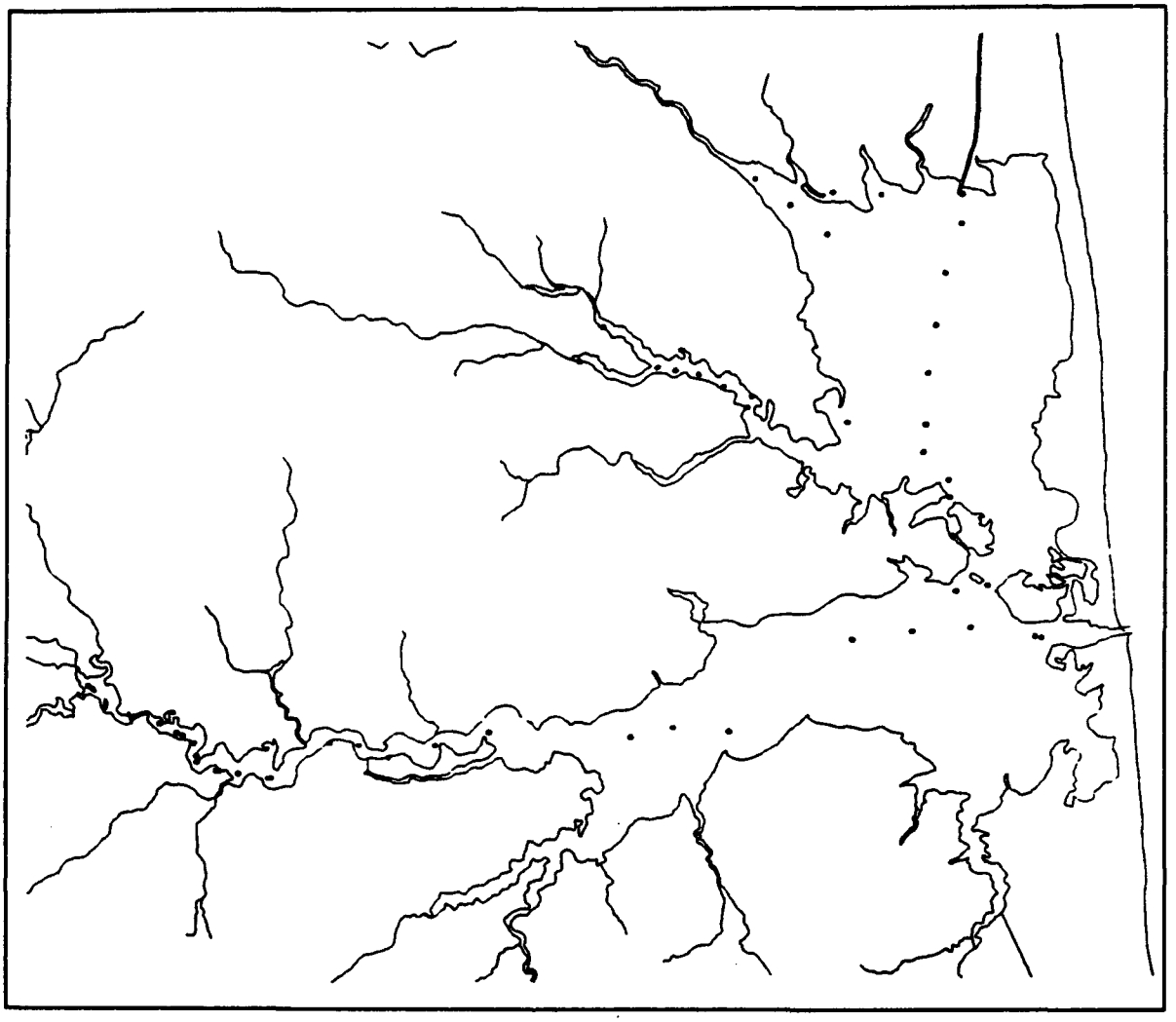

Figure 2-3. University of Delaware Data Stations, 1989

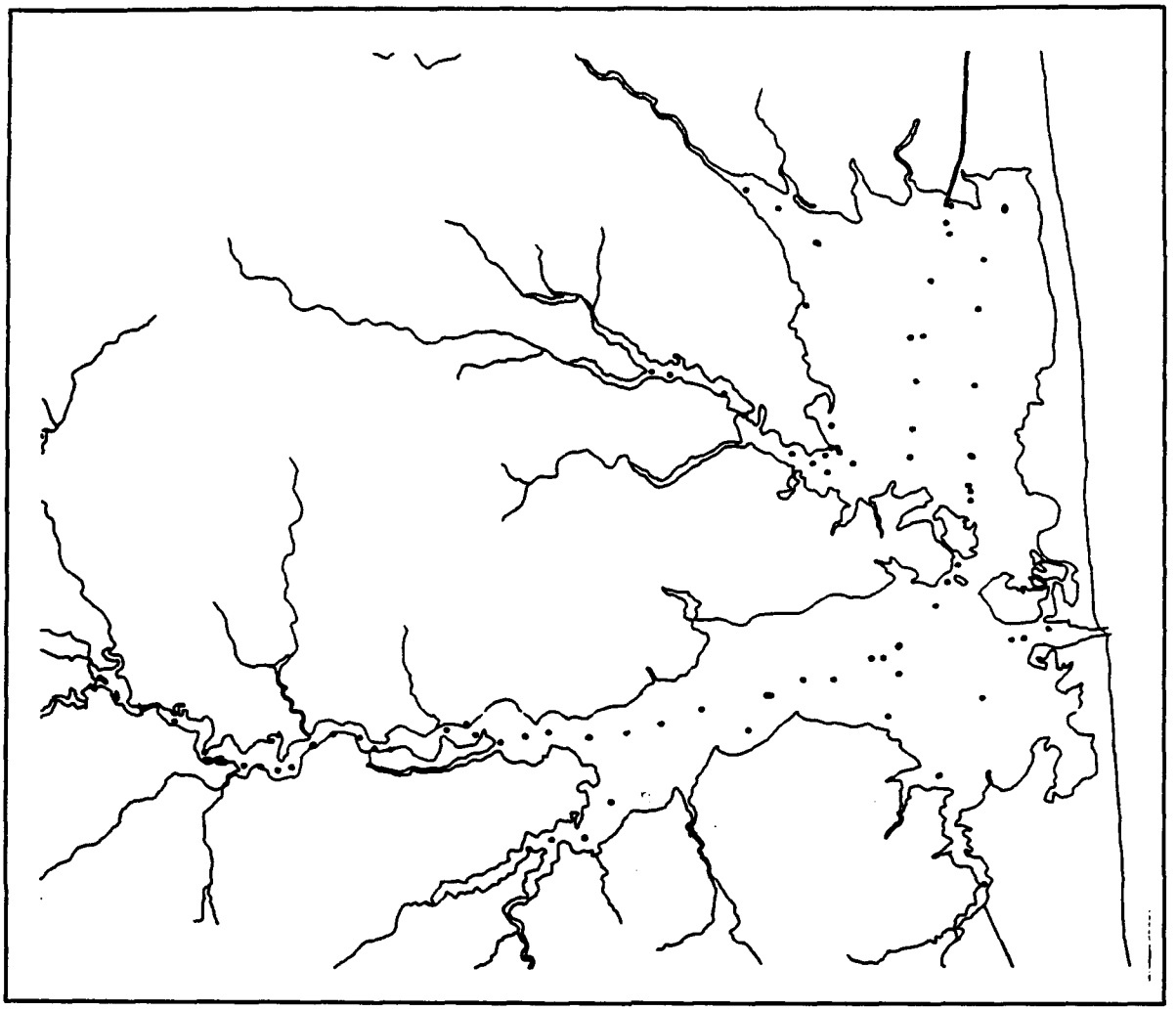

Figure 2-4. University of Delaware Data Stations, 1990

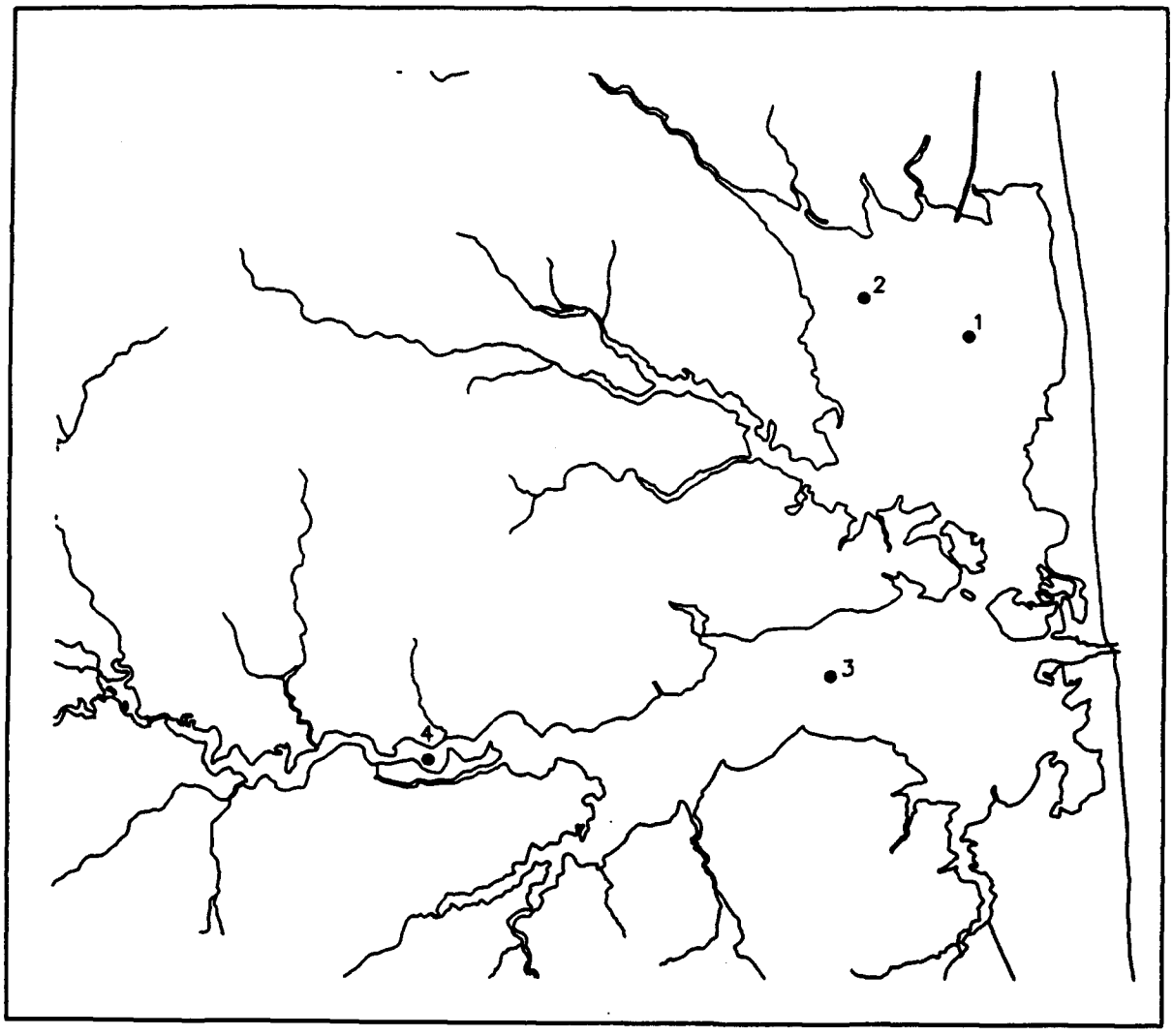

Figure 2-5. Locations of Sediment-Water Flux Measures

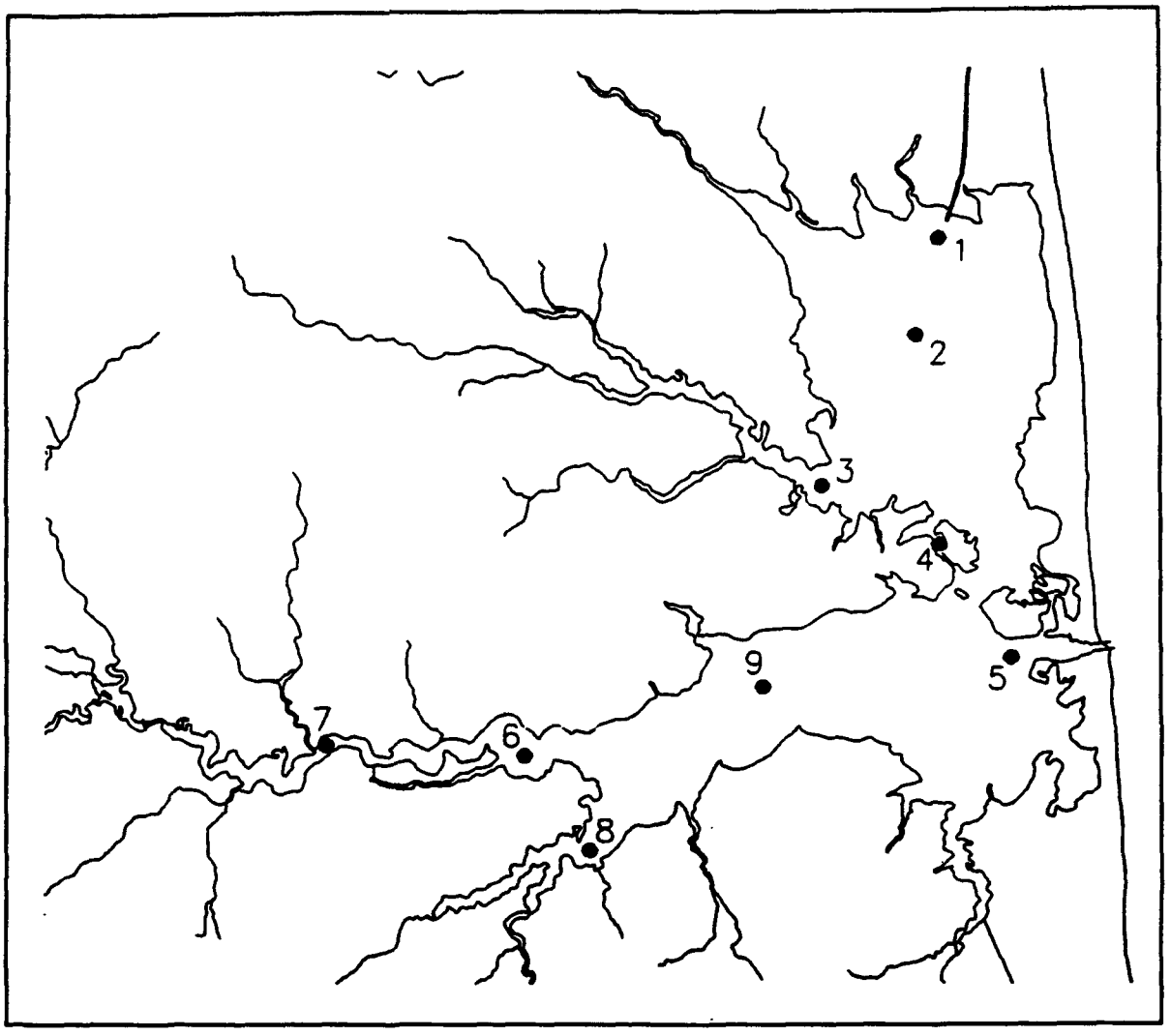

Figure 2-6. Location of Academy of Natural Sciences Disk Visibility Measures

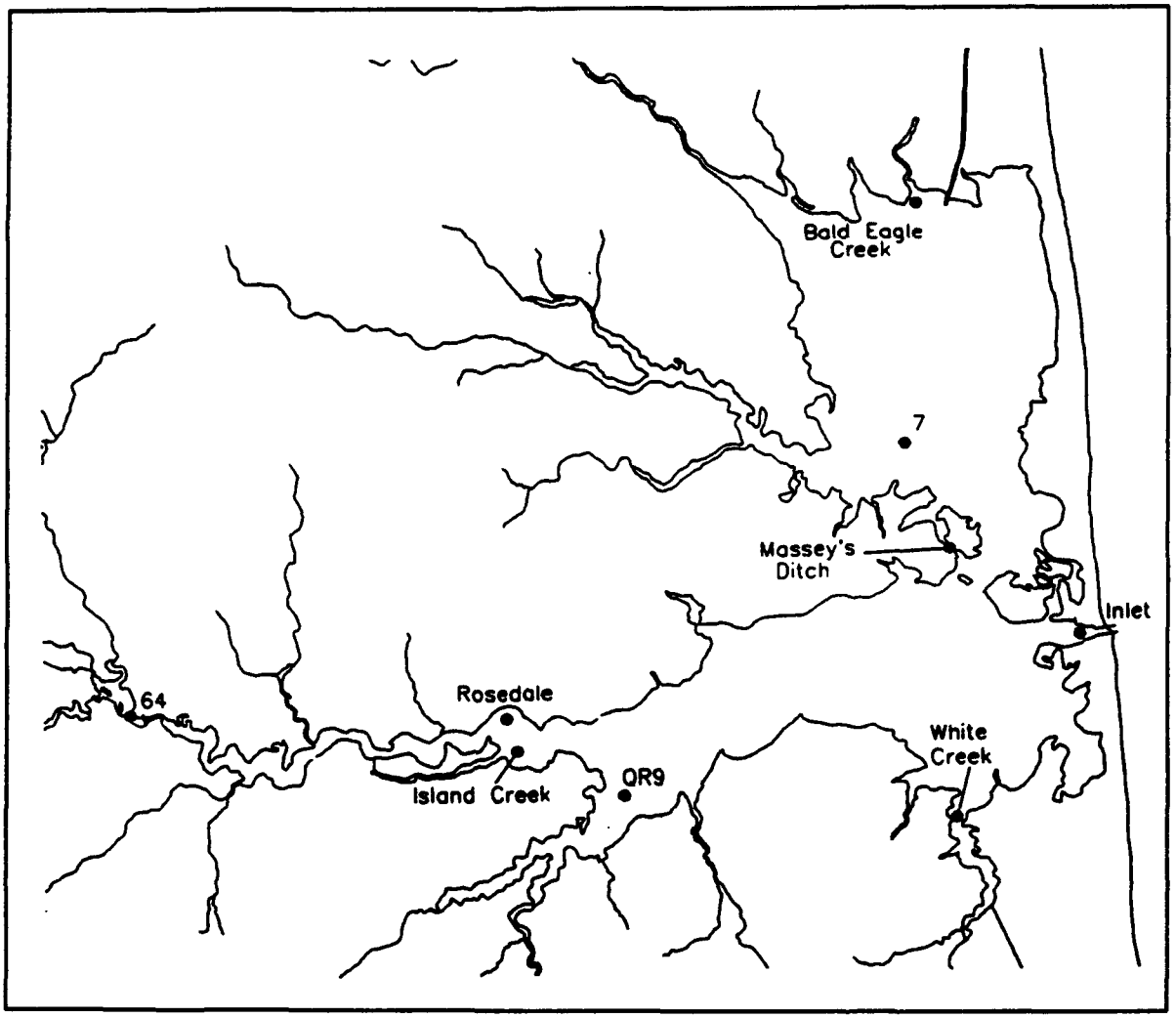

Figure 2-7. Location of Diurnal Dissolved Oxygen Surveys

Chapter III: Flows and Loads

Flows

Freshwater Runoff

The volumetric freshwater runoff rate was one of the forcing functions required to drive the hydrodynamic portion of the Indian River/Rehoboth Bay model. Both the time series and spatial distribution of runoff were necessary. Runoff volume was also required to compute the distributed loads of nutrients and organic matter to the system. The drainage basin contained only one stream gauge, on Stockley Branch (Figure 3-1), active during the entire study period. The strategy adopted to get flow throughout the basin was to convert Stockley volumetric flow (e.g. m^3 sec^{-1}) to flow per unit area (e.g. cm day^{-1}). This flow per unit area was multiplied by drainage areas of subbasins within the watershed to get the volumetric flow in each subbasin. Subbasin locations and areas were obtained from Ritter (1986) who identified 16 subbasins in the Indian River/Rehoboth Bay watershed. Of these, three contributed to Millsboro Pond upstream of the dam and were combined by us into one. Land areas draining directly into Indian River and Rehoboth Bay were named as individual watersheds by Ritter. We allocated the direct discharge area to tributary subbasins so that the total number of subbasins considered in this study was twelve (Table 3-1). Flows from each subbasin were input to the model at the discrete location (Figure 3-1) at which the subbasin tributary entered the receiving water. Flows were updated on a daily basis throughout the three-year study period.

Millsboro Pond

Flow from the largest of the subbasins (Figure 3-2) entered the tidal system across the Millsboro spillway. A gauging station (USGS 0148455525) operated at the spillway during a portion of the study. Comparison of flows at Stockley and Millsboro (on a per unit area basis) showed the impoundment exerted a smoothing effect (Figure 3-3). Peak flows at Millsboro were dampened relative to the Stockley gauge while minimum flow from the impoundment was higher than gauged at the upland station. Due to the smoothing effect, the Stockley flow per unit area was not used to provide flows at

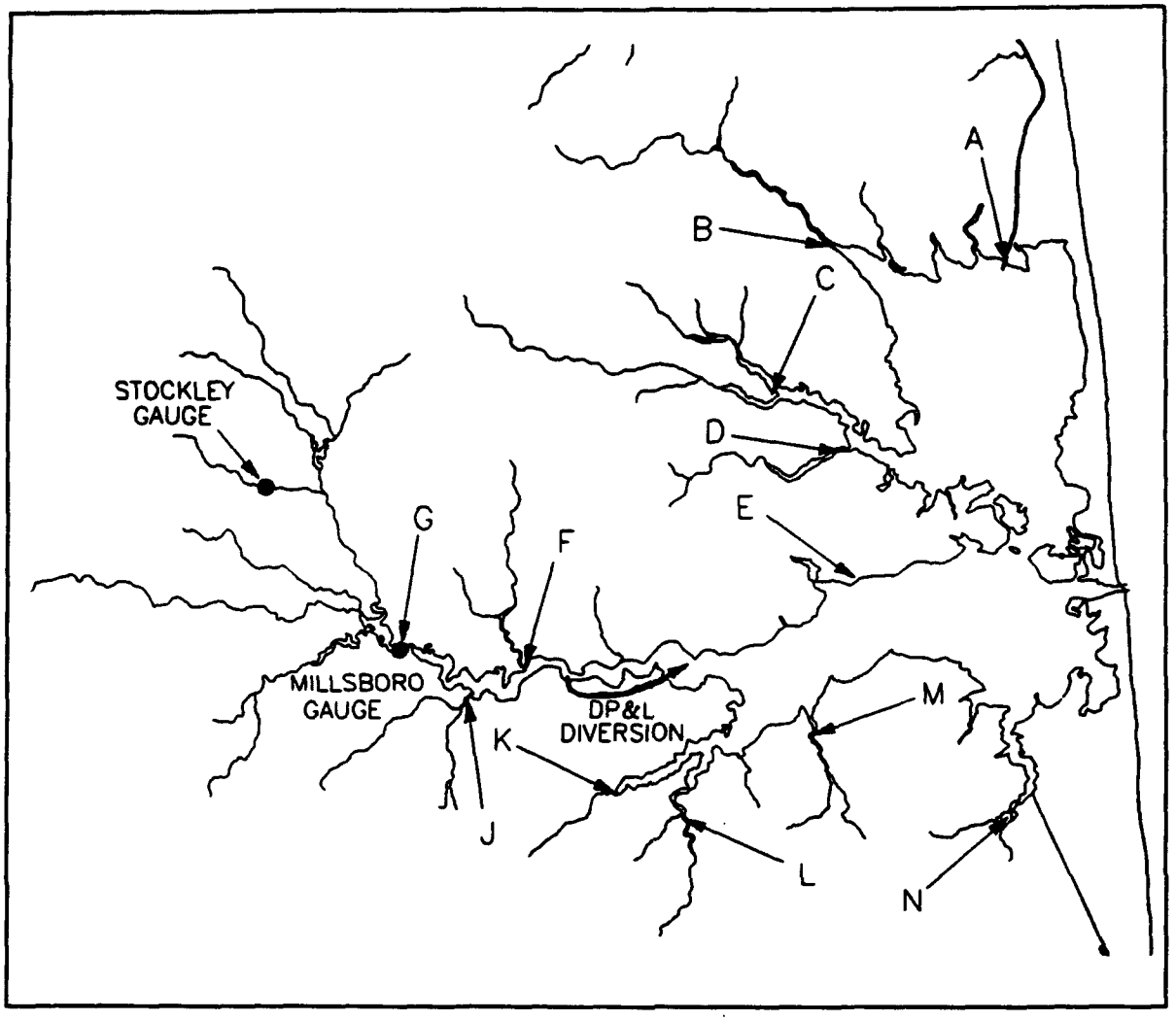

Figure 3-1. Locations of distributed flows

Millsboro. Rather, a regression relationship was derived that related flow at Millsboro to flow on the Nanticoke River near Bridgeville. The Nanticoke gauge (USGS 01487000) was nearby but outside the Indian River watershed. The Nanticoke drainage area (19529 hectares) was an order of magnitude larger than the Stockley drainage area (1357 hectares). The large drainage area of the Nanticoke gauge apparently exerted a smoothing effect on flow similar to the smoothing effect of the Millsboro impoundment. The relationship was:

$$FMB = 1.22\ FNT - 0.133 \qquad (3\text{-}1)$$

in which:

FMB = flow at Millsboro (cm)

FNT = flow at Nanticoke (cm)

Table 3-1
Subbasins in Indian River Rehoboth Bay Watershed

Code	Basin	Area (hectares)
A	Lewes–Rehoboth Canal	3785
B	Love Creek	5682
C	Herring Creek	6397
D	Gunea Creek	3547
E	Lingo Creek	1801
F	Swan Creek	5527
G	Millsboro Pond	14339
J	Iron Branch	5997
K	Pepper Creek	4154
L	Vines Creek	4027
M	Blackwater Creek	3549
N	White Creek	3385

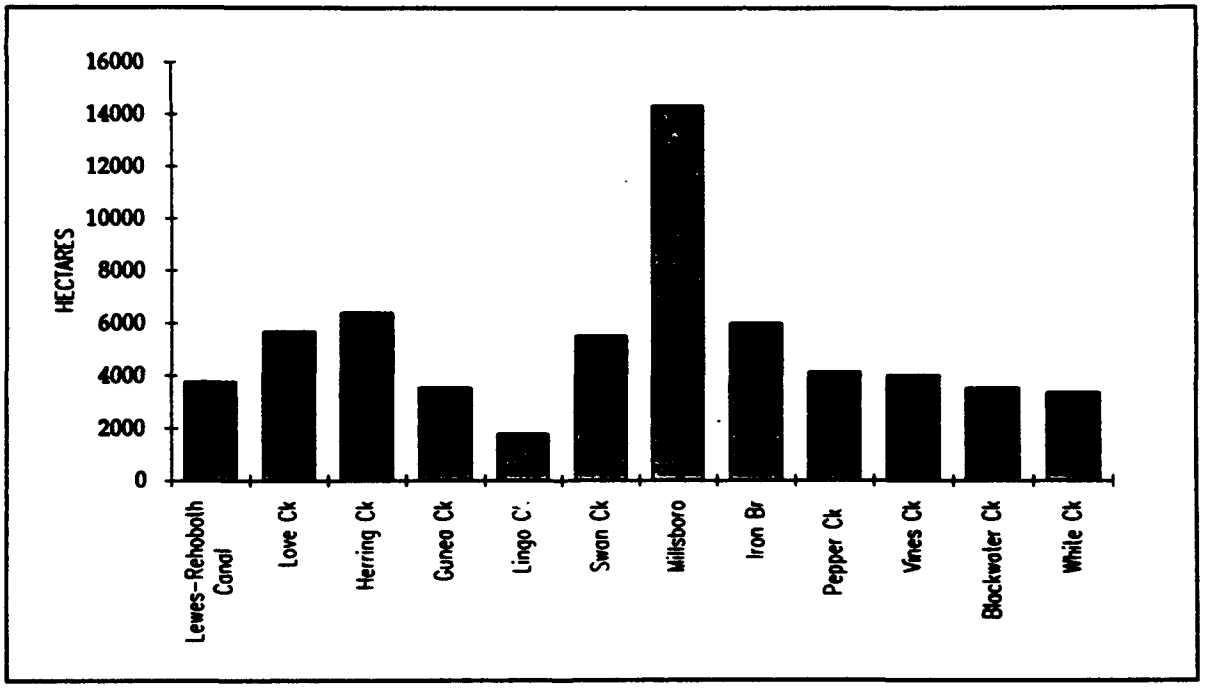

Figure 3-2. Subbasin areas

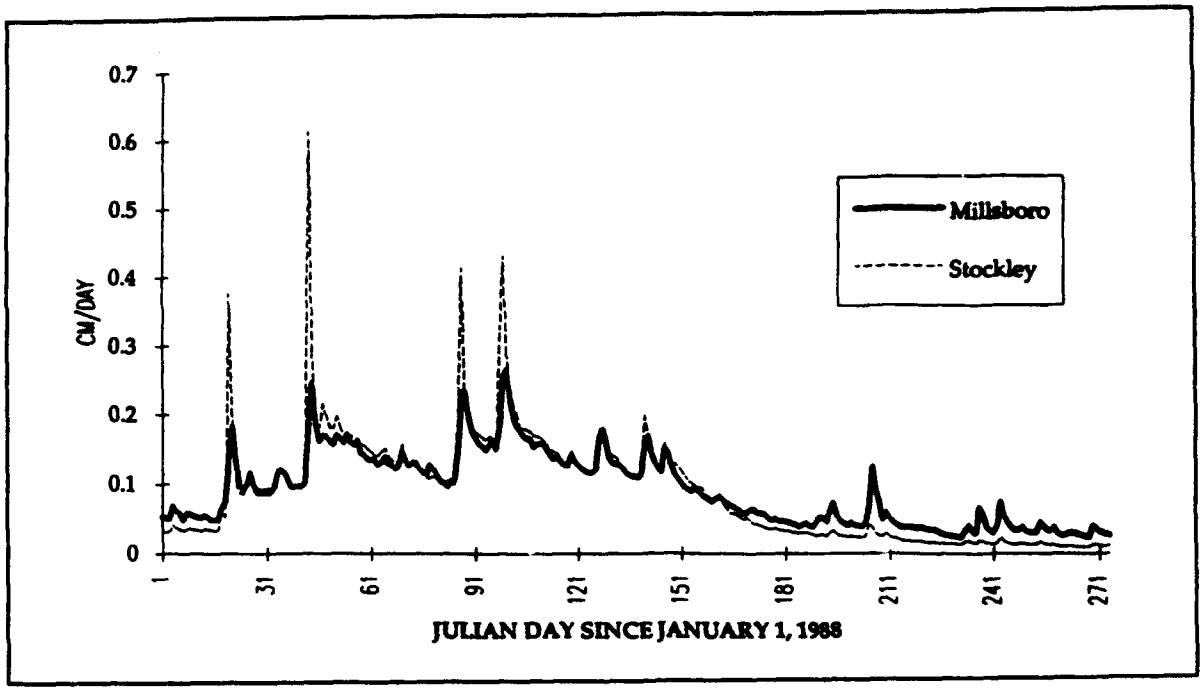

Figure 3-3. Comparison of flow per unit area at Stockley and Millsboro

The R^2 for the relationship was 0.95 for monthly-average flows.

Delmarva Power and Light Diversion

The Delmarva Power and Light Company operates a power plant on the southern shore of Indian River. Three once-through cooling units divert water from Indian River, through the power plant condensers, and into Island Creek. Discharge water flows down the creek and rejoins Indian River downstream of the intake, close to the location where the riverine portion opens out into Indian River Bay (Figure 3-1). The cooling water diversion was included in the hydrodynamic model. Flow through the power plant, at monthly intervals, was obtained from discharge monitoring records (DMRs) provided by the Department of Natural Resources and Economic Conservation. The flow diversion was 12 to 16 m^3 sec^{-1} (Figure 3-4). Interpolated flows were employed to fill gaps in the DMRs.

Relation to Groundwater Flow

Roughly 80% of stream flow in the Indian River/Rehoboth Bay watershed is base flow contribution from groundwater (Johnston 1976). The runoff per unit area records derived from the Stockley gauge included both groundwater and overland runoff. Extension of the Stockley record to the entire watershed extended both overland and groundwater runoff volumes. Independent estimates (Andres 1992) have been made of the groundwater contribution to

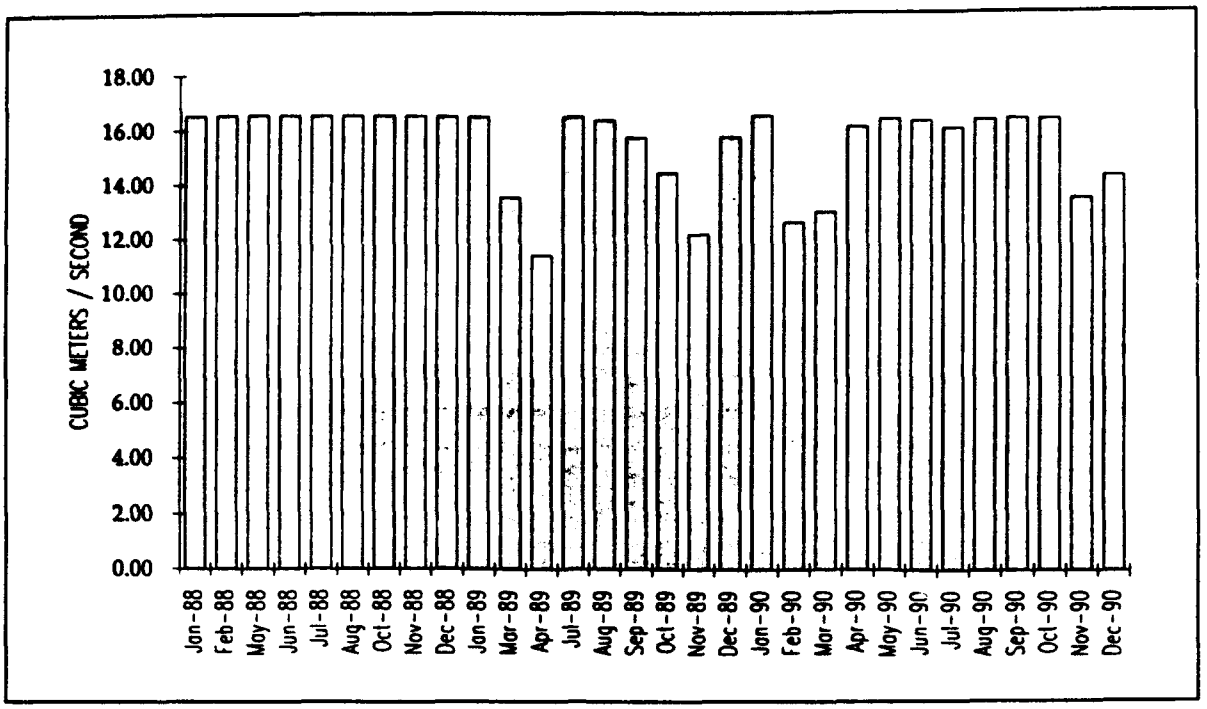

Figure 3-4. Volumetric flow diverted through Delmarva Power and Light cooling units

Indian River/Rehoboth Bay from drainage immediately adjacent to the shoreline. Since this area was represented in our twelve subbasins, no additional accounting for groundwater was required.

Flows Through Navigation Canals

Canals connect Rehoboth Bay with Delaware Bay and Indian River Bay with Little Assawoman Bay. At present, no information exists on flow and material exchange through these canals. As a first approximation, we assumed no net flow occurs through the canals.

Hydrologic Characterization

Runoff at the Stockley gauge during the study period is summarized in Figure 3-5. Two years, 1988 and 1990, had typical hydrographs. Flow was highest during the first half of the year and lowest during spring and fall. The hydrograph for 1989 was unusual, however. Peak flow occurred during August and flow in all months exceeded the long-term average. Recurrence relationships (Table 3-2) indicate the flows that occurred in 1989 are exceeded by less than 8% of the years on record. Flows that occurred during summer 1989 are exceeded by less than 2% of the years on record. Calendar year 1989 was extremely wet. By contrast, annual flow in 1990 was close to long-term median flow while 1988 annual flow was below average. Summer flows

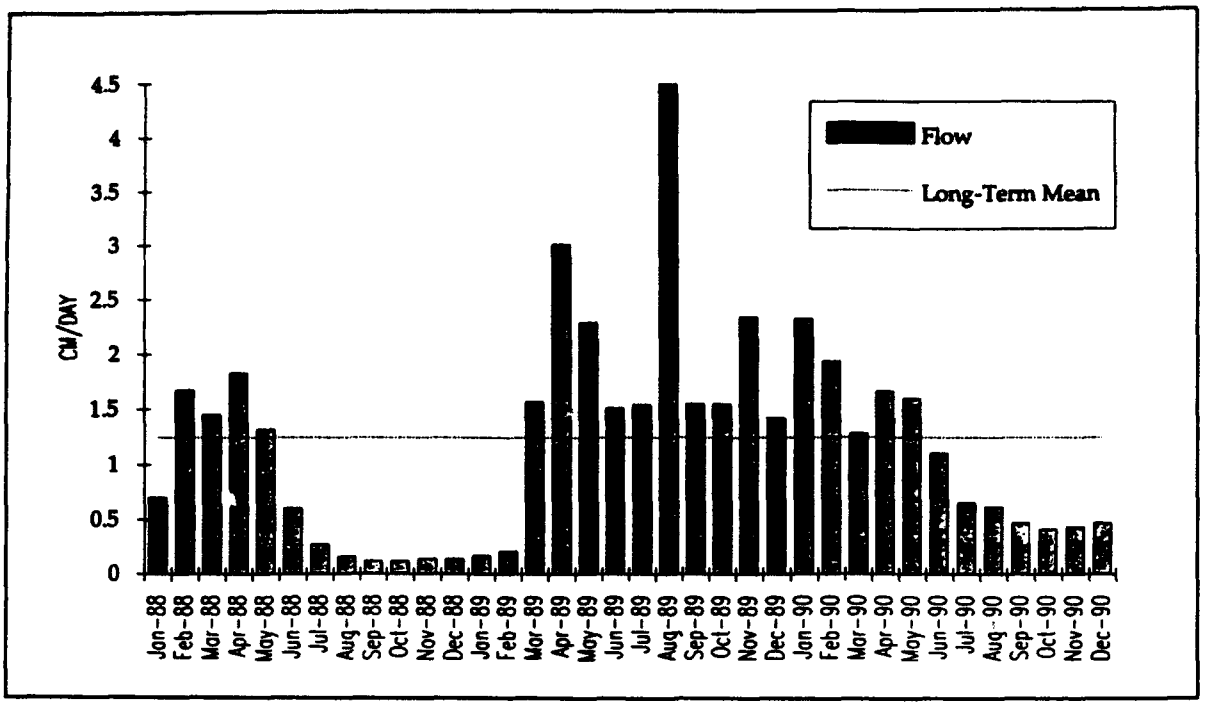

Figure 3-5. Monthly flow per unit area at Stockley 1988 - 1990

Table 3-2
Hydrologic Characterization

Period	Percent of Years That Exceed This One[1]	Characterization
Twelve Months, 1988	70.2	Dry
Twelve Months, 1989	7.4	Wet
Twelve Months, 1990	54.2	Average
July – September, 1988	43.6	Average
July – September, 1989	1.1	Wet
July – September, 1990	39.3	Average

[1] Obtained from SMullen 1992

in 1988 and 1990 were similar and close enough to the median to be characterized as "average".

Loads

The water quality model requires nutrient and organic loads to Indian River/Rehoboth Bay as forcing functions for computation of receiving water quality. Loads can be divided into three classes: Distributed Loads, Point-Source Loads, and Atmospheric Loads. Distributed loads enter the system as runoff from the watersheds that drain into the tidal waters. Point-source loads originate in industries and treatment plants along the shoreline. Atmospheric loads are deposited directly on the water surface in rainfall and as dryfall. Both the time series and locations of these loads are required for the model.

Distributed Loads

Distributed loads were computed as the product of runoff volume and concentration of nutrient or organic substance. Runoff volumes were the same as those used to drive the hydrodynamic model. Monthly loads were computed for each subbasin and input to the model at the same locations as the flows (Figure 3-1). Concentrations in the runoff were obtained from analysis of the "Upland" stations in the STORET data base. Separate analyses were conducted for the Millsboro subbasin and for the remaining watersheds. We conducted separate analyses to allow for concentration differences between freeflowing streams and water leaving the impoundment.

Freeflowing Streams. Our analysis of the data indicated no relationship between concentration and location or flow. Observations of most substances exhibited a high degree of variability. Mean concentrations were unduly influenced by a few extreme observations. We characterized concentrations in the runoff (Table 3-3) as the median value of all observations since the median statistic is less influenced by extreme values than the mean. No temporal or spatial variability in concentration was considered except for nitrate which exhibited a temporal pattern; concentration was generally higher in late autumn and winter than in summer (Figure 3-6). Monthly median concentrations were employed to compute nitrate loads.

Millsboro Spillway. Analysis of concentrations in water leaving the Millsboro impoundment parallelled analysis of concentration in freeflowing streams. No relationship of concentration to flow or season was evident except for nitrate which showed a temporal pattern similar to freeflowing streams (Figure 3-6). Concentrations were characterized as the median of all observations (Table 3-4) except for nitrate. For nitrate, monthly median values were employed.

Total Organic Carbon. The water quality model employs organic carbon as a state variable. Runoff observations included BOD5, but not organic carbon. No direct conversion of BOD to organic carbon exists but empirical relationships can sometimes be found. We examined a data base of total

Table 3-3
Concentrations in Freeflowing Streams

Month	Ammonium gm m^{-3}	Nitrate gm m^{-3}	Total Kjeldahl Nitrogen gm m^{-3}	Phosphate gm m^{-3}	Organic Phosphorus gm m^{-3}	Total Organic Carbon gm m^{-3}
Jan	0.1	2.98	0.88	0.11	0.03	9
Feb	0.1	2.58	0.88	0.11	0.03	9
Mar	0.1	2.65	0.88	0.11	0.03	9
Apr	0.1	2.04	0.88	0.11	0.03	9
May	0.1	1.62	0.88	0.11	0.03	9
Jun	0.1	0.86	0.88	0.11	0.03	9
Jul	0.1	0.23	0.88	0.11	0.03	9
Aug	0.1	1.13	0.88	0.11	0.03	9
Sep	0.1	1.69	0.88	0.11	0.03	9
Oct	0.1	0.39	0.88	0.11	0.03	9
Nov	0.1	1	0.88	0.11	0.03	9
Dec	0.1	2.43	0.88	0.11	0.03	9

organic carbon (TOC) and CBOD5 observations collected in freeflowing streams tributary to the upper Potomac River. A loose curvilinear relationship was evident (Figure 3-7). TOC concentration at Millsboro and in freeflowing streams was obtained visually from the figure as the TOC concentration (9 gm m^{-3}) corresponding to median BOD5 concentration (2.5 gm m^{-3}) in the "Upland" data set.

Point-source Loads

Thirteen point sources exist within the Indian River/Rehoboth Beach watershed (Figure 3-8). One of these, the Lewes STP, discharges near the northern terminus of the canal that connects Delaware and Rehoboth Bays. Consistent with our assumption of no net flow through the canal, we assumed that Lewes effluent does not travel the length of the canal to Rehoboth Bay. The Rehoboth Beach WWTF and lesser point sources that discharge near the southern terminus of the canal were included as Rehoboth Bay point sources. The Georgetown STP discharges into a tributary of the Millsboro impoundment. Loads from Georgetown do not require explicit treatment since they are included in the distributed load assigned to the Millsboro spillway. (Analysis

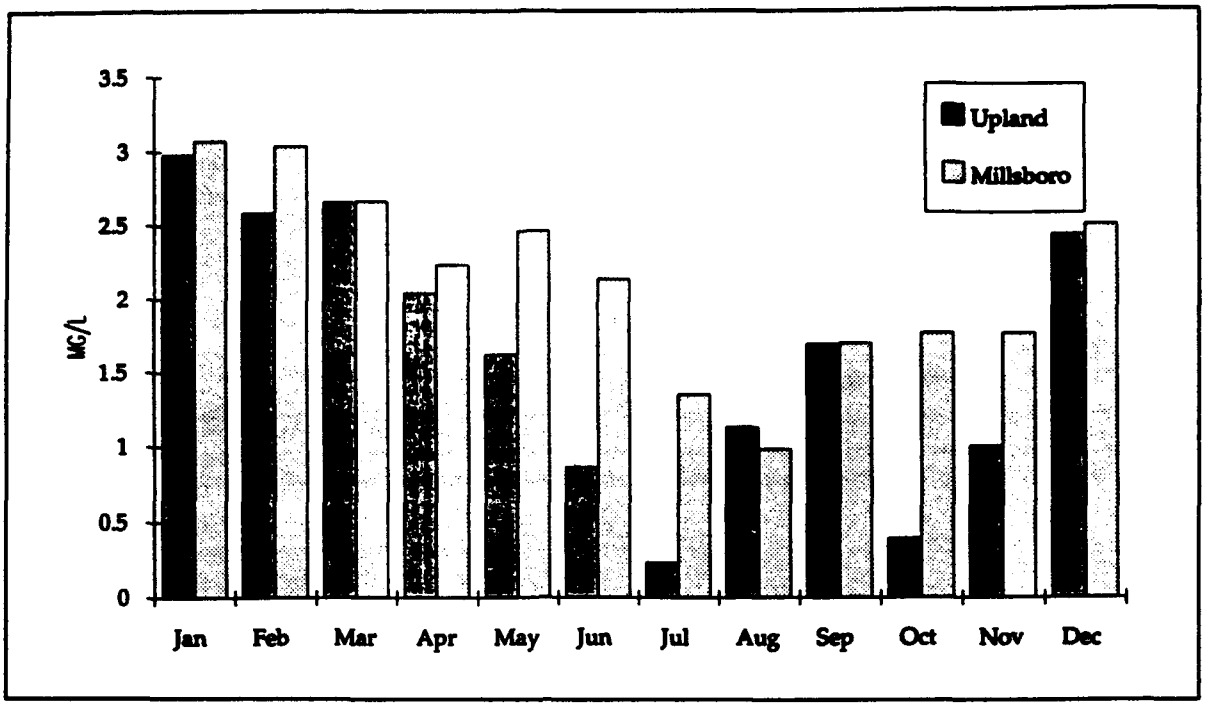

Figure 3-6. Monthly median nitrate concentration at Millsboro spillway and in freeflowing streams

indicates Georgetown loads are less than 5% of the total load at Millsboro.) Deletion of Lewes and Georgetown leaves 11 point sources for consideration.

Flows and Concentrations. Loads from each point source were computed as the product of volumetric flow rate and substance concentration. Flow and concentration data were supplied by DNREC. Flow data was mostly complete, on a monthly basis, especially for the larger point sources. Flows in missing months were obtained by substituting flows from the same months in alternate years. Concentration observations were sporadic, however. For some sources, data were available only for 1991 or 1992, after the study period. We found no rational basis for assigning temporal variability to the point-source concentrations. Mean concentration of all available observations was assigned to each point source (Table 3-5). Consequently, temporal variations in computed point-source loads were due exclusively to variations in flow rather than concentration.

Total Organic Carbon. The water quality model employs organic carbon as a state variable. Point-source monitoring included BOD5, but not organic carbon. Following the pattern set for distributed loads, we attempted to find an empirical relationship between the two substances. We examined a data base of total organic carbon (TOC) and CBOD5 observations collected in point sources discharging to the upper Potomac River. No relationship was evident (Figure 3-9). We selected from the data base the median concentration, 18 gm m^{-3}, to characterize effluent TOC in Indian River/Rehoboth Bay.

Table 3-4
Concentrations in Millsboro Spillway

Ammonium gm m^{-3}	Nitrate gm m^{-3}	Total Kjeldahl Nitrogen gm m^{-3}	Phosphate gm m^{-3}	Organic Phosphorus gm m^{-3}	Total Organic Carbon gm m^{-3}
0.1	3.07	0.8	0.03	0.02	9
0.1	3.03	0.8	0.03	0.02	9
0.1	2.66	0.8	0.03	0.02	9
0.1	2.23	0.8	0.03	0.02	9
0.1	2.45	0.8	0.03	0.02	9
0.1	2.13	0.8	0.03	0.02	9
0.1	1.35	0.8	0.03	0.02	9
0.1	0.98	0.8	0.03	0.02	9
0.1	1.7	0.8	0.03	0.02	9
0.1	1.76	0.8	0.03	0.02	9
0.1	1.76	0.8	0.03	0.02	9
0.1	2.5	0.8	0.03	0.02	9

Delmarva Power and Light. Information and data on Delmarva Power and Light operations were supplied by Mr. Robert Jubic of DP&L. DP&L has several operations which require consideration in computation of point-source loads. The largest flow through the plant is cooling water for Units 1 - 3. No material is added to the once-through cooling water. We assumed, however, that viable algae do not survive the trip through the condensers. Code was installed in the model so that algae withdrawn through the diversion from Indian River were discharged as equivalent amounts of nutrients and organic substances into Island Creek. No material was added to the cooling water, however.

Water increases in temperature as it passes through the condensers so that discharge temperature is higher than withdrawal temperature. Cooling of discharge water occurs in Island Creek before the water rejoins Indian River. Since our model does not include Island Creek we could not use plant records of discharge temperature. We had no way to compute the cooling effect in the Creek. Instead we used STORET data, supplemented by University of Delaware observations, to derive temperature differences between observations collected near the DP&L intake and the mouth of Island Creek. Temperature increase between the intake and creek mouth ranged from 0.95 to 7.5 C° (Figure 3-10). Average increase was 4.2 C°. Code was installed in the model to

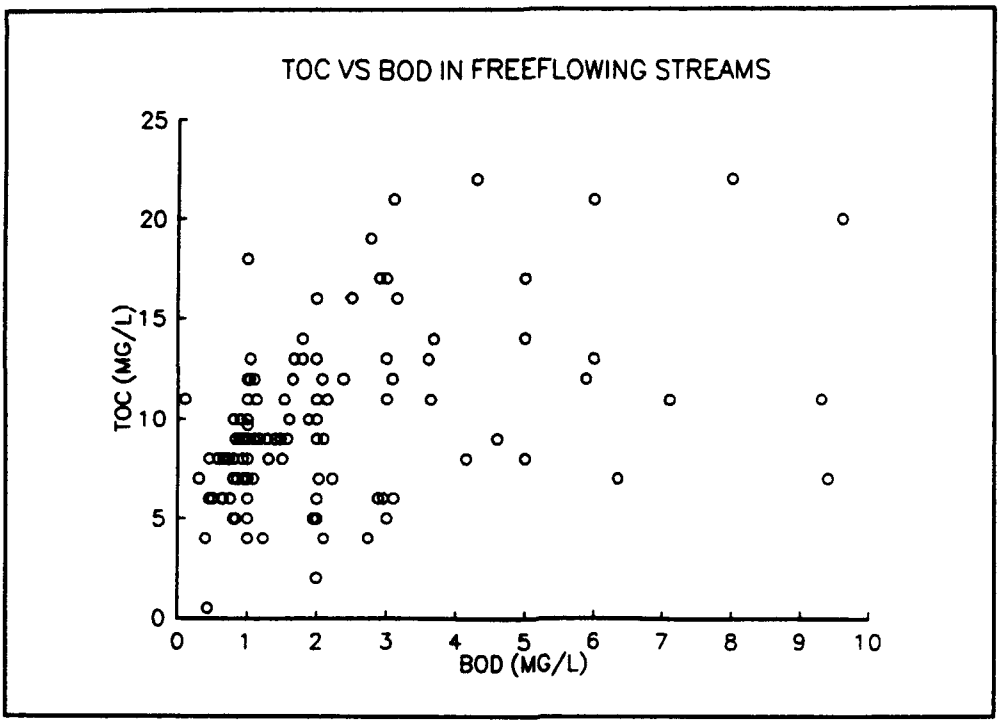

Figure 3-7. Total organic carbon versus CBOD5 in freeflowing streams tributary to the Potomac River below Washington, DC

increase by the mean value temperature of water diverted through the DP&L plant.

A small portion of condenser discharge is diverted into the Unit 4 cooling tower. The tower operates through evaporative cooling so that substance concentrations increase in the cooling water. When solids concentration in the water increases by a factor of three to four, the tower is "blown down" (emptied) via Discharge 027. Total nitrogen concentration in "blow down" water is three to four times higher than intake water (Figure 3-11), consistent with the increase in solids. Nitrate concentration increases by an order of magnitude, however, and total Kjeldahl nitrogen concentration decreases despite the evaporative water loss. The data suggest mineralization of organic nitrogen and subsequent nitrification occur in the tower. To account for this effect we converted appropriate amounts of organic nitrogen in DP&L diversion water (≈30 kg day^{-1}) to nitrate. No net addition or subtraction of total nitrogen was considered, however.

For two of the three study years, 1988 and 1989, phosphorus detergent was added to the cooling tower water. Monthly data on phosphorus use was provided by DP&L. We added these phosphorus loads to the DP&L diversion water. Phosphorus use at the plant ceased after December, 1989.

No data was available to assess the effect of the cooling tower on total organic carbon. We assumed no net addition or change through the tower.

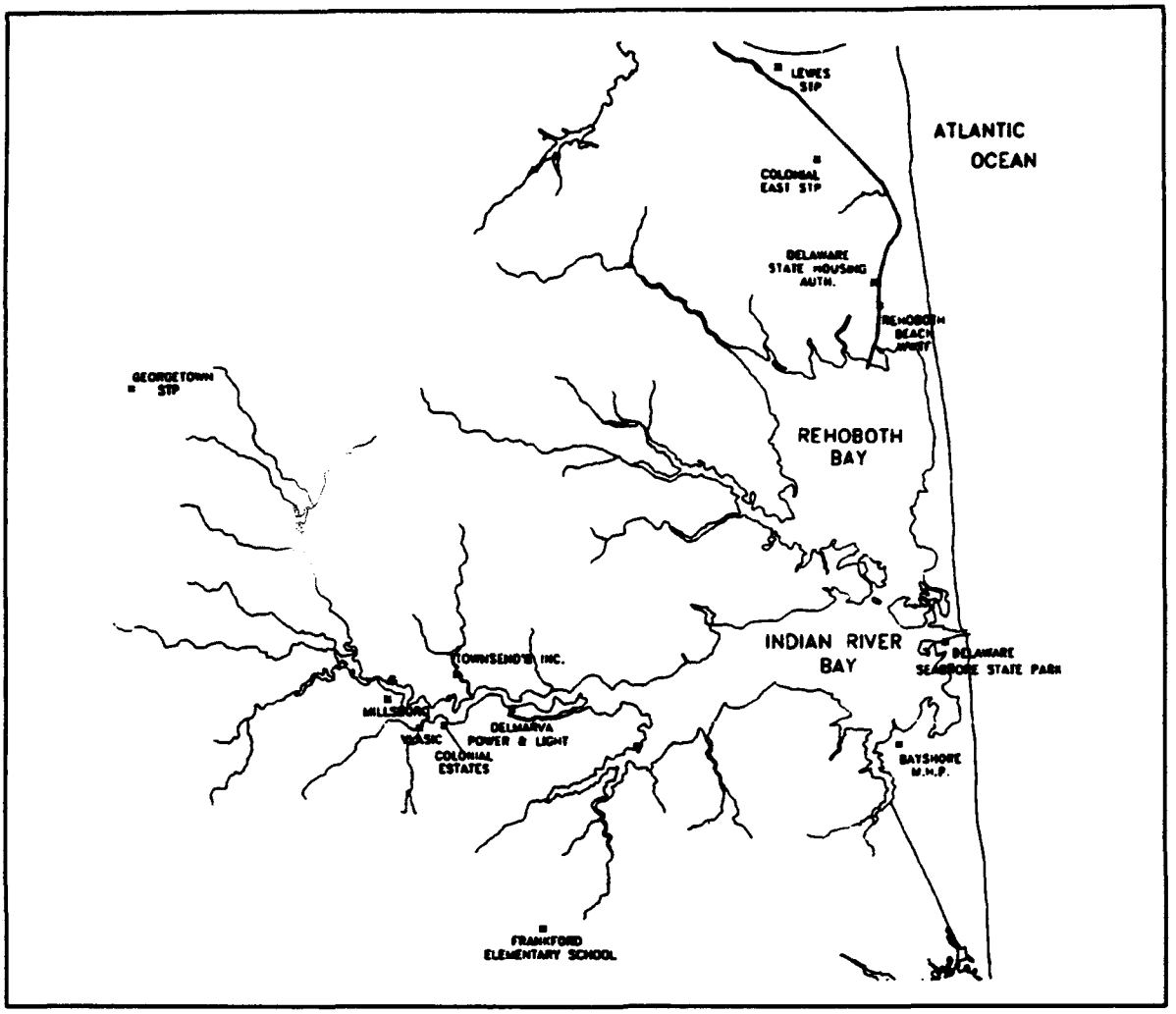

Figure 3-8. Point sources in the Indian River/Rehoboth Bay drainage basin

The DP&L plant has a small sanitary facility (Discharge 028). This facility was considered separately from the cooling water. Analysis and treatment of the sanitary facility was identical to the other point sources in the system.

Atmospheric Loads

Data to compute atmospheric nutrient loads, collected at nearby Cape Henlopen Delaware, were supplied by Dr. Joseph Scudlark of the University of Delaware. Mean ammonium load in rainfall was 2.6 kg N hectare^{-1} year^{-1}. Mean nitrate load was 14.1 kg N hectare^{-1} year^{-1}. Organic nitrogen load was estimated as 15% of the inorganic load. No atmospheric load of phosphorus was detected. A "rule of thumb" in consideration of atmospheric loads is that dryfall, difficult or impossible to measure, equals wetfall. To account for dryfall, the measures and estimates of nitrogen in rainfall were doubled. Atmospheric loads were applied uniformly throughout the study period to all

Table 3-5
Point-Source Concentrations

	Ammonium gm m^{-3}	Nitrate gm m^{-3}	Total Kjeldahl Nitrogen gm m^{-3}	Phosphate gm m^{-3}	Organic Phosp. gm m^{-3}	Total Org. Carb. gm m^{-3}
Delaware Seashore State Park	7.2	17.3	7.2	3.8	0.6	18
Frankford Elementary School	9.86	22.7	9.86	5.5	1	18
Town of Millsboro	7.1	2.6	8.7	2.4	0.3	18
Townsend's Inc.	1	21.8	6	0.1	0	18
Vlassic Food	0.06	3.1	1.36	0.064	0.066	18
Colonial East Mobile Home Pk.	9.7	6.85	9.7	2.2	0.4	18
Rehoboth Beach WWTF	0.95	0.62	5.76	3.46	0.61	18
Delaware State Housing Authority	1.15	28.8	1.15	4.25	0.75	18
Bayshore Mobile Home Pk.	7.2	17.3	7.2	3.8	0.6	18
Colonial Estates	7.9	10.7	7.9	3.1	0.5	18
Delmarva Power and Light (028)	0.9	15.2	3.1	1.26	0.14	18

portions of the water surface. No attempt was made to account for spatial or temporal variations in load. The total atmospheric nitrogen load to the water surface was 765 kg day^{-1}.

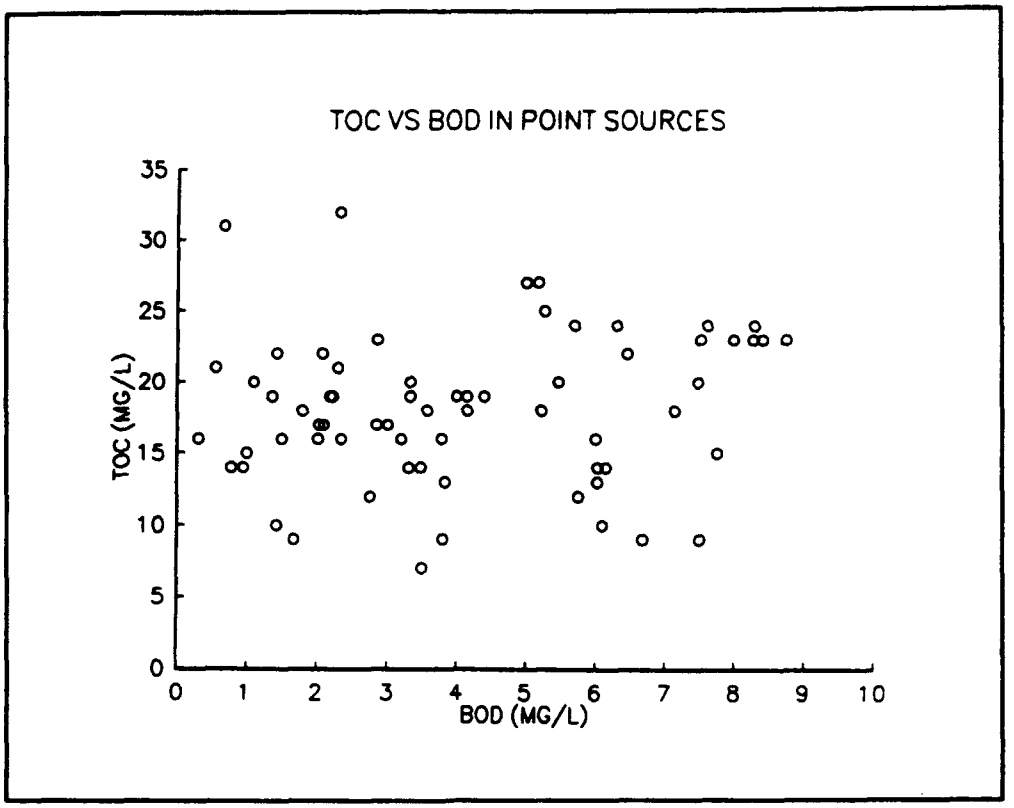

Figure 3-9. Total organic carbon versus CBOD5 in point sources discharging to the Potomac River below Washington DC

Summary of Loads

Distributed Loads. A summary of the subbasin loads, averaged throughout the study period (Table 3-6, Figure 3-12), indicates that nitrogen loads are distributed roughly in accordance with subbasin area. Millsboro is the largest subbasin and the largest distributed nitrogen source. Millsboro is also the largest distributed phosphorus source (Figure 3-13) but is not as dominant as for nitrogen. The relatively large distributed phosphorus loads from the free-flowing subbasins occur because total phosphorus concentration attributed to these basins is nearly three times larger than concentration at Millsboro. The concentration disparity suggests phosphorus settling occurs in the pond but the apparent differences may also be an artifact of the data analysis. Alternate treatments of the data can be conducted that indicate no difference in phosphorus concentration. Total organic carbon loads from the subbasins (Figure 3-14) reflect exactly the relative areas of the basins since concentration is uniform across all subbasins. Millsboro is the largest distributed source of total organic carbon.

Point-Source Loads. A summary of the point-source loads, averaged throughout the study period (Table 3-7), indicates that the Townsend's plant is by far the largest point source of nitrogen (Figure 3-15). Rehoboth Beach

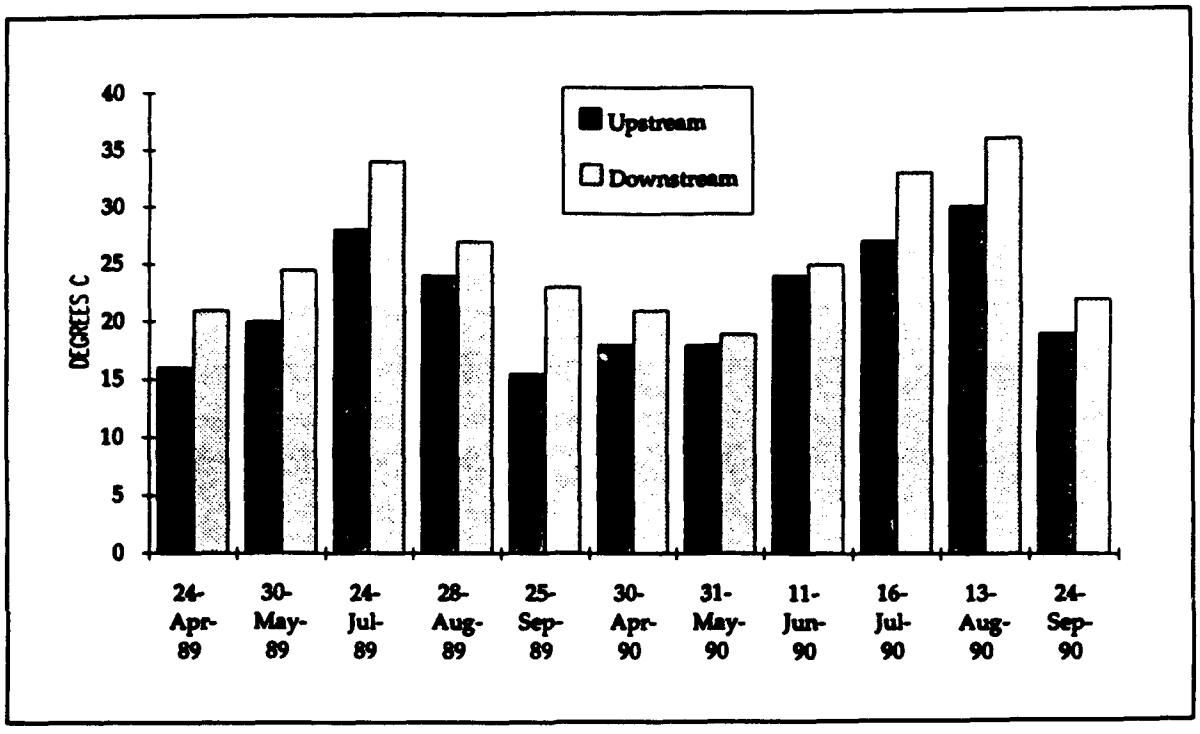

Figure 3-10. Temperature difference between DP&L intake and discharge to Indian River

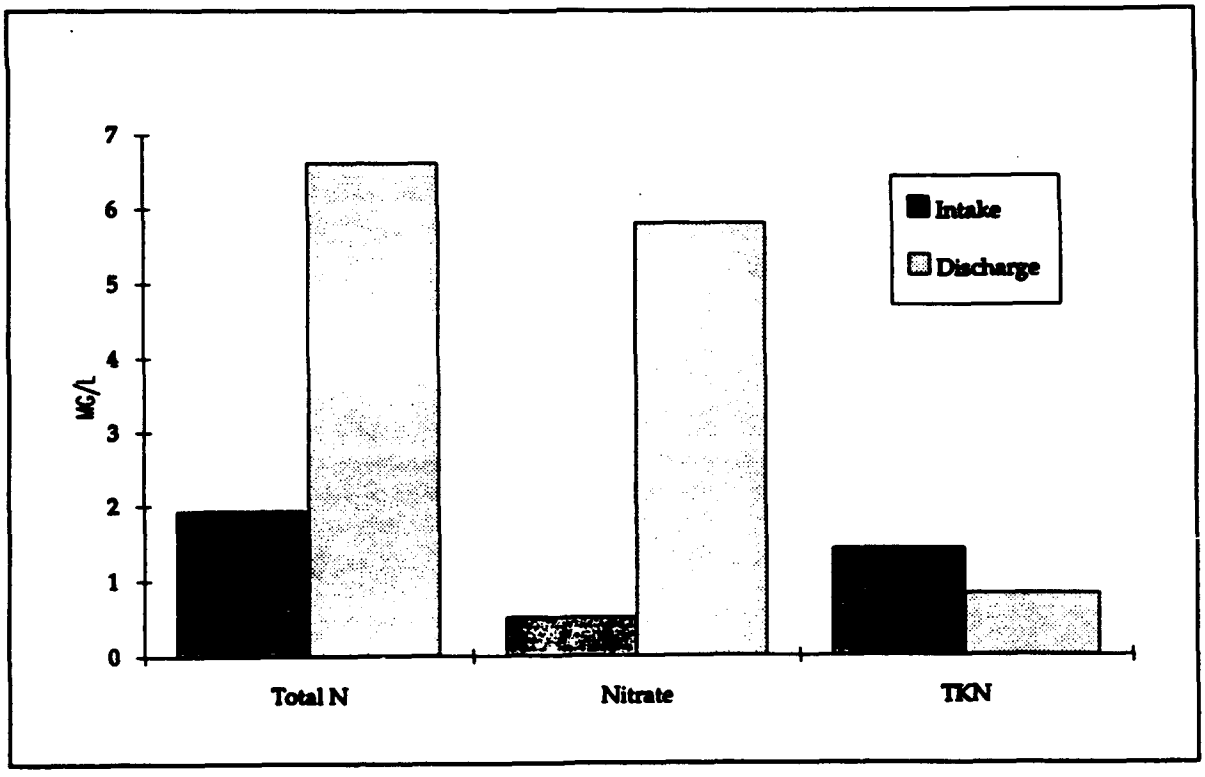

Figure 3-11. Nitrogen concentrations in cooling tower intake and discharge

Table 3-6
Mean Distributed Loads 1988-1990

Basin	Total Nitrogen kg day^{-1}	Total Phosphorus kg day^{-1}	Total Organic Carbon kg day^{-1}
Lewes–Rehoboth Canal	96	5.16	332
Love Creek	155	8.34	536
Herring Creek	177	9.53	613
Guinea Creek	88	4.76	306
Lingo Creek	39	2.13	137
Swan Creek	155	8.37	538
Iron Branch	170	9.15	588
Pepper Creek	113	6.07	390
Vines Creek	109	5.85	376
Blackwater Creek	94	5.05	325
White Creek	89	4.78	307
Millsboro Spillway	717	11.90	2143
Total	2000	81.09	6591

WWTF dominates the phosphorus point sources (Figure 3-16) and is the second largest nitrogen contributor. Town of Millsboro is the second largest phosphorus contributor followed by the DP&L "blow down" water (027). Note that the loads for DP&L are averaged across the three-year study period. For two years, 1988 and 1989, the DP&L load was roughly equivalent to the Town of Millsboro. The DP&L load in 1990 was zero, however, and does not currently exist. Townsend's and Rehoboth Beach also lead in point-source total organic carbon (Figure 3-17).

Relative Loading. Distributed loads comprise the largest nitrogen source to the system (Figure 3-18). In 1988 and 1990, largest nitrogen loads occurred in the first six months. This pattern reflected both the hydrograph and the temporal pattern in nitrate concentration. In 1989, the extremely wet summer was mirrored by unusually large nitrogen loads in the summer months. Atmospheric nitrogen loads are the next largest source. During the dry summer months of 1988 and 1990, periods of high algal and low dissolved oxygen concentration, atmospheric loads equaled or exceeded distributed loads. Point sources are the least of the nitrogen loads although point-source loads approached distributed loads in magnitude during the dry summer of 1988.

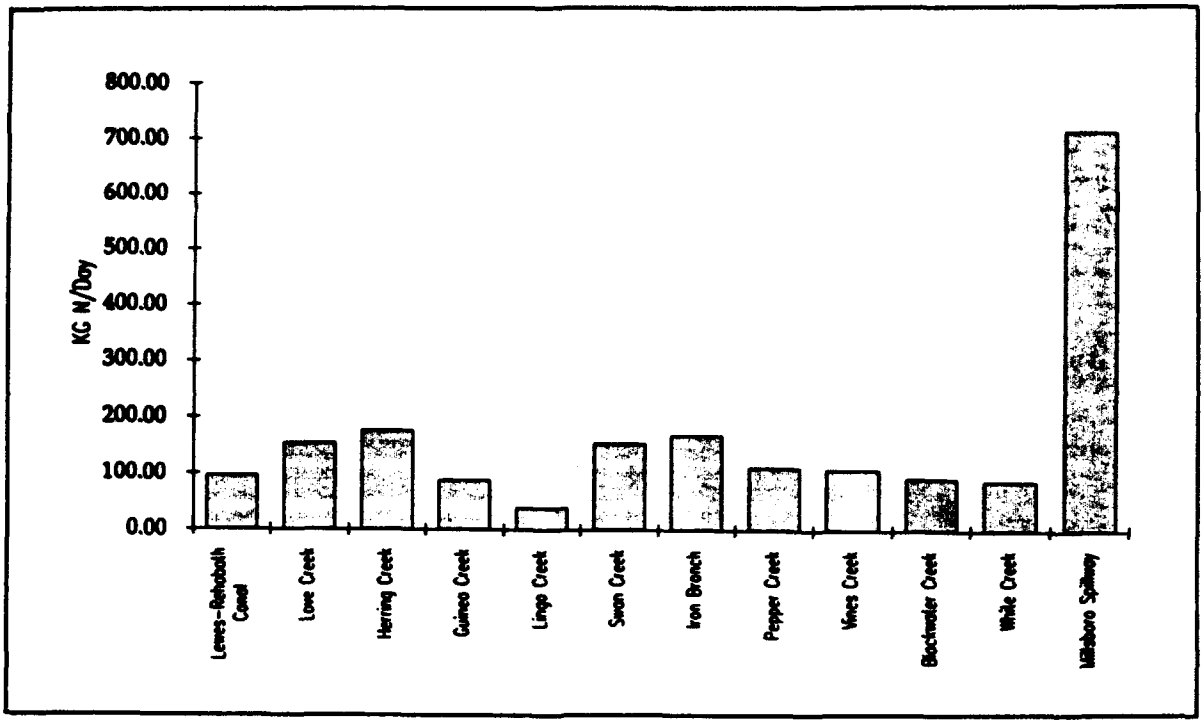

Figure 3-12. Mean total nitrogen load from subbasins

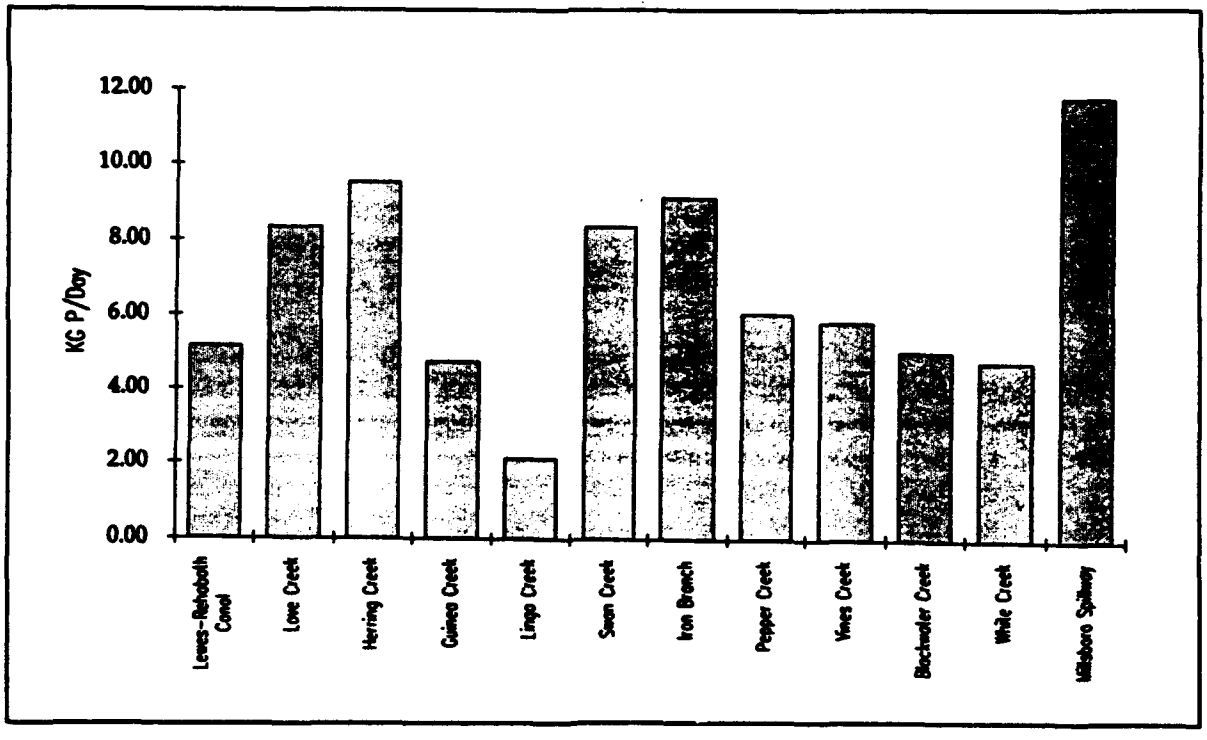

Figure 3-13. Mean total phosphorus load from subbasins

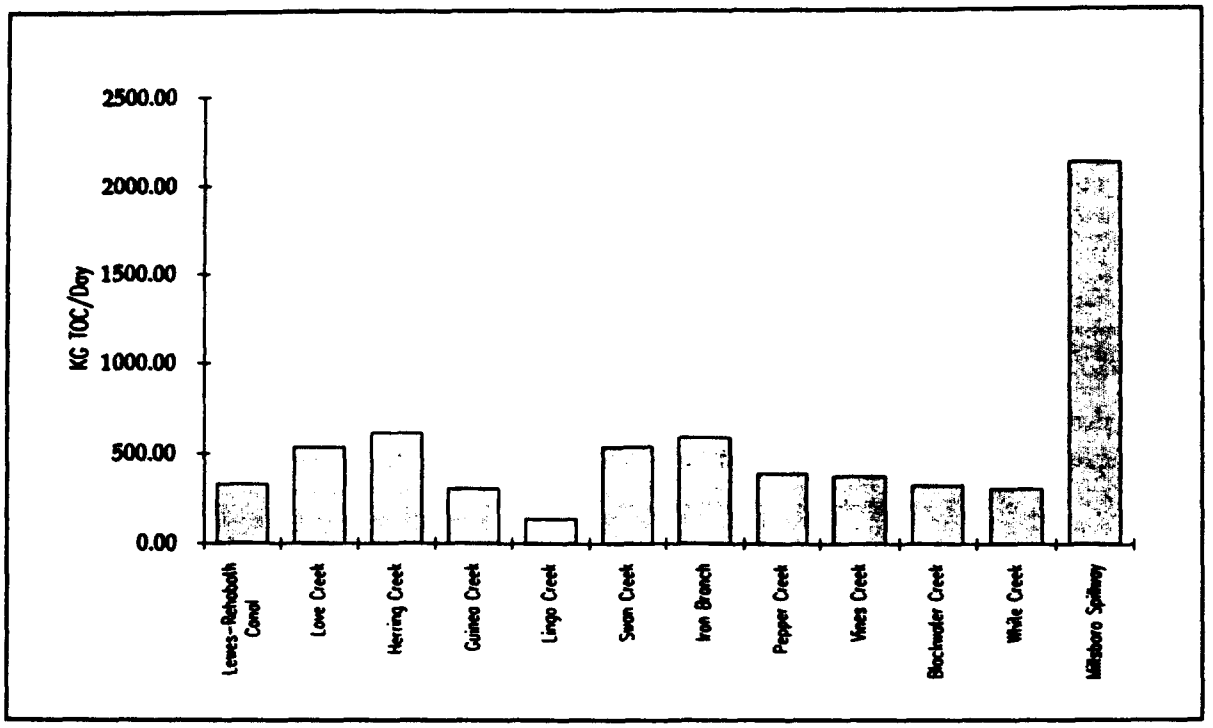

Figure 3-14. Mean total organic carbon load from subbasins

Distributed loads are also the largest source of phosphorus (Figure 3-19). The distributed phosphorus load mirrors exactly the hydrograph since no temporal variation in phosphorus concentration is considered. In 1988 and 1990, largest phosphorus loads occurred in the first six months of the year. In 1989, largest phosphorus loads occurred in summer due to the unusually large summer flows. Point-source phosphorus loads are less than distributed loads although during the dry summer of 1988 point-source loads exceeded distributed loads. The point-source loads exhibit a periodicity. Highest loads occur in June, July, and August due to flow variations at the Rehoboth Beach facility, the largest phosphorus point source. Flows in summer months are three or four times greater than in winter months.

As with nitrogen and phosphorus, distributed total organic carbon loads exceed point-source loads (Figure 3-20). The distributed loads dominate throughout the year in dry or wet hydrology.

Comparison to Previous Estimates. "Desktop" estimates of loads to Indian River/Rehoboth Bay for "Wet", "Dry", and "Normal" years were completed by Ritter (1986). We compared our loads to the previous estimates. Our loads for 1988, 1989, and 1990 were compared to previous estimates for "Dry", "Wet", and "Normal" years respectively (Table 3-8). Our total nitrogen loads are comparable to previous estimates but average roughly 15% less. Comparison of loads by category indicates rough equivalence of distributed

Table 3-7
Mean Point-Source Loads 1988-1990

Source	Total Nitrogen kg day	Total Phosphorus kg day	Total Organic Carbon kg day
Delaware Seashore State Park	1.37	0.30	1.23
Delmarva Power and Light (027)	0.00	1.64	0.00
Frankford Elementary School	0.27	0.05	0.15
Town of Millsboro	11.87	2.84	18.91
Townsend's Inc.	145.23	0.52	94.04
Vlassic Food	4.79	0.14	19.34
Colonial East Mobile Home Pk.	1.14	0.18	1.25
Rehoboth Beach WWTF	25.76	16.43	72.67
Delaware State Housing Authority	0.94	0.16	0.57
Bayshore Mobile Home Pk.	0.26	0.06	0.24
Colonial Estates	0.90	0.17	0.87
Delmarva Power and Light (028)	0.53	0.04	0.52
Georgetown[1]	34.37	0.48	27.18
Lewes STP[2]	32.29	7.77	37.50
Total Contributing Point Sources	193.06	22.54	209.77

[1] Load from this point source is included in the distributed load from the Millsboro subbasin.
[2] Not considered as a load to Rehoboth Bay. Shown only for comparison.

nitrogen loads. Comparison of other categories indicates significant differences, however. Our point-source nitrogen loads are only a third of previous estimates. This difference may be due to a reduction in point-source loads since the previous estimates were completed or else improved quantification due to availability of additional, contemporary data. Our atmospheric nitrogen loads are triple the previous estimates. In view of the nature and extent of the Cape Henlopen data base, current estimates must be regarded as the best available. The differences in current and previous estimates of point-source and atmospheric loads offset. Total nitrogen loads would be nearly equivalent except for additional loads considered by Ritter. The excess in previous estimates over current estimates is due to septic tank loads considered by Ritter but omitted from this study.

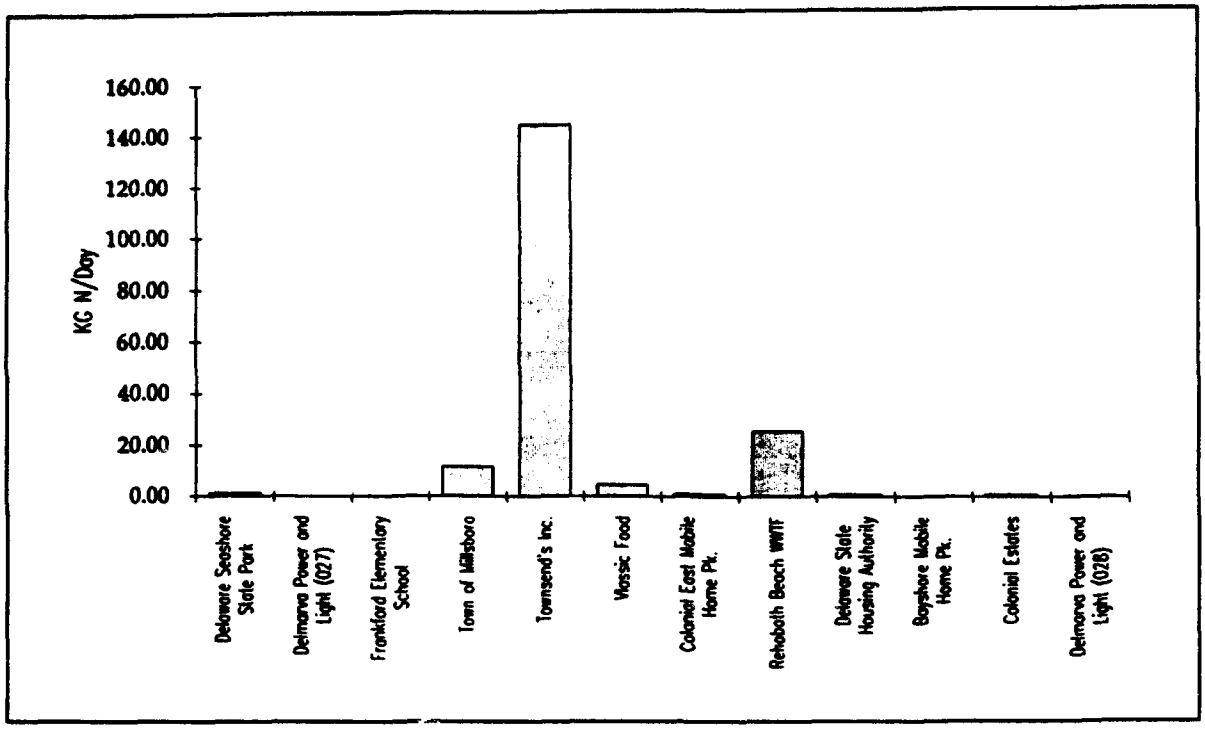

Figure 3-15. Mean total nitrogen load from point sources

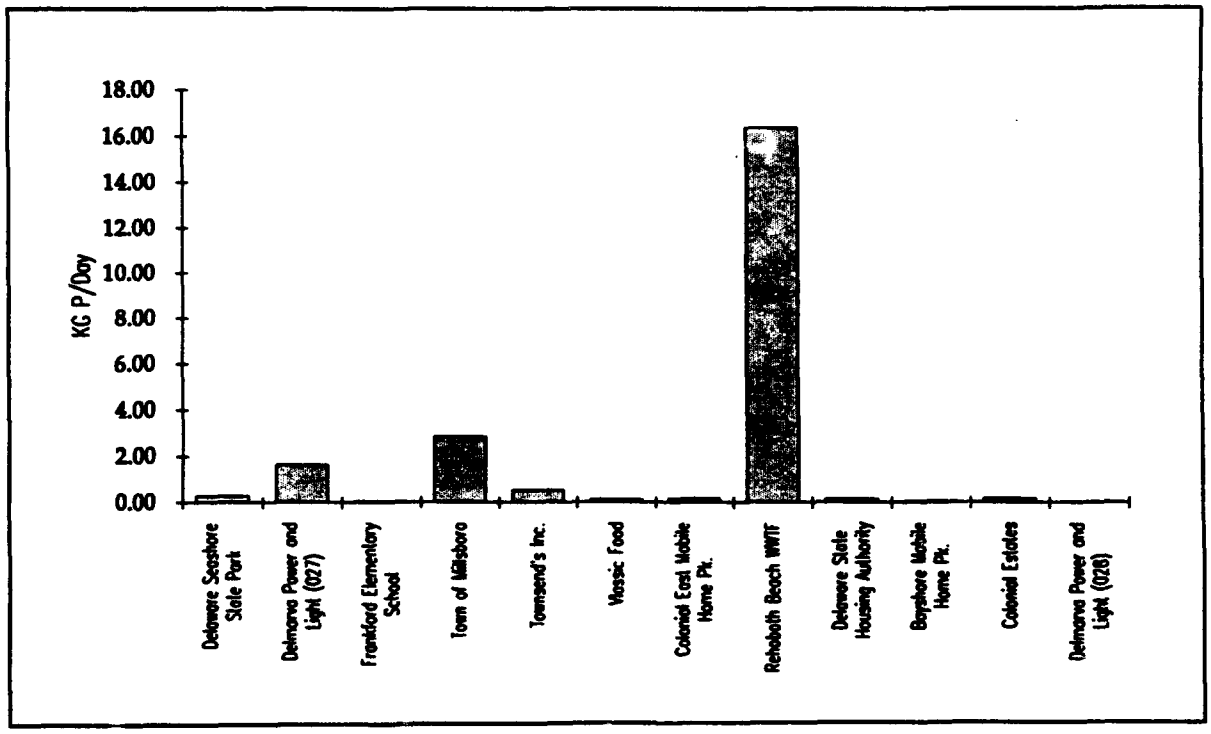

Figure 3-16. Mean total phosphorus load from point sources

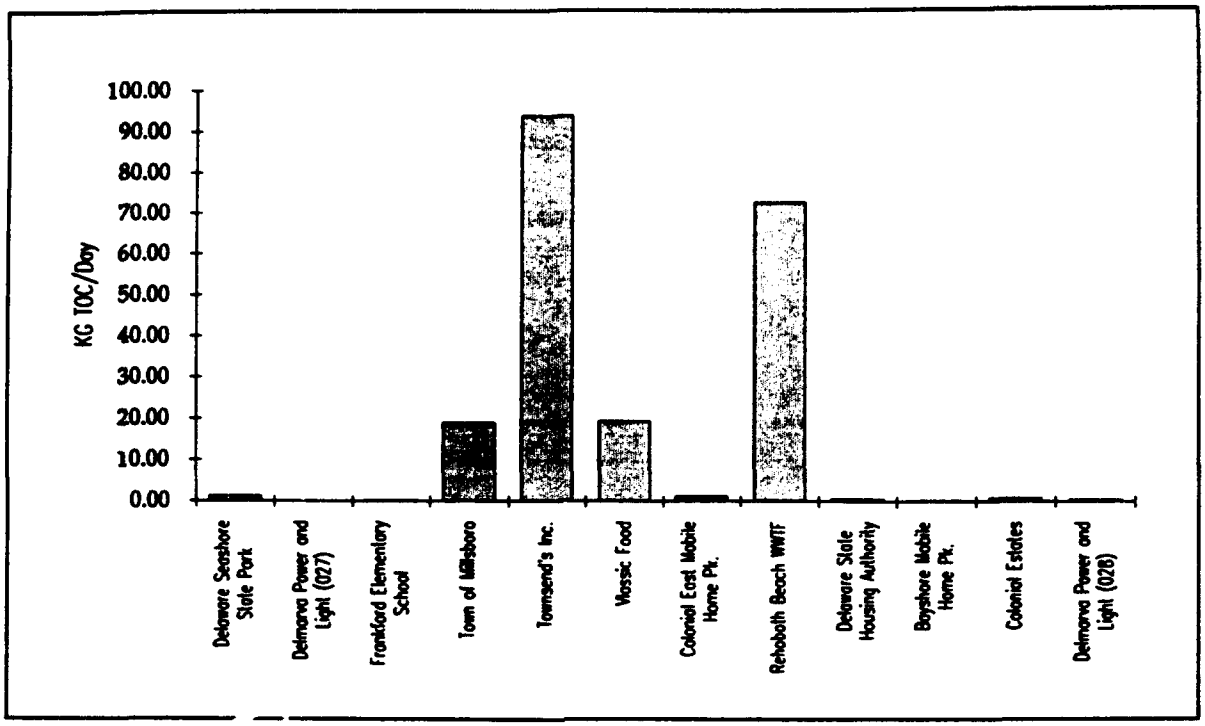

Figure 3-17. Mean total organic carbon load from point sources

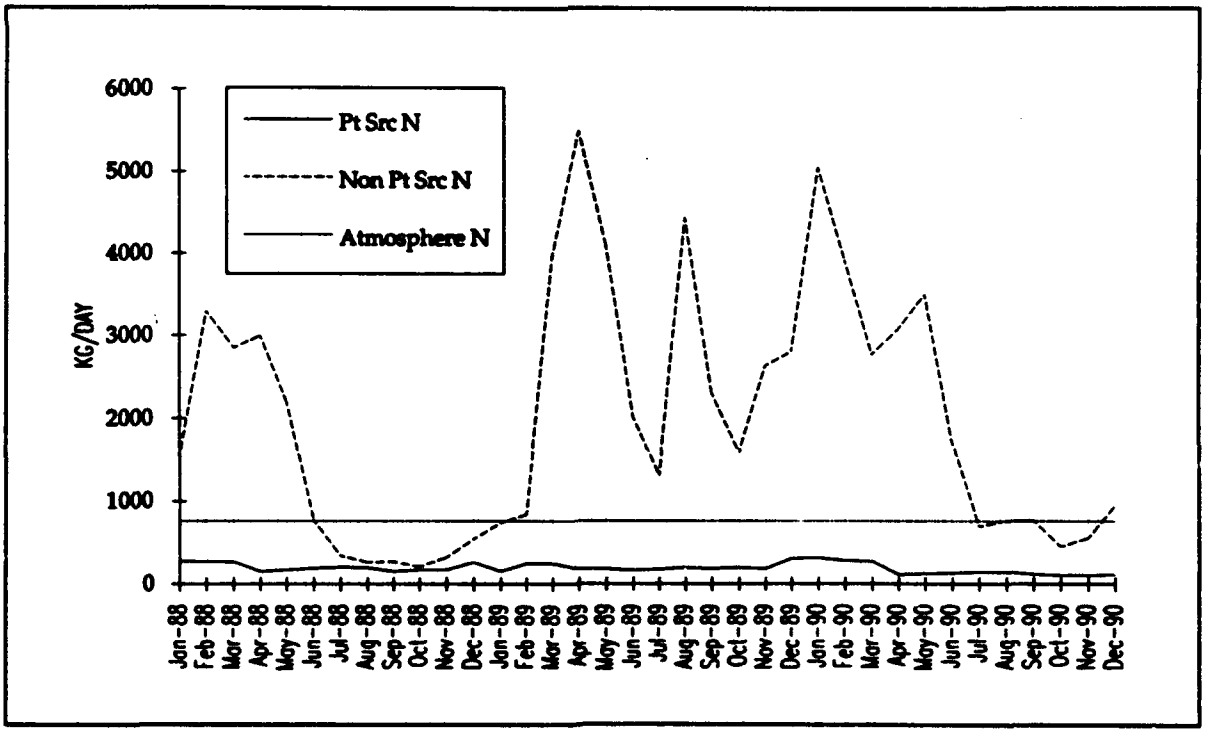

Figure 3-18. Time series of point-source, distributed, and atmospheric nitrogen loads

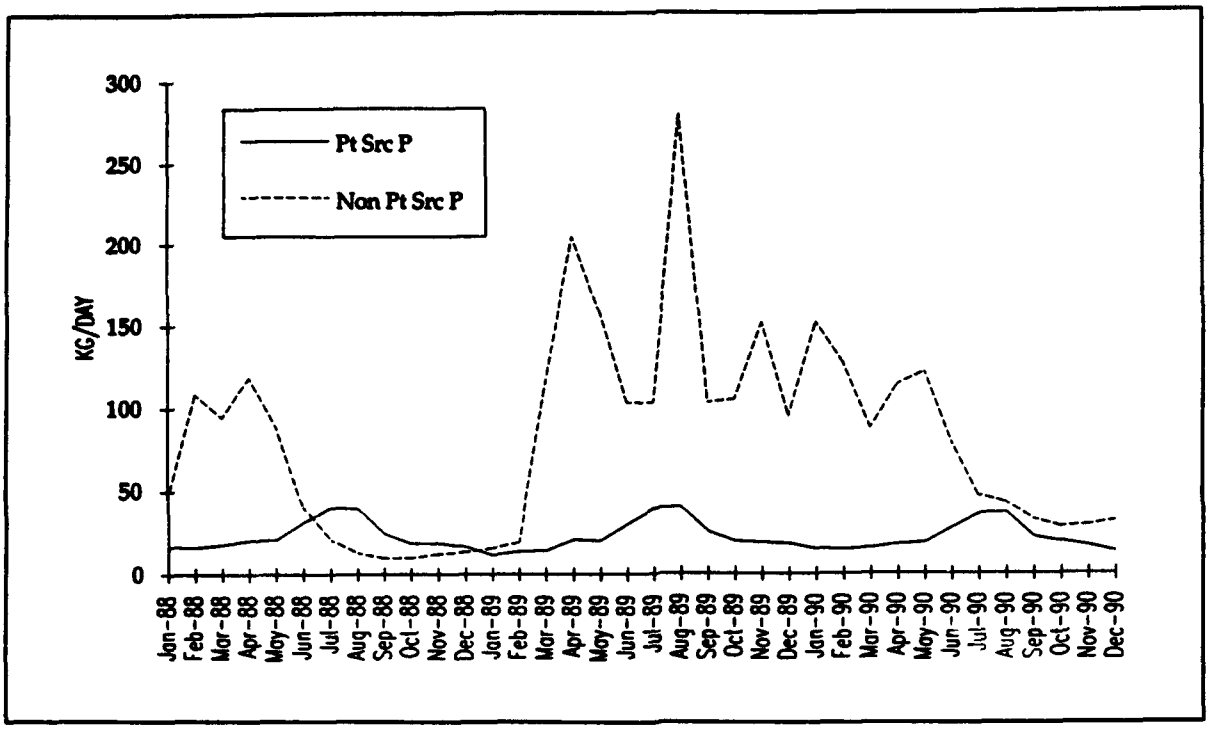

Figure 3-19. Time series of point-source and distributed phosphorus loads

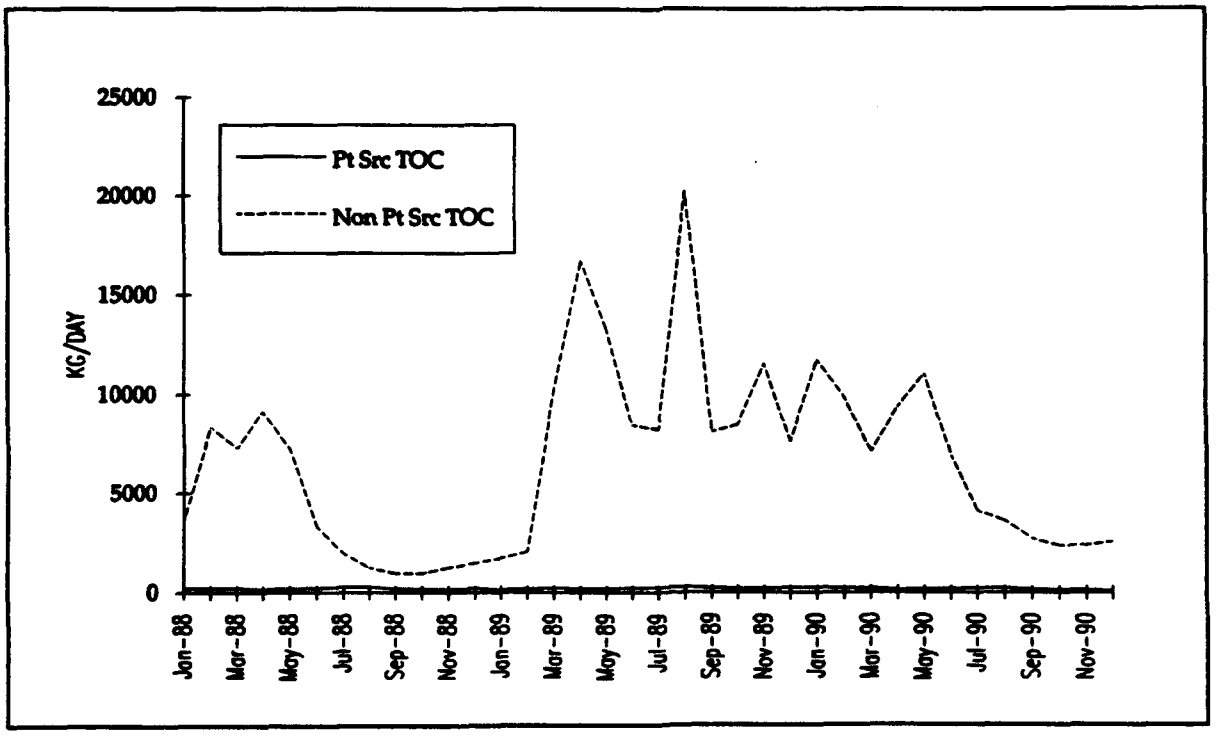

Figure 3-20. Time series of point-source and distributed total organic carbon loads

Table 3-8
Comparison of Loads

Nitrogen	1988 kg day^{-1}	Dry kg day^{-1}	1989 kg day^{-1}	Wet kg day^{-1}	1990 kg day^{-1}	Normal kg day^{-1}
Point Sources	209	634	204	634	166	634
Distributed Loads	1300	1091	2683	3240	2017	2186
Atmospheric	765	171	765	342	765	174
Other	0	515	0	515	0	515
Total	2275	2410	3652	4730	2948	3509
Phosphorus	**1988**	**Dry**	**1989**	**Wet**	**1990**	**Normal**
Point Sources	24	72	23	72	21	72
Distributed Loads	48	52	121	159	74	104
Atmospheric	0	11	0	21	0	16
Other	0	14	0	14	0	14
Total	72	149	144	267	96	206

Current estimates of total phosphorus loads are less than previous estimates for all loading categories. The sum of all current loads is half the previous estimate. Differences in distributed loads are small relative to the uncertainty in the load estimates. Differences in point-source and atmospheric loading likely occur due to the availability to us of additional, contemporary data. As with nitrogen, phosphorus loads from sources considered by Ritter, primarily septic tanks, were omitted in this study.

Chapter IV: Description of the Hydrodynamic Model

The numerical hydrodynamic model CH3D (Curvilinear Hydrodynamics in Three Dimensions) was used to provide detailed hydrodynamic flow field information as input to the water quality model. The basic model was developed by Sheng (1986) but was modified extensively in its application to the Chesapeake Bay study (Johnson et al. 1991). These modifications include implementing different basic numerical formulations of the governing equations as well as substantial recoding to obtain a more computationally efficient model. Physical processes impacting circulation which can be modeled include tide, wind, river inflow, and the effect of the earth's rotation (i.e., Coriolis effect).

A key attribute of CH3D is its ability to define a basin in a boundary-fitted coordinate system, allowing grid coordinate lines to conform with irregular coastal features, such as a shoreline or navigation channel. The solution algorithm employs an external-internal mode-splitting technique. In the external mode, finite difference approximations of the vertically-integrated Navier-Stokes equations are solved, yielding water surface elevations and depth-averaged x- and y-directed unit flow rates. This information is then processed in the internal mode to determine the x-, y-, and z-directed velocity distributions through the water column. Because the Indian River-Rehoboth Bay model application is a two-dimensional, depth-averaged (i.e., external) mode application, the internal mode is not discussed in this chapter.

This chapter describes the governing equations used in CH3D and the formulation of bottom and surface shear stress terms as well as the Coriolis effect. The process of transforming and non-dimensionalizing the governing equations is discussed and finite-difference approximations of the governing equations are presented.

Governing Equations

The hydrodynamic equations used in CH3D are derived from the classical Navier-Stokes equations formulated in a Cartesian coordinate system

(Figure 4-1). Assuming that the vertical water accelerations are small in comparison with the gravitational acceleration (i.e., hydrostatic pressure conditions exist) and that the fluid is homogeneous and incompressible, the depth-averaged approximation yields the following in-plan, two-dimensional form of the governing equations:

x-Momentum

$$\frac{\partial U}{\partial t} + \frac{\partial}{\partial x}\left(\frac{UU}{H}\right) + \frac{\partial}{\partial y}\left(\frac{UV}{H}\right) + gH\frac{\partial S}{\partial x} - fV - \frac{\tau_{sx}}{\rho} + \frac{\tau_{Bx}}{\rho} + A_H\left(\frac{\partial^2 U}{\partial x^2} + \frac{\partial^2 U}{\partial y^2}\right) + \frac{1}{\rho}\frac{\partial p}{\partial x} = 0 \quad (1)$$

y-Momentum

$$\frac{\partial V}{\partial t} + \frac{\partial}{\partial x}\left(\frac{UV}{H}\right) + \frac{\partial}{\partial y}\left(\frac{VV}{H}\right) + gH\frac{\partial S}{\partial y} + fU - \frac{\tau_{sy}}{\rho} + \frac{\tau_{By}}{\rho} + A_H\left(\frac{\partial^2 V}{\partial x^2} + \frac{\partial^2 V}{\partial y^2}\right) + \frac{1}{\rho}\frac{\partial p}{\partial y} = 0 \quad (2)$$

Continuity

$$\frac{\partial S}{\partial t} + \frac{\partial U}{\partial x} + \frac{\partial V}{\partial y} = 0 \quad (3)$$

where

x, y, t = independent space and time variables

U, V = unit flow rate components in the x- and y-directions, respectively

H = total water depth $(h+S)$

S = water surface displacement measured relative to an arbitrary datum

h = static water depth measured from the same datum

g = gravitational acceleration

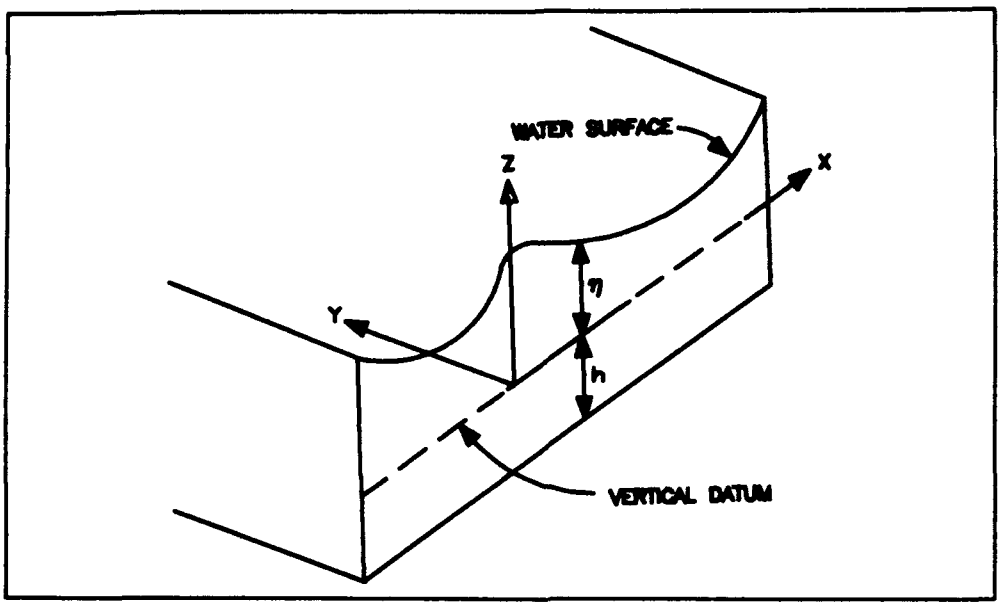

Figure 4-1. Cartesian coordinate system definition sketch

f = Coriolis parameter

τ_{sx}, τ_{sy} = surface shear stress in the x- and y-directions, respectively

τ_{Bx}, τ_{By} = bottom shear stress in the x- and y-directions, respectively

ρ = water density (assumed to be constant)

A_H = generalized dispersion coefficient

p = pressure

Bottom Shear Stress Formulation

CH3D uses the following quadratic expression to represent the bottom shear stress in the x-momentum equation:

$$\tau_{Bx} = \frac{g}{C_z^2 H^2}\sqrt{U^2 + V^2}\, U \qquad (4)$$

where

C_z = Chezy's resistance factor

A similar expression is used for τ_{By} in the y-momentum equation.

Rather than specifying the Chezy resistance factor, Manning's n, which is independent of depth, is input to the model. These coefficients are related through the following equation:

$$C_z = \frac{H^{1/6}}{n} \tag{5}$$

In addition, CH3D has an option for designating Manning's n as a function of depth to specify changes in bottom roughness at different water depths.

Surface Shear Stress Formulation

The surface shear stress τ_s is formulated as:

$$\tau_s = \rho_a C_D |W| W \tag{6}$$

where ρ_a is the air density, W is the wind velocity, and C_D is a dimensionless wind drag coefficient. CH3D uses the wind drag formulation presented in Garratt (1977):

$$C_D = \frac{(0.75 + 0.067\omega)}{1000} \tag{7}$$

where ω is the wind speed. This formulation requires wind speeds specified in units of meters per second. An upper limit of 3.0×10^{-3} is applied to this coefficient. Thus, for wind speeds greater than 65 knots, a constant drag coefficient is applied.

Coriolis Effect

Although it is not a true force, the Coriolis effect accounts for the apparent deflection in a fluid's trajectory that is induced by the rotation of the Earth. The Coriolis parameter f is expressed as:

$$f = 2\nu \sin\lambda \tag{8}$$

where v is the angular speed of the Earth's rotation (7.292 x 10^{-5} rad/sec) and λ is the latitude of the study area (38 deg 36.5 min).

Non-Dimensionalization of Governing Equations

The dimensionless form of the governing equations are used to facilitate relative magnitude comparisons of the various terms in the governing equations and to minimize the effects of round-off errors during computations. The following dimensionless variables are used:

$$(u^*, v^*, w^*) = (u, v, wX_r/Z_r)/U_r$$

$$(x^*, y^*, z^*) = (x, y, zX_r/Z_r)/X_r$$

$$(\tau_x^*, \tau_y^*) = (\tau_x^w, \tau_y^w)/\rho_o f Z_r U_r$$

$$t^* = tf$$

$$S^* = gS/fU_rX_r = S/S_r$$

$$A_H^* = A_H/A_{Hr}$$

$$K_H^* = K_H/K_{Hr}$$

These definitions yield the following dimensionless parameters in the governing equations:

Froude Number:	$F_r = U_r/(gZ_r)^{1/2}$
Rossby Number:	$R_o = U_r/fX_r$
Densimetric Froude Number:	$Fr_D = F_r / \sqrt{\varepsilon}$

where

$$\varepsilon = (\rho_r - \rho_o)/\rho_o$$

U_r, ρ_r, X_r, Z_r, A_{Hr}, and K_{Hr} are arbitrary reference values of the velocity, density, length, depth, dispersion, and diffusion.

Using the dimensionless variables (asterisks have been dropped) and the parameters previously defined, the vertically integrated equations constituting the external mode are:

ξ-Momentum

$$\frac{\partial U}{\partial t} + R_o\left[\frac{\partial}{\partial x}\left(\frac{UU}{H}\right) + \frac{\partial}{\partial y}\left(\frac{UV}{H}\right)\right] + H\frac{\partial S}{\partial x}$$

$$- V - \tau_{sx} + R_o\tau_{bx} + E_H\left[\frac{\partial}{\partial x}\left(A_H\frac{\partial U}{\partial x}\right) + \frac{\partial}{\partial y}\left(A_H\frac{\partial U}{\partial y}\right)\right] \qquad (9)$$

$$+ \frac{R_o}{Fr_D^2}\frac{H^2}{2}\frac{\partial \rho}{\partial x} = 0$$

η-Momentum

$$\frac{\partial V}{\partial t} + R_o\left[\frac{\partial}{\partial x}\left(\frac{UV}{H}\right) + \frac{\partial}{\partial y}\left(\frac{VV}{H}\right)\right] + H\frac{\partial S}{\partial y}$$

$$+ U - \tau_{sy} + R_o\tau_{by} + E_H\left[\frac{\partial}{\partial x}\left(A_H\frac{\partial V}{\partial x}\right) + \frac{\partial}{\partial y}\left(A_H\frac{\partial V}{\partial y}\right)\right] \qquad (10)$$

$$+ \frac{R_o}{Fr_D^2}\frac{H^2}{2}\frac{\partial \rho}{\partial y} = 0$$

Continuity

$$\frac{\partial S}{\partial t} + \beta\left(\frac{\partial U}{\partial x} + \frac{\partial V}{\partial y}\right) = 0 \qquad (11)$$

where

$$\beta = gZrlf^2X_r^2 \equiv (R_o/F_r)^2$$

Transformation of Governing Equations

The governing equations contained in CH3D were developed in a non-orthogonal curvilinear coordinate system. This system, however, necessitates the transformation of the governing equations into a non-orthogonal curvilinear or boundary-fitted coordinate system (ξ,η). Both independent (e.g., *x*, *y*) and dependent variables (e.g., *U*, *V*) in the governing equations are

transformed into the (ξ,η) curvilinear system. CH3D employs contravariant components (as opposed to covariant components) in the transformation of the governing equations, therefore velocities are defined perpendicular to a cell face, as opposed to parallel to a cell face.

The flow rate components in physical space (i.e., $U(i)$ and $V(j)$) are related to the contravariant components (i.e., U^i, V^i, U^j, V^j) by the following equations:

$$U(i) = \frac{g_{11}}{|g|} U^i + \frac{g_{12}}{|g|} V^i \tag{12}$$

$$V(j) = \frac{g_{21}}{|g|} U^j + \frac{g_{22}}{|g|} V^j \tag{13}$$

where g_{ij} is the metric tensor defined as:

$$g_{ij} = \begin{bmatrix} x_\xi^2 + y_\xi^2 & x_\xi x_\eta + y_\xi y_\eta \\ x_\eta x_\xi + y_\eta y_\xi & x_\eta^2 + y_\eta^2 \end{bmatrix} \tag{14}$$

or

$$g_{ij} = \begin{bmatrix} g_{11} & g_{12} \\ g_{21} & g_{22} \end{bmatrix} \tag{15}$$

and $|g|$ is the determinant of the metric tensor g_{ij}:

$$|g| = g_{11}g_{22} - g_{12}g_{21} \tag{16}$$

Whereas scalar quantities in the physical plane are identical in the transformed plane, all spatial derivatives containing these terms must be transformed. The surface slope terms are transformed as follows:

$$\frac{\partial S}{\partial x} = g^{11}\frac{\partial S}{\partial \xi} + g^{12}\frac{\partial S}{\partial \eta} \tag{17}$$

$$\frac{\partial S}{\partial y} = g^{21}\frac{\partial S}{\partial \xi} + g^{22}\frac{\partial S}{\partial \eta} \tag{18}$$

where g^{ij} are inverse metric tensor components:

$$g^{ij} = \frac{1}{|g|}\begin{bmatrix} x_\eta^2 + y_\eta^2 & -(x_\eta x_\xi + y_\eta y_\xi) \\ -(x_\xi x_\eta + y_\xi y_\eta) & x_\xi^2 + y_\xi^2 \end{bmatrix} = \frac{1}{|g|}\begin{bmatrix} g_{22} & -g_{21} \\ -g_{12} & g_{11} \end{bmatrix} \tag{19}$$

or

$$g^{ij} = \begin{bmatrix} g^{11} & g^{12} \\ g^{21} & g^{22} \end{bmatrix} \tag{20}$$

The transformed governing equations developed by Sheng (1986) are as follows. The inertial and diffusion terms in contravariant coordinates are quite lengthy and thus are omitted in this report. However, these terms are presented in Johnson et al. (1991).

<u>ξ-Momentum</u>

$$\frac{\partial U}{\partial t} + R_o Inertia^* + H\left(g^{11}\frac{\partial S}{\partial \xi} + g^{12}\frac{\partial S}{\partial \eta}\right) - \frac{g_{12}}{|g_u|}U$$

$$-\frac{g_{22}}{|g_u|}\bar{V} - \tau_{s\xi} + \frac{R_o g(g_{11}U^2 + 2g_{12}U\bar{V} + g_{22}\bar{V}^2)^{1/2}}{C_z^2 H^2}U \tag{21}$$

$$+E_H Diffusion^* + \frac{R_o H^2}{Fr_D^2\ 2}\left(g^{11}\frac{\partial p}{\partial \xi} + g^{12}\frac{\partial p}{\partial \eta}\right)U = 0$$

η-Momentum

$$\frac{\partial V}{\partial t} + R_o Inertia^* + H\left(g^{21}\frac{\partial S}{\partial \xi} + g^{22}\frac{\partial S}{\partial \eta}\right) + \frac{g_{11}}{|g_v|}\bar{\bar{U}}$$

$$\frac{g_{12}}{|g_v|}V - \tau_{s\eta} + R_o g\frac{(g_{11}\bar{\bar{U}}^2 + 2g_{12}\bar{\bar{U}}V + g_{22}V^2)^{1/2}}{C_z^2 H^2}V \qquad (22)$$

$$+ E_H Diffusion^* + \frac{R_o}{Fr_D^2}\frac{H^2}{2}\left(g^{21}\frac{\partial \rho}{\partial \xi} + g^{22}\frac{\partial \rho}{\partial \eta}\right) = 0$$

Continuity

$$\frac{\partial S}{\partial t} + \beta\frac{1}{|g_s|}\frac{\partial}{\partial \xi}\left(|g_u|U\right) + \beta\frac{1}{|g_s|}\frac{\partial}{\partial \eta}\left(|g_v|V\right) = 0 \qquad (23)$$

where

U,V = contravariant unit flow rate components in the transformed plane (superscripts have been dropped for convenience)

$|g_s|$ = determinant of the metric tensor, $|g|$, at an *S*-point (Figure 4-2)

$|g_u|, |g_v|$ = determinant of the metric tensor, $|g|$, at a U-face and V-face, respectively

$\bar{\bar{U}}$ = average x-direction unit flow rate at a *V*-face

$\bar{\bar{V}}$ = average y-direction unit flow rate at a *U*-face

Finite Difference Approximations of Governing Equations

The finite difference approximations to the governing equations are based on a Eulerian system where the velocities and water surface fluctuations are computed at discrete locations within the flow field. A network of grid cells is used to define the parameter locations. A representative grid cell in computational space (ξ,η) is shown in Figure 2. In this staggered grid, the water surface fluctuation is defined at the cell center (i,j), ξ-direction unit

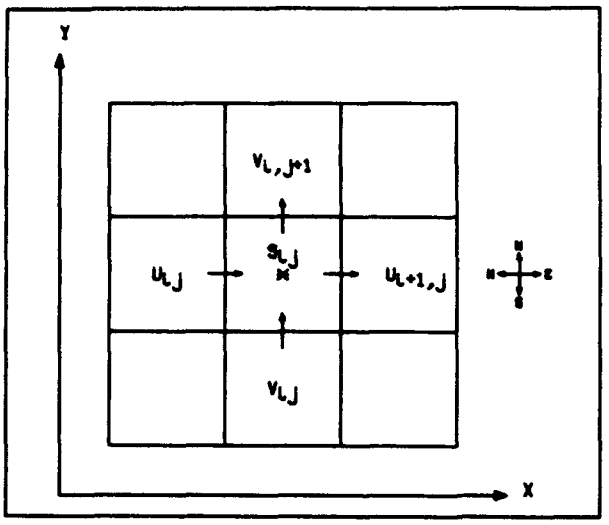

flow rates (U) are defined at the "west" (i,j) and "east" ($i+1,j$) cell faces, and the η-direction unit flow rates (V) are computed at the "south" (i,j) and "north" ($i,j+1$) cell faces. The finite difference approximations of the governing equations follow. Note that the continuity equation is split into two parts. The sum of these equations is the original continuity equation.

Figure 4-2. Variable positions

<u>ξ-Momentum</u>

$$\frac{U^*_{i,j} - U^n_{i,j}}{\Delta t} + R_o J^n_{i,j} + \theta Hg^{11}\left(\frac{S^*_{i,j} - S^*_{i-1,j}}{\Delta\xi}\right) + (1-\theta)Hg^{11}\left(\frac{S^n_{i,j} - S^n_{i-1,j}}{\Delta\xi}\right)$$

$$+ Hg^{12}\left(\frac{S^n_{i-1/2,j+1/2} - S^n_{i-1/2,j-1/2}}{\Delta\eta}\right) - \frac{g_{12}}{|g_u|}U^n_{i,j} - \frac{g_{22}}{|g_u|}\bar{V} - \tau_{s\xi} \qquad (24)$$

$$+ \theta R_o(FRC)U^*_{i,j} + (1-\theta)R_o(FRC)U^n_{i,j} + E_H D^n_{i,j} + \theta\frac{R_o}{Fr_D^2}\frac{H^2}{2}g^{11}\left(\frac{\rho^*_{i,j} - \rho^*_{i-1,j}}{\Delta\xi}\right)$$

$$(1-\theta)\frac{R_o}{Fr_D^2}\frac{H^2}{2}g^{11}\left(\frac{\rho^n_{i,j} - \rho^n_{i-1,j}}{\Delta\xi}\right) + \frac{R_o}{Fr_D^2}\frac{H^2}{2}g^{12}\left(\frac{\rho^n_{i-1/2,j+1/2} - \rho^n_{i-1/2,j-1/2}}{\Delta\eta}\right) = 0$$

where

n = previous time level

$*$ = intermediate time level

$n+1$ = solve for this time level

θ = weighting factor between successive time levels

I = inertia

FRC = friction

D = dispersion

η-Momentum

$$\frac{V_{ij}^{n+1}-V_{ij}^{n}}{\Delta t} + R_o I_{ij}^{n} + Hg^{21}\left(\frac{S_{i+1/2,j-1/2}^{n}-S_{i-1/2,j-1/2}^{n}}{\Delta\xi}\right) + \theta Hg^{22}\left(\frac{S_{ij}^{n+1}-S_{ij-1}^{n+1}}{\Delta\eta}\right)$$

$$+ (1-\theta)Hg^{22}\left(\frac{S_{ij}^{n}-S_{ij-1}^{n}}{\Delta\eta}\right) + \frac{g_{11}}{|g_v|}\bar{U} + \frac{g_{12}}{|g_v|}V_{i,j}^{n} - \tau_{s\eta} + \theta R_o(FRC)V_{ij}^{n+1}$$

$$+ (1-\theta)R_o(FRC)V_{i,j}^{n} + E_H D_{i,j}^{n} + \frac{R_o}{Fr_D^{\,2}}\frac{H^2}{2}g^{21}\left(\frac{\rho_{i+1/2,j-1/2}^{n}-\rho_{i-1/2,j-1/2}^{n}}{\Delta\xi}\right)$$

$$+ \theta\frac{R_o}{Fr_D^{\,2}}\frac{H^2}{2}g^{22}\left(\frac{\rho_{ij}^{n+1}-\rho_{ij-1}^{n+1}}{\Delta\eta}\right) + (1-\theta)\frac{R_o}{Fr_D^{\,2}}\frac{H^2}{2}g^{22}\left(\frac{\rho_{i,j}^{n}-\rho_{ij-1}^{n}}{\Delta\eta}\right) \quad (25)$$

ξ-Continuity

$$\frac{S_{ij}^{*}-S_{ij}^{n}}{\Delta t} + \beta\theta\frac{|g_u|}{|g_s|}\left(\frac{U_{i+1,j}^{*}-U_{ij}^{*}}{\Delta\xi}\right) + \beta(1-\theta)\frac{|g_u|}{|g_s|}\left(\frac{U_{i+1,j}^{n}-U_{ij}^{n}}{\Delta\xi}\right)$$

$$+ \beta\frac{|g_v|}{|g_s|}\left(\frac{V_{ij+1}^{n}-V_{ij}^{n}}{\Delta\eta}\right) = 0 \quad (26)$$

η-Continuity

$$\frac{S_{ij}^{n+1} - S_{ij}^{*}}{\Delta t} + \beta\theta\frac{|g_v|}{|g_s|}\left(\frac{V_{ij+1}^{n+1} - V_{ij}^{n+1}}{\Delta\eta}\right) + \beta(1-\theta)\frac{|g_v|}{|g_s|}\left(\frac{V_{ij+1}^{n} - V_{ij}^{n}}{\Delta\eta}\right)$$

$$- \beta\frac{|g_v|}{|g_s|}\left(\frac{V_{ij+1}^{n} - V_{ij}^{n}}{\Delta\eta}\right) = 0 \qquad (27)$$

The computational procedure used in CH3D is based on an Alternating Direction Implicit scheme (Roache 1976). Using this method, the ξ- and η-momentum equations are solved separately, and each calculation in time is made in two stages. In the first stage, the ξ-continuity and ξ-momentum equations are solved along each row of the grid to progress from time level *n* to an intermediate time level *, indicated by superscript *. The ξ-direction unit flow rate components and water surface fluctuations are solved implicitly, and the η-direction unit flow rate components are supplied from time level *n*. The ξ-direction unit flow rates from this step represent those at time level *n+1* , whereas the water surface fluctuations are only an approximation to those at time level *n+1*. The η-direction unit flow rate components remain at time level *n*. In the second stage, the η-continuity and η-momentum equations are solved along each column for the η-direction unit flow rates and the water surface fluctuations at time level *n+1*. ξ-direction unit flow rate components are supplied from the first stage calculations.

As shown in the finite difference approximations to the governing equations, a weighting factor θ is used to place the water surface slope and bottom friction terms between time levels *n* and *n+1*. When the weighting factor equals 0.0, these terms are evaluated at the previous time level *n* (explicit treatment), whereas when the weighting factor equals 1.0, they are evaluated at the new time level *n+1* (implicit treatment). Usually a value between 0.0 and 1.0 is used.

Chapter V: Hydrodynamic Model Application

In this chapter, the application of CH3D to the Indian River Bay-Rehoboth Bay system is described. A discussion of numerical grid development and the bathymetry used to represent the study area is given. The model calibration and validation procedure is presented, including a discussion of boundary forcing conditions used in the model and an analysis of model results.

Numerical Grid Development

CH3D uses a non-orthogonal, boundary-fitted grid to represent the limits of a study area. Using a boundary-fitted grid allows coordinate lines to conform to the irregular boundaries of land masses. In this way, the delineation between each bay and the surrounding land can be made. Similarly, the delineation between an island and the surrounding water can be made. Note that CH3D does not contain an adaptive gridding algorithm, therefore there is no means to allow for flooding and drying of low-lying areas. To maintain the appropriate water volume in the system, active cell volumes in low-lying areas were increased.

The boundary-conforming grid used for the Indian River Bay-Rehoboth Bay hydrodynamic study was constructed using program Eagle (Thompson 1985). The 73 x 68 cell grid generated by Eagle contains approximately 2000 active cells with cells concentrated through the inlet and Middle Island areas (Figure 5-1). Cell sizes through the inlet were approximately 30-m by 120-m in the north-south and east-west directions, respectively. Cell sizes near the Middle Island area were as small as 60-m by 120-m in the east-west and north-south directions, respectively. A 1988 hydrographic survey of the Indian River Bay-Rehoboth Bay system conducted by the U.S. Army Engineer District, Philadelphia provided the necessary bathymetric information. This information was translated to a depth in each grid cell by applying a 3-point linear interpolation scheme to the data. Depths in the dual bay system are generally less than 2 m mean low water (mlw).

Figure 5-1. Indian River-Rehoboth Bay grid

Model Calibration and Validation

The purpose of the calibration procedure is to insure that the model accurately predicts hydrodynamic conditions within a given study area. The accuracy of model results is greatly influenced by the accuracy of boundary forcing conditions, representation of the geometry of the study area (i.e. bathymetry and land/water interface), and to a lesser degree, the choice of certain "calibration" parameters (Mark et al. 1993). In the calibration procedure, these parameters are adjusted to obtain the best agreement between model results and measured field data. In essence, if the study area is accurately depicted with the numerical grid and the boundary conditions are correct, model results will be "in the ballpark" and the small adjustments to calibration parameters are a means of "fine-tuning" model results.

The purpose of the validation procedure is to confirm that the calibrated model can replicate hydrodynamic conditions independent of the conditions for which it was calibrated. In this procedure, the model is applied without any adjustment to the calibration parameters. A good comparison between model results and measured data in the validation process means that the model should accurately simulate hydrodynamics for other time periods.

The time periods selected for model calibration and validation for the Indian River Bay-Rehoboth Bay system were time periods when there was available field data for comparison to model results with sufficient length of record and sufficient spatial extent to cover the model domain. Another factor influencing the time periods selected was the fact that the hydrodynamic model results were used to supply flow conditions to the water-quality (WQ) model. Therefore, the hydrodynamic model should be tested over a time-span consistent with the transport of contaminants within this system. During a low flow time period, river discharges may lack sufficient momentum to flush contaminants from the system. During extreme events, large oscillations in the water surface and/or high river discharges can provide sufficient momentum to transport contaminants. Because of the importance of these factors, the model was calibrated and validated for a cycle of 7 days.

Calibration Overview

CH3D was calibrated for the Indian River Bay-Rehoboth Bay study area for the one-week time period 29 June - 5 July 1988. Both water surface elevation and velocity data were only available for this time period. Water surface elevation data were also available at all tide gauges from 1 October - 31 December 1988 and comparisons were made for one week during this time period (14 - 20 October 1988) as part of the validation process.

The open boundary in Indian River Inlet was driven with a time series of water surface elevation recorded by the tide gauge adjacent to the U.S. Coast Guard Station (T5 in Figure 2-1). The grid boundary location was selected to coincide with the gauge location. However, grid cells in this region are

approximately 120 m wide and therefore "precise" placement is considered to be within 60 m of the actual gauge location. In addition, the tide gauge is attached to a pier in the Coast Guard Boat Basin and is therefore somewhat sheltered. Because the influence of these factors is not known, water levels were not adjusted in phase or amplitude to account for these factors. As a consequence, water surface levels and velocities computed by the model may contain phase errors of several minutes.

Tide data were collected at the USCG Station at 15-minute intervals, however, water levels were supplied to the model at a 1-hr interval using a lowlow pass (LLP) filter on the recorded time series. Water levels were linearly-interpolated by the model for each time step between the 1-hr input values and were uniformly assigned to every cell on the open boundary. No water surface level gradient was imposed along this boundary.

Note that after completing the initial calibration procedure, a simulation was made using the original 15-min interval tidal data for the inlet boundary forcing function and the results were not altered significantly. Therefore, using the 1-hr filtered data was appropriate.

The time-history of wind speed and directions used in the model were recorded by the Delaware Power and Light (DPL) wind anemometer. These data were selected over wind data at the "old" USCG station because the DPL record was more complete. Short time periods missing from the DPL record were linearly-interpolated between recorded values. DPL data for 30 - 31 October 1988 were extremely high, which when used as input to the hydrodynamic model caused grid cells to become dry, thus leading to model instabilities. After consulting with DPL personnel, it was determined that these extremely high wind velocities were inappropriate and were adjusted to more reasonable estimates for that time period. Wind data were supplied to the model at 1-hr intervals and were linearly-interpolated for time steps between the 1-hr input values.

Discharge data were available from 1 January - 30 September 1988 for Vines Creek and Millsboro Pond (at the head of Indian River). Flows at remaining locations throughout the system (Figure 3-1) were estimated by the ratio technique described in Chapter 3. Estimation techniques were also used to complete the Vines Creek and Millsboro Pond datasets outside the period of record. Discharge data were provided by USGS as daily average flow rates, therefore model input consisted of one flow rate for each day of the simulation. Flow rates were updated at each time step of the simulation by linearly interpolating between daily values.

Data available for comparison with model results included:

1) a time series of water surface elevations recorded at each of the following USGS stations (Figure 2-1):

a) Vines (T1)
b) Potnets (T2)
c) Massey (T3)
d) Dewey (T4)

Water surface elevation data were collected at 15-minute intervals. Water level data collected at the USCG station were used to drive the inlet boundary condition and therefore could not be used for comparison to model results.

2) currents speeds without directions collected at four locations near Middle Island (CM1, CM2, CM3, and CM4 in Figure 2-1).

Calibration Conditions

The hydrodynamic model was used to simulate the year 1988 so that the WQ team could begin simulations with the water quality model. The actual calibration period, however, was only 153 hours (29 June 1500 - 5 July 2400). Data were available at all four tide gauges and current data were also collected for 25 hrs at the 4 velocity stations (30 June hr 0600 - 1 July hr 0700) during this time period. Data at the four tide gauges showed a variation in range from a low of 0.6 m at the Dewey gauge to a high of 1.1 m at the Vines Creek gauge. River discharge for the calibration time period was extremely low. The Millsboro Dam flow rate was 0.76-0.91 m^3/sec and the Vines Creek flow rate was less than 0.03 m^3/sec. Peak flow rates for 1988 were approximately 5.66 m^3/sec at Millsboro Dam and 2.83-4.25 m^3/sec at Vines Creek. Winds during the calibration period were 1.3-5.8 m/sec generally from a northerly direction.

Calibration Procedure

Calibration was achieved primarily through adjustments to the bottom friction coefficient, Manning's n. Initially a global bottom friction coefficient was specified throughout the grid and the model was run repeatedly with different global values (0.020-0.035) to determine an approximate value of n. The best global value was determined by comparing model predicted water surface elevations to measured water surface elevations at the four tide stations described previously. To achieve the more difficult task of replicating water velocities, the global bottom friction coefficient was refined and tested over a narrower range of values. In the last stage, Manning's n values were adjusted locally in shallow regions to account for increased friction drag in these areas. The best comparison between model results and measured data was achieved with a global Manning's n of 0.025. Shallower areas (less than .3 m) were assigned a friction value of 0.045.

Analysis of Calibration Results

Water Surface Elevation

The model accurately reproduced the amplitude of the water surface level time histories recorded at the Vines Creek, Potnets, Massey, and Dewey gauges, however, the model consistently leads the prototype data by 30 min at all gauges (Figures 5-2 through 5-5). The modeled tide travels too quickly from the inlet to the gauges. Scatter plots of predicted versus measured water surface levels show the typical elliptic shape indicative of a phase shift (Figures 5-6 through 5-9). The root-mean-square (rms) error at the Vines, Potnets, Massey, and Dewey gauges was computed to be 7.1, 8.3, 3.0, and 2.7 cm, respectively. A thorough search for the cause of this discrepancy led to many interesting possibilities.

First, water surface level data computed by the model is written to an output file at an interval of 30 minutes -- the exact phase discrepancy. Although this seemed to be a likely source for the discrepancy, it was not the cause in this case. The model was run with an output interval of 15 minutes, and the results were identical to the previous results. Another possibility for the discrepancy was data interpretation, i.e., a plotting error. Rather than plotting the results, the actual values produced by the model were evaluated and compared with the prototype values, and the discrepancy was real.

Interestingly, all four gauges are consistently out of phase with the prototype, regardless of their distance from the inlet. Therefore, the error lies either with the boundary condition imposed at the inlet or between the inlet boundary and the closest gauge (Massey (T3)). First the inlet boundary forcing function was investigated as the source for the discrepancy. The grid boundary location was specifically selected to coincide with the USCG station gauge location (T5). However, grid cells in this region are approximately 120 m wide and therefore "precise" placement is considered to be within 60 m of the actual gauge location. In addition, the tide gauge is attached to a pier in the Coast Guard Boat Basin and is therefore somewhat sheltered. The influence of these factors may contribute to the phase discrepancy observed in the water surface levels computed by the model, however, the contribution would be minor.

Tide data were collected at the USCG Station using a digital recorder with a 15-minute punch interval, however, water levels were supplied to the model at a 1-hr interval using a low-low pass (LLP) filter on the recorded time series. Water levels were linearly-interpolated by the model for each time step between the 1-hr input values and were uniformly assigned to every cell on the open boundary. Could the 1-hr interval between boundary forcing data be the cause for the phase lag? To investigate this, the model was rerun with an inlet boundary forcing interval of 15 minutes. The results were not altered significantly, therefore the 1-hour forcing interval was appropriate.

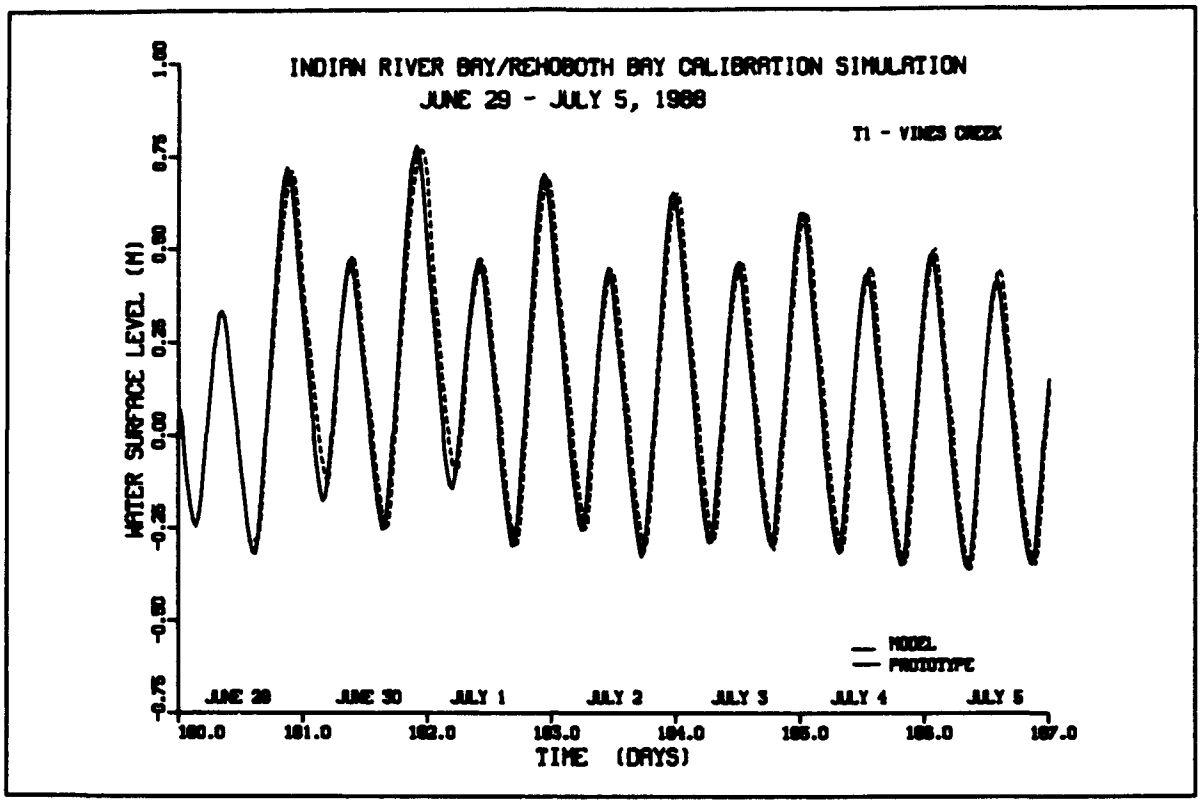

Figure 5-2. Tidal calibration at Vines Creek gauge

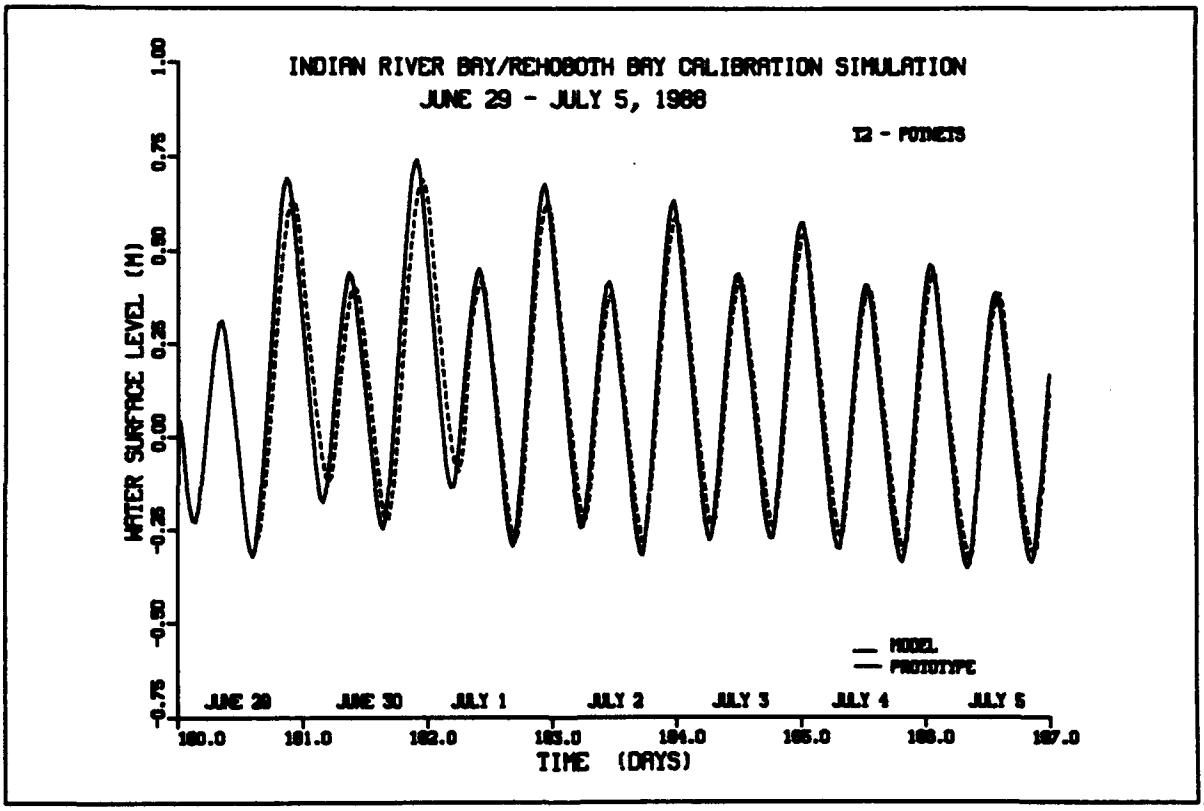

Figure 5-3. Tidal calibration at Potnets gauge

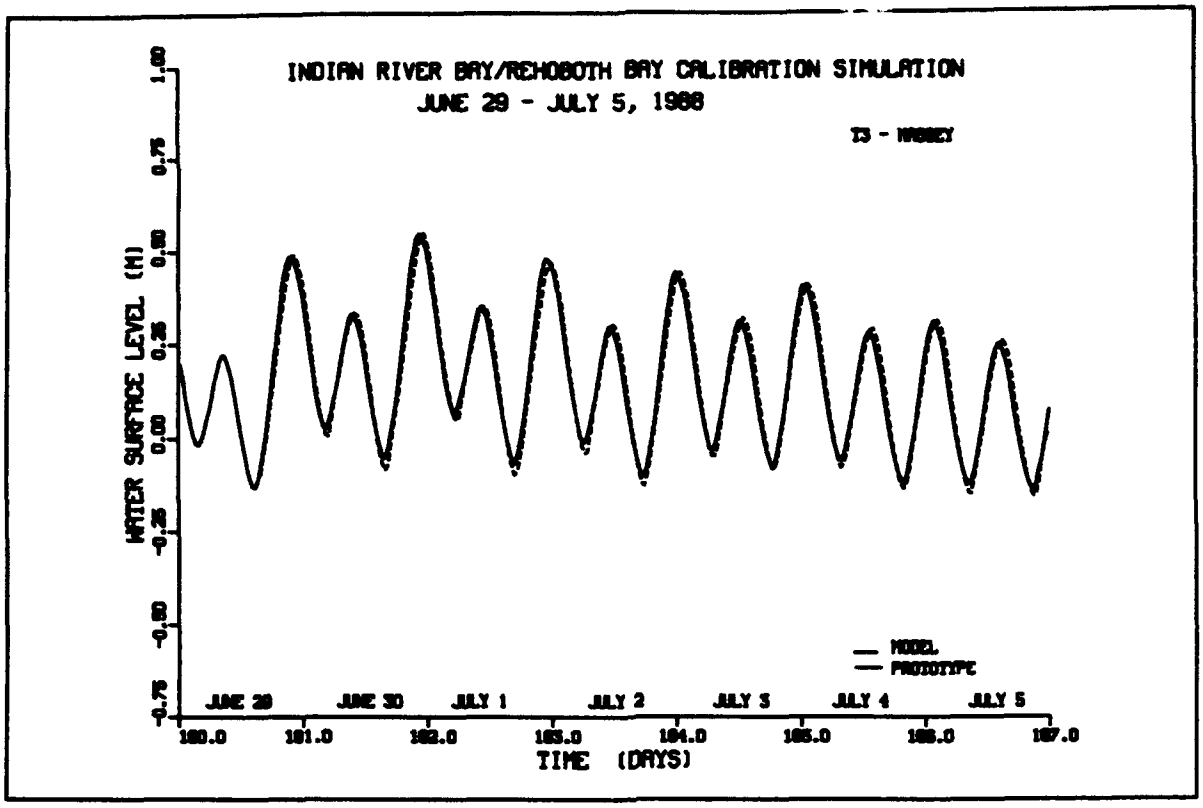

Figure 5-4. Tidal calibration at Massey's Ditch gauge

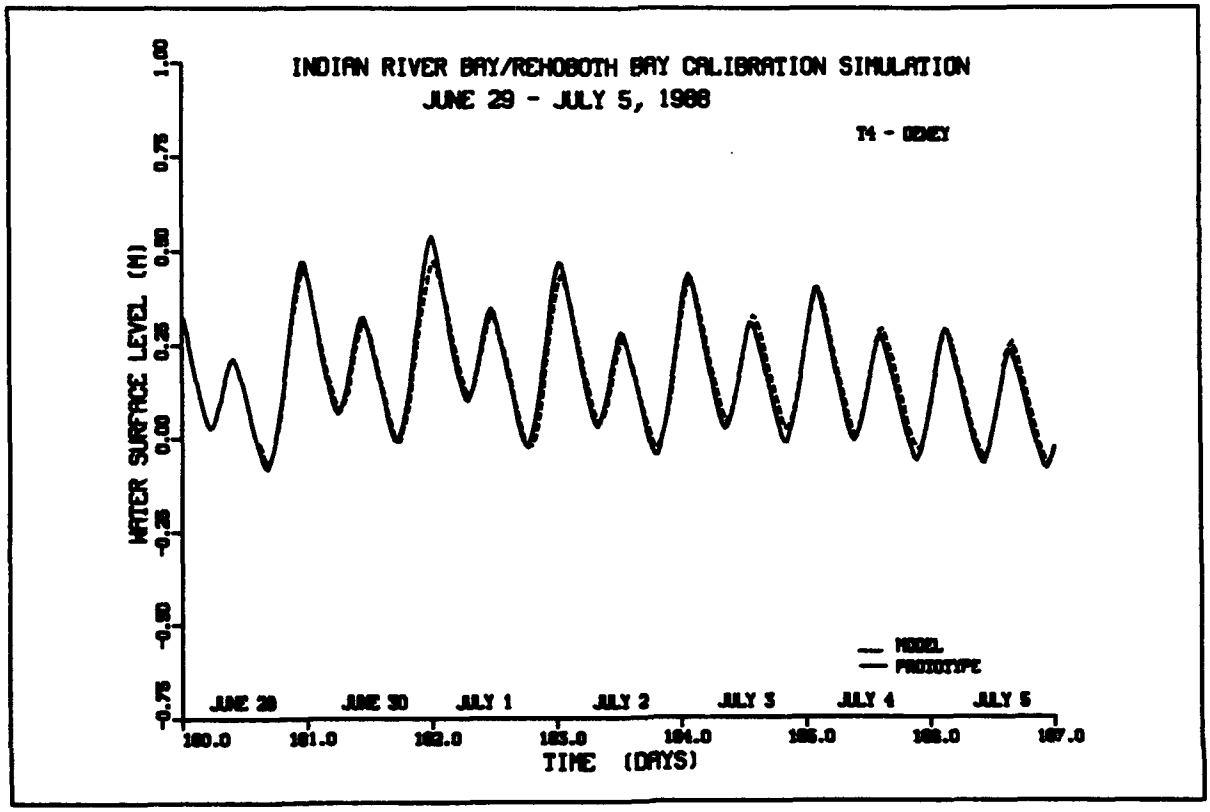

Figure 5-5. Tidal calibration at Dewey Beach gauge

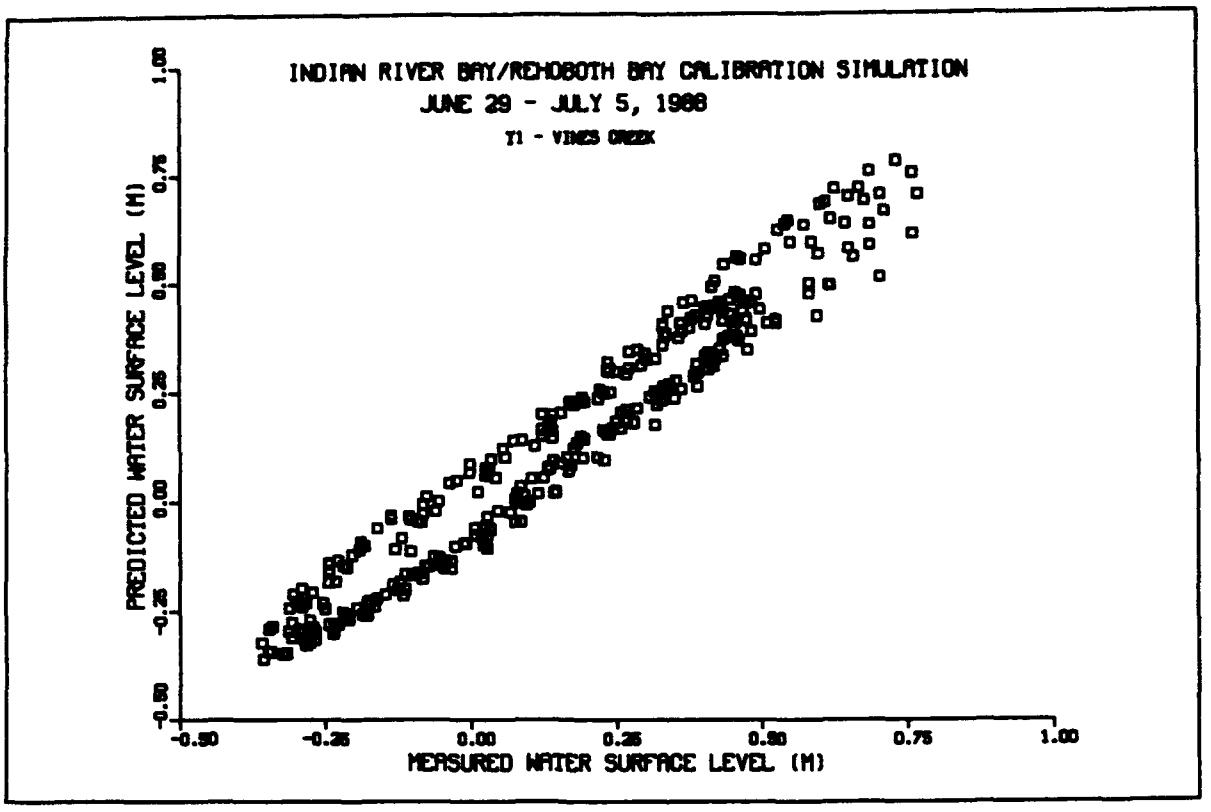

Figure 5-6. Scatter plot of tidal calibration at Vines Creek gauge

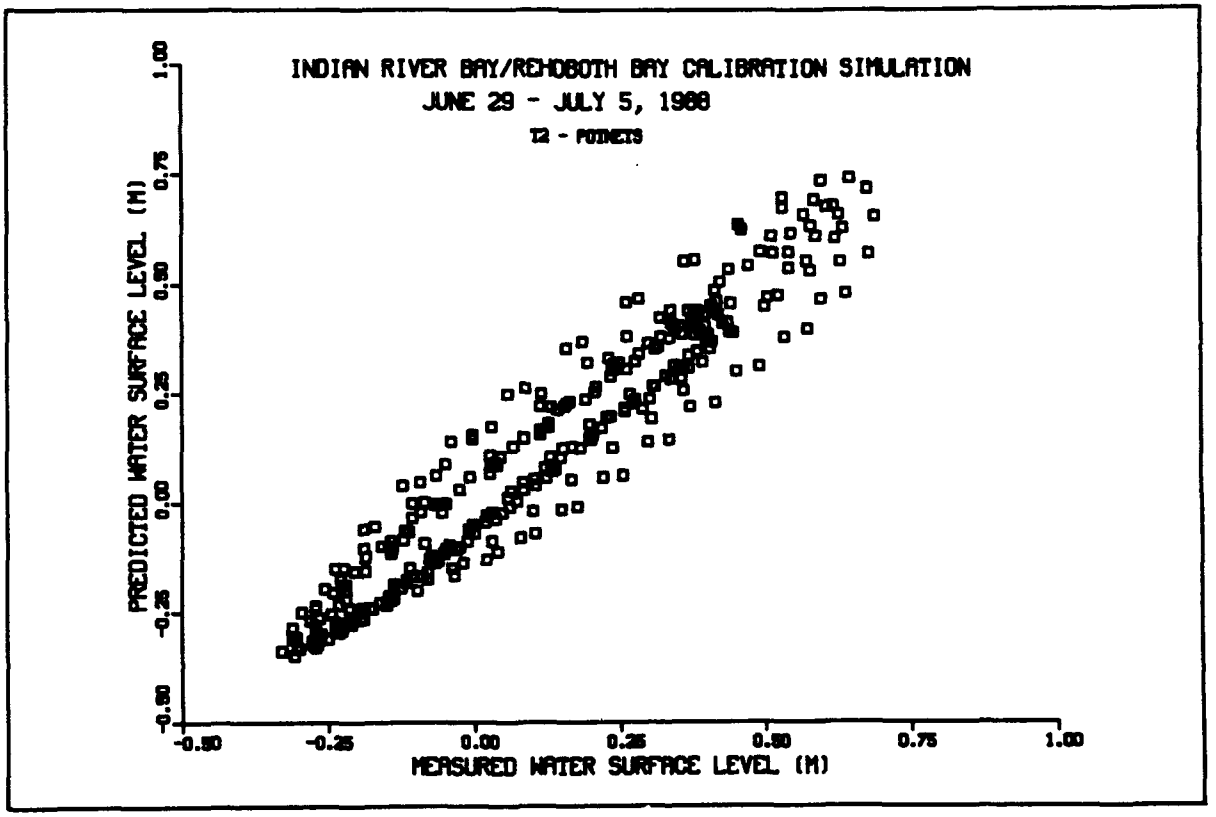

Figure 5-7. Scatter plot of tidal calibration at Potnets gauge

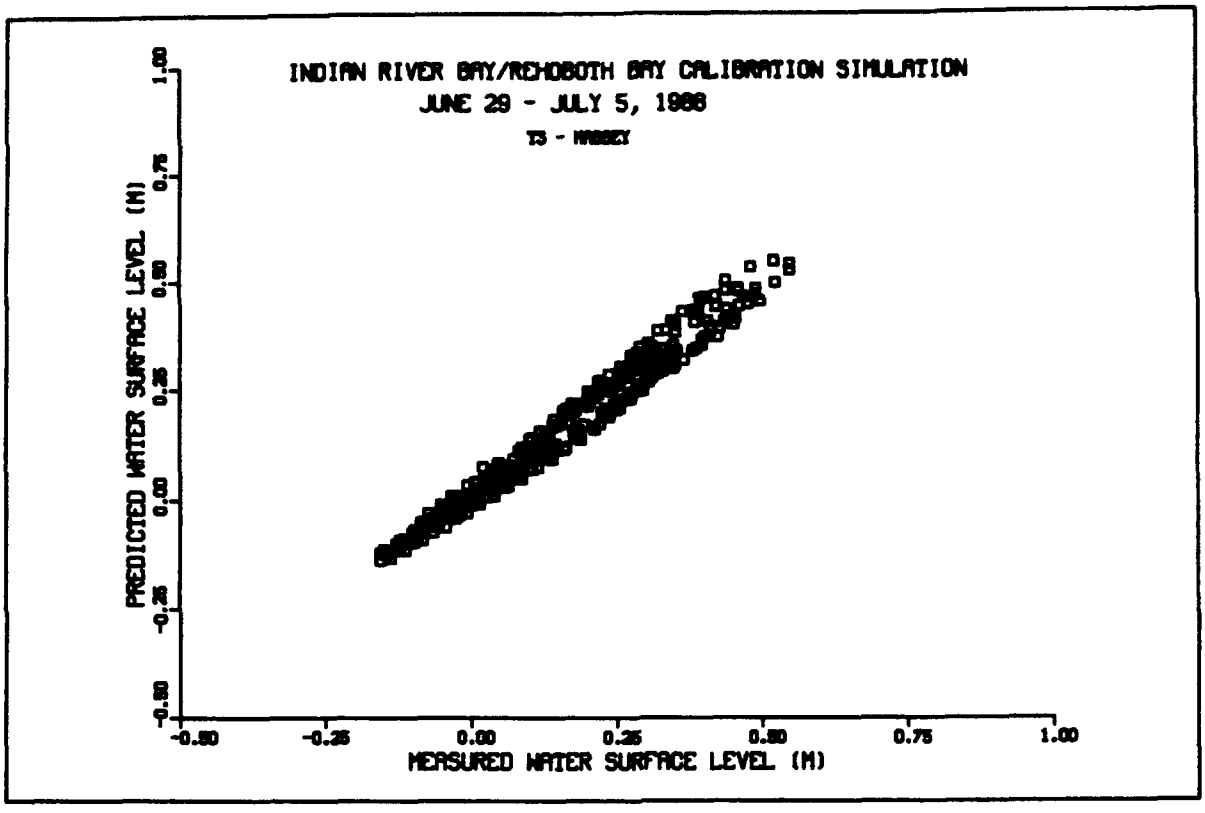

Figure 5-8. Scatter plot of tidal calibration at Massey's Ditch gauge

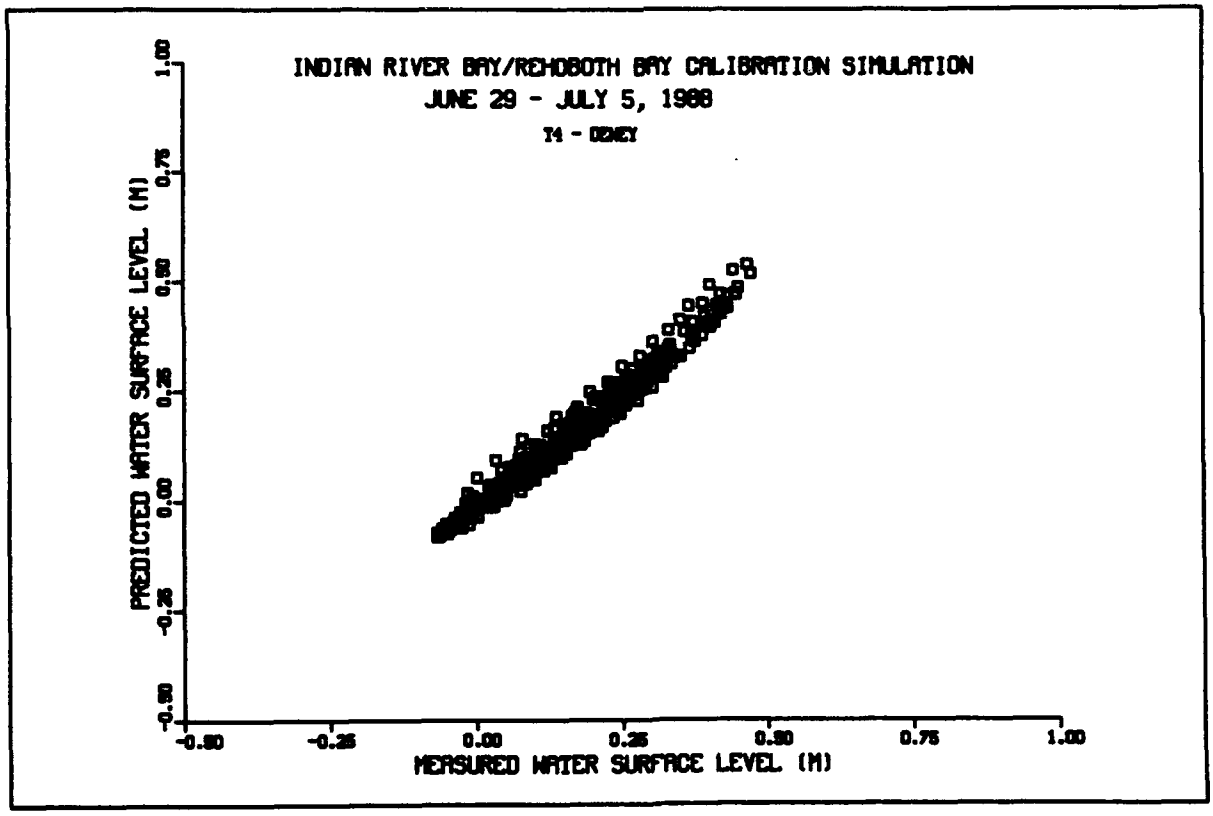

Figure 5-9. Scatter plot of tidal calibration at Dewey Beach gauge

The choice of a water surface level boundary condition was examined. Choosing to force the model at the inlet boundary with water surface elevation data was dictated by the considerable quantity of water surface level data available there. However, velocities through Indian River Inlet are significant (1.5-2.5 m/sec). If the model was forced with flow through the open boundary rather than a water level time series, the boundary condition would include the velocity head contribution. The relative contribution of elevation head and velocity head may not be computed correctly by merely specifying a water surface elevation boundary condition. This factor could have an impact on phasing of the tides. Therefore, it is concluded that the location of the inlet boundary precludes the model from simulating the large head loss through the inlet. The boundary condition applied across the inlet boundary does not include the velocity head contribution nor its interaction with the elevation head. These factors most probably caused the observed phasing discrepancy.

Regardless of the cause of the phase shift, it is insignificant from a water quality standpoint. By adjusting the boundary forcing function 30 minutes, the model results are in phase with the prototype data at all four gauges (Figures 5-10 through 5-13). In addition, the scatter plots of predicted versus measured water surface level lose their elliptic shape and show a linear relationship between model results and prototype data (Figures 5-14 through 5-17). The rms error at the Vines, Potnets, Massey, and Dewey gauges was reduced to 3.1, 4.3, 2.0, and 2.2 cm, respectively.

Velocity

Only 25 hours of velocity data were available for comparison with model results. All four velocity stations (CM1 through CM4) are in the vicinity of Middle Island (Figure 2-1). The model overpredicts the water velocity east of Middle Island (at CM1 and CM2), is fairly accurate west of Middle Island at CM3, and underpredicts flood velocities and overpredicts ebb velocities at CM4 (Figures 5-18 through 5-21).

Validation Conditions

CH3D was validated for the Indian River Bay-Rehoboth Bay study area for the one-week time period 14 - 20 October 1988. Water surface elevation data were available at the same four tide gauges referred to in the calibration, for the validation time period. A comparison of model results to these data was used to validate CH3D. Data at the four tide gauges showed a variation in range from a low of 0.6 m at Dewey gauge and a high of 1.1 m at the Vines gauge.

As in the calibration process, the open boundary at Indian River Inlet was driven with a time series of water surface elevation data recorded by the tide gauge adjacent to the USCG Station (T5 in Figure 2-1). Tide data were collected at the USCG Station at 15-minute intervals, however, water levels were

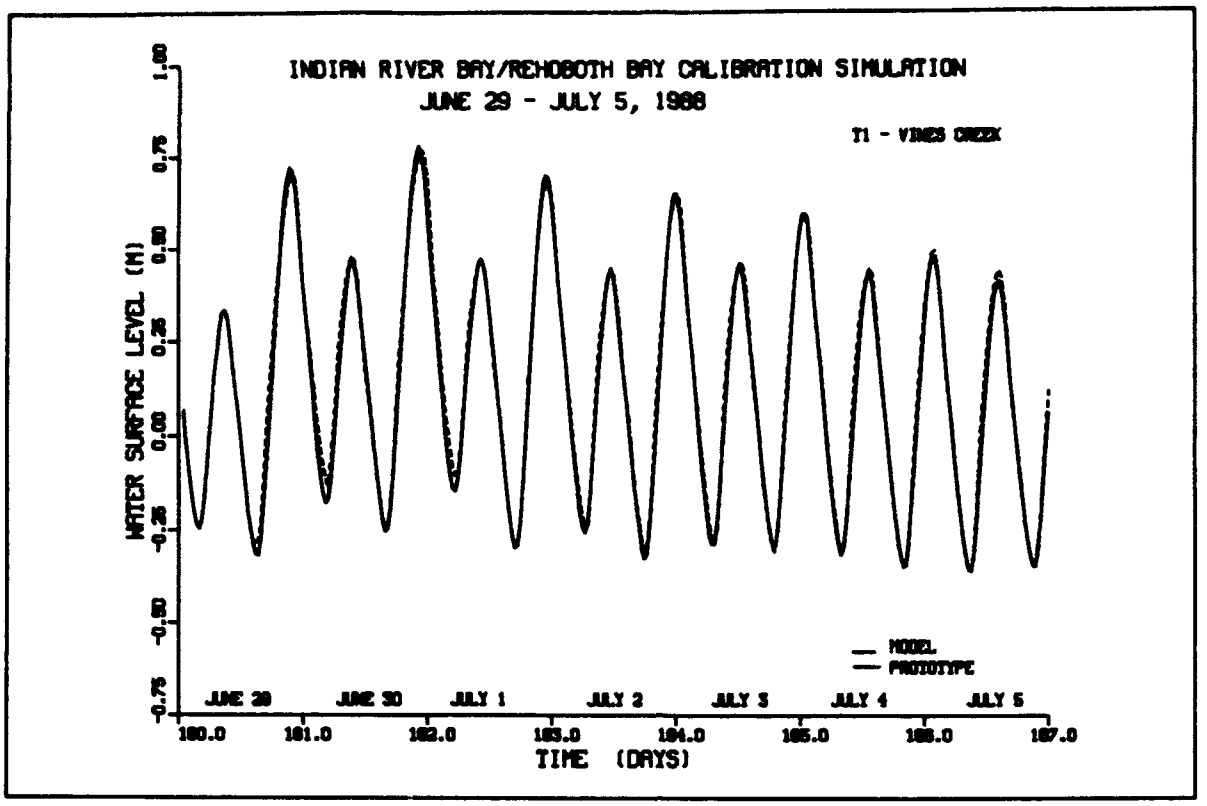

Figure 5-10. Tidal calibration at Vines Creek gauge

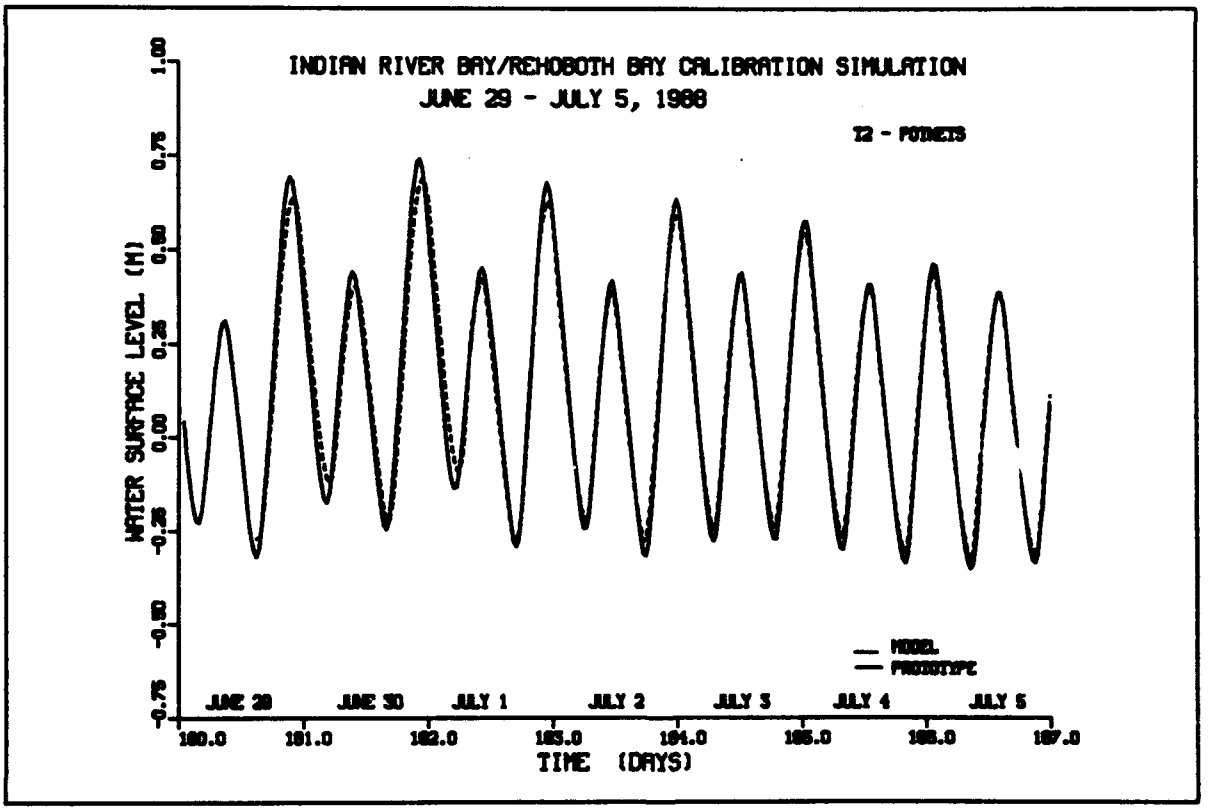

Figure 5-11. Tidal calibration at Potnets gauge

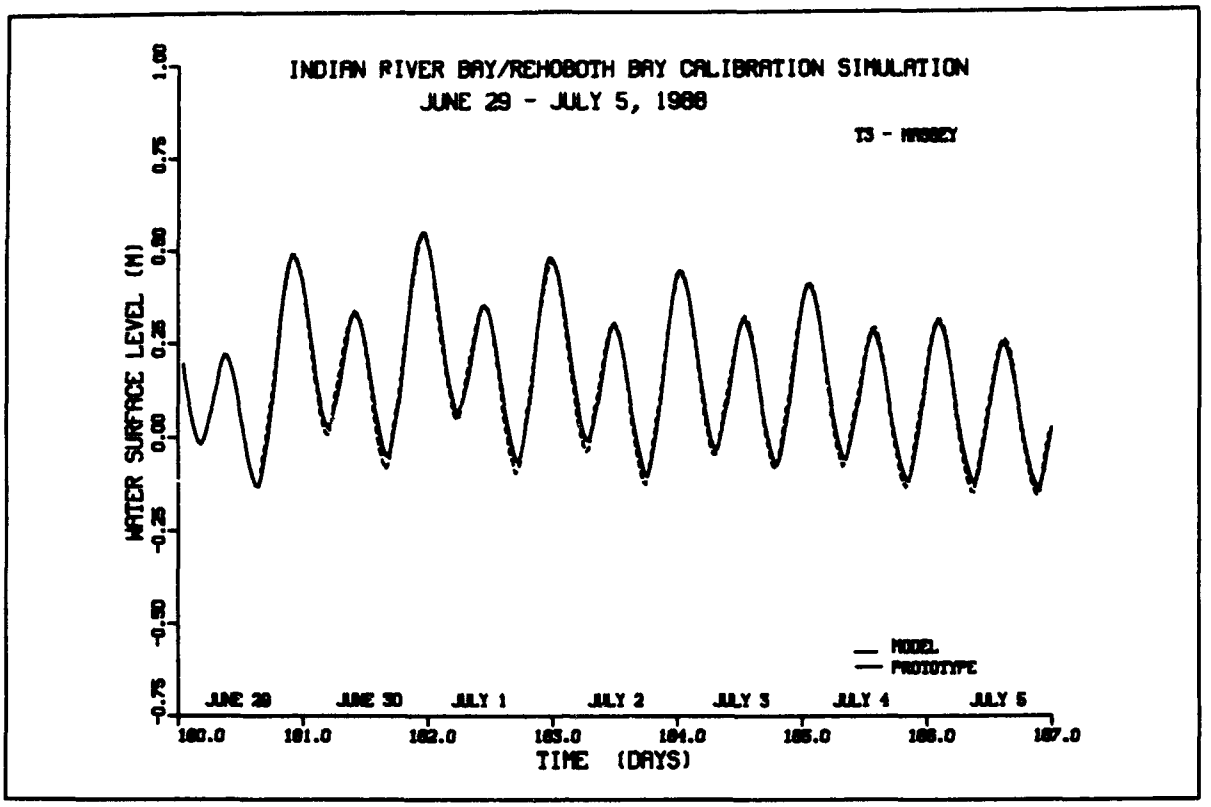

Figure 5-12. Tidal calibration at Massey's Ditch gauge

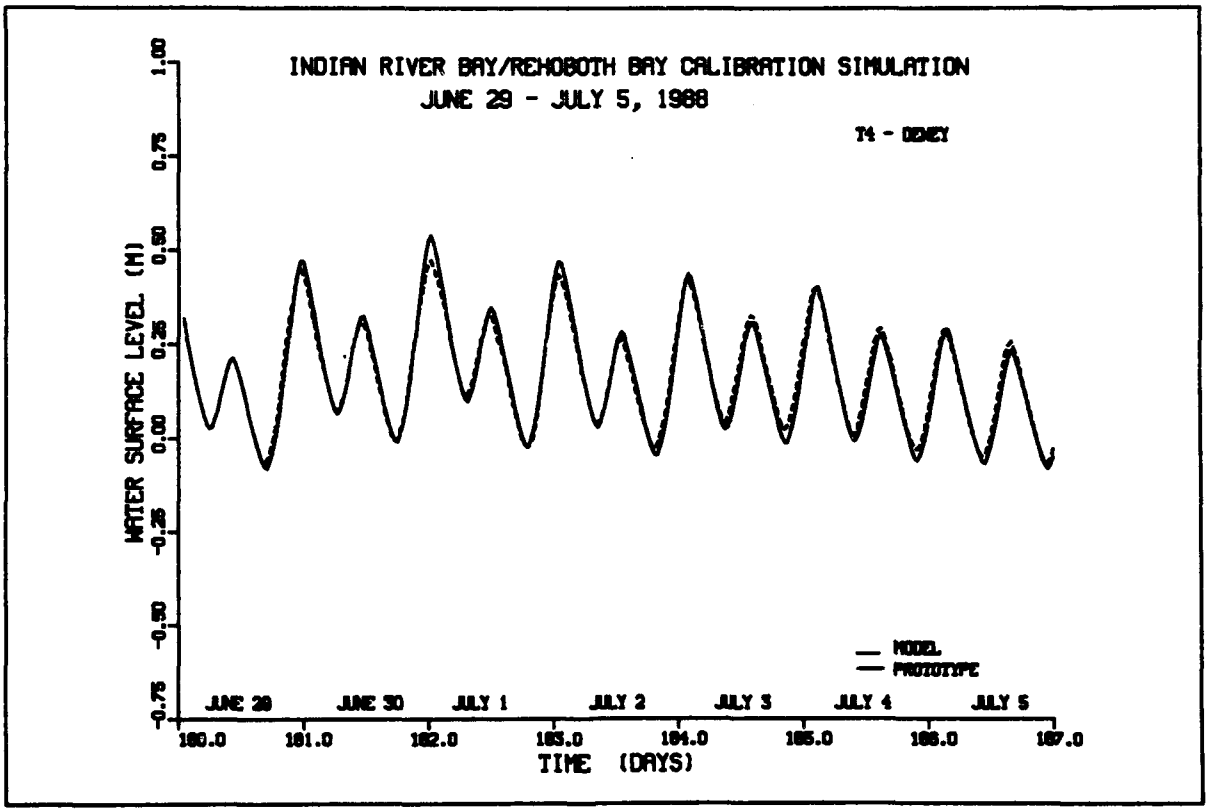

Figure 5-13. Tidal calibration at Dewey Beach gauge

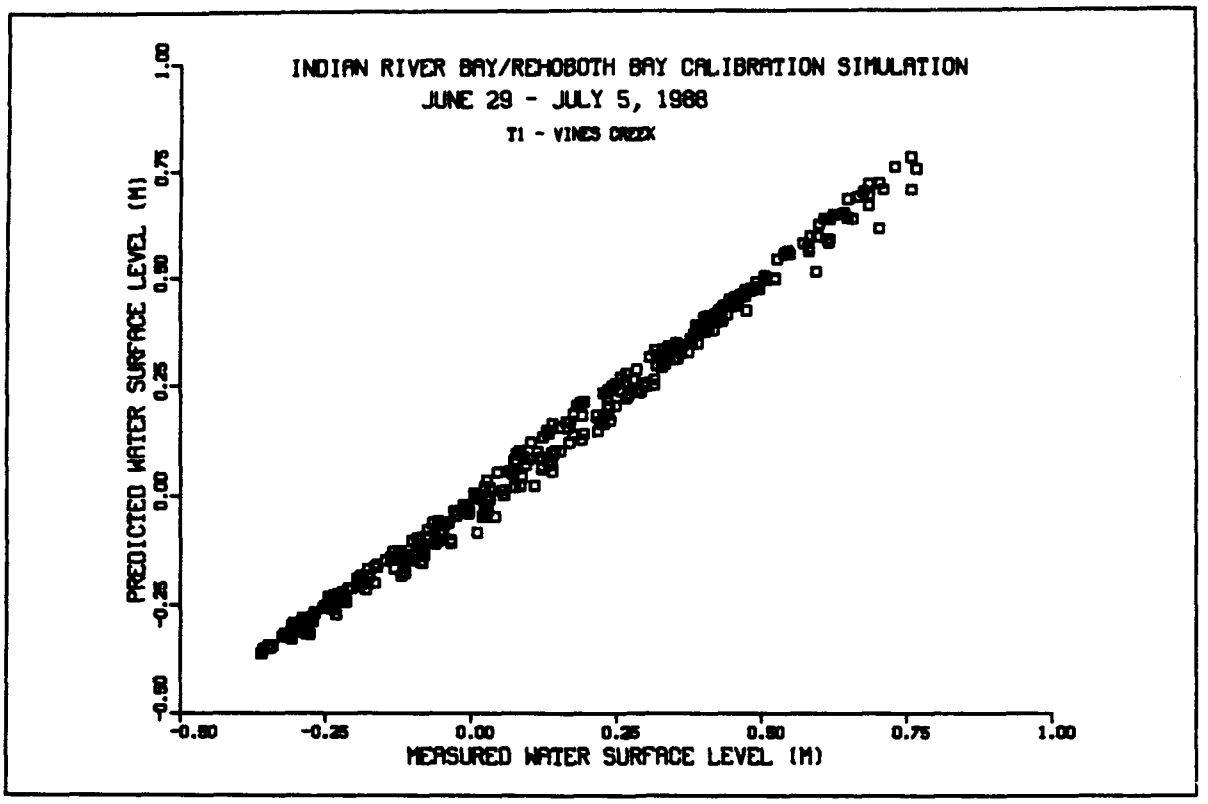

Figure 5-14. Scatter plot of tidal calibration at Vines Creek gauge

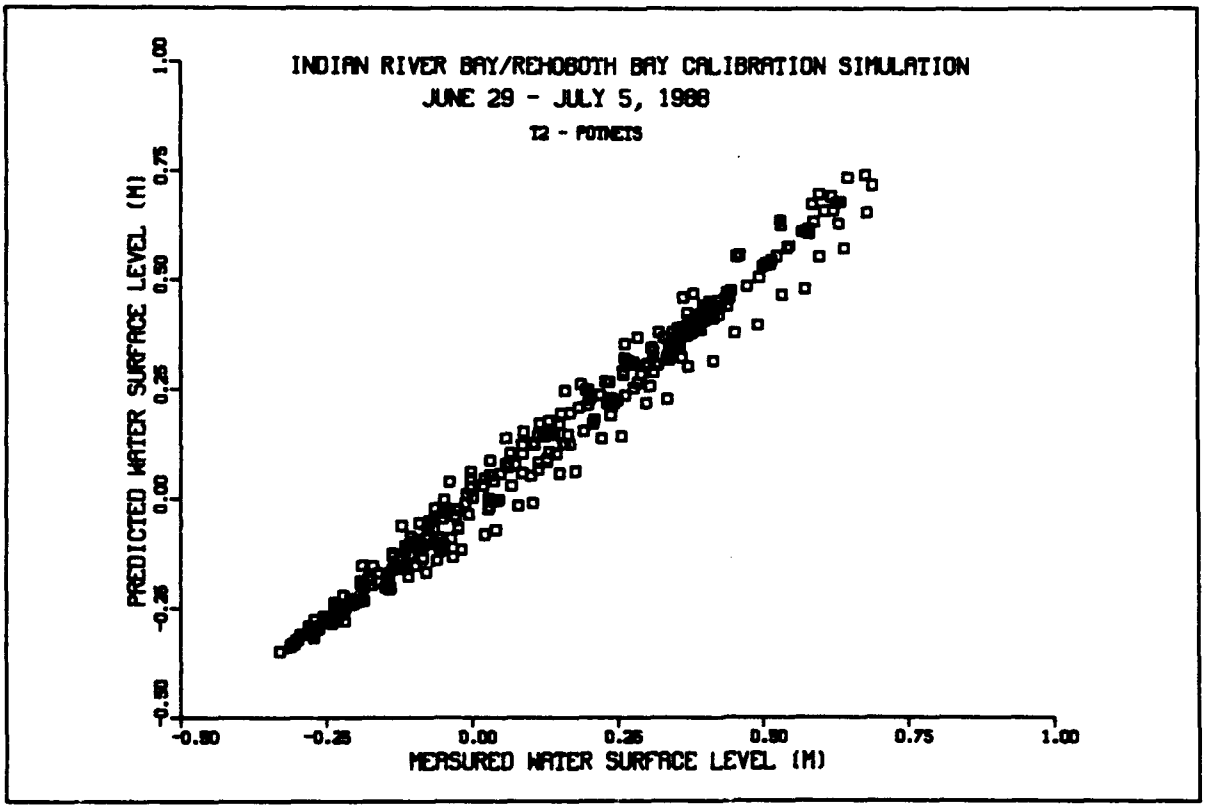

Figure 5-15. Scatter plot of tidal calibration at Potnets gauge

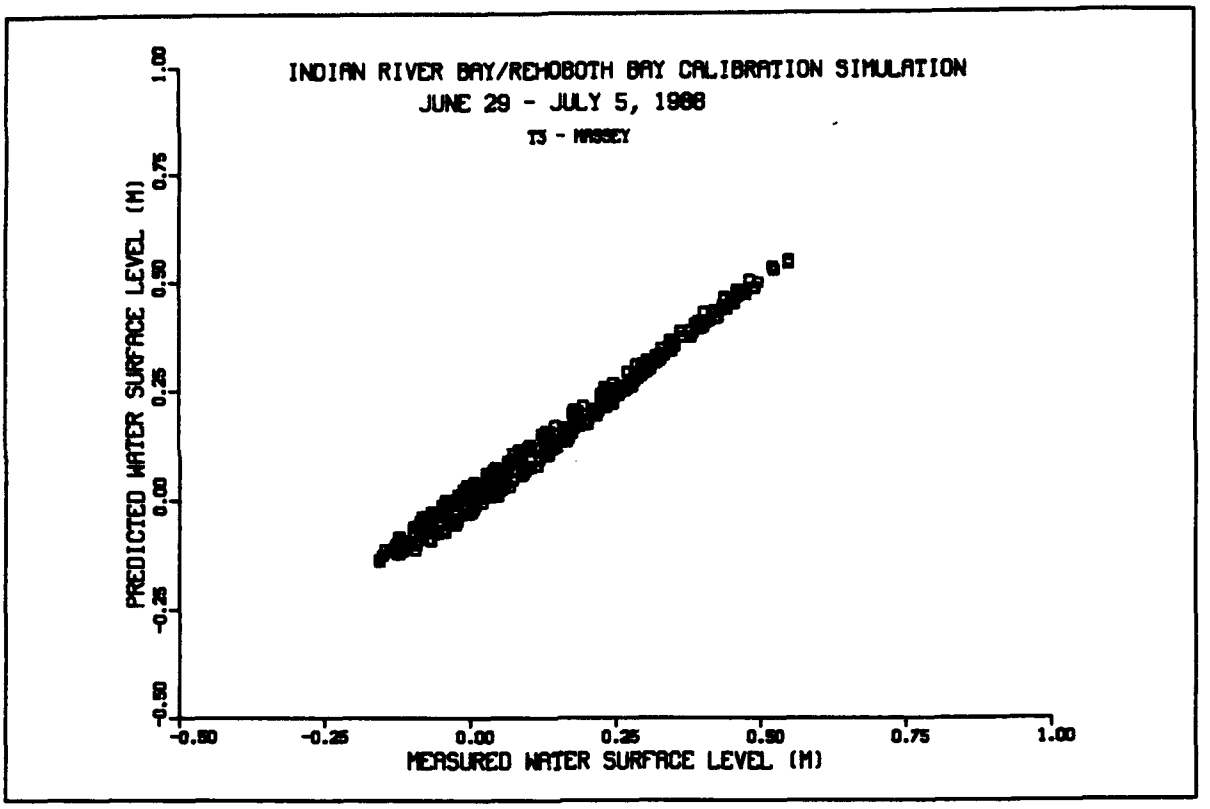

Figure 5-16. Scatter plot of tidal calibration at Massey's Ditch gauge

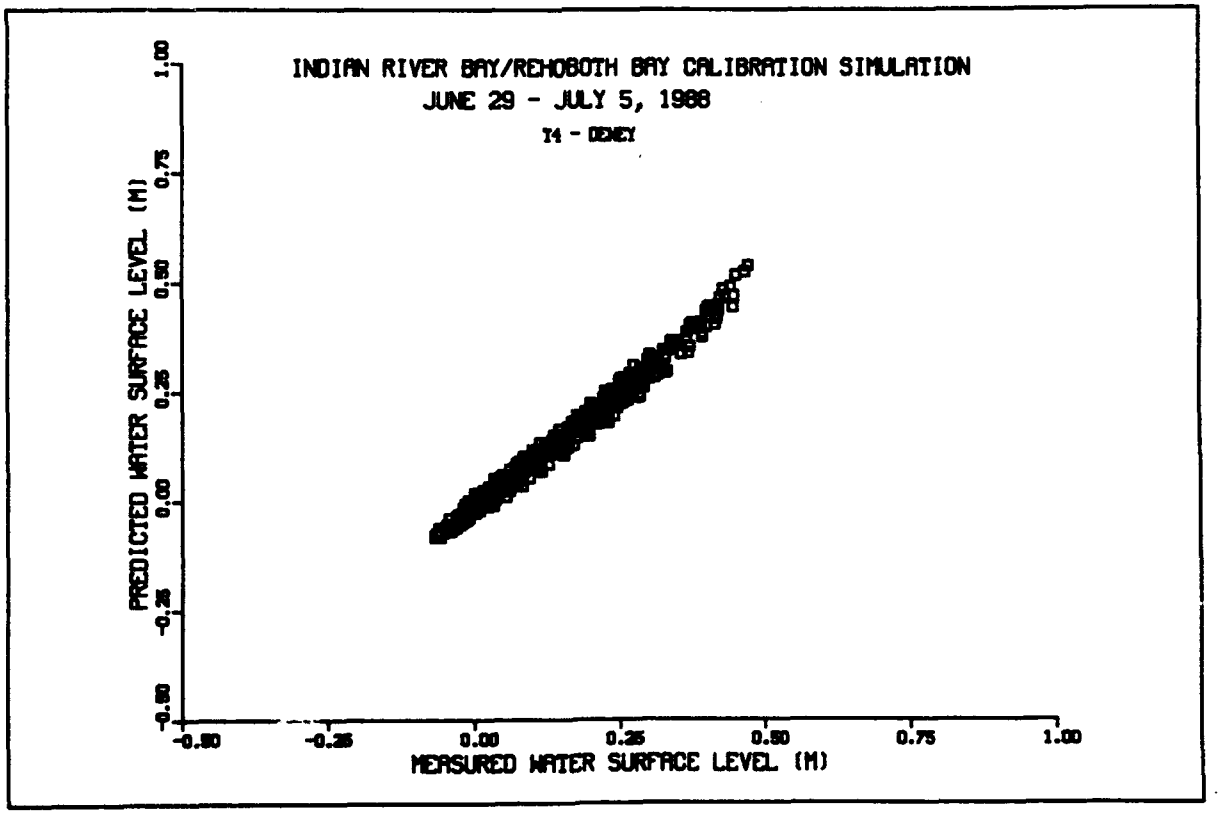

Figure 5-17. Scatter plot of tidal calibration at Dewey Beach gauge

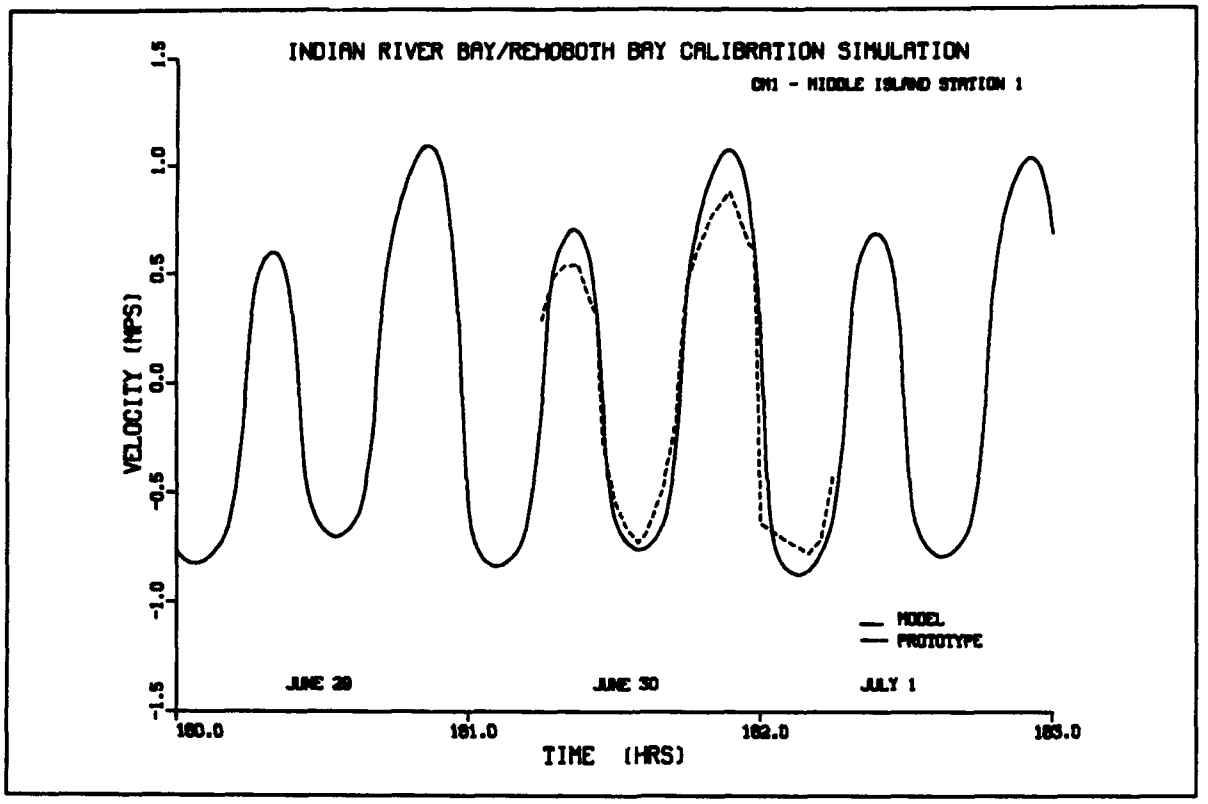

Figure 5-18. Velocity calibration at Middle Island Station 1

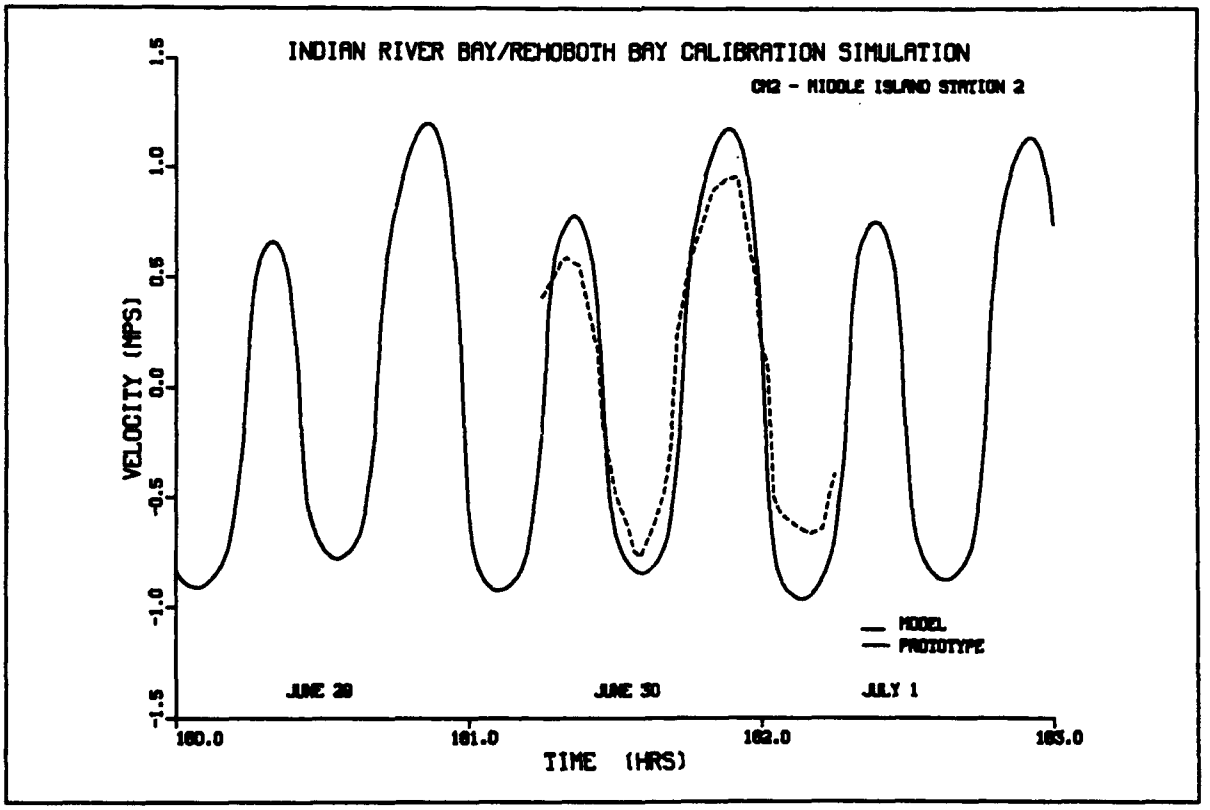

Figure 5-19. Velocity calibration at Middle Island Station 2

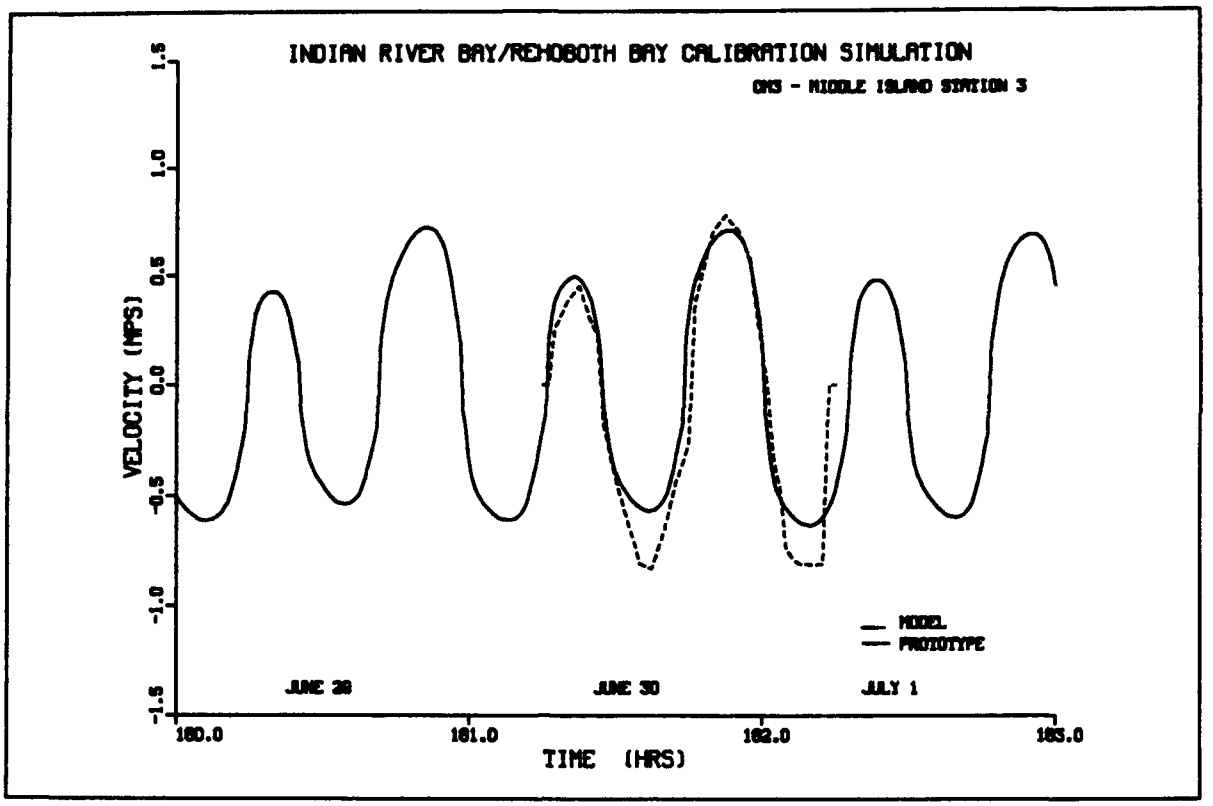

Figure 5-20. Velocity calibration at Middle Island Station 3

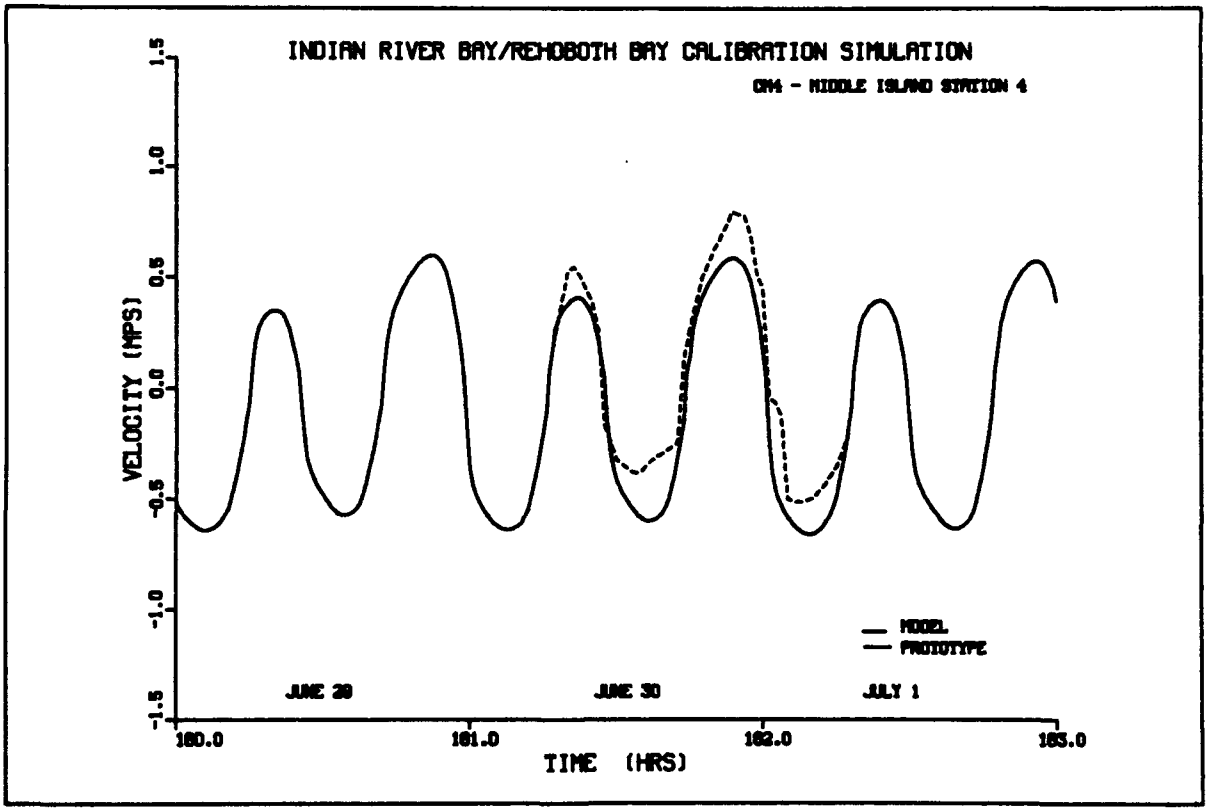

Figure 5-21. Velocity calibration at Middle Island Station 4

supplied to the model at a 1-hr interval using a low-low pass filter on the recorded time series. Water levels were linearly interpolated by the model for each time step between the 1-hr input values and were uniformly assigned to every cell on the open boundary. No water surface level gradient was imposed along this boundary.

Wind speed and direction used in the model were recorded by the Delaware Power and Light (DPL) anemometer. Wind data were supplied to the model at 1-hr intervals and were linearly interpolated for time steps between the 1-hr input values.

Discharge data for the validation period were estimated by ratio techniques described in Chapter 3. River discharge rates for the validation period were average. The Millsboro Dam flow rate was approximately 1.66 m^3/sec and the Vines Creek flow rate was approximately 0.05 m^3/sec. Discharge data were estimated as daily average flow rates, therefore model input consisted of one flow rate for each day of the simulation. Flow rates were updated at each time step of the simulation by linearly interpolating between daily values.

Analysis of Validation Results

As with the calibration period, the model accurately reproduces the amplitude of the water surface level time histories recorded at the Vines Creek, Potnets, Massey, and Dewey gauges, however, the model consistently leads the prototype by 30 minutes at all gauges (Figures 5-22 through 5-25). Scatter plots of predicted versus measured water surface levels show the typical elliptic shape indicative of a phase shift (Figures 5-26 through 5-29). The rms error at the Vines, Potnets, Massey, and Dewey gauges was computed to be 5.1, 4.3, 3.3, and 1.8 cm respectively. Again, the cause of the discrepancy is most likely due to the boundary condition applied across the inlet boundary.

By adjusting the boundary forcing function 30 minutes, the model results are in phase with the prototype data at all four gauges (Figures 5-30 through 5-33). In addition, the scatter plots of predicted versus measured water surface level lose their elliptic shape and show a linear relationship between model results and prototype data (Figures 5-34 through 5-37). The rms error at the Vines, Potnets, and Massey gauges was reduced to 2.8, 2.0, and 1.3 cm, respectively. The rms error at the Dewey gauge did not change.

Salinity Overview

The salinity distribution in the Indian River Bay-Rehoboth Bay system varies both spatially and temporally. Indian River Bay has a strong salinity gradient in the east-west direction, whereas Rehoboth Bay responds fairly uniformly (Figure 5-38). The strong east-west salinity gradient in Indian River Bay is clearly the result of saltwater inflow through Indian River Inlet (to the

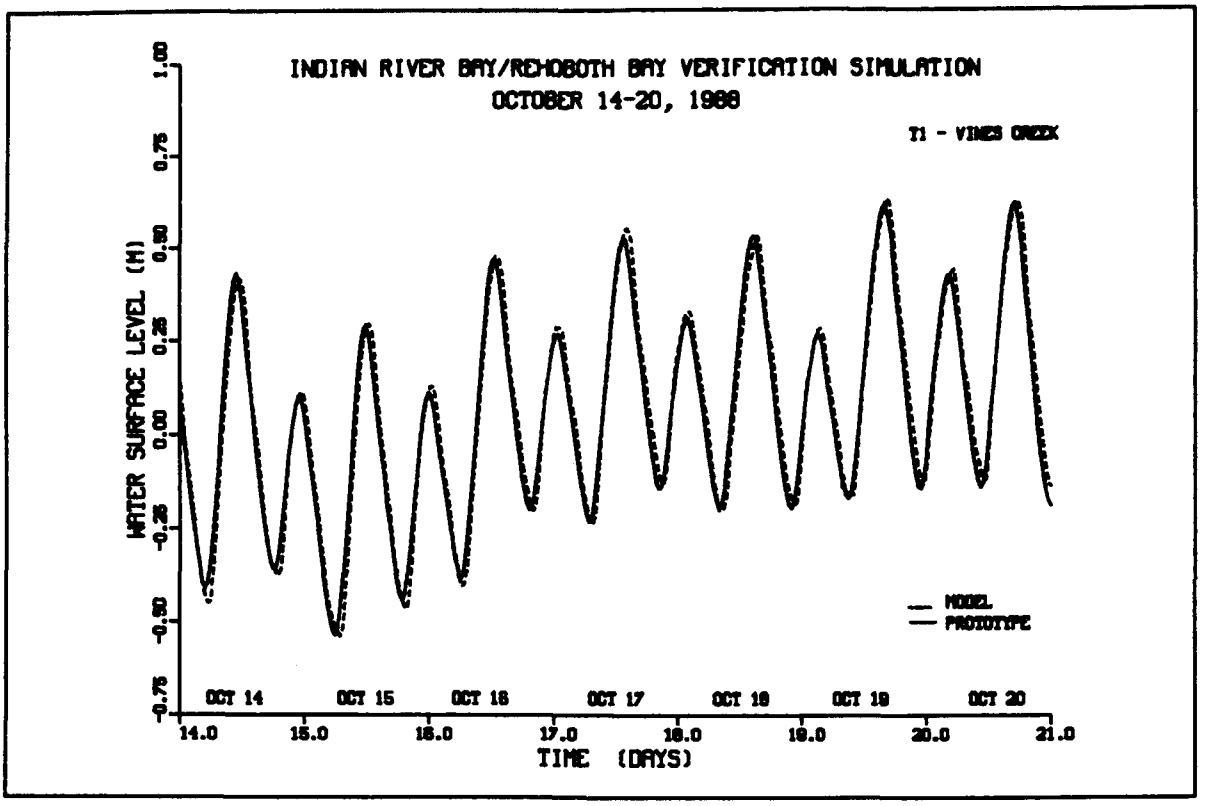

Figure 5-22. Tidal verification at Vines Creek gauge

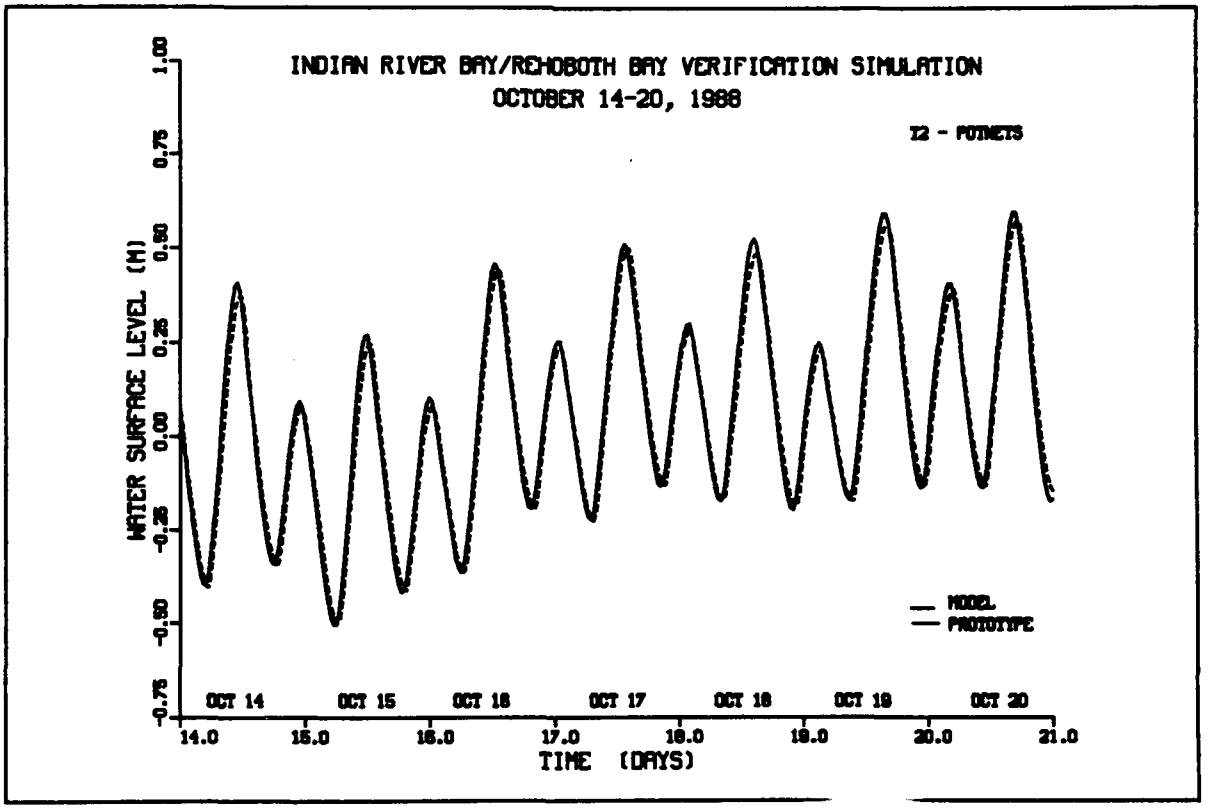

Figure 5-23. Tidal verification at Potnets gauge

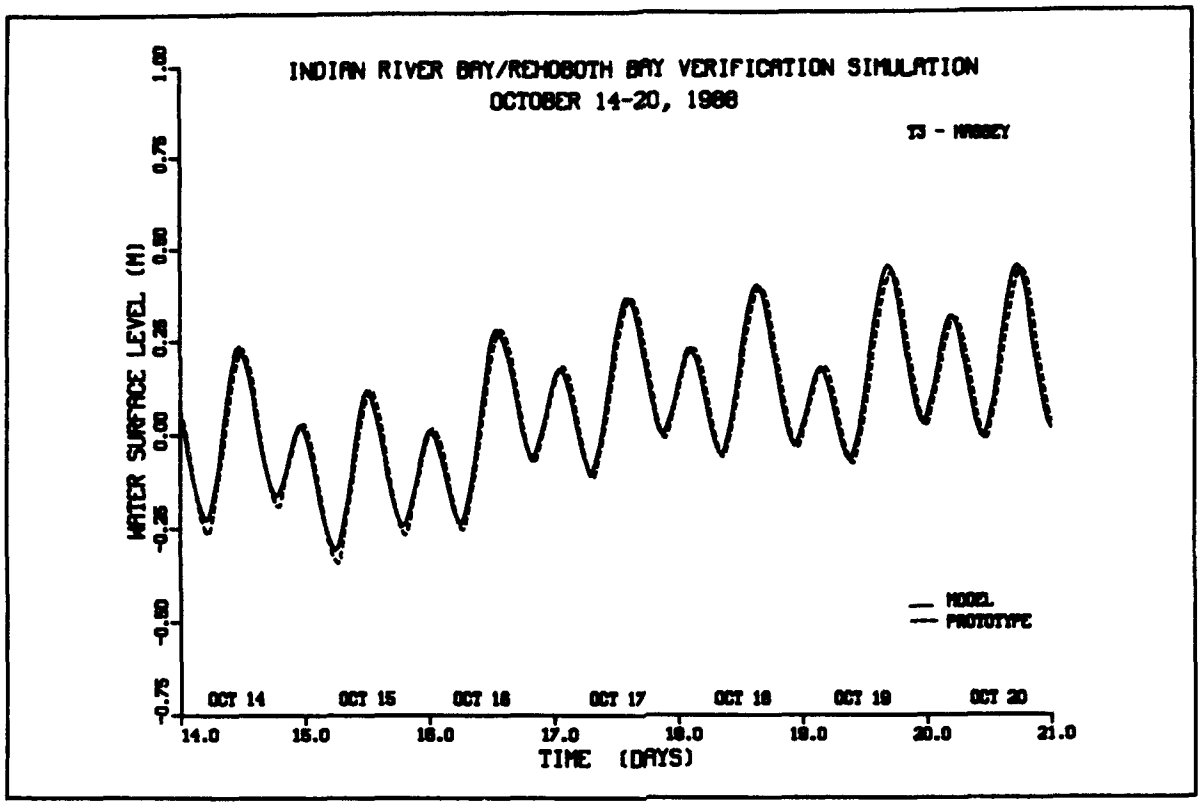

Figure 5-24. Tidal verification at Massey's Ditch gauge

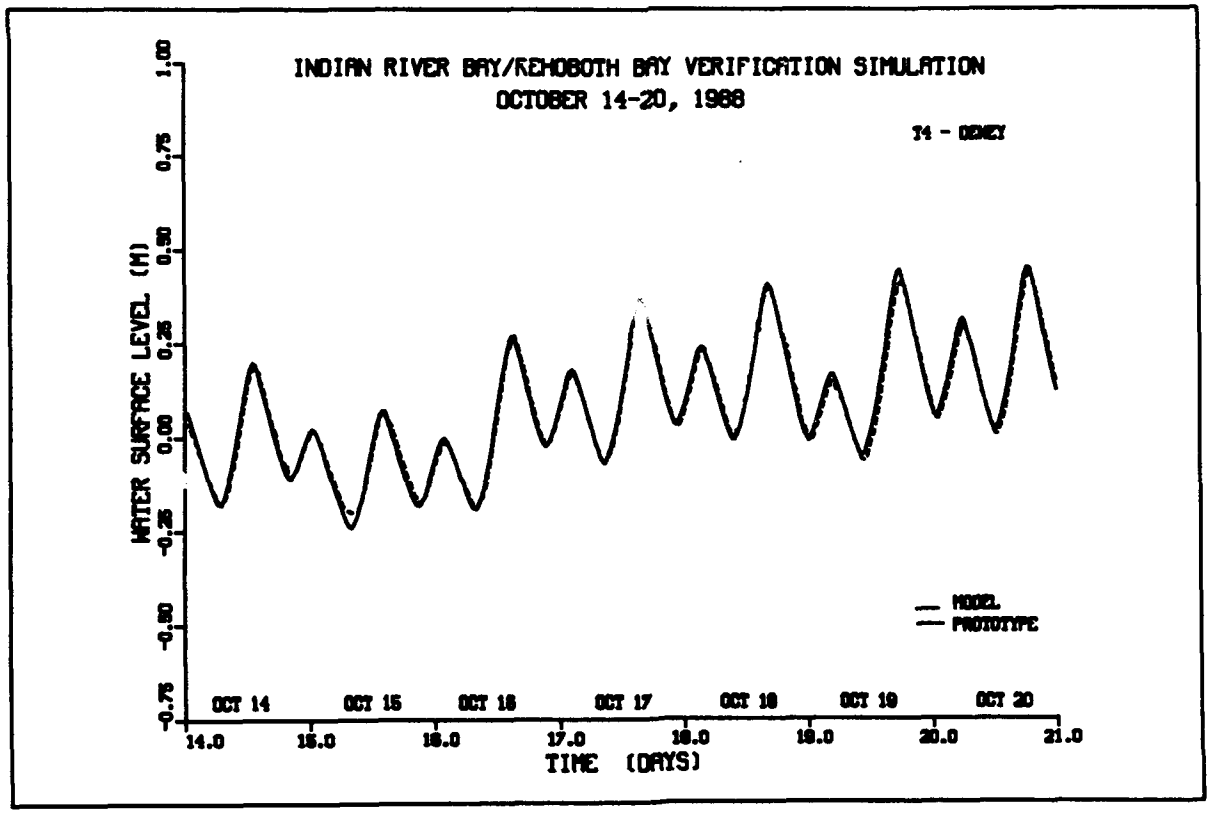

Figure 5-25. Tidal verification at Dewey Beach gauge

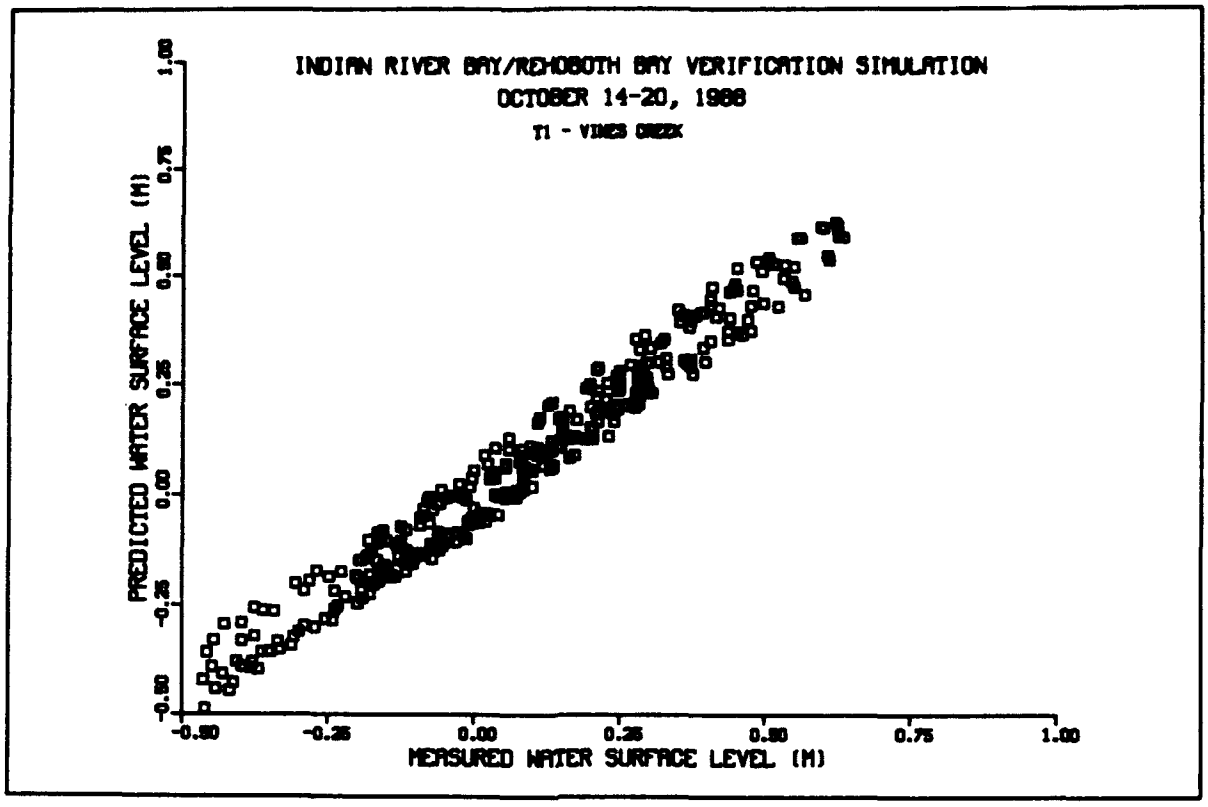

Figure 5-26. Scatter plot of tidal verification at Vines Creek gauge

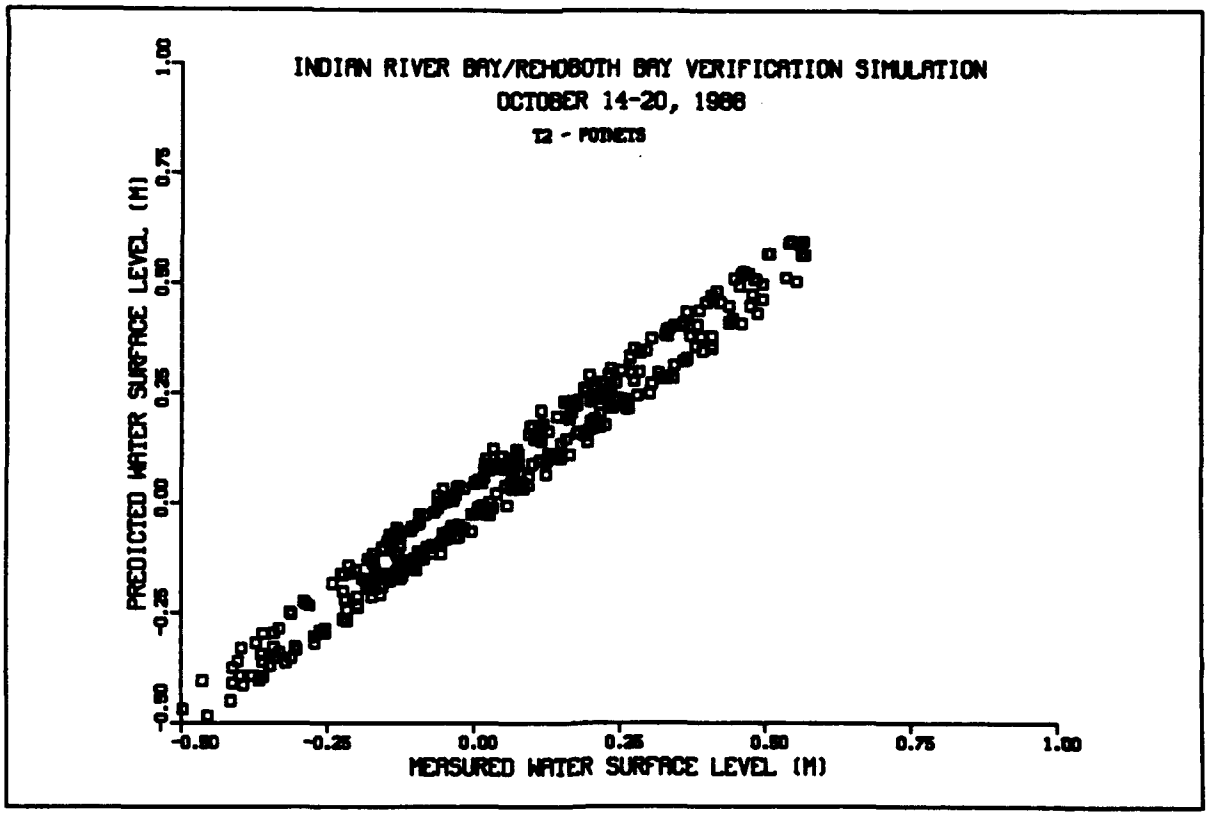

Figure 5-27. Scatter plot of tidal verification at Potnets gauge

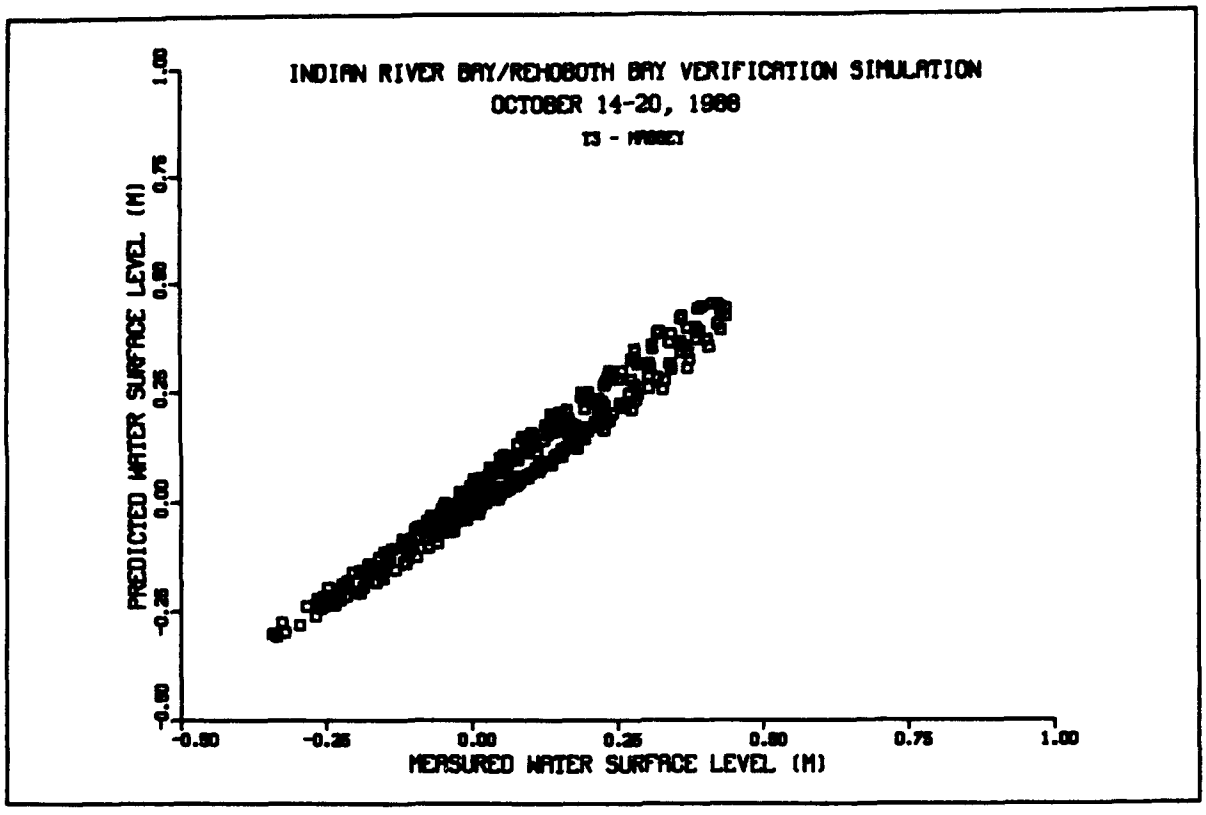

Figure 5-28. Scatter plot of tidal verification at Massey's Ditch gauge

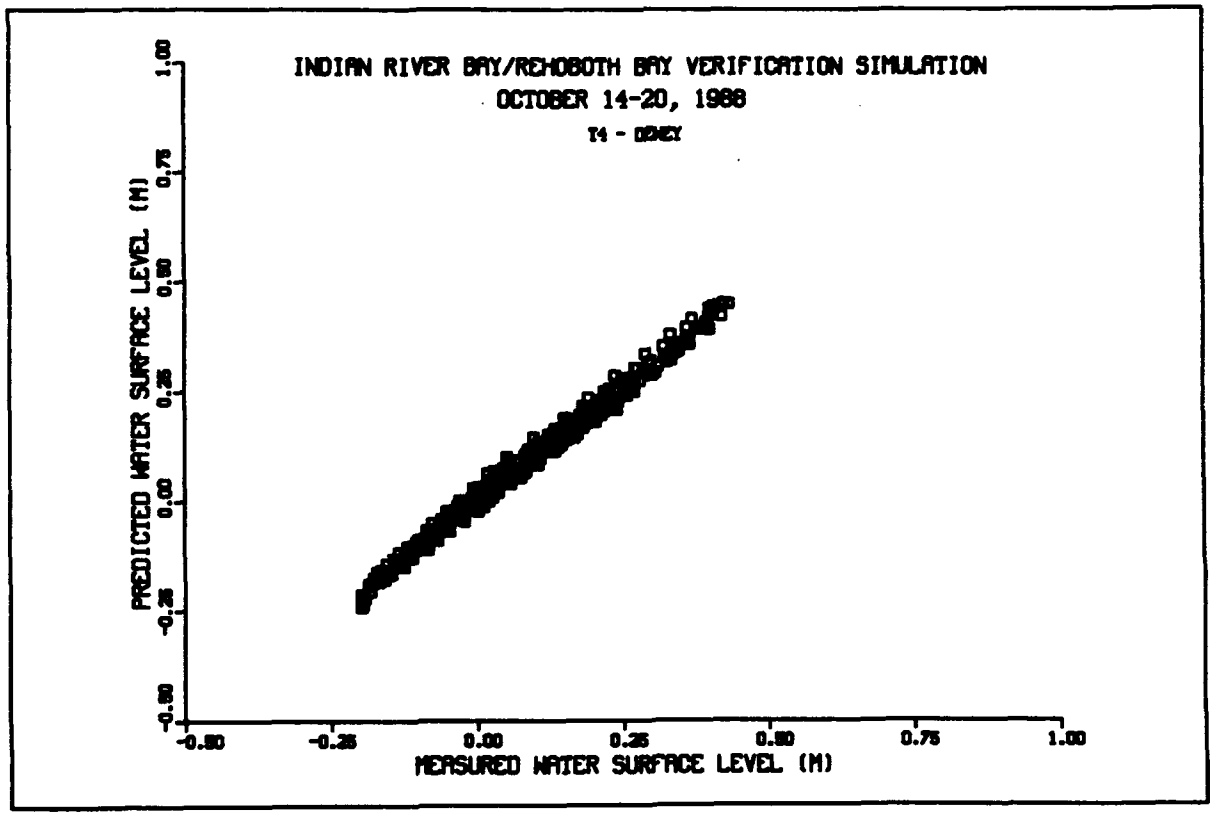

Figure 5-29. Scatter plot of tidal calibration at Dewey Beach gauge

east) and freshwater inflow from Indian River at Millsboro Dam (to the west) (Karpas 1978). For low flow conditions, freshwater does not penetrate as far into Indian River as under high flow conditions, resulting in a lower salinity gradient from the inlet boundary to the river boundary. Conversely, high flow conditions push freshwater far into Indian River, resulting in a higher salinity gradient from the inlet boundary to the river boundary. Comparing high flow conditions during flood and ebb shows the limits of salinity excursion in Indian River Bay are strongly influenced by the tide (time of day). For high river flow conditions and flood flow, salinity in Indian River is compressed by the strong river flow opposing the tidal flood flow resulting in a steep salinity gradient in Indian River Bay. Under ebb conditions, the salinity gradient is still large, but the excursion limits are pushed further east by the strong river flow and ebbing tide.

Rehoboth Bay has no major source of freshwater. Because of this, Rehoboth Bay has a higher salinity concentration than most of Indian River Bay, and Rehoboth Bay responds nearly uniformly to the tidal input of salinity. However, there is a weak east-west gradient as a result of freshwater inflow from two major creeks (Love and Herring) on the western shore of Rehoboth Bay (Karpas 1978) (Figure 5-38).

Temporal variability of salinity is a function of tidal oscillation (salt-water inflow) and variation in freshwater inflow, and the interaction of these two factors. Figures 5-39 and 5-40 show the time variation of salinity from day 260 to day 265 of 1988 (September 16-20) in Indian River and Indian River Bay (grid cells (9,29) and (30,24), respectively), and Figures 5-41 and 5-42 show the time variation of salinity near the center of Rehoboth Bay (grid cells (42,54) and (44,60) respectively).

The time series of salinity in the upper reach of Indian River (Figure 5-39) shows a large variation in salinity with tidal oscillations. Salinity in this region ranges from a low of 13.7 ppt to a high a 21.5 ppt with an average value of approximately 17-18 ppt. The important point is that salinity varies nearly 8 ppt *during one tidal cycle* in the upper reach of Indian River. This is critical from a modeling standpoint because of the sparseness of salinity data for comparison to model results and the missing component of "time of day" in the salinity data collection process.

Figure 5-40 shows that the time variation of salinity in Indian River Bay has less influence from Indian River than the previous location and is therefore more tidally influenced. Salinity in this region ranges from 29.0 to 31.5 ppt with an average value of approximately 30 ppt. At a distance from the influence of freshwater inflow, the variation in salinity is only 2.5 ppt.

Figure 5-41 shows that salinity in the south-central portion of Rehoboth Bay varies slightly with the tide, having a range of only 1 ppt. Salinity in this portion of Rehoboth Bay varies between 30.5 and 31.5 ppt. Figure 5-42 shows that salinity in the north-central portion of Rehoboth Bay is nearly constant

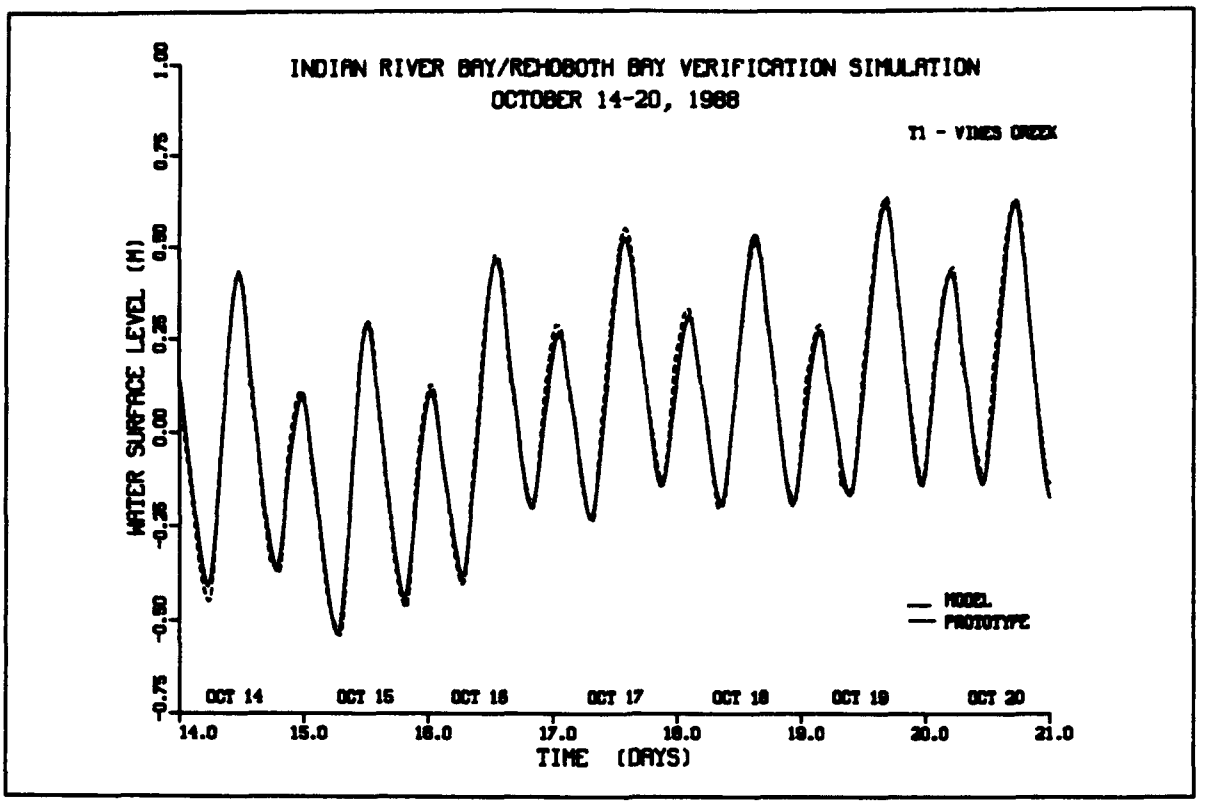

Figure 5-30. Tidal verification at Vines Creek gauge

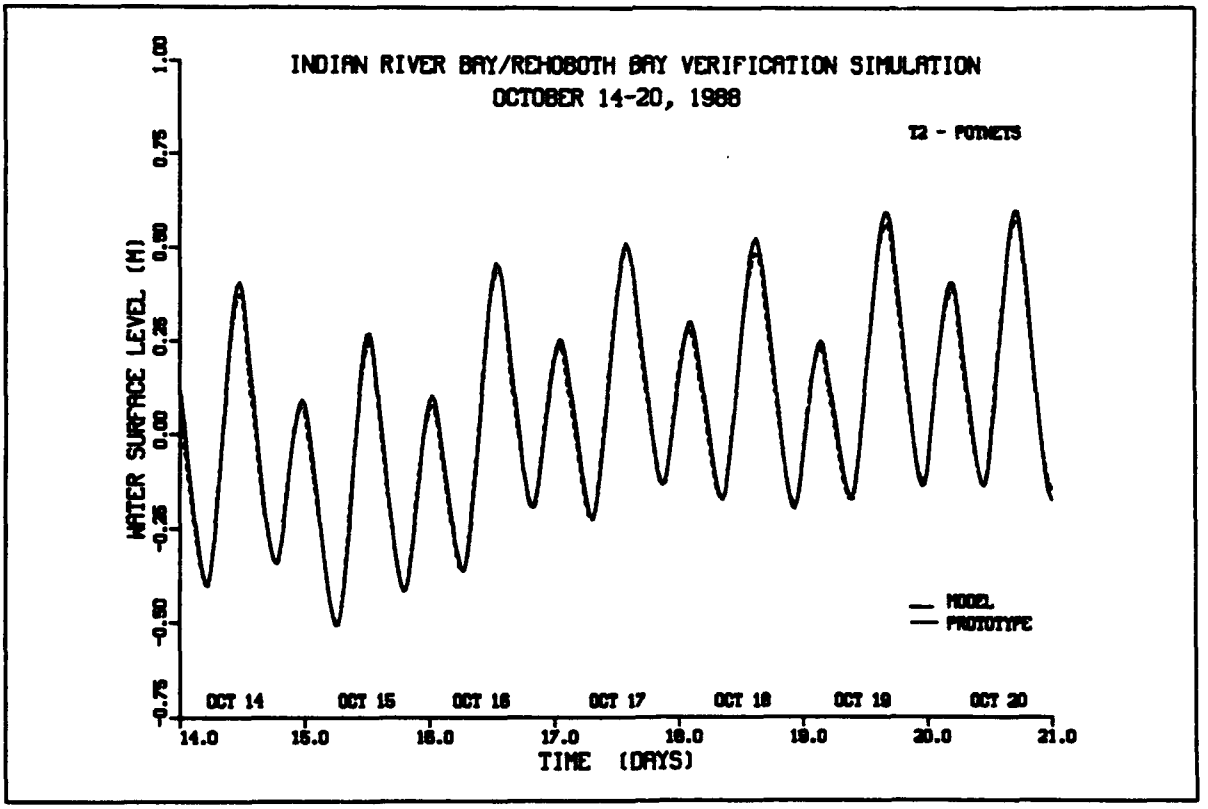

Figure 5-31. Tidal verification at Potnets gauge

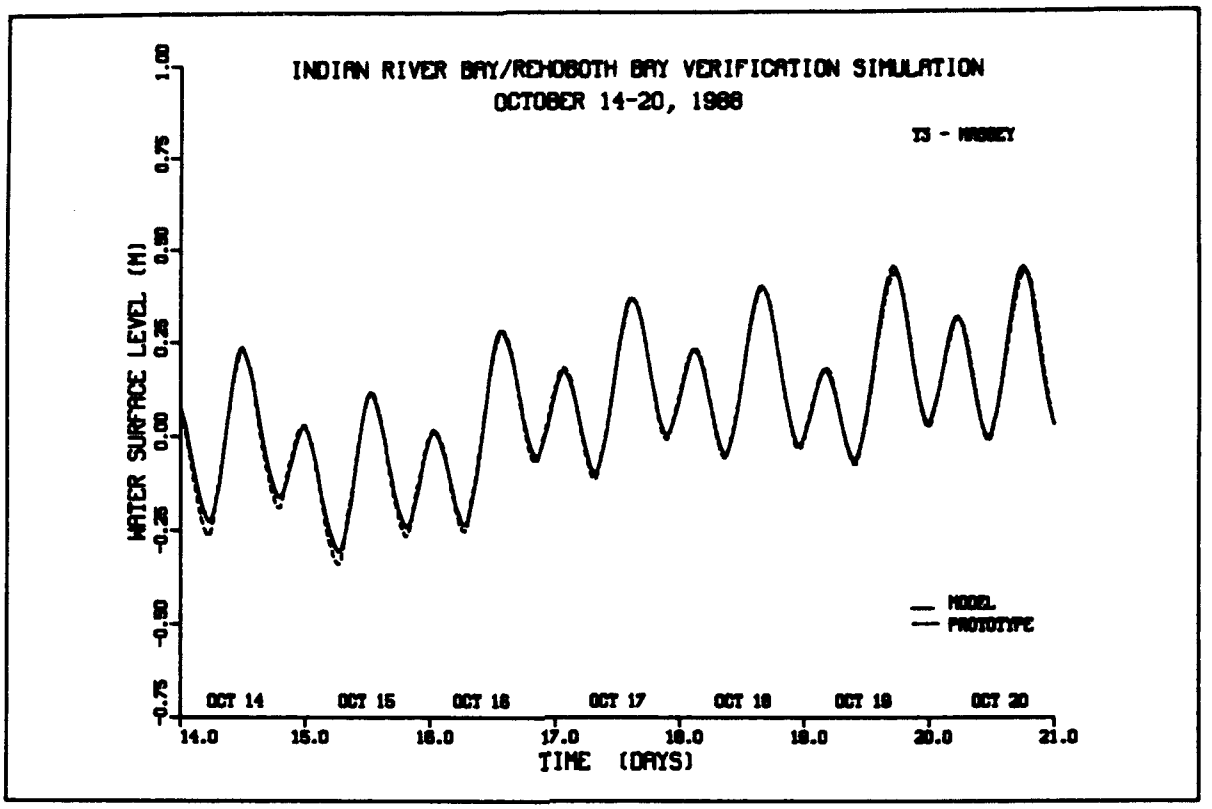

Figure 5-32. Tidal verification at Massey's Ditch gauge

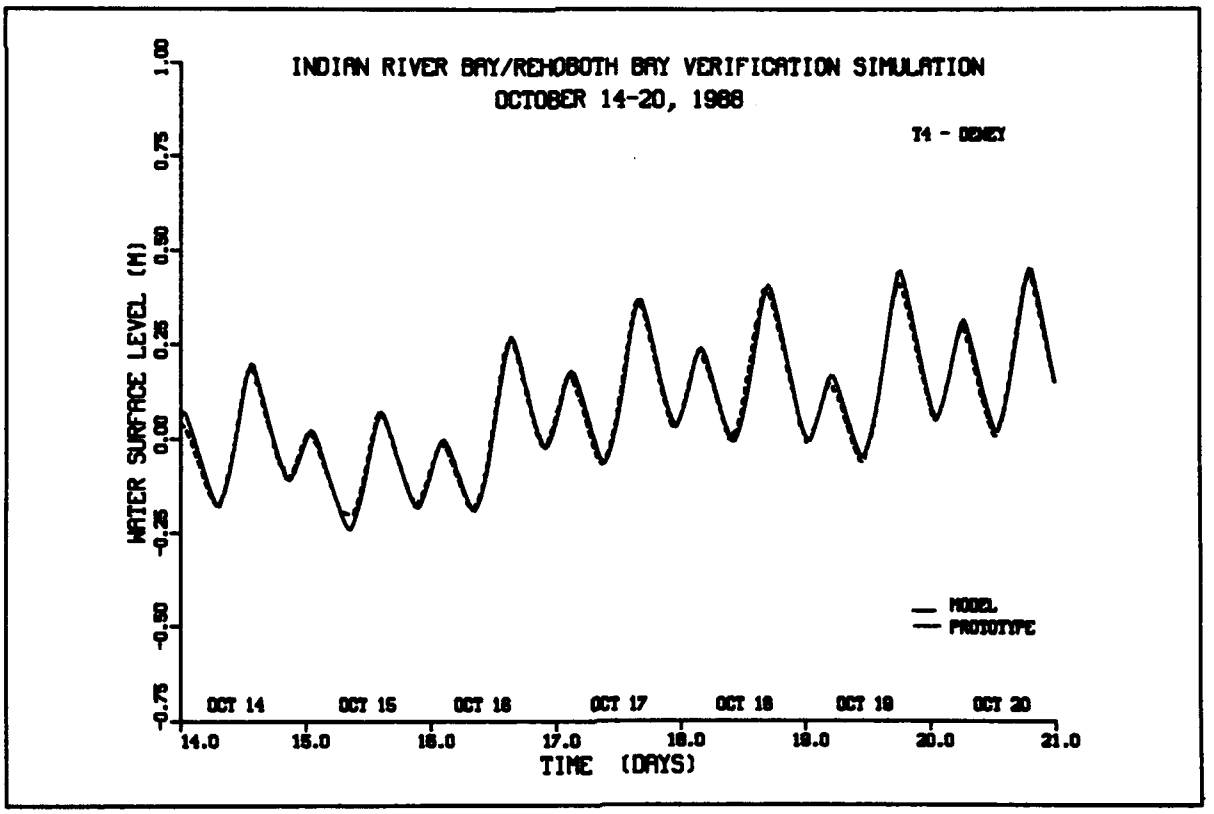

Figure 5-33. Tidal verification at Dewey Beach gauge

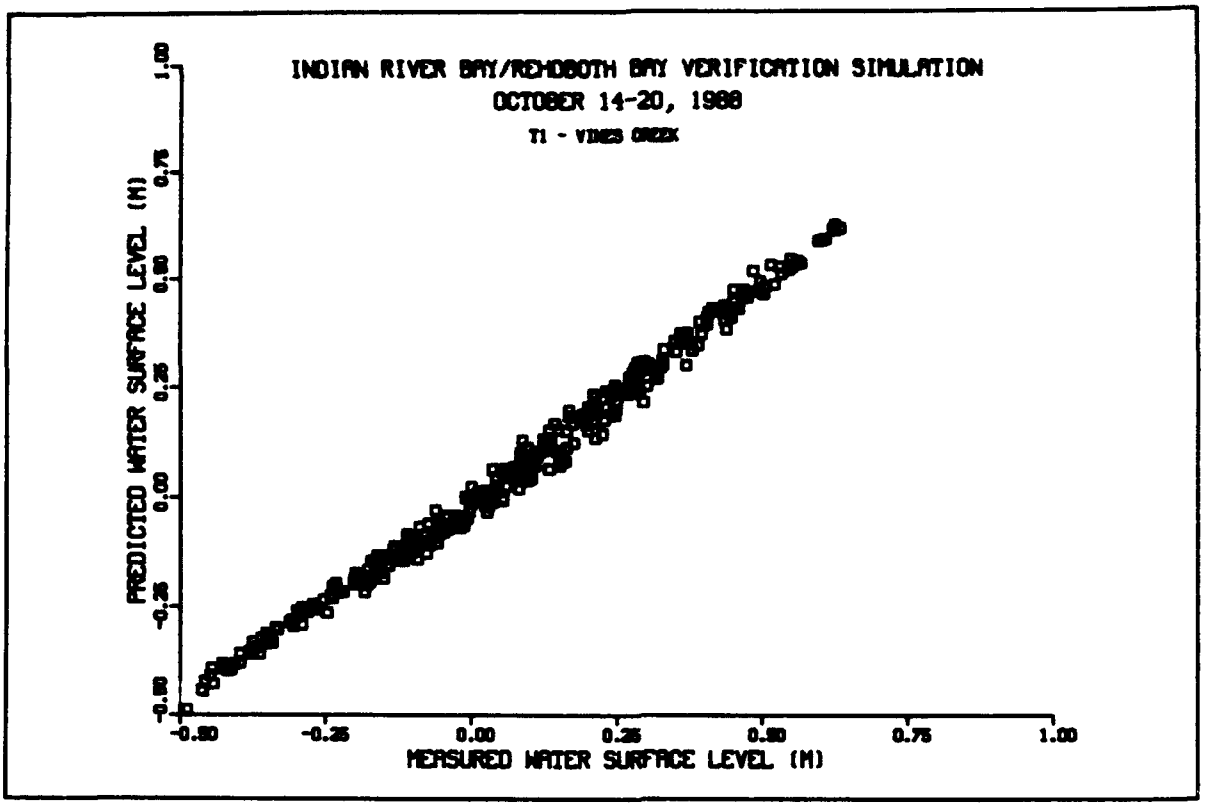

Figure 5-34. Scatter plot of tidal verification at Vines Creek gauge

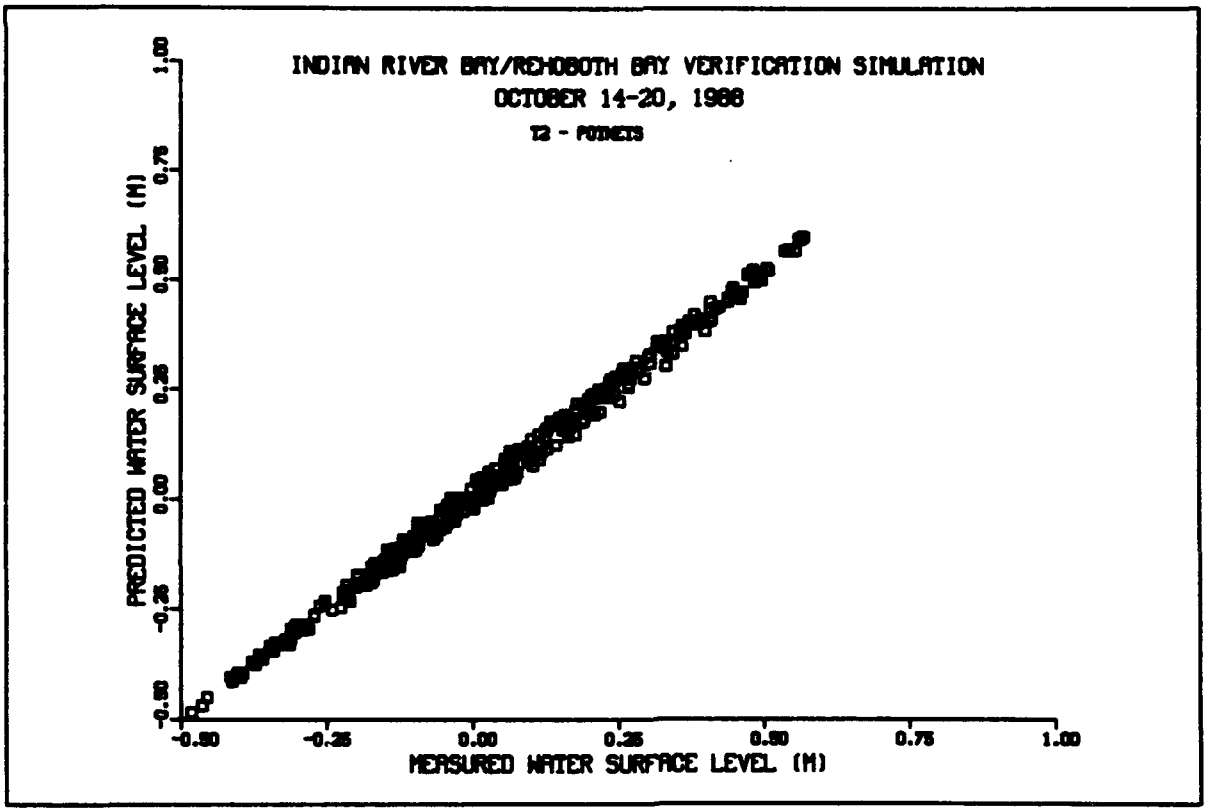

Figure 5-35. Scatter plot of tidal verification at Potnets gauge

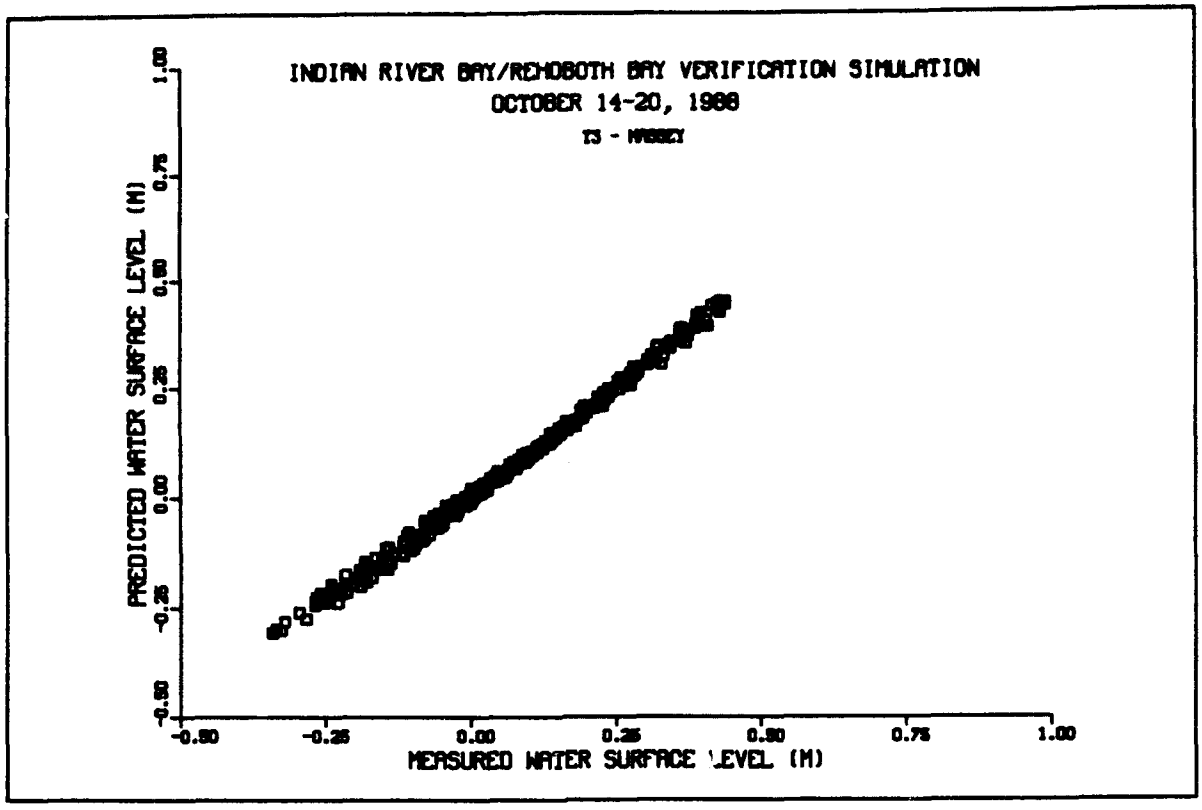

Figure 5-36. Scatter plot of tidal verification at Massey's Ditch gauge

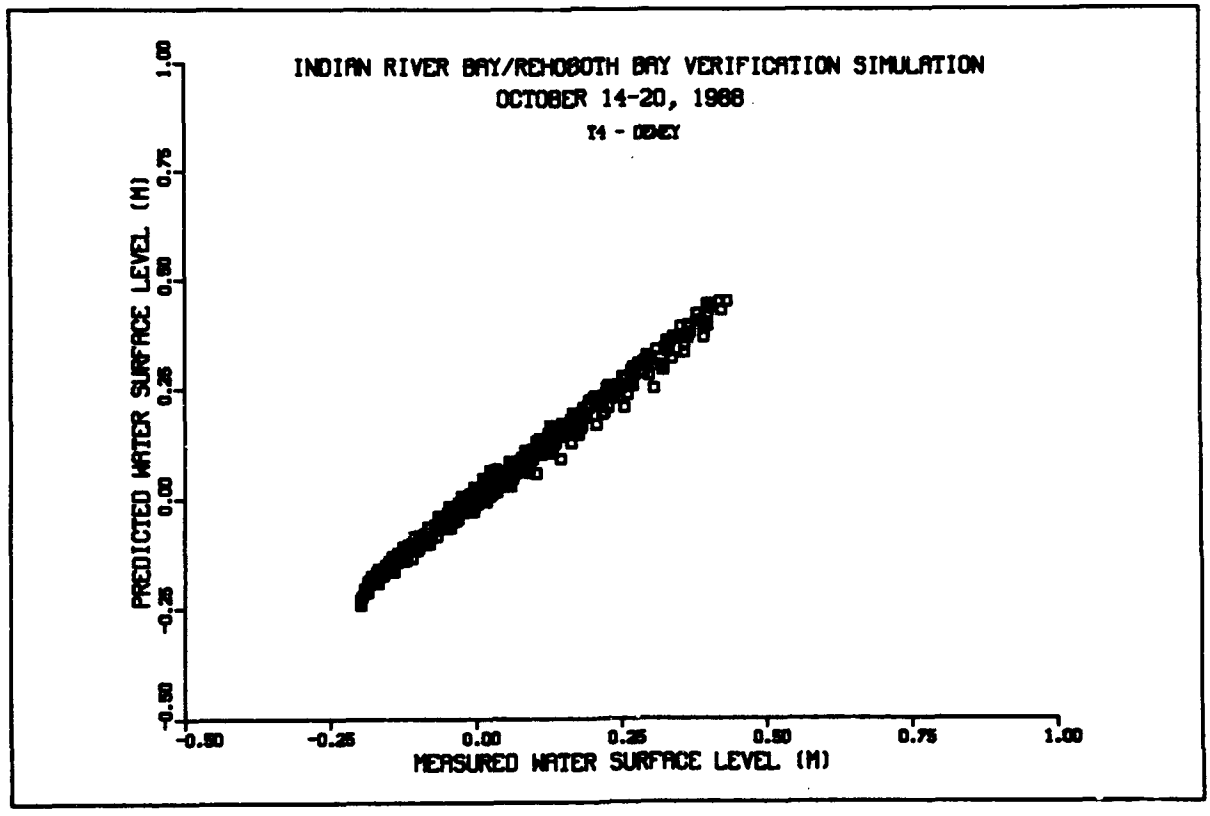

Figure 5-37. Scatter plot of tidal calibration at Dewey Beach gauge

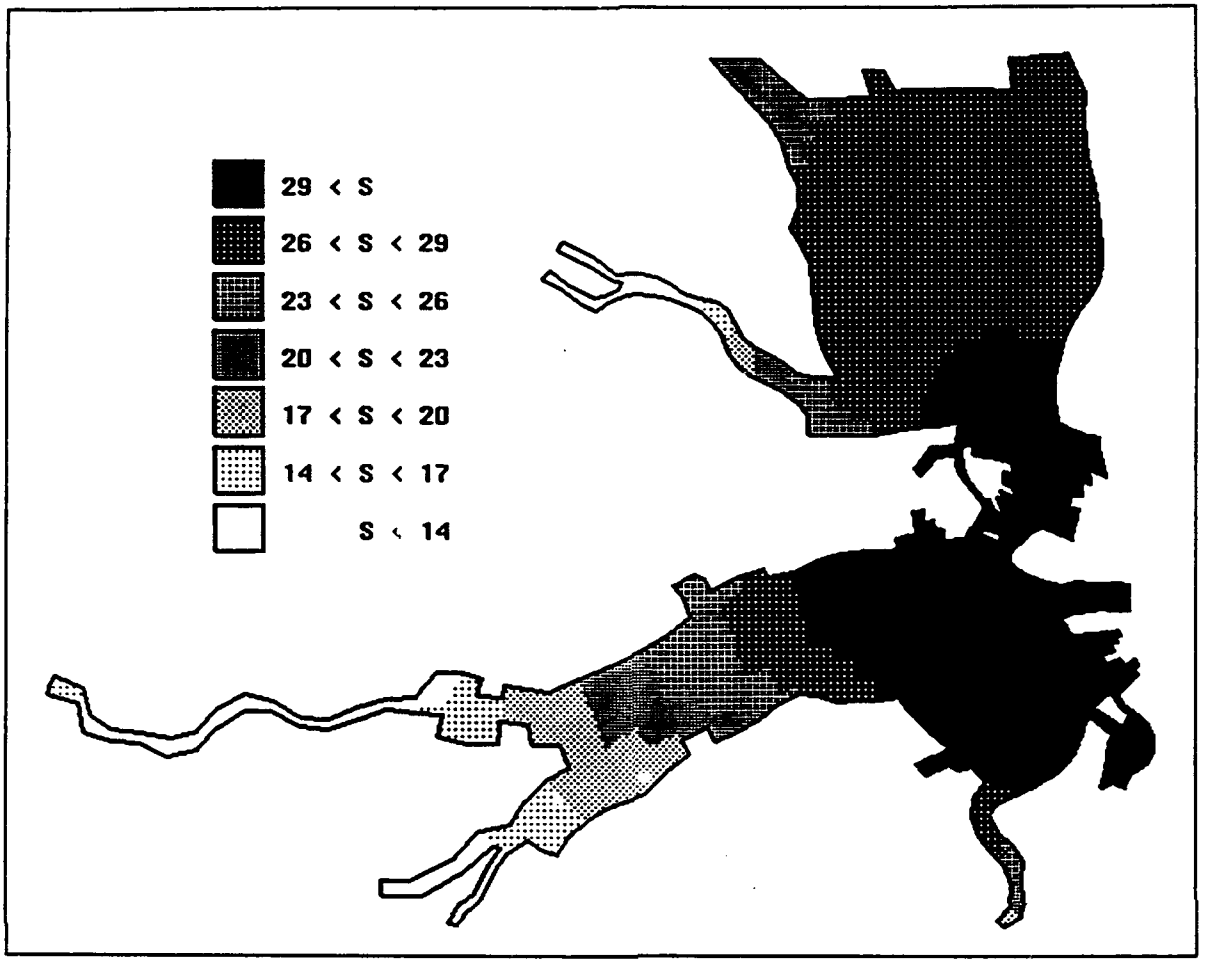

Figure 5-38. Indian River Bay/Rehoboth Bay salinity distribution

with time (31.2 ppt). Rehoboth Bay has no major freshwater inflows and is therefore tidally-dominated.

In conclusion, Indian River Bay is the more complex of the two bays in this system from a salinity standpoint. Salinity varies both spatially and temporally in Indian River Bay due to the interaction of salt water from the inlet and freshwater from Indian River at Millsboro Dam. Rehoboth Bay is nearly homogeneous. There is no major source of freshwater inflow to Rehoboth Bay and it is therefore clearly tidally-dominated.

Salinity Calibration and Validation

A long-term (1 year) simulation was used in the salinity calibration. The model simulation period was year 1988, however prototype data available for this time period was limited to 3 days of spatially-distributed salinity. A time-series of salinity at one location would therefore be limited to 3 values for the

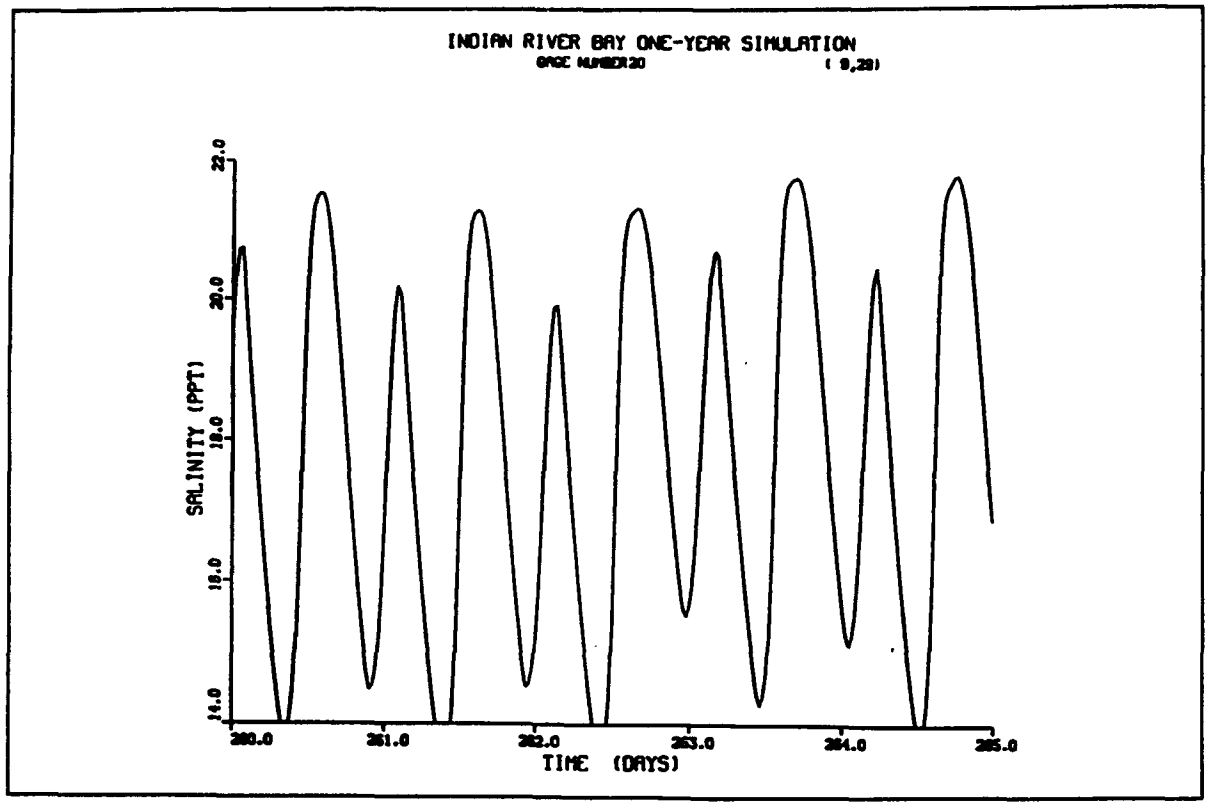

Figure 5-39. Temporal variation of salinity in Indian River

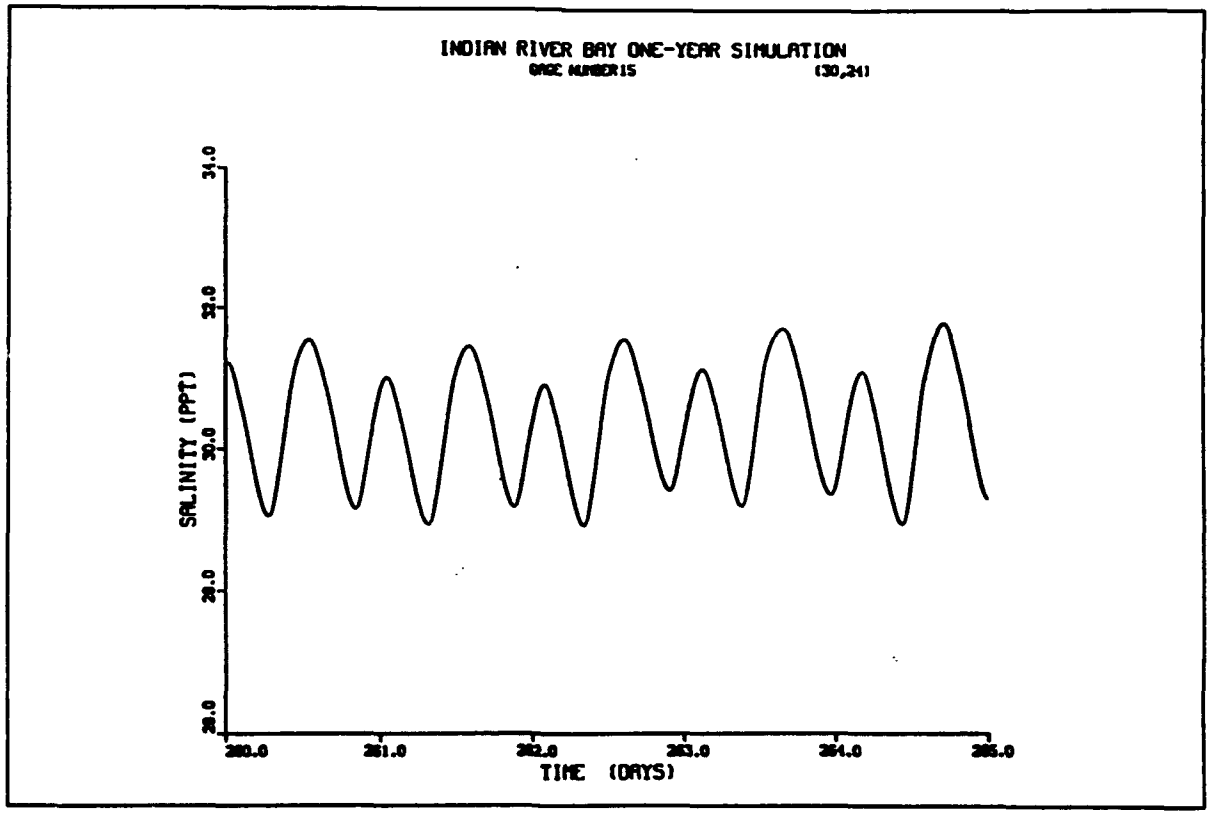

Figure 5-40. Temporal variation of salinity in Indian River Bay

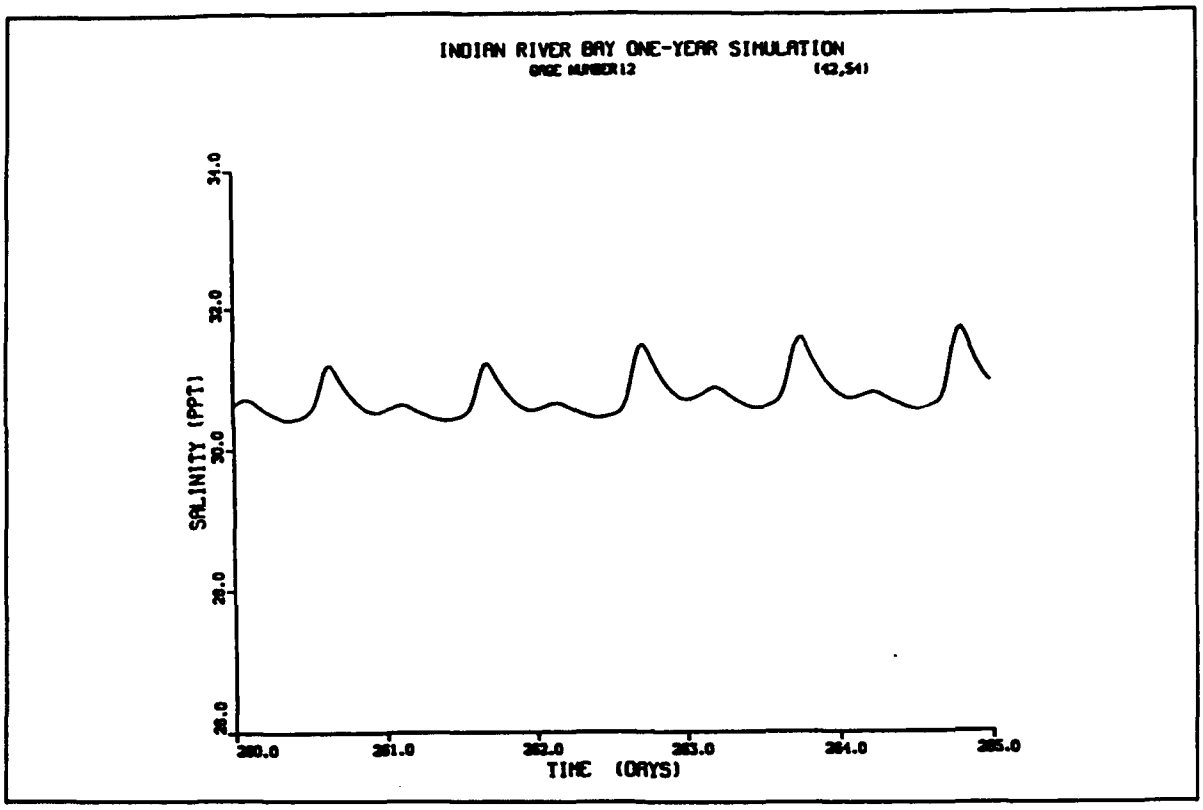

Figure 5-41. Temporal variation of salinity in Rehoboth Bay (42,54)

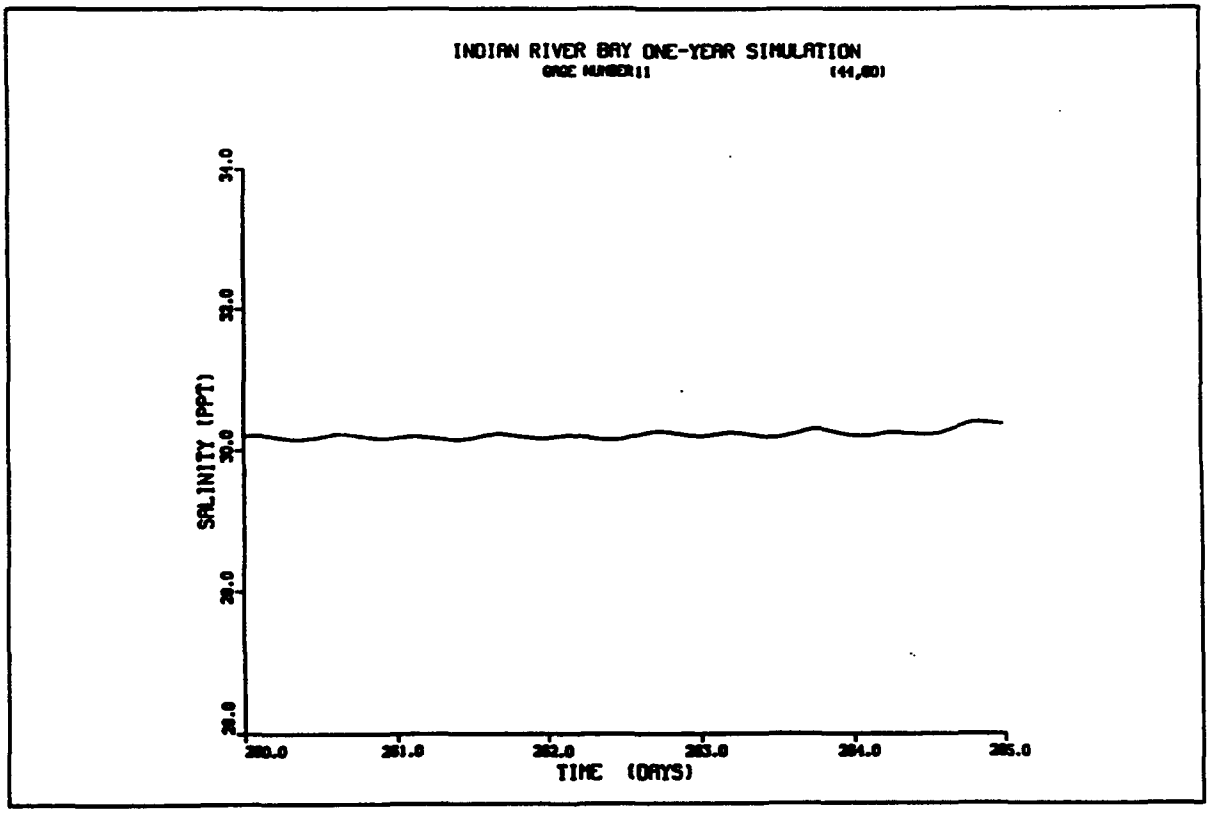

Figure 5-42. Temporal variation of salinity in Rehoboth Bay (44,60)

entire year. Thus, a spatial comparison of model results to prototype data was used. These data provide a picture of the spatial distribution of salinity at 14 stations for June 20, July 25 and September 19, 1988. As previously discussed, it is important to note that the exact time of day for data collection is not available. This factor is most critical in Indian River where the temporal variation of salinity can be as much as 8 ppt during one tidal cycle.

For illustration, Figure 5-43 is a model predicted salinity snapshot of the entire study area at 12 noon on September 19, 1988 with the shaded circles indicating measured salinity values. Note that measured salinity values are single, "instantaneous" values, however the time of day that the data were collected is not known. For this reason, model results were arbitrarily saved at 12 noon. (This is critical in areas where the temporal variability of salinity is significant.) Results in Rehoboth Bay are excellent. Results in Indian River Bay are very good, with the exception of the upper reach of Indian River where the model is underpredicting salinity. The model salinity saved for this region is in the range 14-17 ppt, however, the prototype value is in the 17-20 ppt range.

Reviewing the time-series' of salinity for the central portion of Rehoboth Bay (Figure 5-41 and 5-42) shows that salinity is nearly constant, therefore the time of day for data collection is not critical. In contrast, the time-series of salinity in the upper reach of Indian River (Figure 5-39) shows great variability in salinity with tide (time of day). Thus, the difference between model results and prototype data in Indian River is well within the range of temporal variability of salinity for this region.

Although the model results are within the range of temporal variability, salinity values in Indian River are consistently lower than the prototype values for all three days of data collection in 1988. Therefore, several techniques were examined to obtain a better salinity calibration in the upper reach of Indian River. The technique selected was to increase the size of a few cells in the upper reach of Indian River. The added cell volume decreased the velocity of freshwater inflow thereby allowing salt to penetrate further into Indian River. In addition, a spatially-variable dispersion coefficient was used to calibrate the model. A value of 12 m^2/sec was used in Rehoboth Bay and most of Indian River Bay with the exception of a portion of the middle reach of Indian River (cells 4-14). A spatially variable longitudinal dispersion coefficient was used to calibrate the model to the high salinity gradient observed in this region in 1988, 1989, and 1990. This section of the Indian River is a shallow channel where freshwater from the river meets salt water from the lower estuary in addition to heated water discharged from the DPL power plant. Smith (1976) reported that in the presence of buoyant concentration either from a river or from heated water, the transverse circulation can lead to a marked reduction in longitudinal dispersion. It is believed that this occurred in the central portion of Indian River. For this reason, a smaller dispersion value of 0.6 m^2/sec was used in cells 7 through 11 and was gradually increased to 12 m^2/sec in both the upstream and downstream directions. The desired salinity distribution was thus obtained.

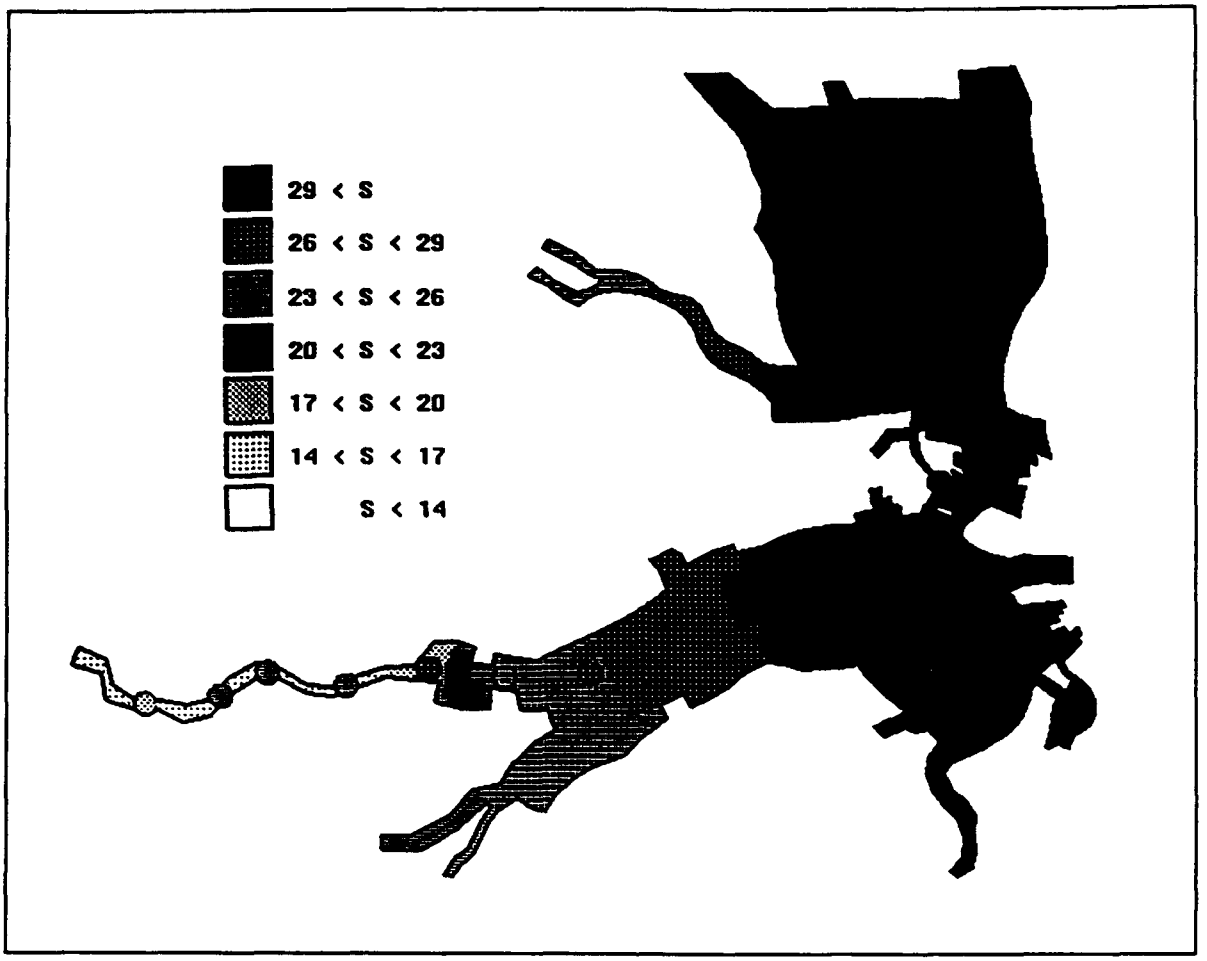

Figure 5-43. Salinity calibration for September 19, 1988

A second long-term (1-year) simulation was used in the salinity validation. The model simulation period was year 1989, however prototype data available for this time period was limited to 2 days of spatially-distributed salinity. A time-series of salinity at one location would therefore be limited to 2 values for the entire year. Thus, a spatial comparison of model results to prototype data was again used. These data provide a picture of the spatial distribution of salinity at 14 stations for April 24 and October 17, 1989. Figure 5-44, depicting the April 24, 1989 model-prototype comparison, is during a period of high flow from Indian River. The results are excellent with the exception of one location in Rehoboth Bay. At gage 5, the prototype data indicates a higher salinity (>29 ppt) than the model predicts (26-29 ppt). However, the actual salinity value is only 29.9 ppt and the discrepancy is therefore small. The lower value of model salinity indicates that the salinity wedge should be forced further into Rehoboth Bay. Figure 5-45, depicting the October 17, 1989 model-prototype comparison, is during a period of low flow from Indian River. Model results are excellent at all gages.

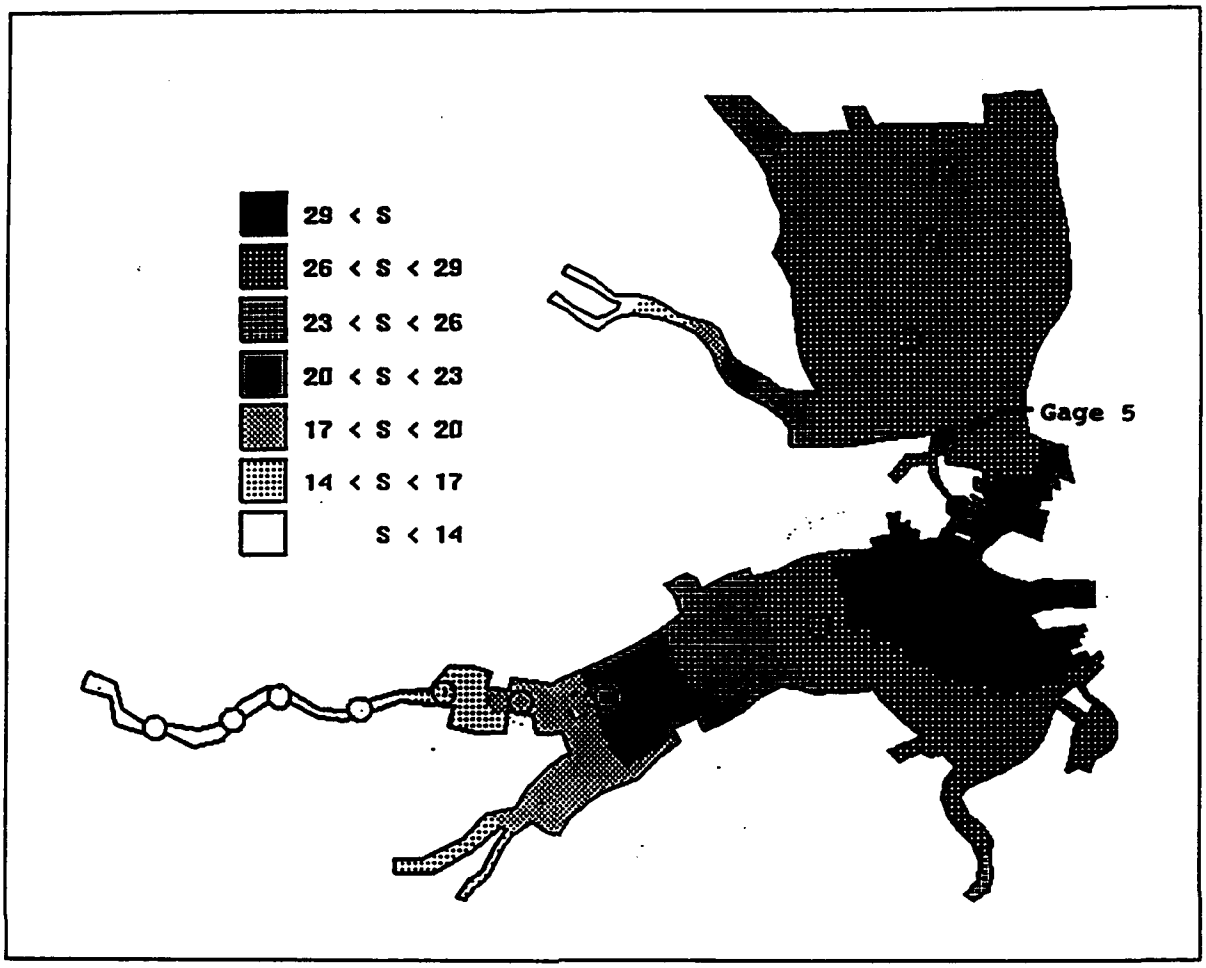

Figure 5-44. Salinity validation for April 24, 1989

Summer Average Salinity

The link between hydrodynamic and water quality modeling is in the conservative property of salinity. In water quality modeling, summer is the chemically- and biologically-active time period. Therefore, a comparison of data and model results in the summer months is important to ensure the accuracy of concentration transport. Since the data available in the summer months precludes a time series comparison, the average summer conditions were modeled and compared to all measured data for the summers of 1988, 1989, and 1990. Summer was defined in the model as July, August, and September. Figures 5-46 through 5-48 show comparisons between model and prototype data for the summers of 1988, 1989, and 1990, respectively. The three-month average of model salinity from the head of the Indian River (Millsboro Pond) to Indian River Inlet is given as a solid line and prototype data at 8 salinity stations on three specific days each year (July 24, 1989, August 28, 1989, September 25, 1989; July 16, 1990, August 13, 1990, September 24, 1990) are given as +'s. In 1988 only two days of salinity data (July 25, September 19) were available. The results confirm that the summer trend for salinity is

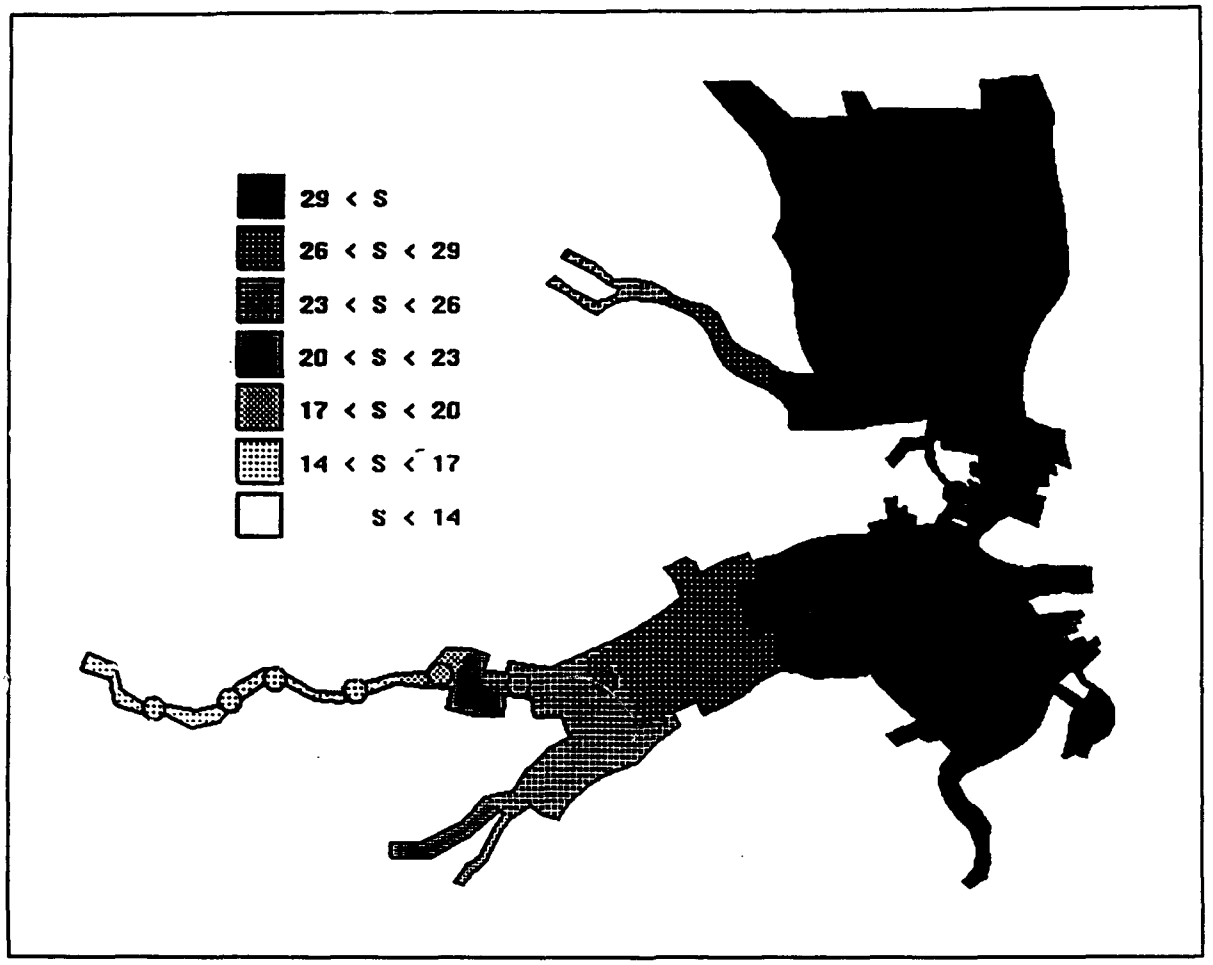

Figure 5-45. Salinity validation for October 17, 1989

captured by the model. Some discrepancy between model and data is evident near Millsboro Pond in 1988 but the discrepancy is more likely due to sparse data than a model deficiency.

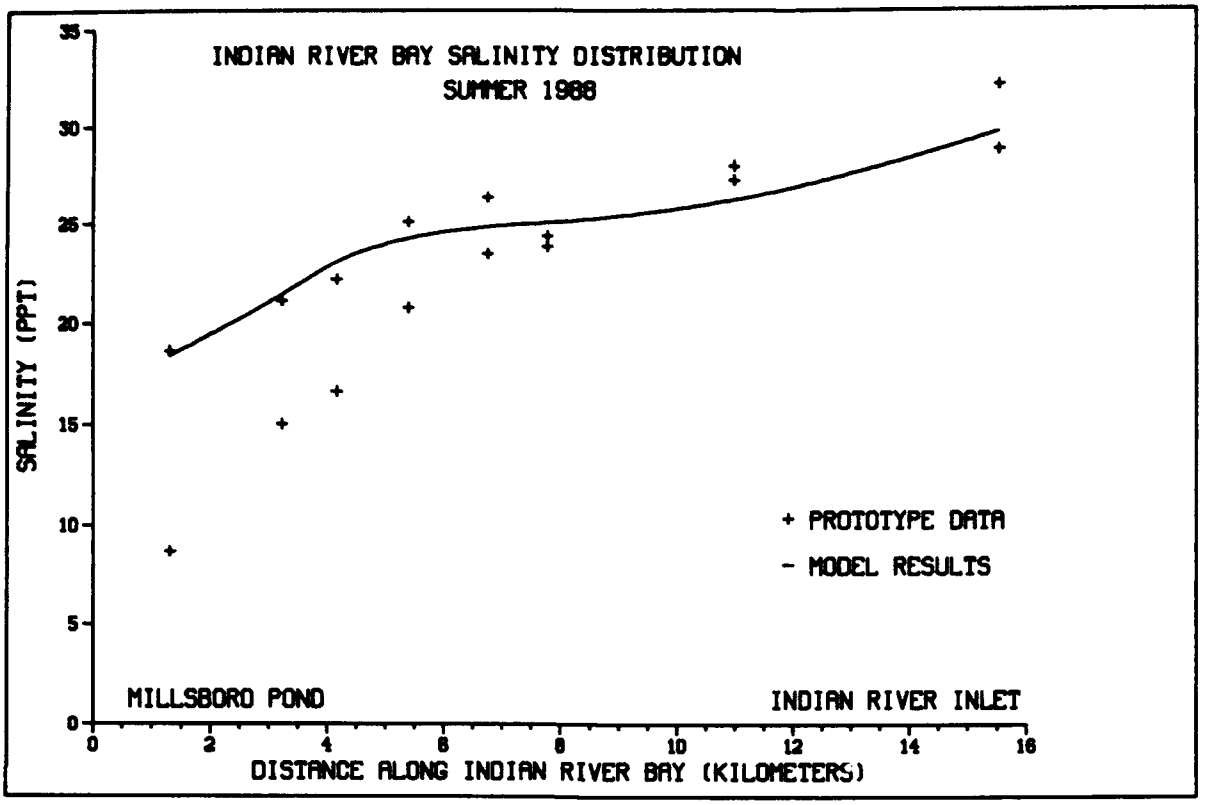

Figure 5-46. Indian River Bay salinity distribution, Summer 1988

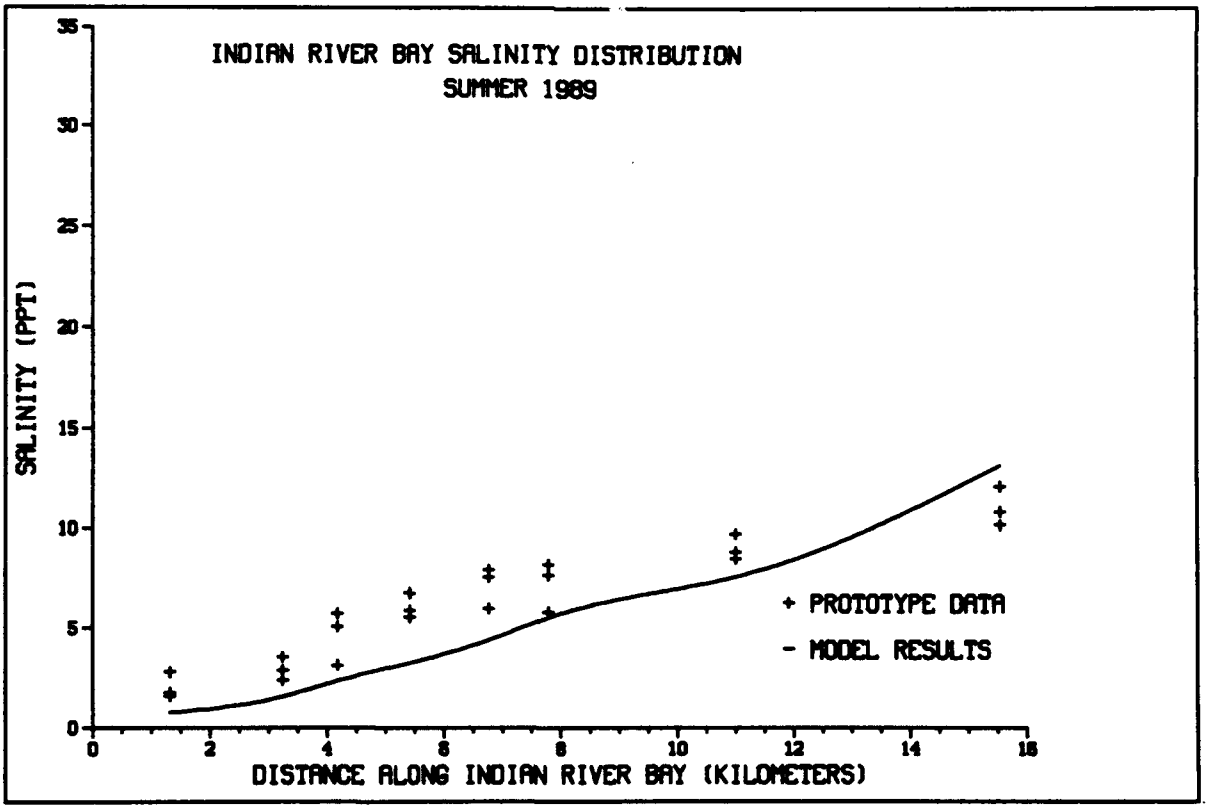

Figure 5-47. Indian River Bay salinity distribution, Summer 1989

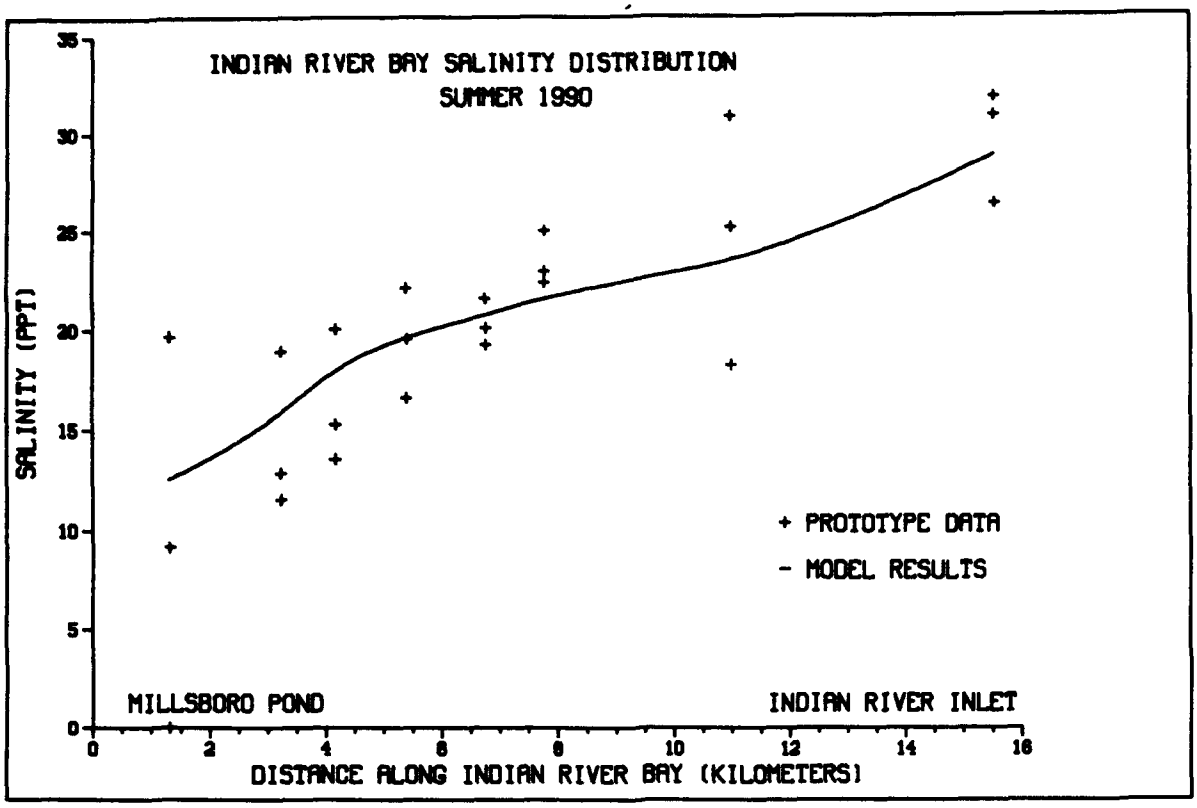

Figure 5-48. Indian River Bay salinity distribution, Summer 1990

Chapter VI: Water Quality Model Kinetics

Introduction

The water quality model, dubbed CE-QUAL-ICM, originated as part of a eutrophication model package applied to Chesapeake Bay (Cerco and Cole 1993). Kinetic formulations from the Chesapeake Bay model were applied to Indian River-Rehoboth Bay with minimal modification. Several state variables present in the original model were dropped, however, consistent with the available data base. Some simplifications were also made, largely through specification of parameter values. The original code is intact and additional state variables and options can be activated in the future. Active state variables in Indian River-Rehoboth Bay are presented in Table 6-1. The remainder of the chapter describes the state variables, details kinetics formulations, and lists coefficient values.

Table 6-1
Water Quality Model State Variables

Temperature	Salinity
Algae	Dissolved Organic Carbon
Labile Particulate Organic Carbon	Refractory Particulate Organic Carbon
Ammonium	Nitrate
Dissolved Organic Nitrogen	Labile Particulate Organic Nitrogen
Refractory Particulate Organic Nitrogen	Total Phosphate
Dissolved Organic Phosphorus	Labile Particulate Organic Phosphorus
Refractory Particulate Organic Phosphorus	Dissolved Oxygen

Algae

Algae are a primary focus of the eutrophication model. Algae play a central role in the carbon, nitrogen and phosphorus cycles. Dissolved oxygen is influenced by algal production and respiration in the water column. Light

extinction is partially dependent attenuation caused by algal chlorophyll. One algal group is currently activated in the model.

Organic Carbon

Three organic carbon state variables are considered: dissolved, labile particulate, and refractory particulate. Labile and refractory distinctions are based upon the time scale of decomposition. Labile organic carbon decomposes on a time scale of days to weeks while refractory organic carbon requires more time. Labile organic carbon decomposes rapidly in the water column or the sediments. Refractory organic carbon decomposes slowly, primarily in the sediments, and may contribute to sediment oxygen demand years after deposition.

Nitrogen

Nitrogen is first divided into organic and mineral fractions. Organic nitrogen state variables are: dissolved organic nitrogen, labile particulate organic nitrogen, and refractory particulate organic nitrogen. Two mineral nitrogen forms are considered: ammonium and nitrate. Both are utilized to fulfill algal nutrient requirements although ammonium is preferred from thermodynamic considerations. The primary reason for distinguishing the two is that ammonium is oxidized by nitrifying bacteria into nitrate. This oxidation can be a significant sink of oxygen in the water column and sediments. An intermediate in the complete oxidation of ammonium, nitrite, also exists. Nitrite concentrations are usually much less than nitrate and for modeling purposes nitrite is combined with nitrate. Hence the nitrate state variable actually represents the sum of nitrate plus nitrite.

Phosphorus

As with carbon and nitrogen, organic phosphorus is considered in three states: dissolved, labile particulate, and refractory particulate. Only a single mineral form, total phosphate, is considered. Total phosphate exists in two states within the model ecosystem: dissolved phosphate and phosphate incorporated in algal cells. Equilibrium partition coefficients distribute the total among two states.

Dissolved Oxygen

Dissolved oxygen is required for the existence of higher life forms. Oxygen availability determines the distribution of organisms and the flows of energy and nutrients in an ecosystem. Dissolved oxygen is a central component of the water quality model.

Salinity

Salinity is a conservative tracer that provides verification of the transport component of the model and facilitates examination of conservation of mass. Salinity also influences the dissolved oxygen saturation concentration.

Temperature

Temperature is a primary determinant of the rate of biochemical reactions. Reaction rates increase as a function of temperature although extreme temperatures result in the mortality of organisms.

Conservation Of Mass Equation

The foundation of CE-QUAL-ICM is the solution of the mass-conservation equation for a control volume. Control volumes in the water quality model correspond to one or more cells on the hydrodynamic model grid. For the Indian River-Rehoboth Bay application, a two-dimensional, vertically integrated form of the mass-conservation equation is employed. CE-QUAL-ICM solves, for each volume and for each state variable, the conservation of mass equation:

$$\frac{\delta V_i C_i}{\delta t} = \sum_{j=1}^{n} Q_j C_j^* + \sum_{j=1}^{n} A_j D_j \frac{\delta C}{\delta x_j} + \sum S_i \qquad (6\text{-}1)$$

V_i = volume of ith control volume (m^3)

C_i = concentration in ith control volume (gm m^{-3})

Q_j = volumetric flow across flow face j of ith control volume (m^3 sec^{-1})

C_j^* = concentration in flow across flow face j (gm m^{-3})

A_j = area of flow face j (m^2)

D_j = diffusion coefficient at flow face j (m^2 sec^{-1})

n = number of flow faces attached to ith control volume

S_i = external loads and kinetic sources and sinks in ith control volume (gm sec^{-1})

t, x = temporal and spatial coordinates

Solution to the mass-conservation equation is via the finite-difference method using the QUICKEST algorithm (Leonard 1979).

The remainder of this chapter details the kinetics portion of the mass-conservation equation for each state variable. Terms are defined where they first appear. Coefficient values are presented in a table at the end of the chapter. For consistency with reported rate coefficients, kinetics are detailed using a temporal dimension of days. Within the CE-QUAL-ICM code, kinetics sources and sinks are converted to a dimension of seconds before employment in the mass-conservation equation.

Algae

Sources and sinks of algae are:

Growth (production)
Basal metabolism
Predation
Settling

The governing equation for algal biomass is:

$$\frac{\delta}{\delta t} B = \left(P - BM - PR - \frac{WSa}{H} \right) B \qquad (6\text{-}2)$$

B = algal biomass, expressed as carbon (gm C m^{-3})

P = production (day^{-1})

BM = basal metabolism (day^{-1})

PR = predation (day^{-1})

WSa = algal settling velocity (m day^{-1})

H = depth of water column (m)

Production

Production by phytoplankton is determined by the availability of nutrients, by the intensity of light, and by the ambient temperature. The effects of each are considered to be multiplicative:

$$P = PM\, f(N)\, f(I)\, f(T) \qquad (6\text{-}3)$$

PM = production under optimal conditions (day^{-1})

f(N) = effect of suboptimal nutrient concentration ($0 \leq f \leq 1$)

f(I) = effect of suboptimal illumination ($0 \leq f \leq 1$)

f(T) = effect of suboptimal temperature ($0 \leq f \leq 1$)

Nutrients

Carbon, nitrogen, phosphorus, and silica are the primary nutrients required for algal growth. Inorganic carbon is usually available in excess and is not considered. Silica is omitted since this nutrient is required only by diatoms which are not distinguished from other algae in the model application. The effects of nitrogen and phosphorus on growth are described by the formulation commonly referred to as "Monod kinetics" (Monod 1949). In the Monod formulation (Figure 6-1) growth is dependent upon nutrient availability at low nutrient concentrations but is independent of nutrients at high concentrations. A key parameter in the formulation is the "half-saturation concentration". Growth rate is half the maximum when available nutrient concentration equals the half-saturation concentration. Liebig's "law of the minimum" (Odum 1971) indicates growth is determined by the nutrient in least supply:

$$f(N) = \text{minimum}\left(\frac{NH_4 + NO_3}{KHn + NH_4 + NO_3}, \frac{PO_4d}{KHp + PO_4d}\right) \qquad (6\text{-}4)$$

NH_4 = ammonium concentration (gm N m^{-3})

NO_3 = nitrate concentration (gm N m^{-3})

KHn = half-saturation constant for nitrogen uptake (gm N m^{-3})

PO_4d = dissolved phosphate concentration (gm P m^{-3})

KHp = half-saturation constant for phosphorus uptake (gm P m^{-3})

Light

Algal production increases as a function of light intensity until an optimal intensity is reached. Beyond the optimal intensity, production declines as

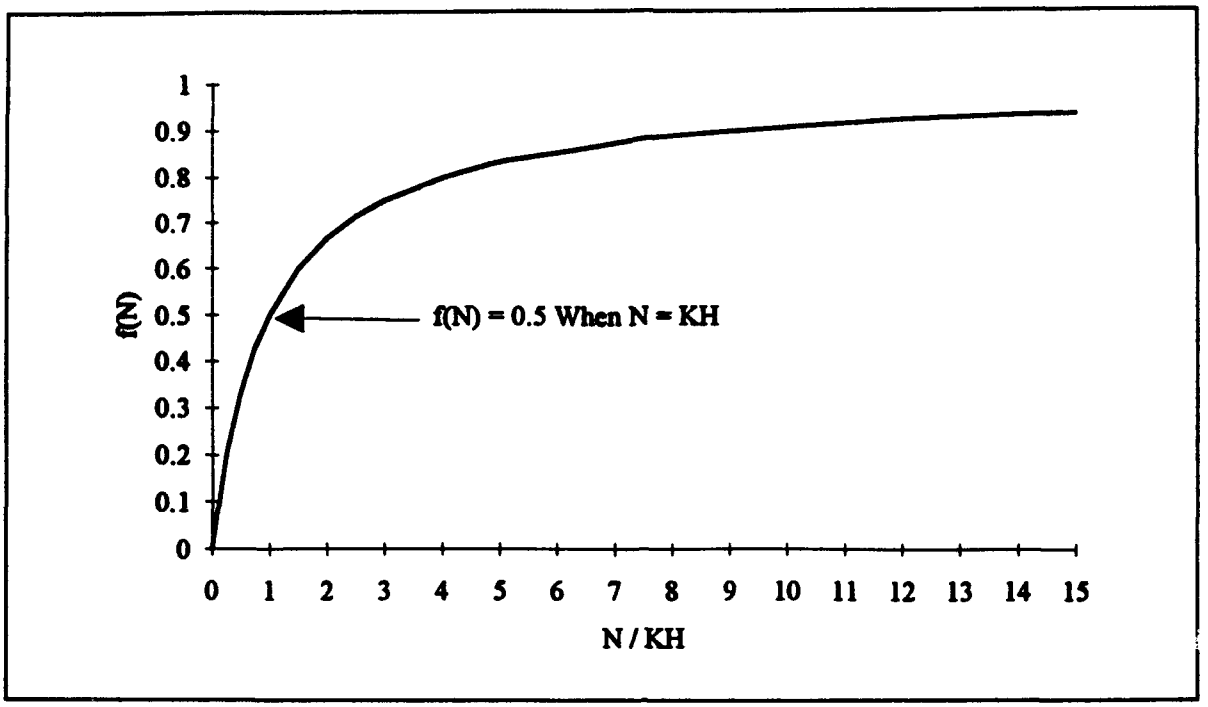

Figure 6-1. The Monod formulation for nutrient-limited growth

intensity increases. Steele's equation (DiToro et al. 1971) describes this phenomenon:

$$f(I) = \frac{I}{Is} e^{1 - \frac{I}{Is}} \qquad (6\text{-}5)$$

I = illumination rate (Langleys day^{-1})

Is = optimal illumination (Langleys day^{-1})

Steele's equation describes the instantaneous light limitation at a point in space. The model, however, computes processes integrated over discrete time intervals and aggregated spatially into model segments. Therefore, Steele's equation must be integrated over an appropriate time interval and averaged over the thickness of each model segment. The integration interval selected is one day. This interval does not preclude computation steps less than a day but frees the model from accounting for illumination in "real time." Daily averaging does preclude computation of diurnal fluctuations in algal production. This restriction is not severe, however, since the classic equations for algal growth are not appropriate for short time scales.

Assuming light intensity declines exponentially with depth, the integrated, averaged form of Steele's equation is:

$$f(I) = \frac{2.72\,FD}{Kess\,H}\left(e^{\alpha b} - e^{\alpha t}\right) \qquad (6\text{-}6)$$

$$\alpha b = -\frac{Io}{FD\,Is}e^{-Kess\,H} \qquad (6\text{-}7)$$

$$\alpha t = -\frac{Io}{FD\,Is} \qquad (6\text{-}8)$$

Io = daily illumination at water surface (Langleys day^{-1})

FD = fractional daylength ($0 \leq FD \leq 1$)

Kess = total light attenuation coefficient (m^{-1})

Light attenuation in the water column is composed of two fractions: a background value dependent on water color and concentration of suspended particles, and extinction due to light absorption by ambient chlorophyll:

$$Kess = Keb + Kechl\frac{B}{CChl} \qquad (6\text{-}9)$$

Keb = background light attenuation (m^{-1})

Kechl = light attenuation coefficient for chlorophyll 'a' ($m^2\ mg^{-1}$)

CChl = algal carbon-to-chlorophyll ratio (gm C mg^{-1} chl)

Optimal illumination for photosynthesis depends on algal taxonomy, duration of exposure, temperature, nutritional status, and previous acclimation. Variations in optimal illumination are largely due to adaptations by algae intended to maximize production in a variable environment. Steele (1962) noted the result of adaptations is that optimal illumination is a consistent fraction (≈ 50%) of daily illumination. Kremer and Nixon (1978) reported an analogous finding that maximum algal production occurs at a constant depth (≈ 1m) in the water column. Their approach is adopted here so that optimal illumination is expressed:

$$Is = Ioavg\, e^{-Kess\ Dopt} \quad (6\text{-}10)$$

Ioavg = adjusted surface illumination (Langleys day^{-1})

Dopt = depth of maximum algal production (m)

A minimum, Ismin, is specified for optimal illumination so that algae do not thrive at extremely low light levels. The time required for algae to adapt to changes in illumination is recognized by computing Is based on a time-weighted average of daily illumination:

$$Ioavg = 0.7\, Io + 0.2\, I1 + 0.1\, I2 \quad (6\text{-}11)$$

I1 = daily illumination one day preceding model day (Langleys day^{-1})

I2 = daily illumination two days preceding model day (Langleys day^{-1})

Four independent parameters influence the effect of light on algal production: FD, Ke, Dopt, and H. The parameters Ke and Dopt, and Ke and H occur as products, however, so the number of independent parameters that determine the light effect is actually three: FD, Ke * Dopt, and Ke * H.

Fractional daylength, FD, occurs as a multiplier and in the exponential terms of the integrated form of Steele's equation (Equation 6-6). The net effect of FD on the light function is nearly linear, however (Figure 6-2). At the latitude of Indian River, FD is limited to the range ≈0.4 to 0.6 so that f(I) varies by ≈50% from the shortest to longest day of the year.

A plot of the effects on growth of the pairs Ke * H and Ke * Dopt (Figure 6-3) has numerous interpretations. For Ke * H >> Ke * Dopt, growth diminishes as Ke * H increases. In other words, growth goes down as light extinction and/or depth increase. For much of the feasible range of Ke * H, growth is only weakly dependent on Dopt. This weak dependence was one factor in the selection of the light-effect formulation. Maximum growth occurs when Ke * H is slightly larger than Ke * Dopt (when H is slightly larger than Dopt). When Ke * H $\leq$ Ke * Dopt (H $\leq$ Dopt), growth is diminished from the maximum due to light levels in the majority of the water column occupying the supersaturated range for algal growth. For small Ke * H (shallow systems with little light attenuation) maximum growth occurs when Dopt = 0. When Dopt = 0, no portion of the water column is in the supersaturated range. For much of the feasible range of Ke * H, however, maximum production occurs when Dopt > 0. For this case, diminished production due to light supersaturation near the surface is offset by increased production at deeper depths.

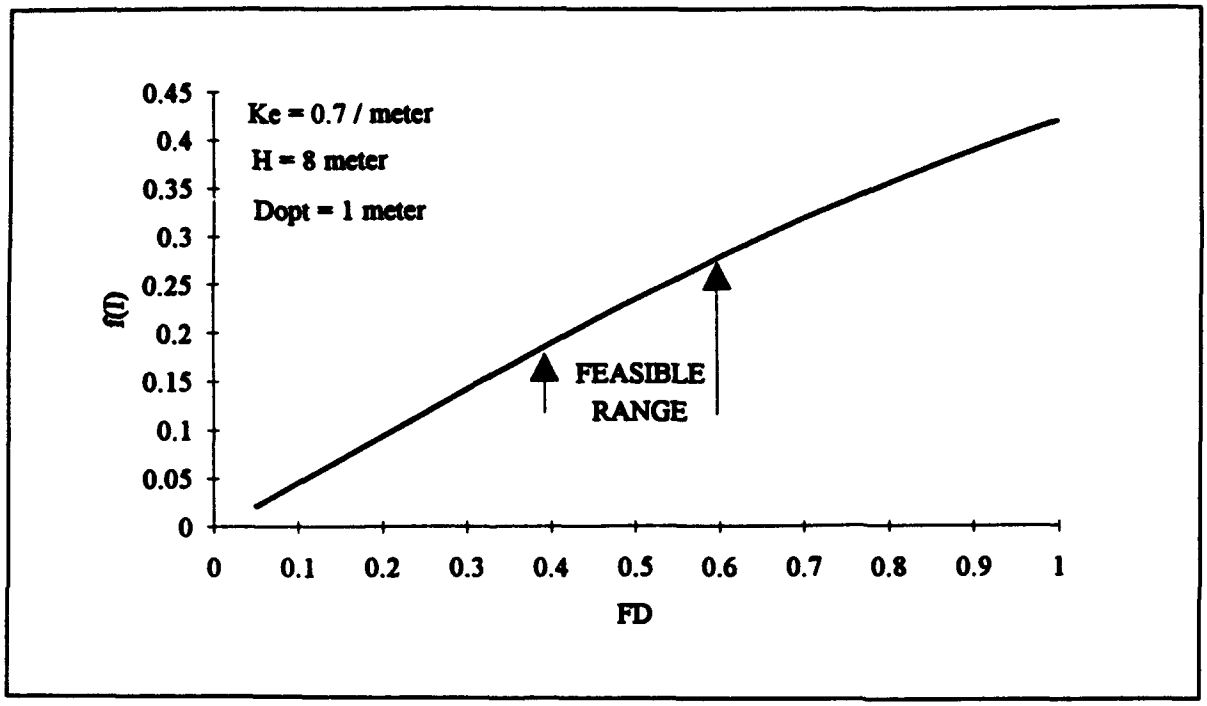

Figure 6-2. Effect of fractional daylength on algal light limitation

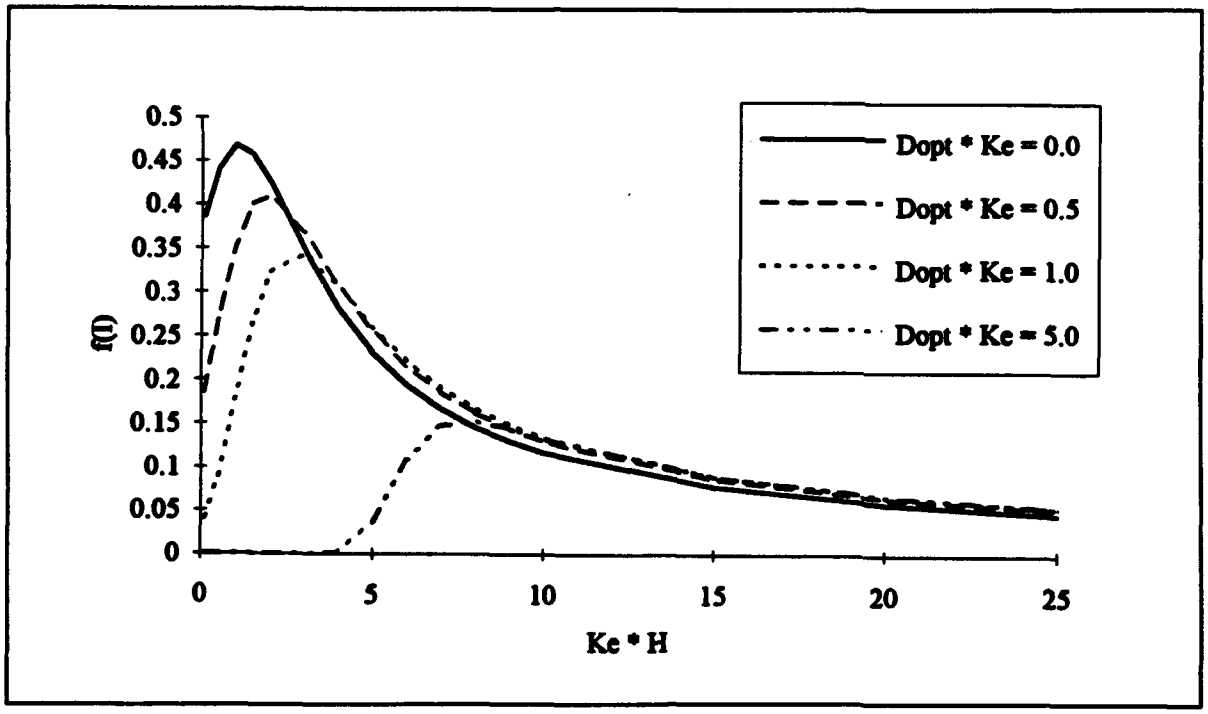

Figure 6-3. Effect of light extinction, total depth, and optimal depth on algal light limitation

Temperature

Algal production increases as a function of temperature until an optimum temperature or temperature range is reached. Above the optimum, production declines until a temperature lethal to the organisms is attained. Numerous functional representations of temperature effects are available. Inspection of growth versus temperature curves indicates a function similar to a Gaussian probability curve (Figure 6-4) provides a good fit to observations:

$$f(T) = e^{-KTg1\,(T - Tm)^2} \text{ when } T \leq Tm$$
$$= e^{-KTg2\,(Tm - T)^2} \text{ when } T > Tm \qquad (6\text{-}12)$$

T = temperature (C^o)

Tm = optimal temperature for algal growth (C^o)

KTg1 = effect of temperature below Tm on growth ($C^{o\,-2}$)

KTg2 = effect of temperature above Tm on growth ($C^{o\,-2}$)

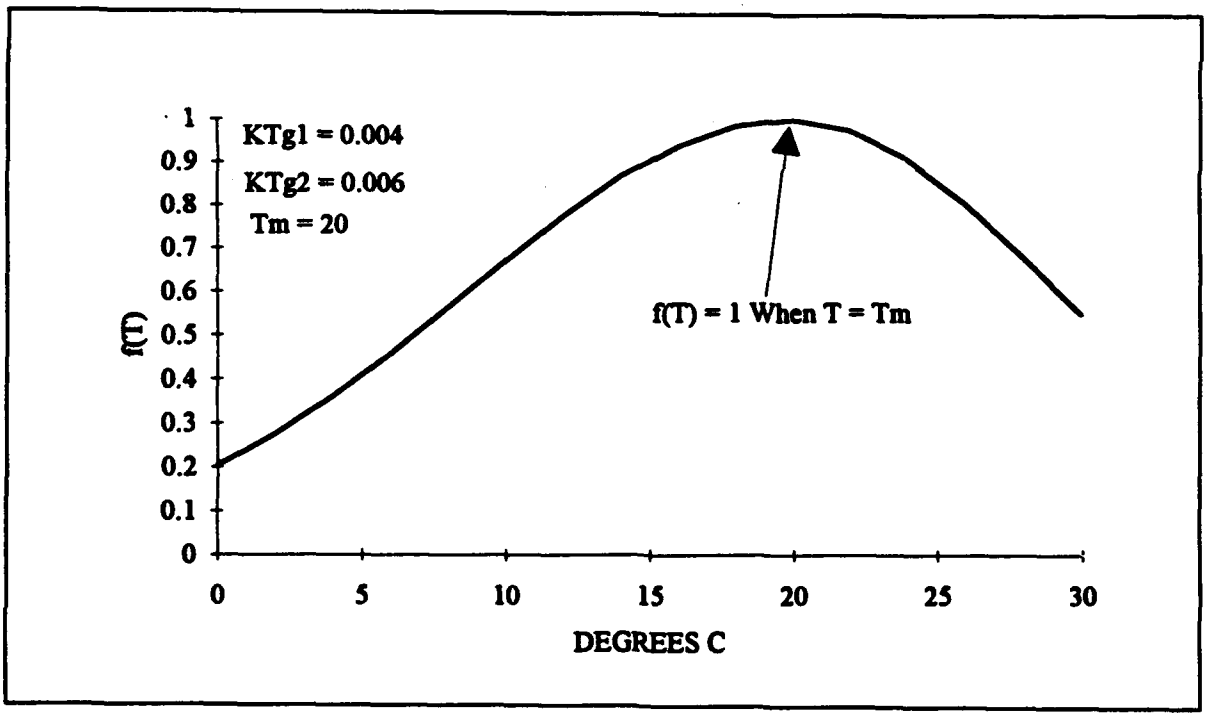

Figure 6-4. Effect of temperature on algal production

Basal Metabolism

As employed here, basal metabolism is the sum of all internal processes that decrease algal biomass. A portion of metabolism is respiration which may be viewed as a reversal of production. In respiration, carbon and nutrients are returned to the environment accompanied by the consumption of dissolved oxygen. A second internal sink of biomass is the excretion of dissolved organic carbon.

Respiration cannot proceed in the absence of oxygen. Basal metabolism cannot decrease in proportion to oxygen availability, however, or algae would approach immortality under anoxic conditions. To solve this dilemma, basal metabolism is considered to be independent of dissolved oxygen concentration but the distribution of metabolism between respiration and excretion is oxygen-dependent. When oxygen is freely available, respiration is a large fraction of the total. When oxygen is restricted, excretion becomes dominant. Formulation of this process is detailed in the text that describes algal effects on carbon and dissolved oxygen.

Basal metabolism is commonly considered to be an exponentially increasing (Figure 6-5) function of temperature:

$$BM = BMr\, e^{KTb\,(T - Tr)} \qquad (6\text{-}13)$$

BMr = metabolic rate at Tr (day^{-1})

KTb = effect of temperature on metabolism ($C^{o\,-1}$)

Tr = reference temperature for metabolism (C^{o})

Predation

Detailed specification of predation rate requires predictive modeling of zooplankton biomass and activity. At present, zooplankton are not included in the model. Consequently, a constant predation rate is specified. This specification implicitly assumes zooplankton biomass is a constant fraction of algal biomass. Zooplankton activity is assumed to be influenced by temperature and is taken into account by incorporating an exponential temperature relationship (Figure 6-5) into the predation term. The predation formulation is identical to basal metabolism. The difference in predation and basal metabolism lies in the distribution of the end products of these processes.

$$PR = BPR\, e^{KTb\,(T - Tr)} \qquad (6\text{-}14)$$

BPR = predation rate at Tr (day^{-1})

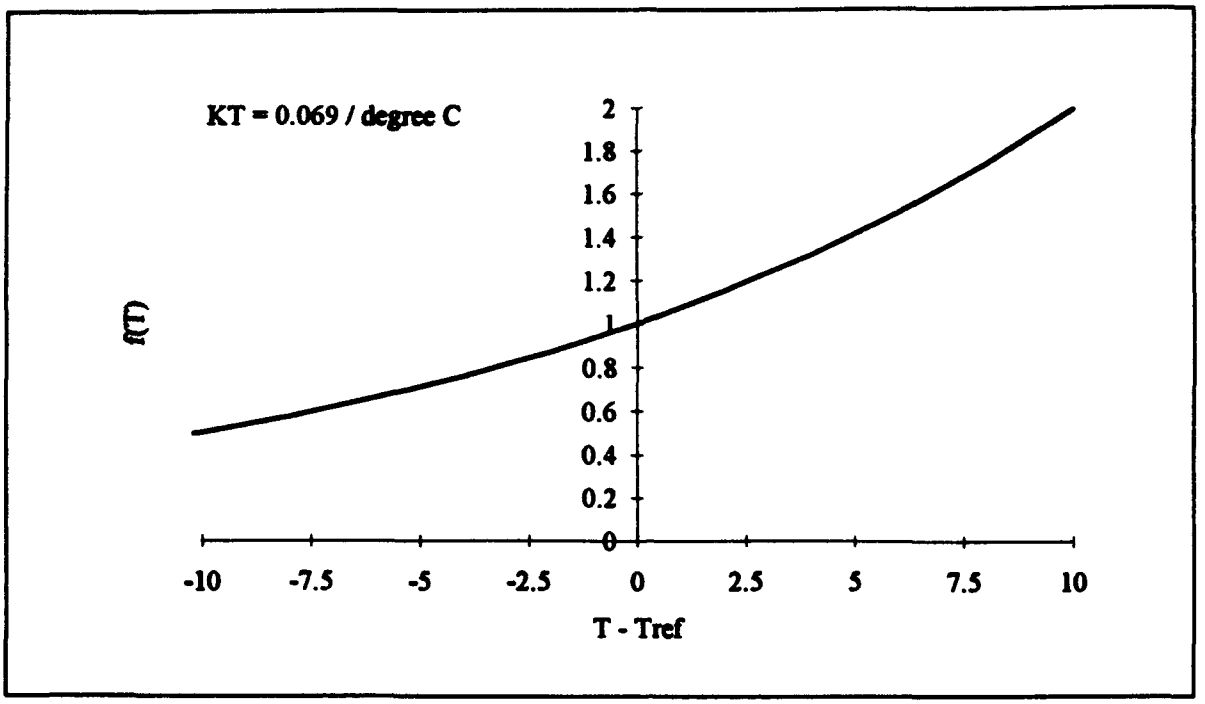

Figure 6-5. Exponential temperature function

Effect of Algae on Organic Carbon

During production and respiration, algae primarily take up and produce carbon dioxide, an inorganic form not considered in the model. A small fraction of basal metabolism is exuded as dissolved organic carbon, however, and in the model this fraction increases as dissolved oxygen becomes scarce. Algae also produce organic carbon through the effects of predation. Zooplankton take up and redistribute algal carbon through grazing, assimilation, respiration, and excretion. Since zooplankton are not included in the model, routing of algal carbon through zooplankton is simulated by empirical distribution coefficients. The effects of algae on organic carbon are expressed:

$$\frac{\delta}{\delta t}\mathrm{DOC} = \left(\left(\mathrm{FCD} + (1 - \mathrm{FCD})\frac{\mathrm{KHr}}{\mathrm{KHr} + \mathrm{DO}}\right)\mathrm{BM} + \mathrm{FCDP}\,\mathrm{PR}\right)\mathrm{B} \qquad (6\text{-}15)$$

$$\frac{\delta}{\delta t}\mathrm{LPOC} = \mathrm{FCLP}\,\mathrm{PR}\,\mathrm{B} \qquad (6\text{-}16)$$

$$\frac{\delta}{\delta t} RPOC = FCRP\ PR\ B \qquad (6\text{-}17)$$

DOC = dissolved organic carbon concentration (gm C m^{-3})

DO = dissolved oxygen concentration (gm O_2 m^{-3})

LPOC = labile particulate organic carbon concentration (gm C m^{-3})

RPOC = refractory particulate organic carbon concentration (gm C m^{-3})

FCD = fraction of basal metabolism exuded as dissolved organic carbon

KHr = half-saturation concentration for algal dissolved organic carbon excretion (gm O_2 m^{-3})

FCDP = fraction of dissolved organic carbon produced by predation

FCLP = fraction of labile particulate carbon produced by predation

FCRP = fraction of refractory particulate carbon produced by predation

The sum of the three predation fractions must equal unity.

Effect of Algae on Phosphorus

Algae take up dissolved phosphate during production and release dissolved phosphate and organic phosphorus through mortality. As with carbon, the fate of algal phosphorus released by metabolism and predation is represented by distribution coefficients. Since the total phosphate state variable includes both intra and extracellular phosphate, no explicit representation of the effect of algae on phosphate is necessary. Distribution of total phosphate is determined by partition coefficients as detailed in the "PHOSPHORUS" section of this chapter. The equations that express the effects of algae on organic phosphorus are:

$$\frac{\delta}{\delta t} DOP = (BM\ FPD + PR\ FPDP)\ APC\ B \qquad (6\text{-}18)$$

$$\frac{\delta}{\delta t} LPOP = (BM\ FPL + PR\ FPLP)\ APC\ B \qquad (6\text{-}19)$$

$$\frac{\delta}{\delta t} RPOP = (BM\ FPR + PR\ FPRP)\ APC\ B \qquad (6\text{-}20)$$

DOP = dissolved organic phosphorus concentration (gm P m^{-3})

LPOP = labile particulate organic phosphorus concentration (gm P m^{-3})

RPOP = refractory particulate organic phosphorus concentration (gm P m^{-3})

APC = algal phosphorus-to-carbon ratio (gm P gm^{-1} C)

FPD = fraction of dissolved organic phosphorus produced by metabolism

FPL = fraction of labile particulate phosphorus produced by metabolism

FPR = fraction of refractory particulate phosphorus produced by metabolism

FPDP = fraction of dissolved organic phosphorus produced by predation

FPLP = fraction of labile particulate phosphorus produced by predation

FPRP = fraction of refractory particulate phosphorus produced by predation

The sums of the metabolism and respiration fractions must each be less than or equal to unity.

Effect of Algae on Nitrogen

Algae take up ammonium and nitrate during production and release ammonium and organic nitrogen through mortality. Nitrate is internally reduced to ammonium before synthesis into biomass occurs (Parsons et al. 1984). Trace concentrations of ammonium inhibit nitrate reduction so that, in the presence of ammonium and nitrate, ammonium is utilized first. The "preference" of algae for ammonium can be expressed empirically (Thomann and Fitzpatrick 1982):

$$PN = NH_4 \frac{NO_3}{(KHn + NH_4)(KHn + NO_3)} + NH_4 \frac{KHn}{(NH_4 + NO_3)(KHn + NO_3)} \qquad (6\text{-}21)$$

PN = algal preference for ammonium uptake ($0 \leq PN \leq 1$)

The ammonium preference function (Figure 6-6) has two limiting values. When nitrate is absent, the preference for ammonium is unity. When ammonium is absent, the preference is zero. In the presence of ammonium and nitrate, the preference depends on the abundance of both forms relative to the half-saturation constant for nitrogen uptake. When both ammonium and nitrate are abundant, the preference for ammonium approaches unity. When ammonium is scarce but nitrate is abundant, the preference decreases in magnitude and a significant fraction of algal nitrogen requirement comes from nitrate.

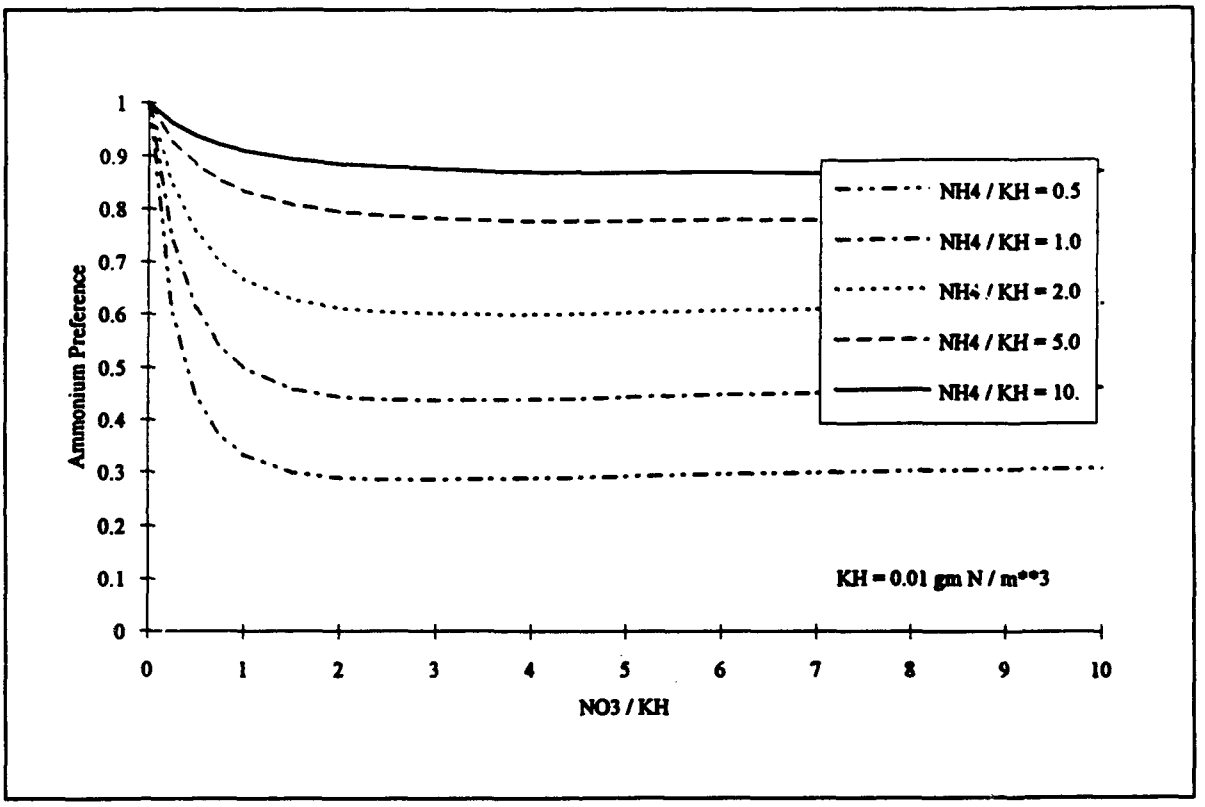

Figure 6-6. Ammonium preference function

The fate of algal nitrogen released by metabolism and predation is represented by distribution coefficients. The effects of algae on the nitrogen state variables are expressed:

$$\frac{\delta}{\delta t} NH_4 = (BM\,FNI + PR\,FNIP - PN\,P)\,ANC\,B \qquad (6\text{-}22)$$

$$\frac{\delta}{\delta t} NO_3 = (PN - 1)\, P\, ANC\, B \qquad (6\text{-}23)$$

$$\frac{\delta}{\delta t} DON = (BM\, FND + PR\, FNDP)\, ANC\, B \qquad (6\text{-}24)$$

$$\frac{\delta}{\delta t} LPON = (BM\, FNL + PR\, FNLP)\, ANC\, B \qquad (6\text{-}25)$$

$$\frac{\delta}{\delta t} RPON = (BM\, FNR + PR\, FNRP)\, ANC\, B \qquad (6\text{-}26)$$

DON = dissolved organic nitrogen concentration (gm N m^{-3})

LPON = labile particulate organic nitrogen concentration (gm N m^{-3})

RPON = refractory particulate organic nitrogen concentration (gm N m^{-3})

ANC = algal nitrogen-to-carbon ratio (gm N gm^{-1} C)

FNI = fraction of inorganic nitrogen produced by metabolism

FND = fraction of dissolved organic nitrogen produced by metabolism

FNL = fraction of labile particulate nitrogen produced by metabolism

FNR = fraction of refractory particulate nitrogen produced by metabolism

FNIP = fraction of inorganic nitrogen produced by predation

FNDP = fraction of dissolved organic nitrogen produced by predation

FNLP = fraction of labile particulate nitrogen produced by predation

FNRP = fraction of refractory particulate nitrogen produced by predation

The sums of the metabolism fractions and the predation fractions must each equal unity.

Algal Stoichiometry

Algal biomass is quantified in units of carbon. In order to express the effects of algae on nitrogen and phosphorus, the ratios of nitrogen-to-carbon and phosphorus-to-carbon in algal biomass must be specified. Global mean values of these ratios are well known (Redfield et al. 1966). Algal composition varies, however, especially as a function of nutrient availability. As nitrogen and phosphorus become scarce, algae adjust their composition so that smaller quantities of these vital nutrients are required to produce carbonaceous biomass (Droop 1973; DiToro 1980; Parsons et al. 1984).

Observations from upper Chesapeake Bay were examined to assess the potential variability of algal stoichiometry (Cerco and Cole 1993). The variation of carbon-to-nitrogen stoichiometry in the upper Bay was small. As a consequence of these observations, the model formulation specified constant algal nitrogen-to-carbon ratio, ANC. Large variations in carbon-to-phosphorus ratio occurred, however. To account for this effect, a variable algal phosphorus-to-carbon ratio, APC, was formulated in the model. Variable stoichiometry was not employed in the Indian River-Rehoboth Bay application. The formulation that allowed variable APC required distinctive treatment of the phosphate state variable, however.

Effect of Algae on Dissolved Oxygen

Algae produce oxygen during photosynthesis and consume oxygen through respiration. The quantity produced depends on the form of nitrogen utilized for growth. More oxygen is produced, per unit of carbon fixed, when nitrate is the algal nitrogen source than when ammonium is the source. Equations describing algal uptake of carbon and nitrogen and production of dissolved oxygen (Morel 1983) are:

$$106\,CO_2 + 16\,NH_4^+ + H_2PO_4^- + 106\,H_2O \rightarrow \text{protoplasm} + 106\,O_2 + 15\,H^+ \qquad (6\text{-}27)$$

$$106\,CO_2 + 16\,NO_3^- + H_2PO_4^- + 122\,H_2O + 17\,H^+ \rightarrow \text{protoplasm} + 138\,O_2 \qquad (6\text{-}28)$$

When ammonium is the nitrogen source, one mole oxygen is produced per mole carbon dioxide fixed. When nitrate is the nitrogen source, 1.3 moles oxygen are produced per mole carbon dioxide fixed.

The equation that describes the effect of algae on dissolved oxygen in the model is:

$$\frac{\delta}{\delta t} DO = \left((1.3 - 0.3\,PN)\,P - \frac{DO}{KHr + DO} BM \right) AOCR\,B \qquad (6\text{-}29)$$

AOCR = dissolved oxygen-to-carbon ratio in respiration (2.67 gm O_2 gm^{-1} C)

The magnitude of AOCR is derived from a simple representation of the respiration process:

$$CH_2O + O_2 = CO_2 + H_2O \qquad (6\text{-}30)$$

The quantity (1.3 - 0.3 PN) is the photosynthesis ratio and expresses the molar quantity of oxygen produced per mole carbon fixed. The photosynthesis ratio approaches unity as the algal preference for ammonium approaches unity.

Organic Carbon

Organic carbon undergoes innumerable transformations in the water column. The model carbon cycle (Figure 6-7) consists of the following elements:

Phytoplankton production
Phytoplankton exudation
Predation on phytoplankton
Dissolution of particulate carbon
Heterotrophic respiration
Denitrification
Settling

Algal production is the primary carbon source although carbon also enters the system through external loading. Predation on algae releases particulate and dissolved organic carbon to the water column. A fraction of the particulate organic carbon undergoes first-order dissolution to dissolved organic carbon. The remainder settles to the sediments. Dissolved organic carbon

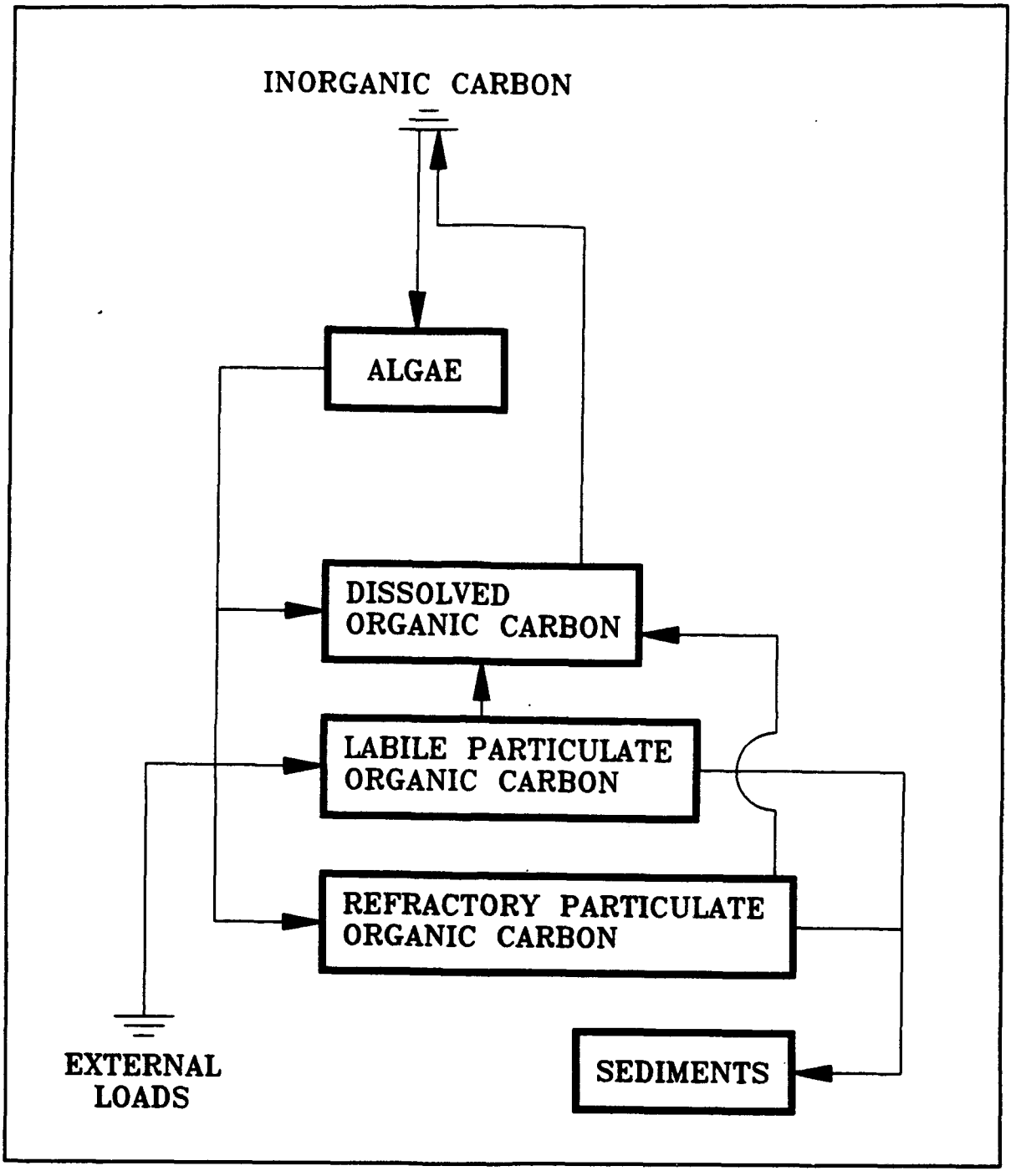

Figure 6-7. The model carbon cycle

produced by phytoplankton exudation, by predation, and by dissolution is respired or denitrified at a first-order rate to inorganic carbon. No carbon is recycled from the sediments to the water column.

Dissolution and Respiration Rates

Dissolution and respiration rates depend on the availability of carbonaceous substrate and on heterotrophic activity. Heterotrophic activity and biomass have been correlated with algal activity and biomass across a wide range of natural systems (Bird and Kalff 1984; Cole et al. 1988). Consequently, algal biomass can be incorporated into dissolution and respiration rate formulations as a surrogate for heterotrophic activity. The correlation between algae and heterotrophs occurs because algae produce labile carbon that fuels heterotrophic activity. Dissolution and respiration processes do not require the presence of algae, however, and may be fueled entirely by external carbon inputs. Representation of dissolution and respiration in the model allows specification of algal-dependent and algal-independent rates:

$$Kdoc = Kdc + Kdcalg\,B \tag{6-31}$$

Kdoc = respiration rate of dissolved organic carbon (day^{-1})

Kdc = minimum respiration rate (day^{-1})

Kdcalg = constant that relates respiration to algal biomass ($m^3\ gm^{-1}$ C day^{-1})

$$Klpoc = Klc + Klcalg\,B \tag{6-32}$$

Klpoc = dissolution rate of labile particulate organic carbon (day^{-1})

Klc = minimum dissolution rate (day^{-1})

Klcalg = constant that relates dissolution to algal biomass ($m^3\ gm^{-1}$ C day^{-1})

$$Krpoc = Krc + Krcalg\,B \tag{6-33}$$

Krpoc = dissolution rate of refractory particulate organic carbon (day^{-1})

Krc = minimum dissolution rate (day^{-1})

Krcalg = constant that relates dissolution to algal biomass ($m^3\ gm^{-1}$ C day^{-1})

An exponential function (Figure 6-5) relates dissolution and respiration to temperature.

Denitrification

As oxygen is depleted from natural systems, oxidation of organic matter is effected by the reduction of alternate oxidants (referred to as "alternate electron acceptors"). The sequence in which alternate acceptors are employed is determined by the thermodynamics of oxidation-reduction reactions. The first substance reduced in the absence of oxygen is nitrate. A representation of the denitrification reaction can be obtained by balancing standard half-cell redox reactions (Stumm and Morgan 1981):

$$4\,NO_3^- + 4\,H^+ + 5\,CH_2O \longrightarrow 2\,N_2 + 7\,H_2O + 5\,CO_2 \qquad (6\text{-}34)$$

Equation 6-34 describes the stoichiometry of the denitrification reaction. The kinetics of the reaction, represented in the model, are first-order. The dissolved organic carbon respiration rate, Kdoc, is modified so that significant decay via denitrification occurs only when nitrate is freely available and dissolved oxygen is depleted (Figure 6-8). A parameter is included so that the anoxic respiration rate is slower than oxic respiration:

$$\text{Denit} = \frac{\text{KHodoc}}{\text{KHodoc} + \text{DO}} \frac{NO_3}{\text{KHndn} + NO_3} \text{AANOX Kdoc} \qquad (6\text{-}35)$$

Denit = denitrification rate of dissolved organic carbon (day^{-1})

AANOX = ratio of denitrification to oxic carbon respiration rate ($0 \leq \text{AANOX} \leq 1$)

KHodoc = half-saturation concentration of dissolved oxygen required for oxic respiration (gm O_2 m^{-3})

KHndn = half-saturation concentration of nitrate required for denitrification (gm N m^{-3})

An exponential function (Figure 6-5) relates denitrification to temperature. Coefficient values in the function are the same as for dissolved organic carbon respiration.

Dissolved Organic Carbon

The complete representation of all dissolved organic carbon sources and sinks in the model ecosystem is:

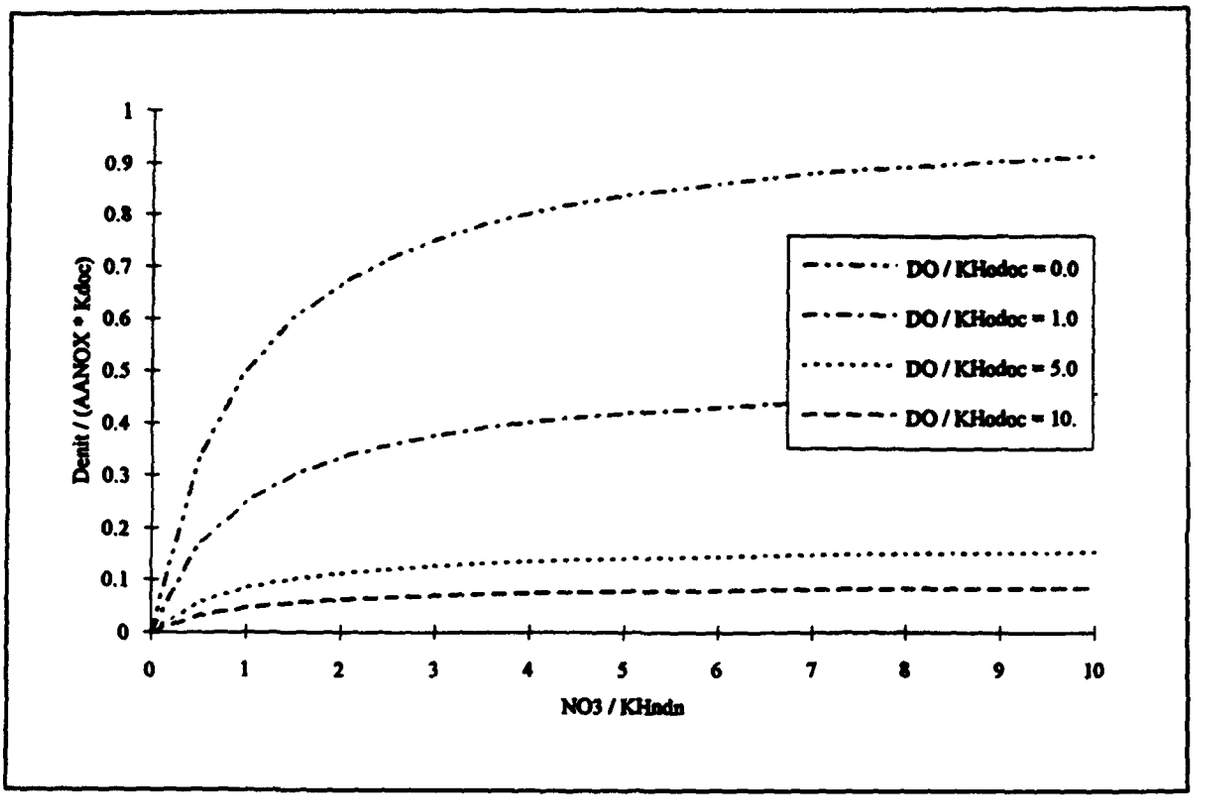

Figure 6-8. Effect of nitrate and dissolved oxygen on denitrification rate

$$\frac{\delta}{\delta t} DOC =$$

$$\left(\left(FCD + (1 - FCD)\frac{KHr}{KHr + DO}\right)BM + FCDP\,PR\right)B \qquad (6\text{-}36)$$

$$+ Klpoc\,LPOC + Krpoc\,RPOC - \frac{DO}{KHodoc + DO} Kdoc\,DOC$$

$$- Denit\,DOC$$

Labile Particulate Organic Carbon

The complete representation of all labile particulate organic carbon sources and sinks in the model ecosystem is:

$$\frac{\delta}{\delta t} LPOC = FCLP\,PR\,B - Klpoc\,LPOC - \frac{WSl}{H} LPOC \qquad (6\text{-}37)$$

WSl = settling velocity of labile particles (m day^{-1})

Refractory Particulate Organic Carbon

The complete representation of all refractory particulate organic carbon sources and sinks in the model ecosystem is:

$$\frac{\delta}{\delta t} RPOC = FCRP\,PR\,B - Krpoc\,RPOC - \frac{WSr}{H} RPOC \qquad (6\text{-}38)$$

WSr = settling velocity of labile particles (m day^{-1})

Phosphorus

The model phosphorus cycle (Figure 6-9) includes the following processes:

Algal production and metabolism
Predation
Hydrolysis of particulate organic phosphorus
Mineralization of dissolved organic phosphorus
Settling

External loads provide the ultimate source of phosphorus to the system. Dissolved phosphate is incorporated by algae during growth and released as phosphate and organic phosphorus through respiration and predation. A portion of the particulate organic phosphorus hydrolyzes to dissolved organic phosphorus. Dissolved organic phosphorus is mineralized to phosphate. Particulate organic phosphorus which is not mineralized in the water column settles to the sediments. The sediments recycle phosphorus to the water column as dissolved phosphate. Direct, mechanistic linkage of phosphorus release to settling of organic phosphorus is not activated in this model application, however.

Effects on phosphorus of algal production, metabolism, and predation have already been detailed. Descriptions of hydrolysis and mineralization and of the total phosphate system follow.

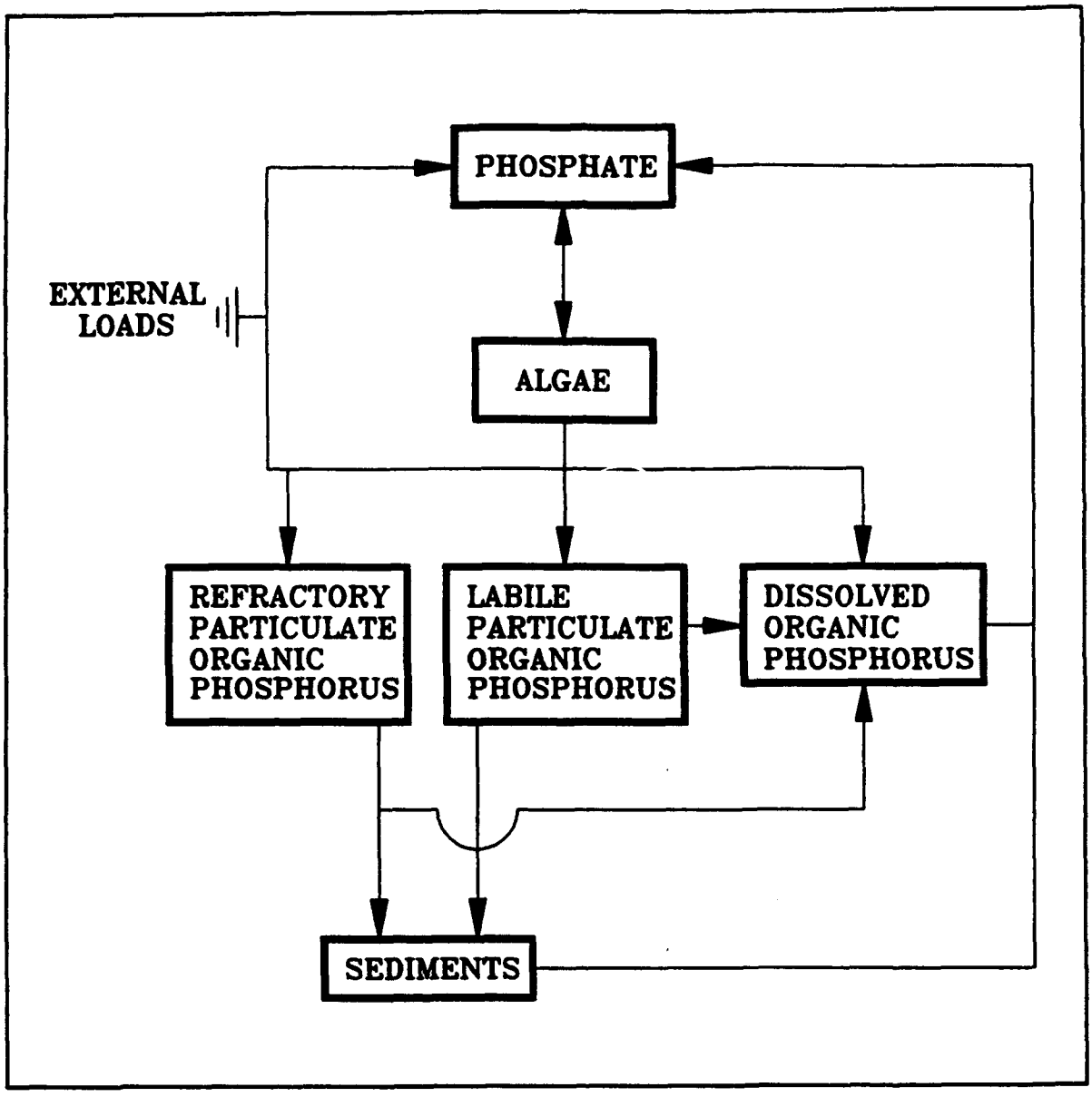

Figure 6-9. The model phosphorus cycle

Hydrolysis and Mineralization

Within the model, hydrolysis is defined as the process by which particulate organic substances are converted to dissolved organic form. Mineralization is defined as the process by which dissolved organic substances are converted to dissolved inorganic form. Conversion of particulate organic phosphorus to phosphate proceeds through the sequence of hydrolysis and mineralization. Direct mineralization of particulate organic phosphorus does not occur.

Mineralization of organic phosphorus is mediated by the release of nucleotidase and phosphatase enzymes by bacteria (Ammerman and Azam 1985; Chrost and Overbeck 1987) and algae (Matavulj and Flint 1987; Chrost and

Overbeck 1987; Boni et al. 1989). Since the algae themselves release the enzyme and since bacterial abundance is related to algal biomass, the rate of organic phosphorus mineralization is related, in the model, to algal biomass. A most remarkable property of the enzyme process is that alkaline phosphatase activity is inversely proportional to ambient phosphate concentration (Chrost and Overbeck 1987; Boni et al. 1989). Put in different terms, when phosphate is scarce, algae stimulate production of an enzyme that mineralizes organic phosphorus to phosphate. This phenomenon is simulated by relating mineralization to the algal phosphorus nutrient limitation. Mineralization is highest when algae are strongly phosphorus limited and is least when no limitation occurs.

Expressions for mineralization and hydrolysis rates are:

$$Kdop = Kdp + \frac{KHp}{KHp + PO_4d} Kdpalg\ B \qquad (6\text{-}39)$$

Kdop = mineralization rate of dissolved organic phosphorus (day^{-1})

Kdp = minimum mineralization rate (day^{-1})

Kdpalg = constant that relates mineralization to algal biomass ($m^3\ gm^{-1}\ C\ day^{-1}$)

$$Klpop = Klp + \frac{KHp}{KHp + PO_4d} Klpalg\ B \qquad (6\text{-}40)$$

Klpop = hydrolysis rate of labile particulate phosphorus (day^{-1})

Klp = minimum hydrolysis rate (day^{-1})

Klpalg = constant that relates hydrolysis to algal biomass ($m^3\ gm^{-1}\ C\ day^{-1}$)

$$Krpop = Krp + \frac{KHp}{KHp + PO_4d} Krpalg\ B \qquad (6\text{-}41)$$

Krpop = hydrolysis rate of refractory particulate phosphorus (day^{-1})

Krp = minimum hydrolysis rate (day^{-1})

Krpalg = constant that relates hydrolysis to algal biomass ($m^3\ gm^{-1}\ C\ day^{-1}$)

An exponential function (Figure 6-5) relates mineralization and hydrolysis rates to temperature.

Potential effects of algal biomass and nutrient limitation on mineralization and hydrolysis rates shown in Figure 6-10. When nutrient concentration greatly exceeds the half-saturation concentration for algal uptake, the rate roughly equals the minimum. Algal biomass has little influence. As nutrient becomes scarce relative to the half-saturation concentration, the rate increases. The magnitude of increase depends on algal biomass. Factor of two to three increases are feasible.

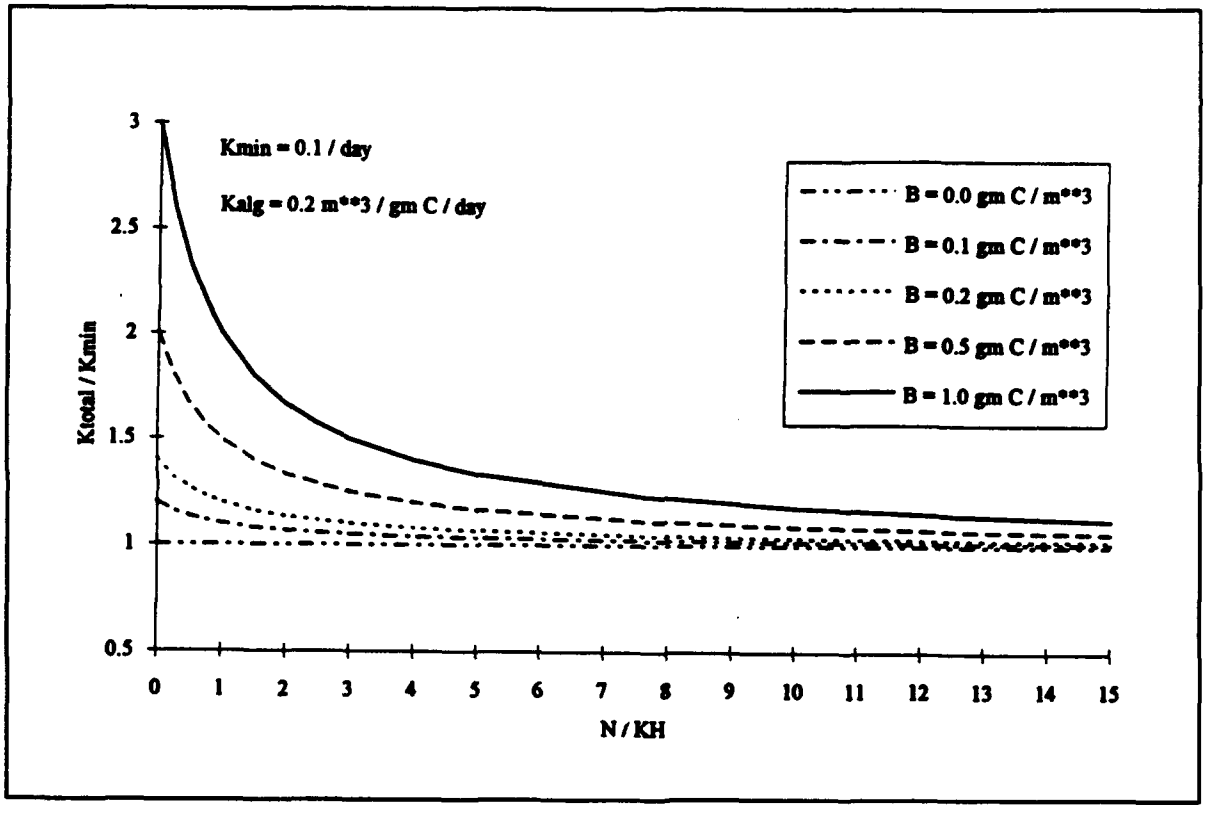

Figure 6-10. Effect of algal biomass and nutrient concentration on hydrolysis and mineralization

The Total Phosphate System

The model phosphate state variable is defined as the sum of dissolved phosphate and algal phosphorus content:

$$PO_4t = PO_4d + PO_4a \quad (6\text{-}42)$$

PO_4t = total phosphate (gm P m^{-3})

PO_4d = dissolved phosphate (gm P m^{-3})

PO_4a = algal phosphorus (gm P m^{-3})

The partitioning of phosphate into extra-cellular and intra-cellular fractions is required in the formulation of variable phosphorus stoichiometry. When variable stoichiometry is activated, algal phosphate is computed as a function of available nutrient. In the Indian River-Rehoboth Bay application, however, constant phosphorus stoichiometry is employed. Algal phosphate is computed:

$$PO_4a = APC\,B \quad (6\text{-}43)$$

Dissolved phosphate is the fraction of total phosphate not incorporated in algal biomass:

$$PO_4d = PO_4t - APC\,B \quad (6\text{-}44)$$

Phosphate

The balance of the equations describing phosphorus are straightforward summations of previously-described sources and sinks:

$$\frac{\delta}{\delta t} PO_4t = - \frac{WSa}{H} APC\,B + Kdop\,DOP \quad (6\text{-}45)$$

Algal uptake and release of phosphate represents an exchange of phosphate fractions rather than a phosphate source or sink. Consequently, no algal source or sink terms are included in the phosphate mass-conservation equation. The settling term represents the settling of phosphate incorporated in algal biomass.

Dissolved Organic Phosphorus

$$\frac{\delta}{\delta t} DOP = (BM\,FPD + PR\,FPDP)\,APC\,B + Klpop\,LPOP + Krpop\,RPOP - Kdop\,DOP \quad (6\text{-}46)$$

Labile Particulate Organic Phosphorus

$$\frac{\delta}{\delta t} LPOP = (BM\,FPL + PR\,FPLP)\,APC\,B - Klpop\,LPOP - \frac{WSl}{H} LPOP \quad (6\text{-}47)$$

Refractory Particulate Organic Phosphorus

$$\frac{\delta}{\delta t} RPOP = (BM\,FPR + PR\,FPRP)\,APC\,B - Krpop\,RPOP - \frac{WSr}{H} RPOP \quad (6\text{-}48)$$

Nitrogen

The model nitrogen cycle (Figure 6-11) includes the following processes:

Algal production and metabolism
Predation
Hydrolysis of particulate organic nitrogen
Mineralization of dissolved organic nitrogen
Settling
Nitrification
Denitrification

External loads provide the ultimate source of nitrogen to the system. Inorganic nitrogen is incorporated by algae during growth and released as ammonium and organic nitrogen through respiration and predation. A portion of the particulate organic nitrogen hydrolyzes to dissolved organic nitrogen.

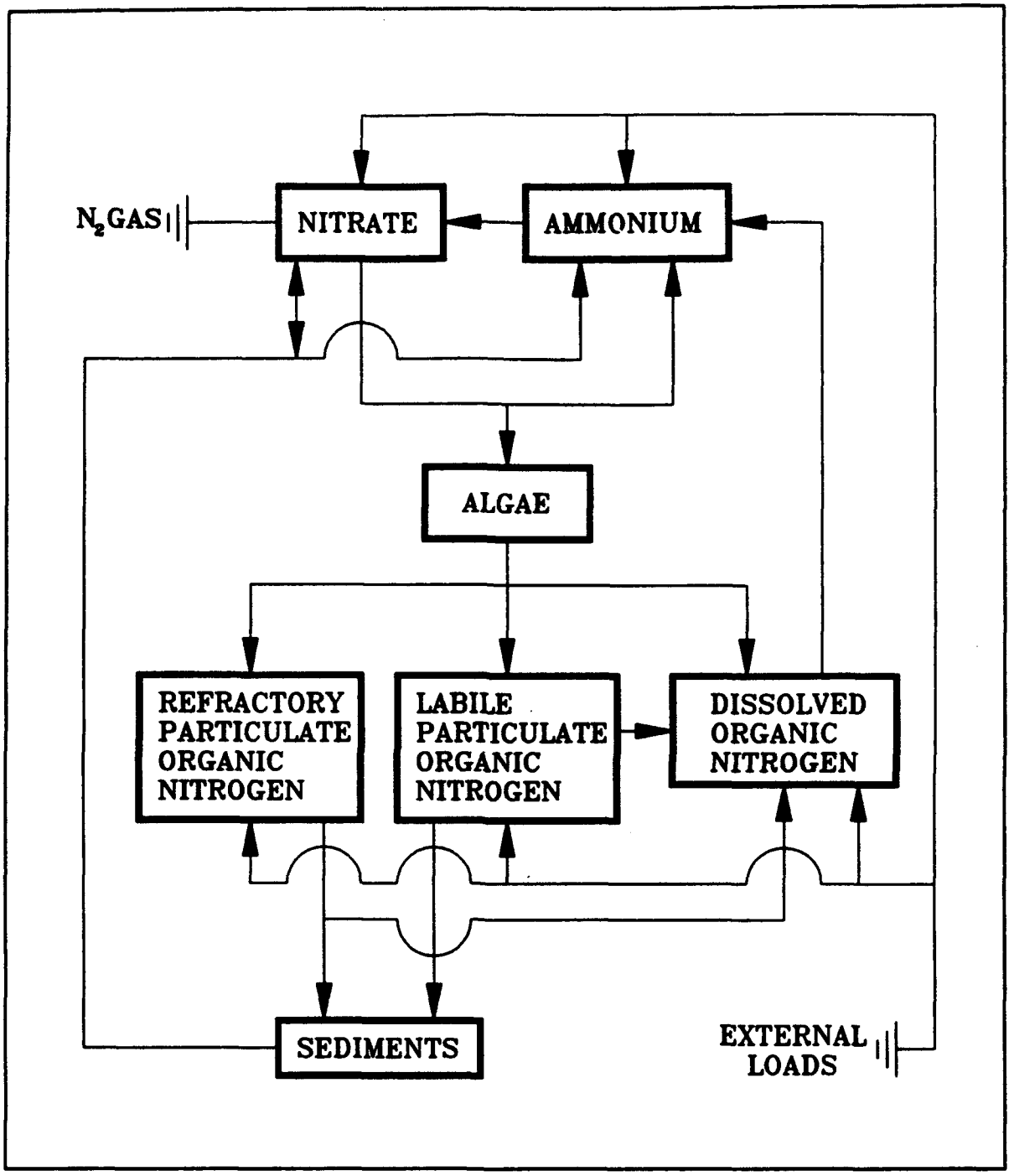

Figure 6-11. The model nitrogen cycle

The balance settles to the sediments. Dissolved organic nitrogen is mineralized to ammonium. In an oxygenated water column, a fraction of the ammonium is subsequently oxidized to nitrate through the nitrification process. In anoxic water, nitrate is lost to nitrogen gas through denitrification. Particulate nitrogen that settles to the sediments is mineralized and recycled to the water column, primarily as ammonium. Direct, mechanistic linkage of ammonium

release to nitrogen settling is not activated in this model application, however. Nitrate moves in both directions across the sediment-water interface, depending on relative concentrations in the water column and sediment interstices.

Effects on nitrogen of algal production, metabolism, and predation have already been detailed. Descriptions of hydrolysis, mineralization, nitrification and denitrification follow.

Hydrolysis and Mineralization

In the model, particulate organic nitrogen is converted to the dissolved organic form via hydrolysis. Dissolved organic nitrogen is converted to ammonium through mineralization. Conversion of particulate nitrogen to ammonium proceeds through the sequence of hydrolysis and mineralization. Direct mineralization of particulate nitrogen does not occur. The argument for accelerated hydrolysis and mineralization during nutrient-limited conditions is not as clear for nitrogen as for phosphorus. The same formulations are made available for nitrogen as for phosphorus, however. Accelerated processes can be activated or deactivated through parameter selection. The nitrogen hydrolysis and mineralization formulations are:

$$Kdon = Kdn + \frac{KHn}{KHn + NH_4 + NO_3} Kdnalg\ B \qquad (6\text{-}49)$$

Kdon = mineralization rate of dissolved organic nitrogen (day^{-1})

Kdn = minimum mineralization rate (day^{-1})

Kdnalg = constant that relates mineralization to algal biomass ($m^3\ gm^{-1}\ C\ day^{-1}$)

$$Klpon = Kln + \frac{KHn}{KHn + NH_4 + NO_3} Klnalg\ B \qquad (6\text{-}50)$$

Klpon = hydrolysis rate of labile particulate nitrogen (day^{-1})

Kln = minimum hydrolysis rate (day^{-1})

Klnalg = constant that relates hydrolysis to algal biomass ($m^3\ gm^{-1}\ C\ day^{-1}$)

$$Krpon = Krn + \frac{KHn}{KHn + NH_4 + NO_3} Krnalg\ B \qquad (6\text{-}51)$$

Krpon = hydrolysis rate of refractory particulate nitrogen (day^{-1})

Krn = minimum hydrolysis rate (day^{-1})

Krnalg = constant that relates hydrolysis to algal biomass ($m^3\ gm^{-1}$ C day^{-1})

An exponential function (Figure 6-5) relates mineralization and hydrolysis rates to temperature.

Nitrification

Nitrification is a process mediated by specialized groups of autotrophic bacteria that obtain energy through the oxidation of ammonium to nitrite and oxidation of nitrite to nitrate. A simplified expression for complete nitrification (Tchobanoglous and Schroeder 1987) is:

$$NH_4^+ + 2\,O_2 \longrightarrow NO_3^- + H_2O + 2\,H^+ \qquad (6\text{-}52)$$

The equation indicates that two moles of oxygen are required to nitrify one mole of ammonium into nitrate. The simplified equation is not strictly true, however. Cell synthesis by nitrifying bacteria is accomplished by the fixation of carbon dioxide so that less than two moles of oxygen are consumed per mole ammonium utilized (Wezernak and Gannon 1968).

The kinetics of complete nitrification are modelled as a function of available ammonium, dissolved oxygen, and temperature:

$$NT = \frac{DO}{KHont + DO} \frac{NH_4}{KHnnt + NH_4} f(T)\,NTm \qquad (6\text{-}53)$$

NT = nitrification rate (gm N m^{-3} day^{-1})

KHont = half-saturation constant of dissolved oxygen required for nitrification (gm O_2 m^{-3})

KHnnt = half-saturation constant of NH_4 required for nitrification (gm N m^{-3})

NTm = maximum nitrification rate at optimal temperature (gm N m^{-3} day^{-1})

The kinetics formulation (Figure 6-12) incorporates the products of two "Monod" functions. The first function diminishes nitrification at low dissolved oxygen concentration. The second function expresses the influence of ammonium concentration on nitrification. When ammonium concentration is low, relative to KHnnt, nitrification is proportional to ammonium concentration. For NH4 << KHnnt, the reaction is approximately first-order. (The first-order decay constant ≈ NTm/KHnnt.) When ammonium concentration is large, relative to KHnnt, nitrification approaches a maximum rate. This formulation is based on a concept proposed by Tuffey et al. (1974). Nitrifying bacteria adhere to benthic or suspended sediments. When ammonium is scarce, vacant surfaces suitable for nitrifying bacteria exist. As ammonium concentration increases, bacterial biomass increases, vacant surfaces are occupied, and the rate of nitrification increases. The bacterial population attains maximum density when all surfaces suitable for bacteria are occupied. At this point, nitrification proceeds at a maximum rate independent of additional increase in ammonium concentration.

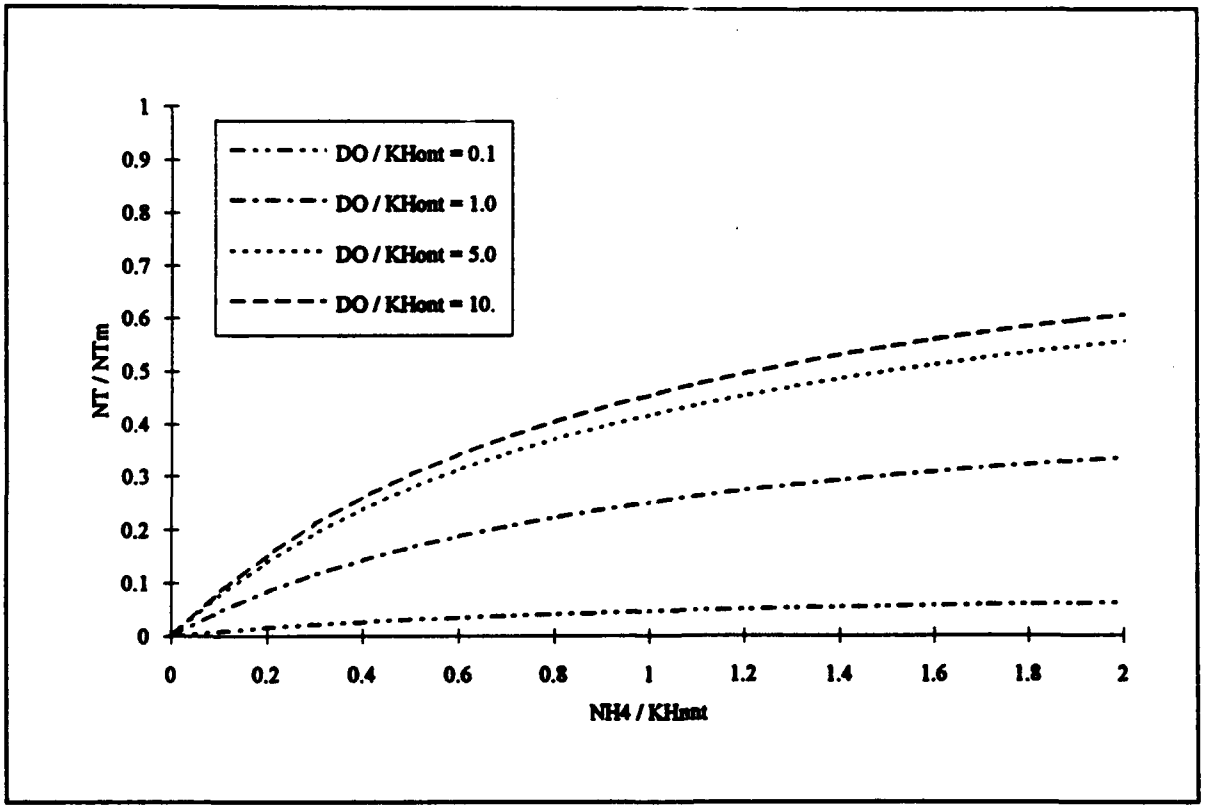

Figure 6-12. Effect of dissolved oxygen and ammonium concentration on nitrification rate

The optimal temperature for nitrification may be less than peak temperatures that occur in coastal waters. To allow for a decrease in nitrification at superoptimal temperature, the effect of temperature on nitrification is modelled in the Gaussian form of Equation 6-4.

Effect of Nitrification on Ammonium

$$\frac{\delta}{\delta t} NH_4 = - NT \qquad (6\text{-}54)$$

Effect of Nitrification on Nitrate

$$\frac{\delta}{\delta t} NO_3 = NT \qquad (6\text{-}55)$$

Effect of Nitrification on Dissolved Oxygen

$$\frac{\delta}{\delta t} DO = - AONT\, NT \qquad (6\text{-}56)$$

AONT = mass dissolved oxygen consumed per mass ammonium-nitrogen nitrified (4.33 gm O_2 gm^{-1} N)

Effect of Denitrification on Nitrate

The effect of denitrification on dissolved organic carbon has been described. Denitrification removes nitrate from the system in stoichiometric proportion to carbon removal as determined by Equation 6-34:

$$\frac{\delta}{\delta t} NO_3 = - ANDC\, Denit\, DOC \qquad (6\text{-}57)$$

ANDC = mass nitrate-nitrogen reduced per mass dissolved organic carbon oxidized (0.933 gm N gm^{-1} C)

Nitrogen Mass Balance Equations

The mass-balance equations for nitrogen state variables are written by summing all previously-described sources and sinks:

Ammonium

$$\frac{\delta}{\delta t} NH_4 = (BM\,FNI + PR\,FNIP - PN\,P)\,ANC\,B + Kdon\,DON - NT \tag{6-58}$$

Dissolved Organic Nitrogen

$$\frac{\delta}{\delta t} DON = (BM\,FND + PR\,FNDP)\,ANC\,B + Klpon\,LPON + Krpon\,RPON - Kdon\,DON \tag{6-59}$$

Labile Particulate Organic Nitrogen

$$\frac{\delta}{\delta t} LPON = (BM\,FNL + PR\,FNLP)\,ANC\,B - Klpon\,LPON - \frac{WSl}{H} LPON \tag{6-60}$$

Refractory Particulate Organic Nitrogen

$$\frac{\delta}{\delta t} RPON = (BM\,FNR + PR\,FNRP)\,ANC\,B - Krpon\,RPON - \frac{WSr}{H} RPON \tag{6-61}$$

Nitrate

$$\frac{\delta}{\delta t} NO_3 = (PN - 1)\, P\, ANC\, B + NT - ANDC\, Denit\, DOC \quad (6\text{-}62)$$

Dissolved Oxygen

Sources and sinks of dissolved oxygen in the water column (Figure 6-13) include:

Algal photosynthesis
Atmospheric reaeration
Algal respiration
Heterotrophic respiration
Nitrification

Reaeration

The rate of reaeration is proportional to the dissolved oxygen deficit in surface waters:

$$\frac{\delta}{\delta t} DO = \frac{Kr}{H} (DOs - DO) \quad (6\text{-}63)$$

Kr = reaeration coefficient (m day^{-1})

DOs = dissolved oxygen saturation concentration (gm O_2 m^{-3})

The surface renewal concept, attributed to Danckwerts by O'Connor and Dobbins (1958), indicates:

$$Kr = \sqrt{Dl\, R} \quad (6\text{-}64)$$

Dl = molecular diffusivity of oxygen in water ($\approx$1.7 x 10-4 m^2 day^{-2})

R = surface renewal rate (day^{-1})

Specification of the surface renewal rate is the fundamental problem in reaeration theory. O'Connor and Dobbins (1958) state that, in isotropic turbulence, surface renewal can be approximated as the ratio of stream velocity to

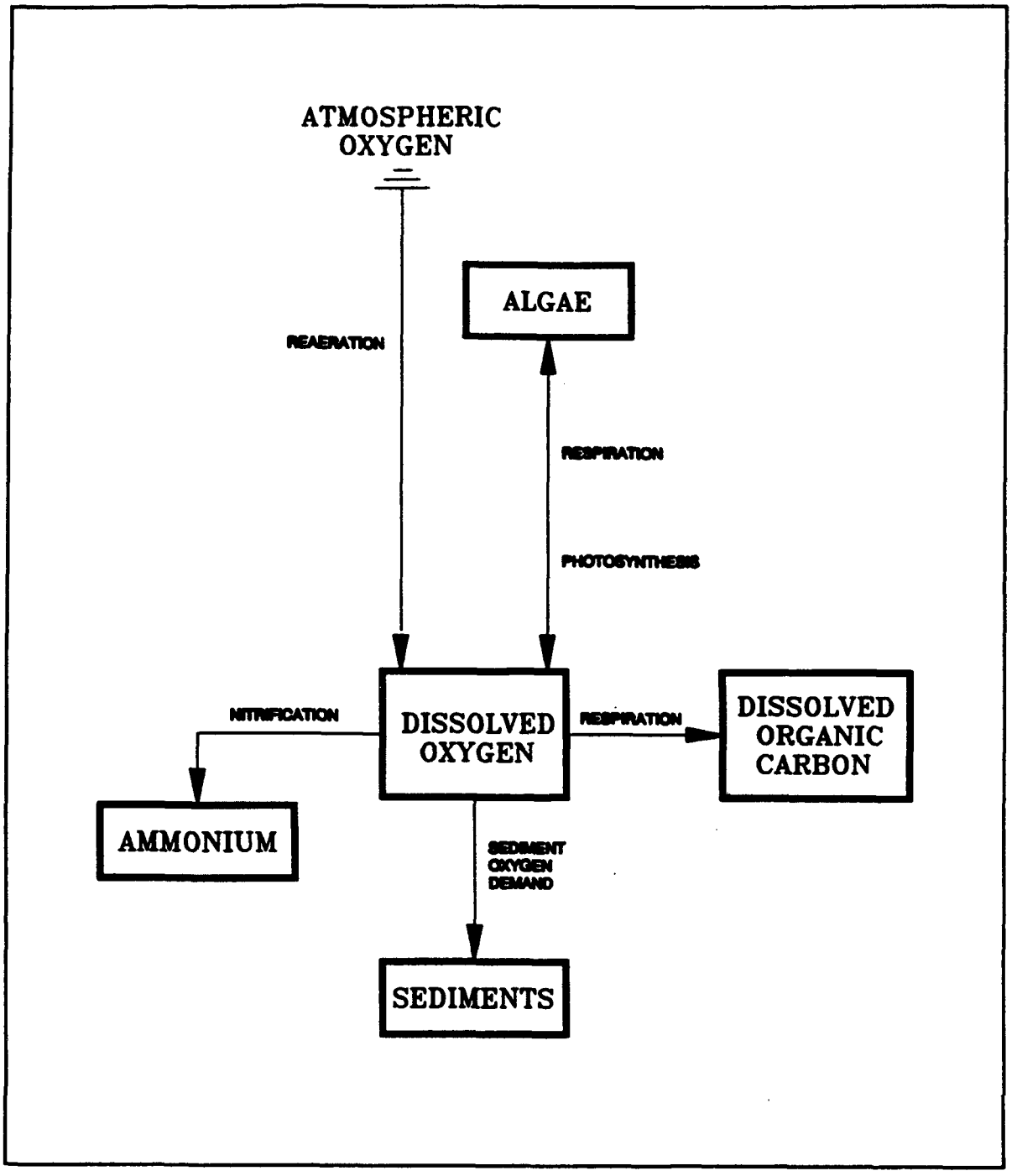

Figure 6-13. Dissolved oxygen sources and sinks

depth. The renewal rate is also influenced by wind, however (O'Connor 1983). Influences on reaeration of temperature (ASCE 1961) and salinity (Wen et al. 1984), most likely effected through changes in diffusivity, have been measured. No single theory that unites all these factors into a formulation of reaeration in an estuary is available. The surface renewal concept is retained in this study with the renewal rate treated as a calibration parameter.

Saturation dissolved oxygen concentration diminishes as temperature and salinity increase. An empirical formula that describes these effects (Genet et al. 1974) is:

$$DOs = 14.5532 - 0.38217\,T + 0.0054258\,T^2 - CL\,(1.665 \times 10^{-4} - 5.866 \times 10^{-6}\,T + 9.796 \times 10^{-8}\,T^2) \quad (6\text{-}65)$$

CL = chloride concentration (= salinity/1.80655)

Summary of Dissolved Oxygen Sources and Sinks

The complete kinetics for dissolved oxygen are:

$$\frac{\delta}{\delta t} DO = \left((1.3 - 0.3\,PN)\,P - \frac{DO}{KHr + DO} BM\right) AOCR\,B - AONT\,NT - \frac{DO}{KHodoc + DO} AOCR\,Kdoc\,DOC + \frac{Kr}{H}(DOs - DO) \quad (6\text{-}66)$$

Salinity

No internal sources or sinks of salinity exist.

Temperature

A conservation of internal energy equation can be written analogous to the conservation of mass equation. The only source or sink of internal energy considered is exchange with the atmosphere. Although solar radiation can penetrate several meters into the water column, radiation-induced increases in internal energy are here assigned entirely to the surface model layer.

For practical purposes, the internal-energy equation can be written as a conservation of temperature equation. Change of temperature due to atmospheric exchange is considered proportional to the temperature difference between the water surface and a theoretical equilibrium temperature (Edinger et al. 1974):

$$\frac{\delta}{\delta t} T = \frac{KT}{\rho Cp H} (Te - T) \qquad (6\text{-}67)$$

Te = equilibrium temperature (C^o)

KT = Heat exchange coefficient (watt m^{-2} $C^{0\ -1}$)

Cp = specific heat of water (4200 watt sec kg^{-1} $C^{o\ -1}$)

ρ = density of water (1000 kg m^{-3})

Summary of Kinetics Coefficients

Initial values of kinetics coefficients were obtained from the Chesapeake Bay model (Cerco and Cole, 1993). These had been determined following an exhaustive literature search and extensive calibration of the model. Many of the initial values were suited for Indian River-Rehoboth Bay with no modification. Values of remaining coefficients were determined through a recursive process in which initial values were altered until optimal agreement between observations and model predictions was achieved. Coefficient values are summarized in Table 6-2. The table also indicates whether coefficients were adopted from Chesapeake Bay (CB) or determined specifically for Indian River-Rehoboth Bay (IRRB).

Table 6-2
Kinetics Coefficients

Symbol	Definition	Value	Origin
AANOX	ratio of denitrification to oxic carbon respiration rate	0.5	CB
ANC	algal nitrogen-to-carbon ratio	0.167 gm N gm^{-1} C	CB
APC	algal phosphorus-to-carbon ratio	0.0167 gm P gm^{-1} C	IRRB
BMr	basal metabolic rate at Tr	0.1 day^{-1}	IRRB
BPR	predation rate at Tr	0.125 day^{-1}	IRRB
CChl	algal carbon-to-chlorophyll ratio	60 gm C mg^{-1} chl	CB
Dopt	depth of maximum algal production	0.5 m	IRRB
FCD	fraction of basal metabolism exuded as dissolved organic carbon	0.0	CB
FCDP	fraction of dissolved organic carbon produced by predation	0.0	IRRB
FCLP	fraction of labile particulate carbon produced by predation	0.7	IRRB
FCRP	fraction of refractory particulate carbon produced by predation	0.3	IRRB
FNI	fraction of inorganic nitrogen produced by metabolism	0.2	IRRB
FNIP	fraction of inorganic nitrogen produced by predation	0.0	IRRB
FND	fraction of dissolved organic nitrogen produced by metabolism	0.8	IRRB
FNDP	fraction of dissolved organic nitrogen produced by predation	0.0	IRRB
FNL	fraction of labile particulate nitrogen produced by metabolism	0.0	IRRB
FNLP	fraction of labile particulate nitrogen produced by predation	0.7	IRRB
FNR	fraction of refractory particulate nitrogen produced by metabolism	0.0	IRRB
FNRP	fraction of refractory particulate nitrogen produced by predation	0.3	IRRB
FPD	fraction of dissolved organic phosphorus produced by metabolism	0.8	IRRB
FPDP	fraction of dissolved organic phosphorus produced by predation	0.0	IRRB
FPL	fraction of labile particulate phosphorus produced by metabolism	0.0	IRRB

(Sheet 1 of 4)

Table 6-2 (Continued)

Symbol	Definition	Value	Origin
FPLP	fraction of labile particulate phosphorus produced by predation	0.7	IRRB
FPR	fraction of refractory particulate phosphorus produced by metabolism	0.0	IRRB
FPRP	fraction of refractory particulate phosphorus produced by predation	0.3	IRRB
Ismin	minimum illumination for algal growth	40 Langleys day^{-1}	CB
Kdc	minimum respiration rate of dissolved organic carbon	0.1 day^{-1}	IRRB
Kdcalg	constant that relates respiration rate to algal biomass	0.0 m^3 gm^{-1} C day^{-1}	CB
Kdn	minimum mineralization rate of dissolved organic nitrogen	0.1 day^{-1}	IRRB
Kdnalg	constant that relates mineralization rate to algal biomass	0.0 m^3 gm^{-1} C day^{-1}	CB
Kdp	minimum mineralization rate of dissolved organic phosphorus	0.1 day^{-1}	CB
Kdpalg	constant that relates mineralization rate to algal biomass	0.2 m^3 gm^{-1} C day^{-1}	CB
Kechl	light attenuation coefficient for chlorophyll 'a'	16 m^2 mg^{-1}	IRRB
KHn	half-saturation concentration for nitrogen uptake	0.01 gm N m^{-3}	CB
KHndn	half-saturation concentration of nitrate required for denitrification	0.1 gm N m^{-3}	CB
KHnnt	half-saturation concentration of NH_4 required for nitrification	1.0 gm N m^{-3}	CB
KHodoc	half-saturation concentration of dissolved oxygen required for oxic respiration	0.5 gm O_2 m^{-3}	CB
KHont	half-saturation concentration of dissolved oxygen required for nitrification	1.0 gm O_2 m^{-3}	CB
KHp	half-saturation concentration for phosphorus uptake	0.001 gm P m^{-3}	CB
KHr	half-saturation concentration for algal dissolved organic carbon excretion	0.5 gm O_2 m^{-3}	CB
Klc	minimum dissolution rate of labile particulate carbon	0.075 day^{-1}	CB

(Sheet 2 of 4)

Table 6-2 (Continued)

Symbol	Definition	Value	Origin
Klcalg	constant that relates dissolution rate to algal biomass	0.0 m^3 gm^{-1} C day^{-1}	CB
Kln	minimum dissolution rate of labile particulate nitrogen	0.075 day^{-1}	CB
Klnalg	constant that relates dissolution rate to algal biomass	0.0 m^3 gm^{-1} C day^{-1}	CB
Klp	minimum dissolution rate of labile particulate phosphorus	0.075 day^{-1}	CB
Klpalg	constant that relates dissolution rate to algal biomass	0.0 m^3 gm^{-1} C day^{-1}	CB
Kr	reaeration coefficient	0.63 m day^{-1}	IRRB
Krc	minimum dissolution rate of refractory particulate carbon	0.005 day^{-1}	CB
Krcalg	constant that relates dissolution rate to algal biomass	0.0 m^3 gm^{-1} C day^{-1}	CB
Krn	minimum dissolution rate of refractory particulate nitrogen	0.005 day^{-1}	CB
Krnalg	constant that relates dissolution rate to algal biomass	0.0 m^3 gm^{-1} C day^{-1}	CB
Krp	minimum dissolution rate of refractory particulate phosphorus	0.005 day^{-1}	CB
Krpalg	constant that relates dissolution rate to algal biomass	0.0 m^3 gm^{-1} C day^{-1}	CB
KTb	effect of temperature on basal metabolism	0.069 $C^{0\ -1}$	CB
KTg1	effect of temperature below Tm on growth	0.012 $C^{0\ -2}$	IRRB
KTg2	effect of temperature above Tm on growth	0.012 $C^{0\ -2}$	IRRB
KThdr	constant that relates hydrolysis rates to temperature	0.069 $C^{0\ -1}$	CB
KTmnl	constant that relates mineralization rates to temperature	0.069 $C^{0\ -1}$	CB
KTnt1	effect of temperature below Tmnt on nitrification	0.09 $C^{0\ -2}$	IRRB

(Sheet 3 of 4)

Table 6-2 (Concluded)

Symbol	Definition	Value	Origin
KTnt2	effect of temperature above Tmnt on nitrification	0.09 $C^{0\ -2}$	IRRB
NTm	maximum nitrification rate at optimal temperature	0.1 gm N m^{-3} day^{-1}	IRRB
PM	production under optimal conditions	2.5 day^{-1}	CB
Tm	optimal temperature for algal growth	25 C^0	CB
Tmnt	optimal temperature for nitrification	30 C^0	IRRB
Tr	reference temperature for metabolism	20 C^0	CB
Trhdr	reference temperature for hydrolysis	20 C^0	CB
Trmnl	reference temperature for mineralization	20 C^0	CB
WSa	algal settling velocity	0.1 m day^{-1}	CB
WSl	settling velocity of labile particles	0.1 m day^{-1}	CB
WSr	settling velocity of refractory particles	0.1 m day^{-1}	CB

(Sheet 4 of 4)

Chapter VII: Linking the Hydrodynamic and Water Quality Models

Introduction

The hydrodynamic and water quality models are indirectly linked. Cell dimensions, flows, and other information from the hydrodynamic model are written to disk for subsequent use by the water quality model. The indirect linkage makes efficient use of computer resources. An unlimited number of water quality model runs can be made using information put out by a single run of the hydrodynamic model. In order to link the models, output from the hydrodynamic model must be "mapped" to the water quality model. That is, information in the x-y plane employed by CH3D must be converted into dimension-free information for use in the control volumes of CE-QUAL-ICM.

The simplest mapping is one-to-one in space and time. In one-to-one mapping, water quality model control volumes correspond in number and size to hydrodynamic grid cells. Flows and other information are stored after each time step of the hydrodynamic model and the two models employ the same time step. One-to-one mapping is the least efficient linkage procedure. Vast amounts of disk space are required to store all hydrodynamic information. The water quality model devotes an unnecessary proportion of execution time to reading hydrodynamic information and integrating the conservation of mass equation using the hydrodynamic time step. For lengthy executions of the hydrodynamic and water quality models, the storage volume and execution time demanded by one-to-one mapping are prohibitive.

Averaging hydrodynamic output before disk storage is one technique employed to increase linkage efficiency. A second technique is the grid overlay in which multiple hydrodynamic model cells are combined into single water quality model control volumes. Both averaging and overlays were employed in the linkage applied to Indian River-Rehoboth Bay. Hydrodynamic information, computed at thirty-second intervals, was averaged into hourly intervals before disk storage. The 2063 CH3D cells were overlaid into a CE-QUAL-ICM grid that contained 281 control volumes (Figure 7-1).

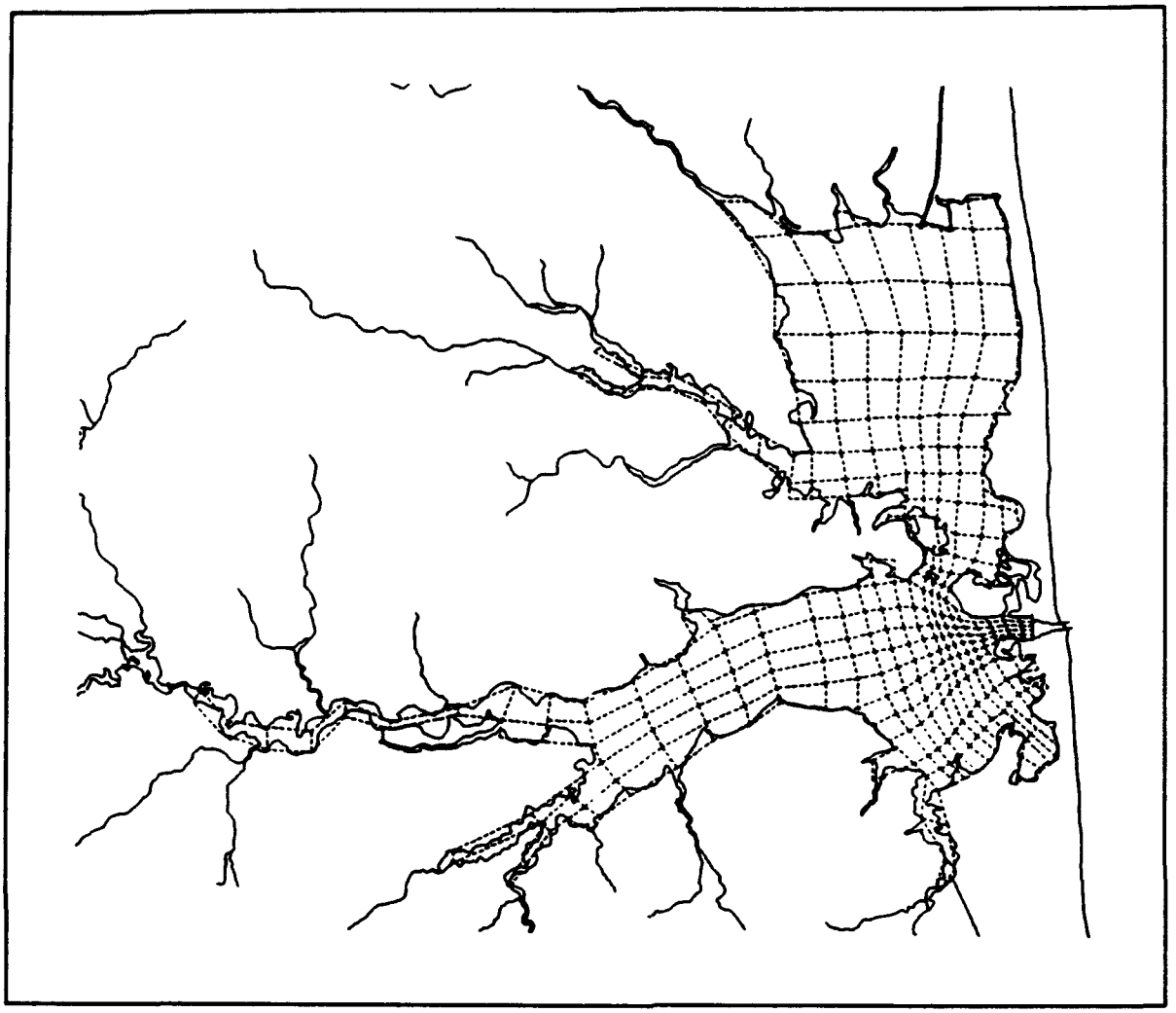

Figure 7-1. Water Quality Model Grid

Water Quality Model Time Step

The interval at which hydrodynamic output is written is not necessarily the appropriate time step for use in the water quality model. Rather, the water quality model time step is determined by the stability requirements of the numerical scheme employed to integrate the conservation of mass equation (Equation 6-1). Typically, the time step determined by stability limits is shorter than the output interval. An "autostepping" algorithm within the water quality model determines the time step. The algorithm computes permissible time step based on flow, dispersion, and cell dimension. If the time step is shorter than the hydrodynamic output interval, flow and dispersion are held constant until hydrodynamic information is updated at the next read operation.

Inspection of the stability region of the one-dimensional QUICKEST algorithm (Leonard 1979) indicates sufficient conditions are:

$$\Delta t \leq \frac{\Delta x}{u} \tag{7-1}$$

and

$$\Delta t \leq \frac{\Delta x^2}{2D} \tag{7-2}$$

Δt = time step (T)

Δx = cell length (L)

u = velocity ($L\ T^{-1}$)

D = diffusion coefficient ($L^2\ T^{-1}$)

The autostepping algorithm examines velocity, diffusion, and cell length at each flow face of the water quality model control volumes. (These correspond to Q_j / A_j, D_j, and δx_j in Equation 6-1). The time step is determined as:

$$\Delta t = \text{minimum}\left(\alpha \frac{\Delta x}{u}, \alpha \frac{\Delta x^2}{2D}\right) \tag{7-3}$$

α = constant that insures time step is less than maximum allowed ($\approx$0.95)

The flow face with the most restrictive time step determines the time step for the entire system.

Although the criteria expressed in Equations 7-1 and 7-2 are not strictly correct for application of QUICKEST in multiple dimensions, we have thus far found the one-dimensional criteria sufficient to determine the time step in multi-dimensional applications. The mean time step determined for the water quality model was $\approx$300 seconds, an order of magnitude greater than the hydrodynamic model time step.

Linkage Testing

Linkage between the two models is accomplished through computer code which is not detailed here. Once the linkage software is complete, the linkage must be tested to insure that transport in the water quality model compares to transport in the hydrodynamic model. For one-to-one linkage the testing is primarily a test of computer code. When hydrodynamic information is correctly mapped into the water quality model, transport in the two models should be identical. When temporal averaging and overlays are employed, factors in addition to coding require consideration. As the averaging interval and overlay size increase, transport in the water quality model diverges from the hydrodynamic model. Judgement is required to determine the acceptable temporal interval and spatial resolution.

The ultimate linkage test is comparison of conservative substance transport in the hydrodynamic and water quality models. To perform our test, we set initial salinity in the hydrodynamic model to zero. The salinity at the interface with the ocean was fixed at 50 ppt. The hydrodynamic model was run for thirty days during which salt was advected and dispersed from the ocean interface into the interior of Indian River and Rehoboth Bay. We ran the water quality model using flow and dispersion from the hydrodynamic model and identical initial and boundary conditions for salinity. One-hour averaging of hydrodynamic information and the overlay grid were employed. Time series of salinity predicted by the two models were compared at several locations on the water quality model grid (Figure 7-2). Each comparison (Figures 7-3 to 7-7) comprised four plots. Time series of salinity predictions, output each hour, were plotted in the upper left. Hourly salinity predictions from the two models were plotted against each other in the upper right. Salinity from both models was averaged over two tidal cycles (≈25 hours) and plotted as time series in the lower left. Tidal-average salinity predictions were plotted against each other in the lower right.

Perfect linkage is indicated when the salinity time series from the two models exactly superimpose. On the corresponding scatterplots, all points will fall on the one-to-one diagonal line. The ideal is nearly realized at cells 52, 127, and 134. These cells lie in regions in which the horizontal gradient of salinity is small. At cells 247 and 117, which lie in regions of substantial horizontal salinity gradient, agreement is less than ideal on the hourly time scale. When results are averaged over two tidal cycles, however, agreement is much improved.

The linkage tests indicate the temporal averaging of hydrodynamic output and the grid overlay are satisfactory for transport problems in which time scales equal or exceed two tidal cycles and spatial concentration gradients are mild. These conditions are typical in eutrophication studies. We conclude the linkage between the two models is correct and suited for eutrophication modeling in Indian River-Rehoboth Bay.

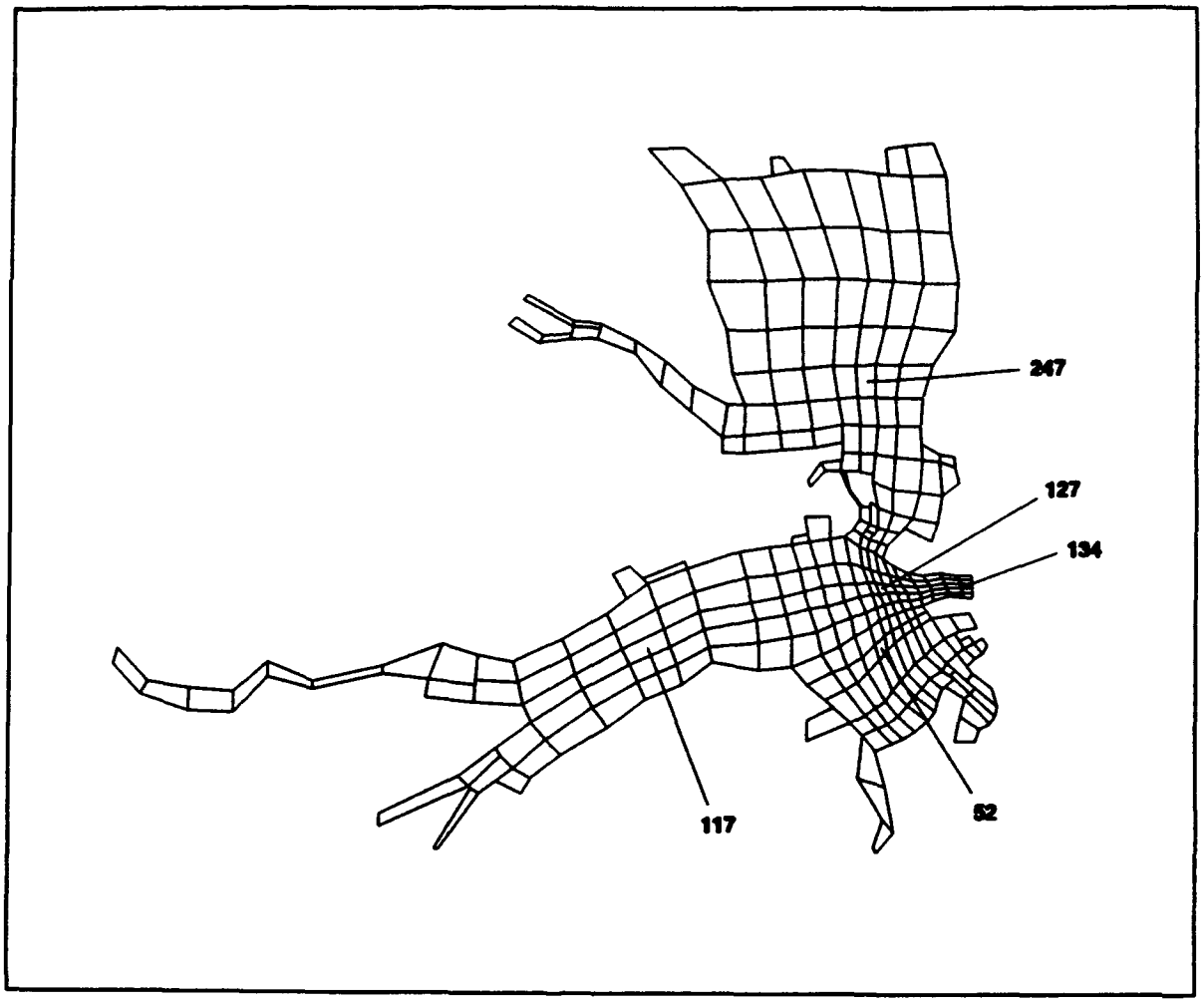

Figure 7-2. Cells Selected for Transport Comparisons

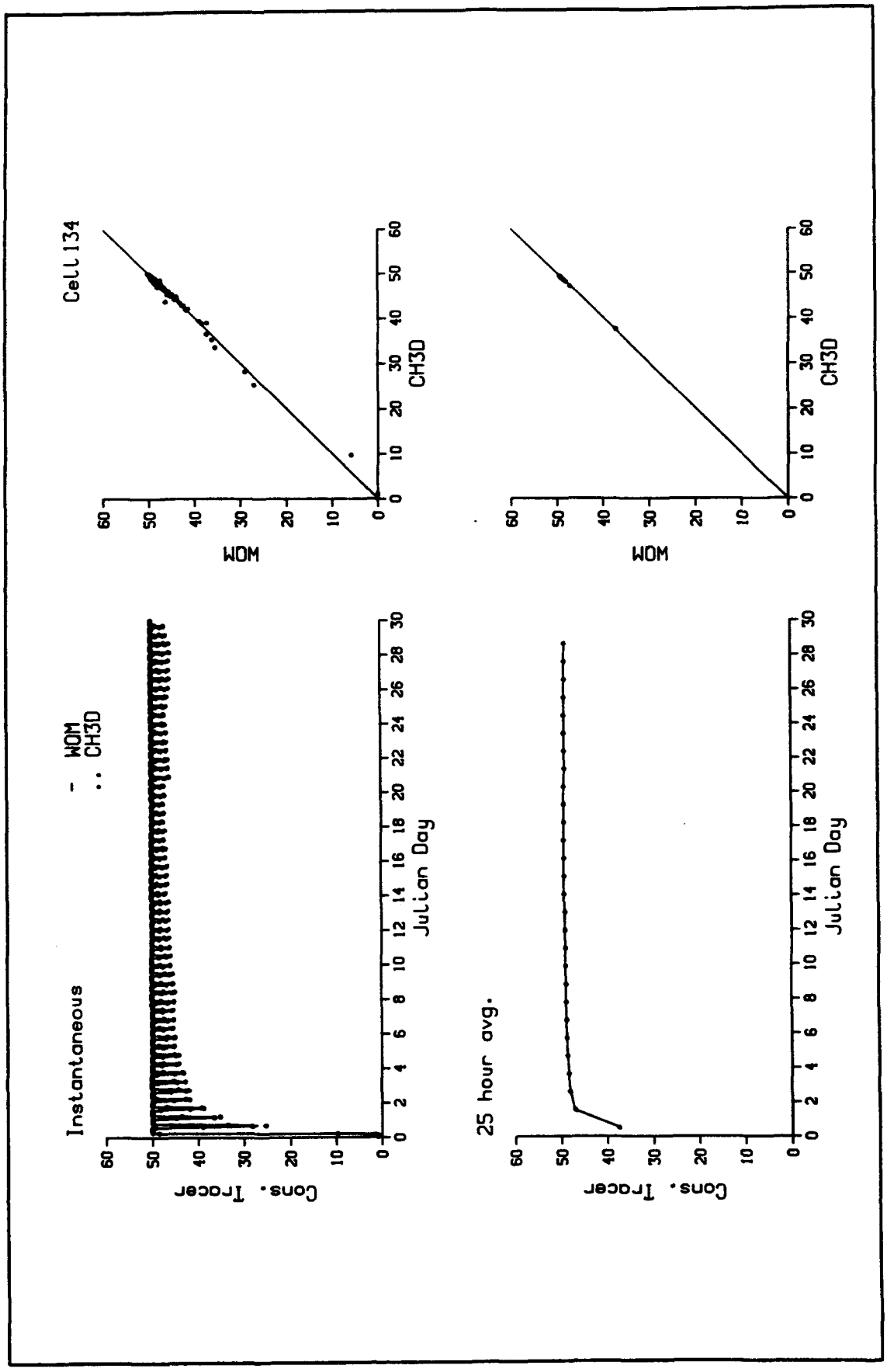

Figure 7-3. Salinity Comparison at Cell 134

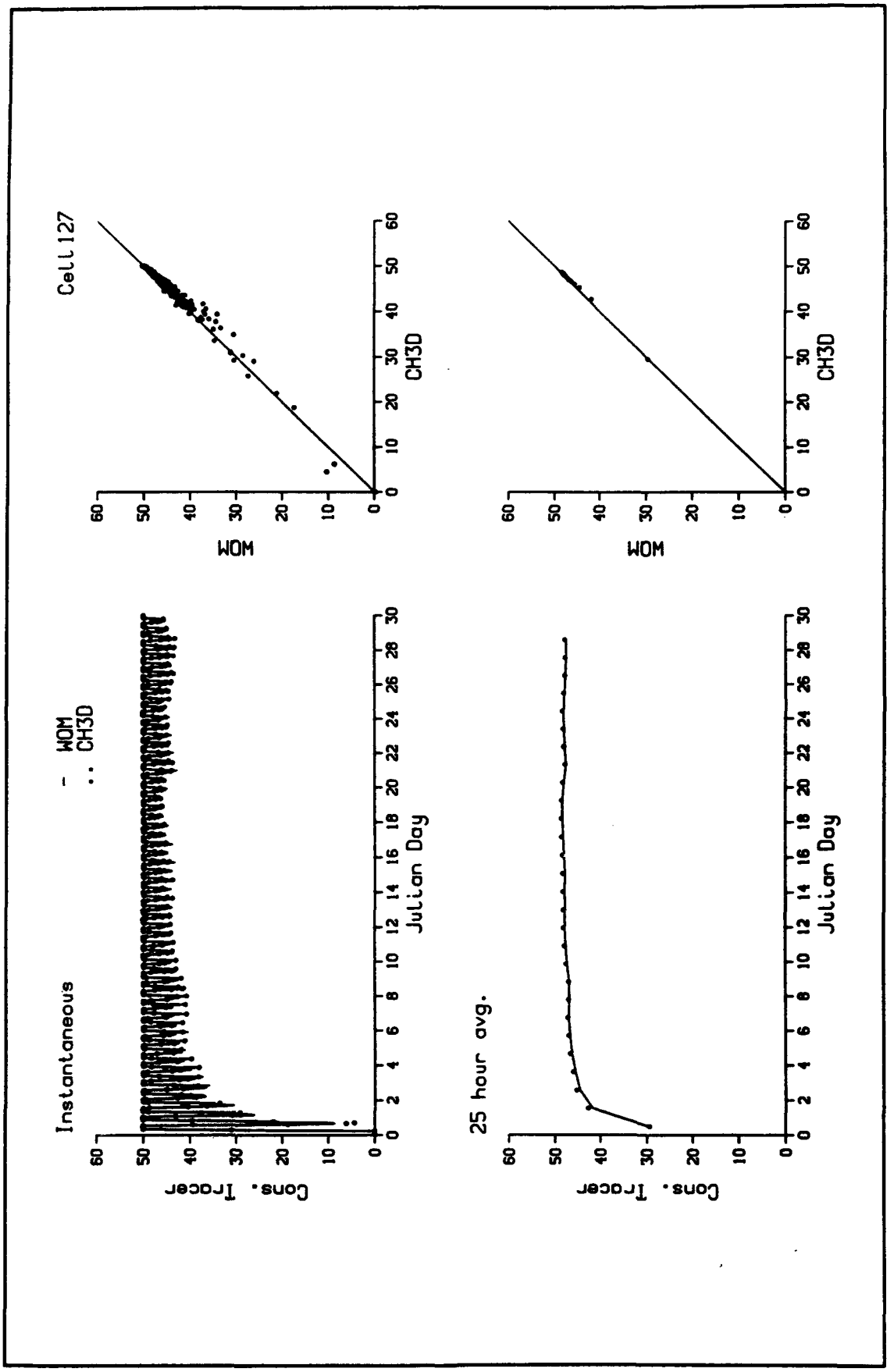

Figure 7-4. Salinity Comparison at Cell 127

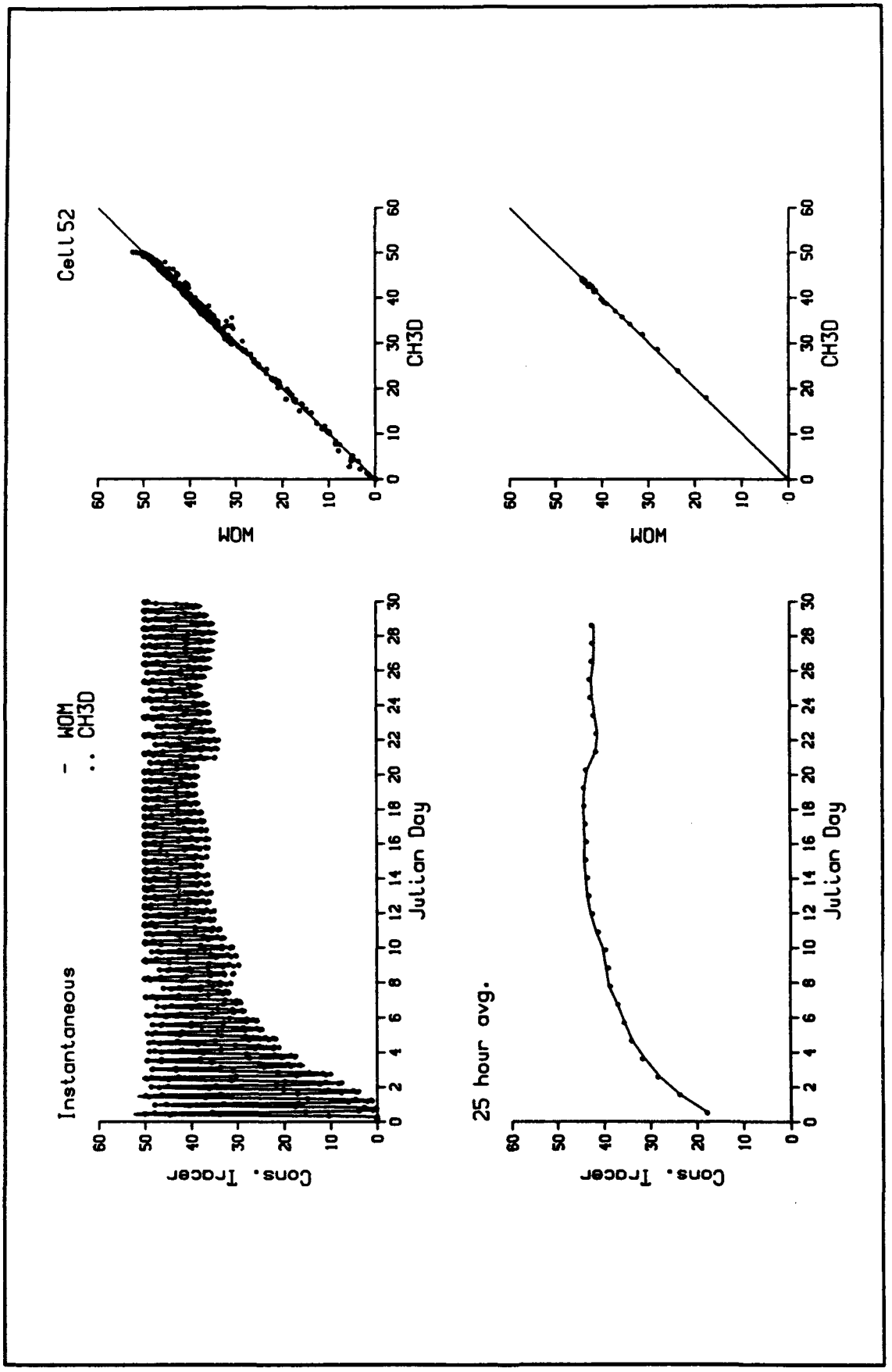

Figure 7-5. Salinity Comparison at Cell 52

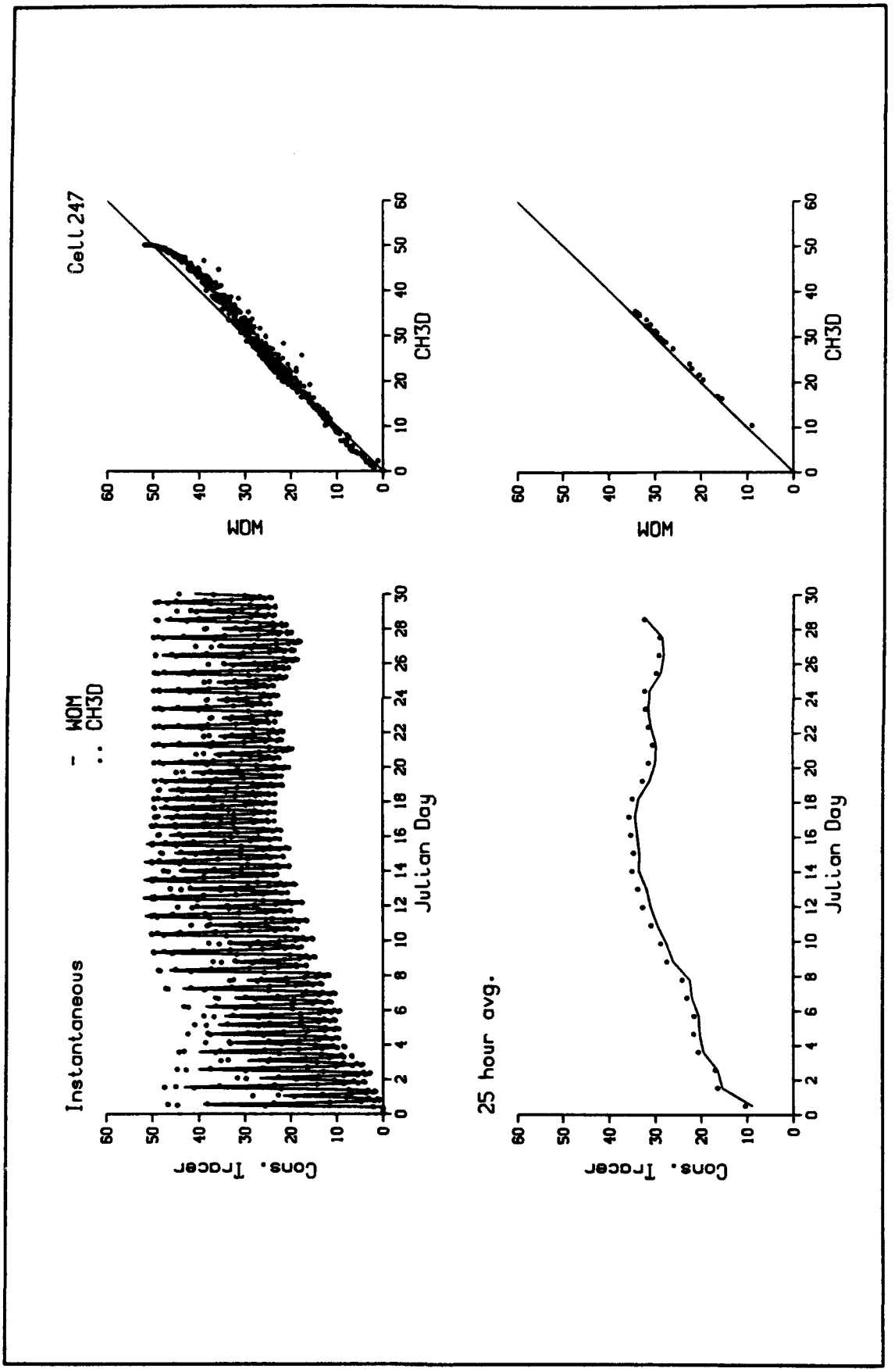

Figure 7-8. Salinity Comparison at Cell 247

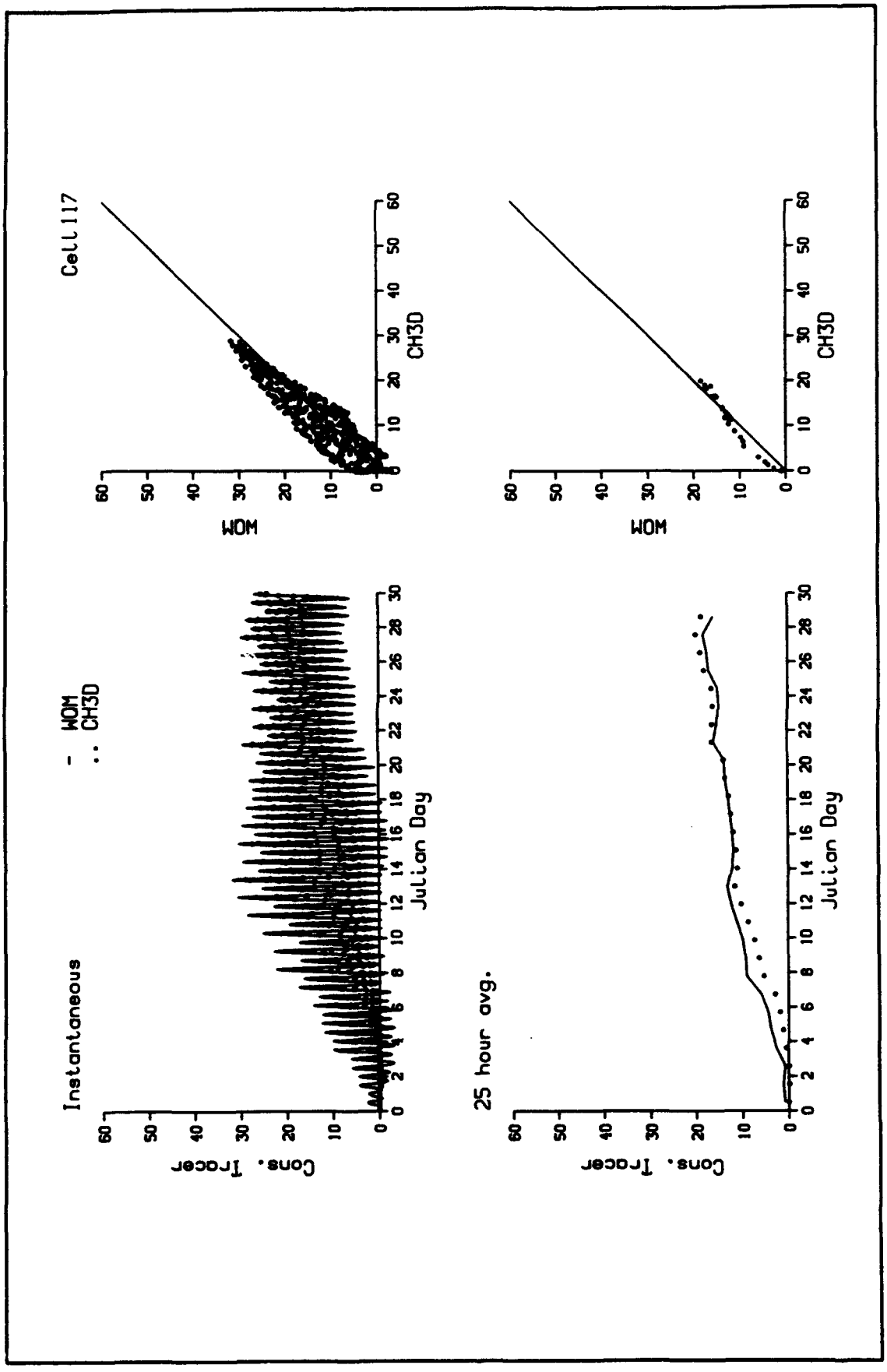

Figure 7-7. Salinity Comparison at Cell 117

Chapter VIII: Additional Model Inputs and Outputs

Introduction

Additional information, beyond loads and calibration parameter values, is required to operate the model. Additional inputs considered here are load partition, open-mouth boundary conditions, light extinction, and sediment-water fluxes. Postprocessing of model state variables into more useful quantities is also desirable. Derivation of BOD concentration and calculation of diurnal fluxes from model computations are detailed.

Partition of Loads

The quantities analyzed in the freeflowing streams and in the point-source discharges required mapping into model state variables (Table 8-1).

Table 8-1
Correspondence of Loads and Model State Variables

Observation	maps into	State Variable
Biochemical Oxygen Demand	——>	Dissolved Organic Carbon
		Labile Particulate Organic Carbon
		Refractory Particulate Organic Carbon
Total Kjeldahl Nitrogen	——>	Dissolved Organic Nitrogen
		Labile Particulate Organic Nitrogen
		Refractory Particulate Organic Nitrogen
Total Phosphorus	——>	Dissolved Organic Phosphorus
		Labile Particulate Organic Phosphorus
		Refractory Particulate Organic Phosphorus

No exact conversion of BOD to organic carbon was possible but reasonable empirical correspondences were employed (Chapter 3). The derived total organic carbon still required partitioning into model state variables, however. Relationships used to derive loads of model state variables from observed loads were:

$$DOC = FDOC * TOC \quad (8\text{-}1)$$

$$LPOC = FLPOC * (TOC - DOC) \quad (8\text{-}2)$$

$$RPOC = (1 - FLPOC) * (TOC - DOC) \quad (8\text{-}3)$$

TOC = total organic carbon (gm m^{-3})

DOC = dissolved organic carbon (gm m^{-3})

LPOC = labile particulate organic carbon (gm m^{-3})

RPOC = refractory particulate organic carbon (gm m^{-3})

FDOC = fraction of total organic carbon that is dissolved

FLPOC = fraction of particulate organic carbon that is labile

$$DON = FDON * (TKN - NH_4) \quad (8\text{-}4)$$

$$LPON = FLPON * (TKN - NH_4 - DON) \quad (8\text{-}5)$$

$$RPON = (1 - FLPON) * (TKN - NH_4 - DON) \quad (8\text{-}6)$$

TKN = total Kjeldahl nitrogen (gm m^{-3})

NH_4 = ammonium (gm m^{-3})

DON = dissolved organic nitrogen (gm m^{-3})

LPON = labile particulate organic nitrogen (gm m^{-3})

RPON = refractory particulate organic nitrogen (gm m^{-3})

FDON = fraction of total organic nitrogen that is dissolved

FLPON = fraction of particulate organic nitrogen that is labile

$$DOP = FDOP * (TOTP - PO_4) \quad (8\text{-}7)$$

$$LPOP = FLPOP * (TOTP - PO_4 - DOP) \quad (8\text{-}8)$$

$$RPOP = (1 - FLPOP) * (TOTP - PO_4 - DOP) \quad (8\text{-}9)$$

TOTP = total phosphorus (gm m^{-3})

PO_4 = dissolved phosphate (gm m^{-3})

DOP = dissolved organic phosphorus (gm m^{-3})

LPOP = labile particulate organic phosphorus (gm m^{-3})

RPOP = refractory particulate organic phosphorus (gm m^{-3})

FDOP = fraction of total organic phosphorus that is dissolved

FLPOP = fraction of particulate organic phosphorus that is labile

Initial values of splits were adopted from values employed in Chesapeake Bay tributaries. These values were refined during calibration of the Indian River-Rehoboth Bay model (Table 8-2).

Open-Mouth Boundary Conditions

Concentrations at the junction of Indian River Inlet with the Atlantic Ocean were specified primarily using data collected offshore of the inlet by the EPA (Chapter 2). Observations were available for 12 of the 36 months covered by model calibration. Boundary conditions in months for which no observations were available were filled in with values observed in the same month in alternate years or values observed at the mouth of Chesapeake Bay. Good correspondence was observed in temperature, salinity, chlorophyll, phosphate, and dissolved oxygen between observations collected offshore of Indian River and at the bottom of the Bay mouth (Figures 8-1 to 8-5). Salinity boundary

Table 8-2
Dissolved and Labile Fractions of Loads

Parameter	Nonpoint-Source Value	Point-Source Value
FDOC	0.8	0.8
FLPOC	0.0	0.15
FDON	0.6	0.8
FLPON	0.0	0.1
FDOP	0.1	0.4
FLPOP	0.0	0.0

conditions for July and August 1989 were specified to match observations collected within Indian River Bay during those unusually wet months.

Light Extinction

Light extinction was specified based on disk visibility measures collected by the Academy of Natural Sciences and the College of Marine Studies (Chapter 2). Disk visibility was converted to light extinction via the relationship:

$$KE = \frac{1.45}{DV} \qquad (8\text{-}10)$$

KE = light extinction (m^{-1})

DV = secchi depth (m)

Light extinction in Indian River-Rehoboth Bay is strongly affected by chlorophyll concentration (Figure 8-6). Light extinction input to the model is background extinction independent of chlorophyll. The effect of chlorophyll is added to the background value based on computed chlorophyll concentration (Equation 6-9). Consequently, the effect of ambient chlorophyll had to be removed from the observed light extinction. Light extinction in the study system may also vary seasonally or regionally. In order to quantify the influence of chlorophyll and detect seasonal and regional trends, a model was proposed:

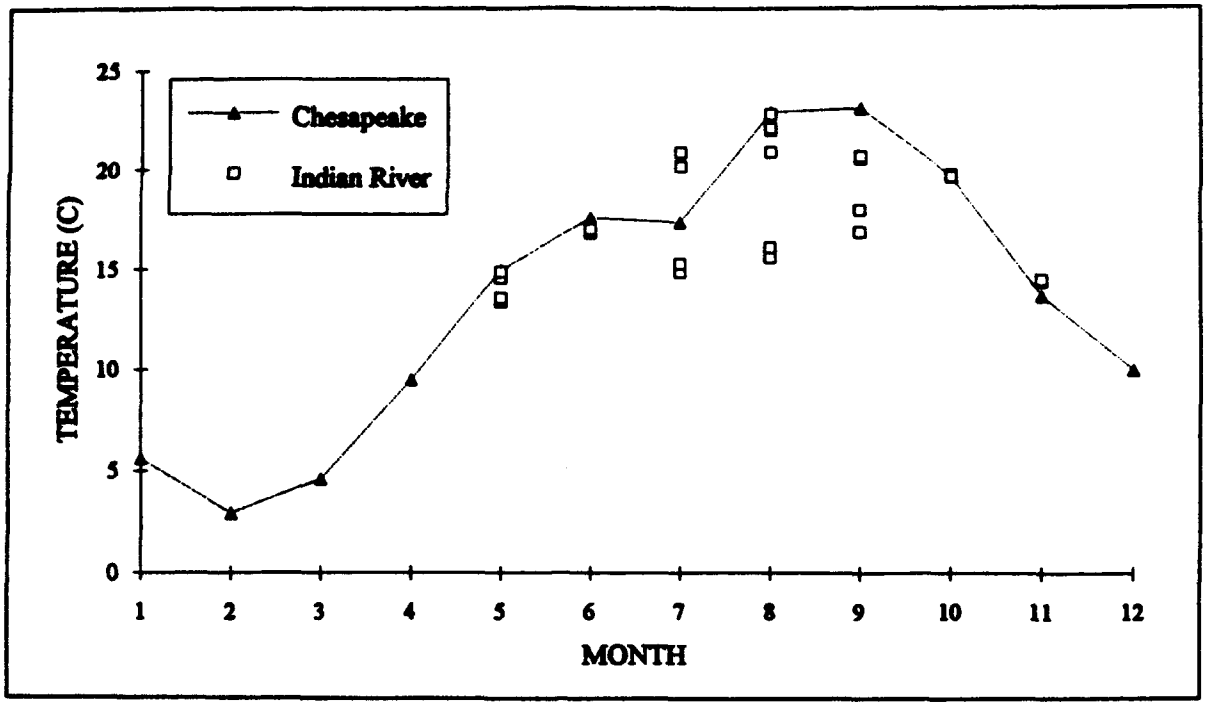

Figure 8-1. Temperature at Mouth of Indian River and Chesapeake Bay

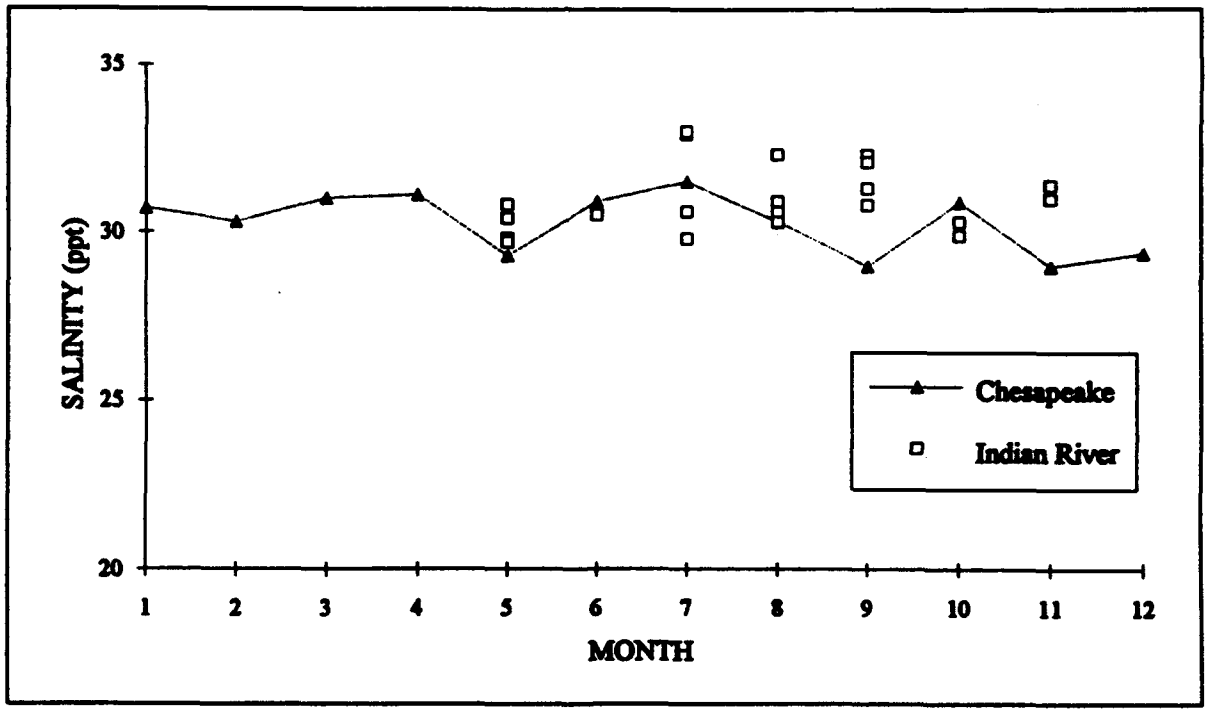

Figure 8-2. Salinity at Mouth of Indian River and Chesapeake Bay

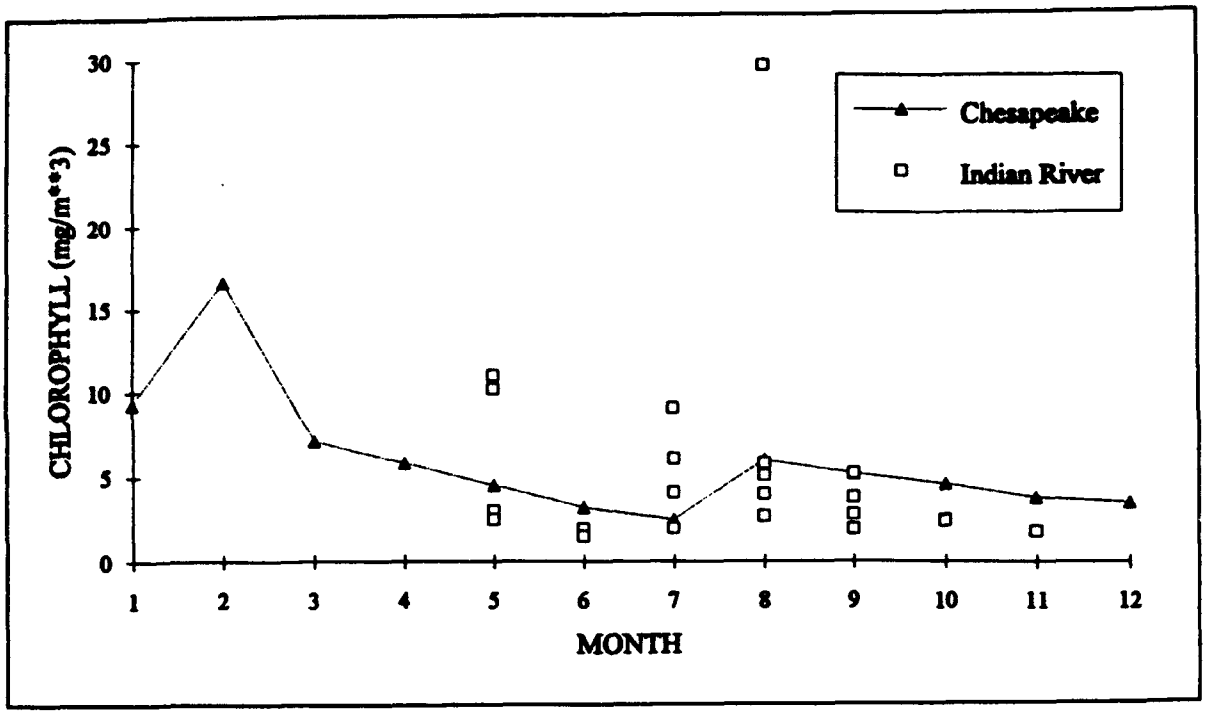

Figure 8-3. Chlorophyll at Mouth of Indian River and Chesapeake Bay

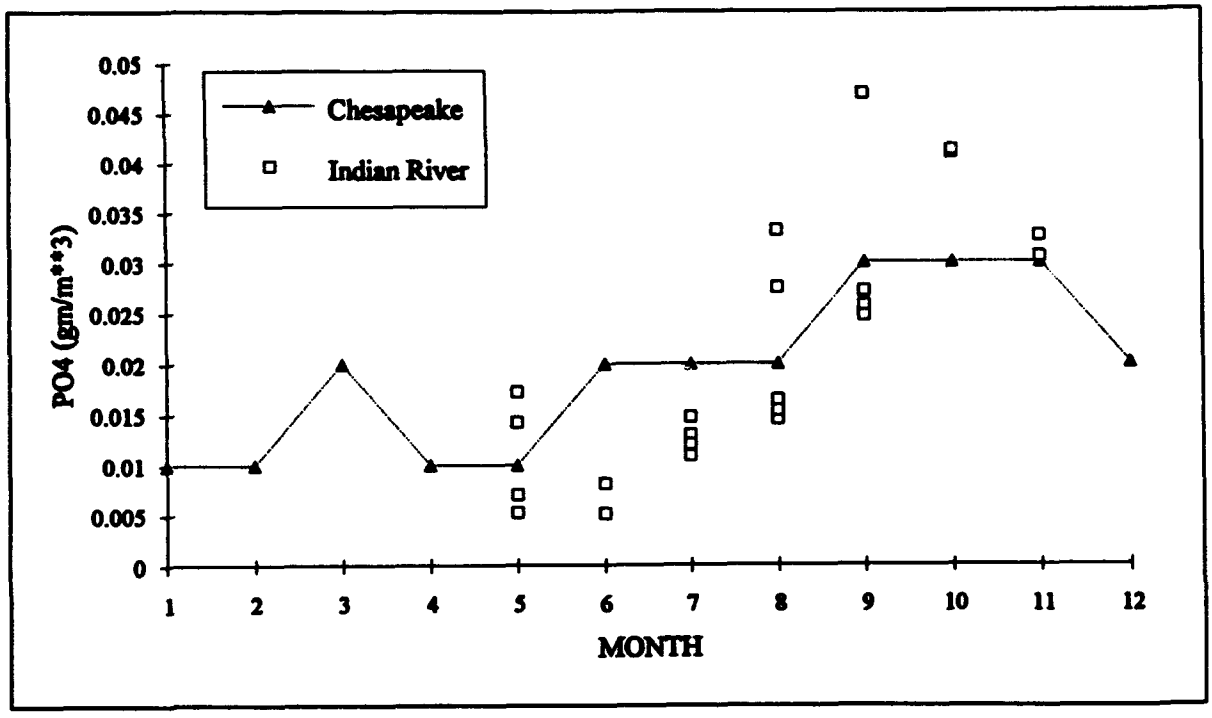

Figure 8-4. Phosphate at Mouth of Indian River and Chesapeake Bay

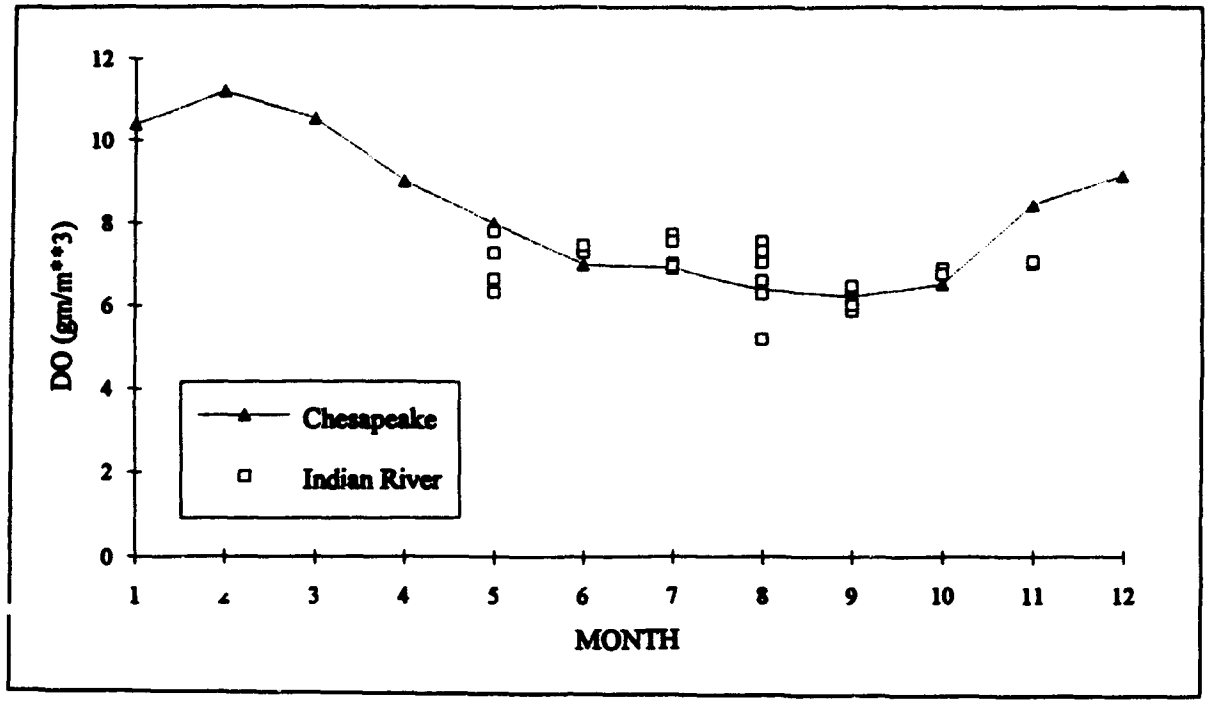

Figure 8-5. Dissolved Oxygen at Mouth of Indian River and Chesapeake Bay

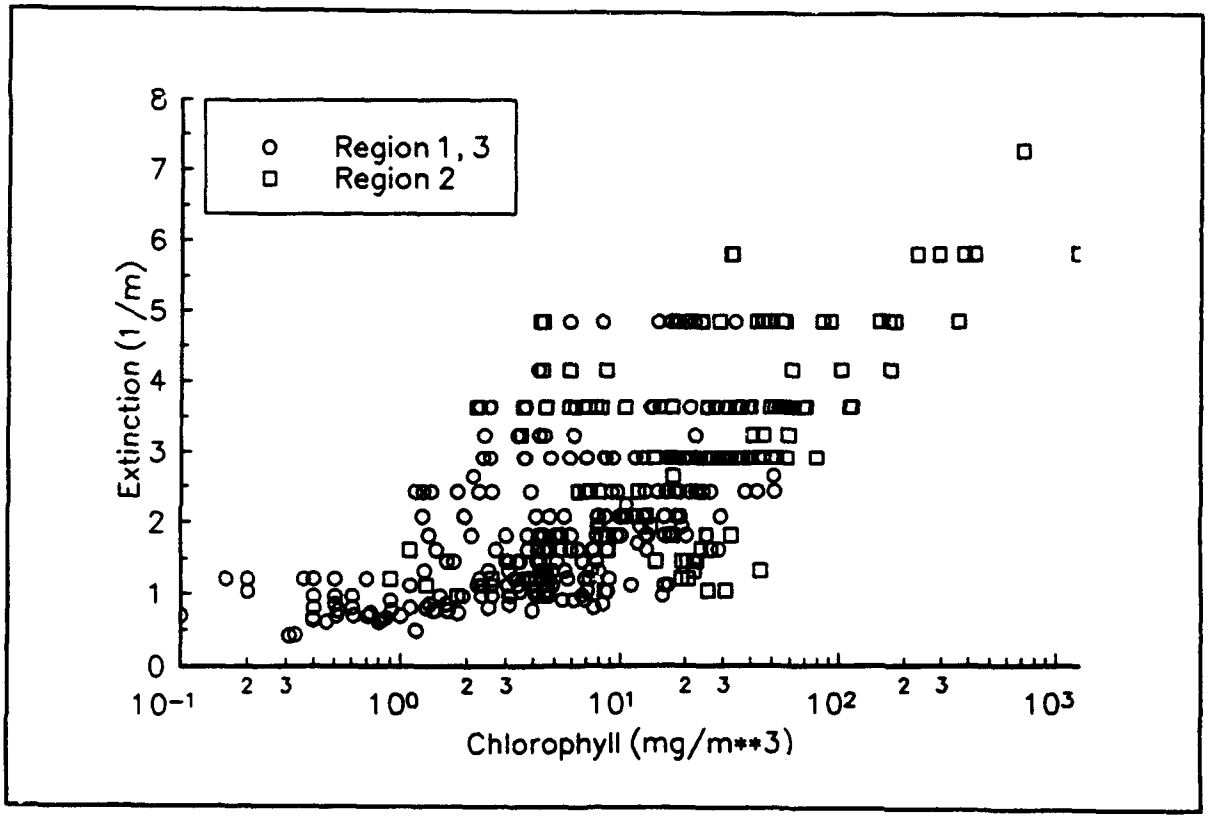

Figure 8-6. Relation of Light Extinction to Chlorophyll Concentration

$$KE = a + bR1 + cR2 + dR3 + e\sin\left(\frac{2\pi}{365}Jday\right) + f\cos\left(\frac{2\pi}{365}Jday\right) + g\,CHL \quad (8\text{-}11)$$

a = annual mean background light extinction (m^{-1})

b = incremental light extinction in Region 1 (m^{-1})

c = incremental light extinction in Region 2 (m^{-1})

d = incremental light extinction in Region 3 (m^{-1})

R1 = 1 in Region 1, 0 elsewhere

R2 = 1 in Region 2, 0 elsewhere

R3 = 1 in Region 3, 0 elsewhere

e, f = parameters that determine amplitude and phase of seasonal variation (m^{-1})

Jday = julian day

g = effect of chlorophyll on light extinction (m^2 mg^{-1} Chl'a')

Stepwise regression was employed to evaluate parameter values. Observed extinction was treated as the dependent variate while region, julian day, and chlorophyll were treated as independent variates. Three regions were defined (Figure 8-7): Region 1 - Lower Indian River, Region 2 - Upper Indian River, Region 3 - Rehoboth Bay.

The analysis (Table 8-3) indicated that chlorophyll was the primary determinant of light extinction in Indian River-Rehoboth Bay. A seasonal trend, independent of chlorophyll was also detected. Background extinction in Upper Indian River was greater than elsewhere but that no difference existed between Lower Indian River and Rehoboth Bay. Monthly values of background light extinction, that accounted for seasonal and regional variation (Figure 8-8), were input to the model.

Sediment-Water Fluxes

Sediment-water fluxes of oxygen and nutrients can be a significant influence on water quality in shallow systems such as Indian River-Rehoboth Bay. One component of the sediment-water system in the shallow bays is a layer of

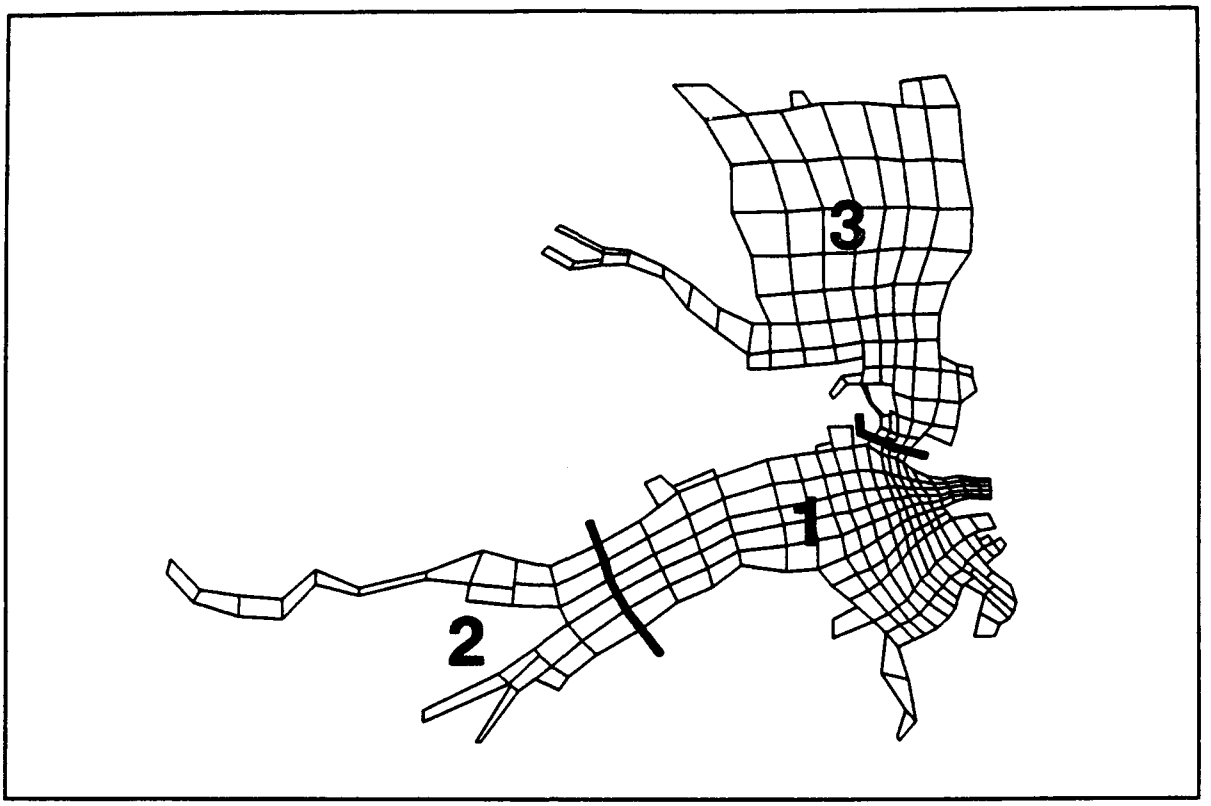

Figure 8-7. Regions in Light Extinction Analysis

Table 8-3
Analysis of Light Extinction

Parameter	Value	Cumulative R^2
a	1.40	
g	0.016	0.30
e	–0.56	0.35
f	–0.74	0.40
c	0.88	0.47

benthic algae that occupies the sediment-water interface in regions where light intercepts the bottom. Actions of the benthic algae modify the sediment-water fluxes that usually occur in a darkened water column. Photosynthesis by benthic algae may induce an apparent sediment release of dissolved oxygen instead sediment oxygen demand. Nutrient uptake by the algae may induce apparent sediment nutrient uptake when release to the water column is expected.

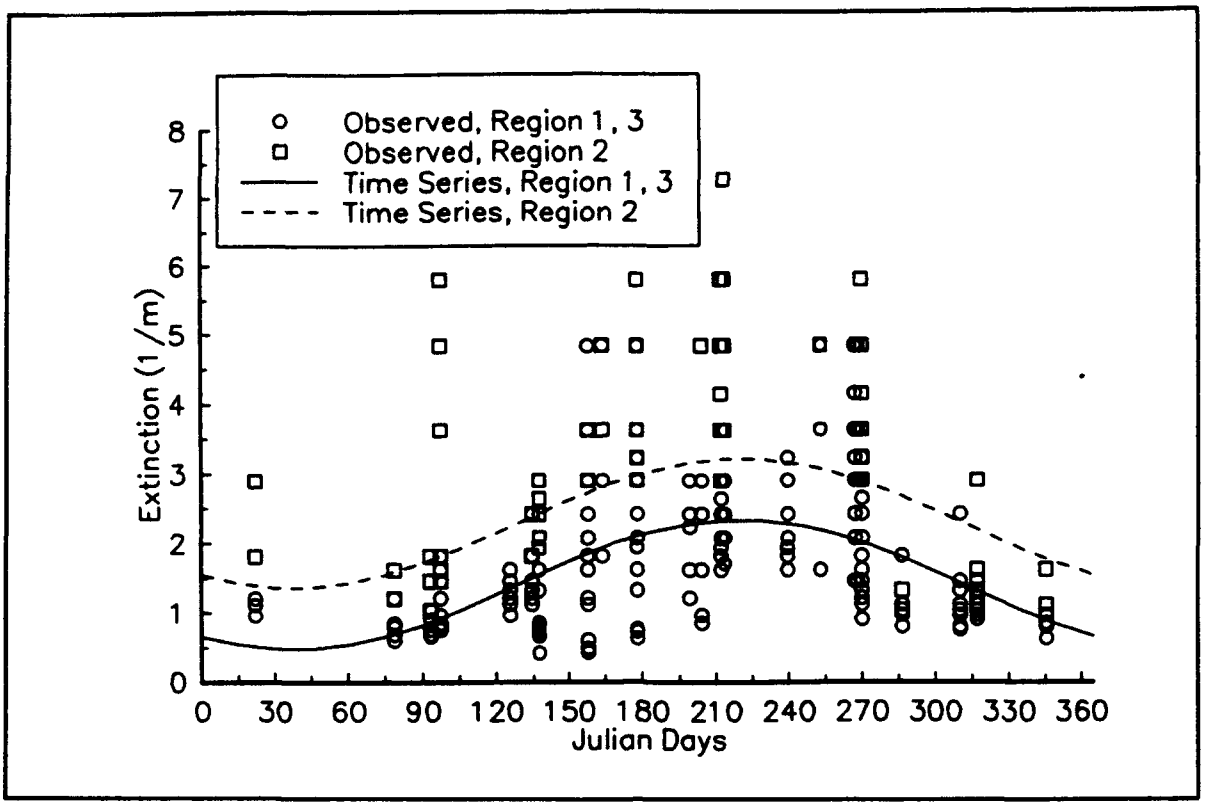

Figure 8-8. Seasonal and Regional Variation in Light Extinction

A series of empirical models of sediment-water fluxes were constructed based on observations collected in Indian River-Rehoboth Bay (Chapter 2). Raw data supplied by the principal investigator consisted of replicate measures collected at varying light intensities. The replicate measures were averaged and scientific units were converted to units employed in the model. Simultaneous measures collected in light and dark were combined into daily-average fluxes that occur during day-night illumination cycles. The observations, treated for analysis, are reported in Table 8-4.

Empirical models were formulated based on examination of the data, on expected actions of benthic algae, and on typical sediment-water interactions in a darkened water column. The sediment oxygen demand model was:

$$SOD = SOD_b e^{\alpha (T - 20)} + b\,Light \qquad (8\text{-}12)$$

SOD = sediment oxygen demand (gm m^{-2} day^{-1})

SOD_b = sediment oxygen demand at 20 C^0 in a darkened water column

Table 8-4
Observed Sediment Water Fluxes

Station	Temp, C^0	Light, langley day^{-1}	SOD, gm m^{-2} day^{-1}	NH_4, mg m^{-2} day^{-1}	NO_3, mg m^{-2} day^{-1}	PO_4, mg m^{-2} day^{-1}
1	12	157.5		0	0	
	12	0	-0.784	52	0.45	
2	12	157.5	0.505	-5.7	-0.76	
	12	0	-1.25	34	0	
3	12	157.5	0.233	-5.5	-0.22	
4	12	6.75	-0.894	39.5	-16	
1	25	63	-1.12	27		1.44
2	25	15.3	-1.06	34		8.56
	25	0	-1.54	150		10.4
3	25	90	-0.209	5.9		0
	25	0	-1.15	107		6.45
4	25	0	-3.48	147		9.67

α = constant that expresses influence of temperature on sediment-water fluxes ($C^{0\ -1}$)

T = temperature (C^0)

b = constant that expresses influence of light on sediment-water fluxes (gm m^{-2} $langley^{-1}$)

Light = illumination at sediment-water interface (langley day^{-1})

By convention in the model, fluxes from sediment to water are positive. Fluxes from water to sediment are negative. The empirical model indicates SOD is negative (oxygen flows from water to sediment) when no light is available at the sediment-water interface (Figure 8-9). The magnitude of SOD increases as a function of temperature. The availability of light at the bottom makes SOD less negative. At low temperatures and high light intensity, the bottom gives off oxygen. At extremely high temperature, however, SOD is negative despite light availability. (To aid in interpretation of the functions, Table 8-5 presents a few reference values of temperature and light.)

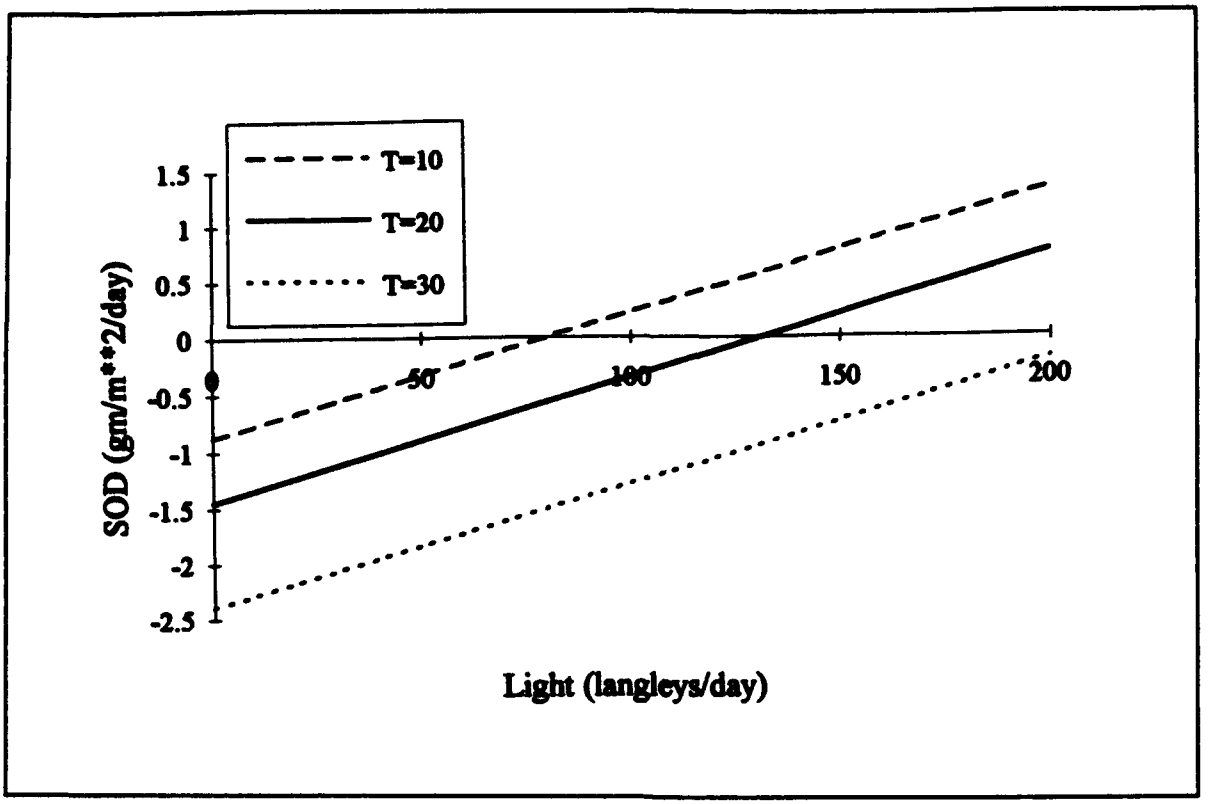

Figure 8-9. Effect of Temperature and Light on Sediment Oxygen Demand

Table 8-5
Temperature and Light at Sediment-Water Interface at Mean Depth of Indian River-Rehoboth Bay

Month	Temperature, C^0	Light, Region 1, 3, langley day^{-1}	Light, Region 2, langley day^{-1}
January	5.3	205	46
July	26.6	18	4

The ammonium flux model was:

$$NH_4flx = NH_4flx_b \, e^{\alpha (T - 20)} - b \, PN \, Nlim \, Light \qquad (8\text{-}13)$$

NH_4flx = ammonium flux (gm m^{-2} day^{-1})

NH_4flx_b = ammonium flux at 20 C^0 in a darkened water column

PN = algal preference for ammonium

Nlim = nitrogenous nutrient limitation for algae

Definitions of remaining terms are the same as for SOD (Equation 8-12).

Ammonium flux is positive, from sediment to water, when no light is available at the bottom (Figure 8-10). Sediment ammonium release increases as an exponential function of temperature. When light is available at the bottom, ammonium release is diminished. Under strong illumination at low temperature, sediments take up ammonium. The nutrient preference and limitation terms are identical to the terms specified for phytoplankton (Equations 6-4 and 6-21). These terms prevent sediment ammonium uptake when none is available in the water column.

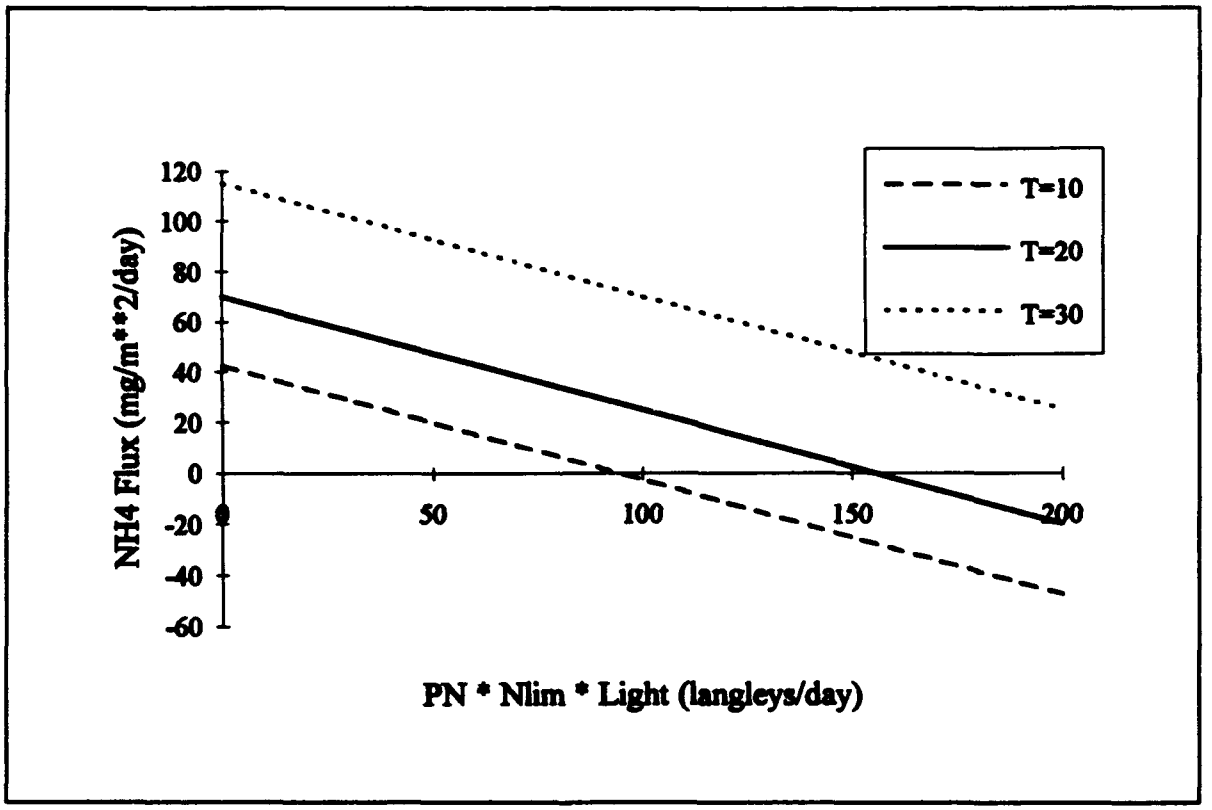

Figure 8-10. Effect of Temperature and Light on Sediment-Water Ammonium Flux

Nitrate moves in both directions across the sediment-water interface. This effect is influenced by concentration in the water, independent of benthic algae. When nitrate is abundant in the water, nitrate flows to the sediments where it is denitrified to a gaseous form. When nitrate is absent from the water, small sediment release occurs due to production by nitrification in the sediments (Figure 8-11). The empirical nitrate model was:

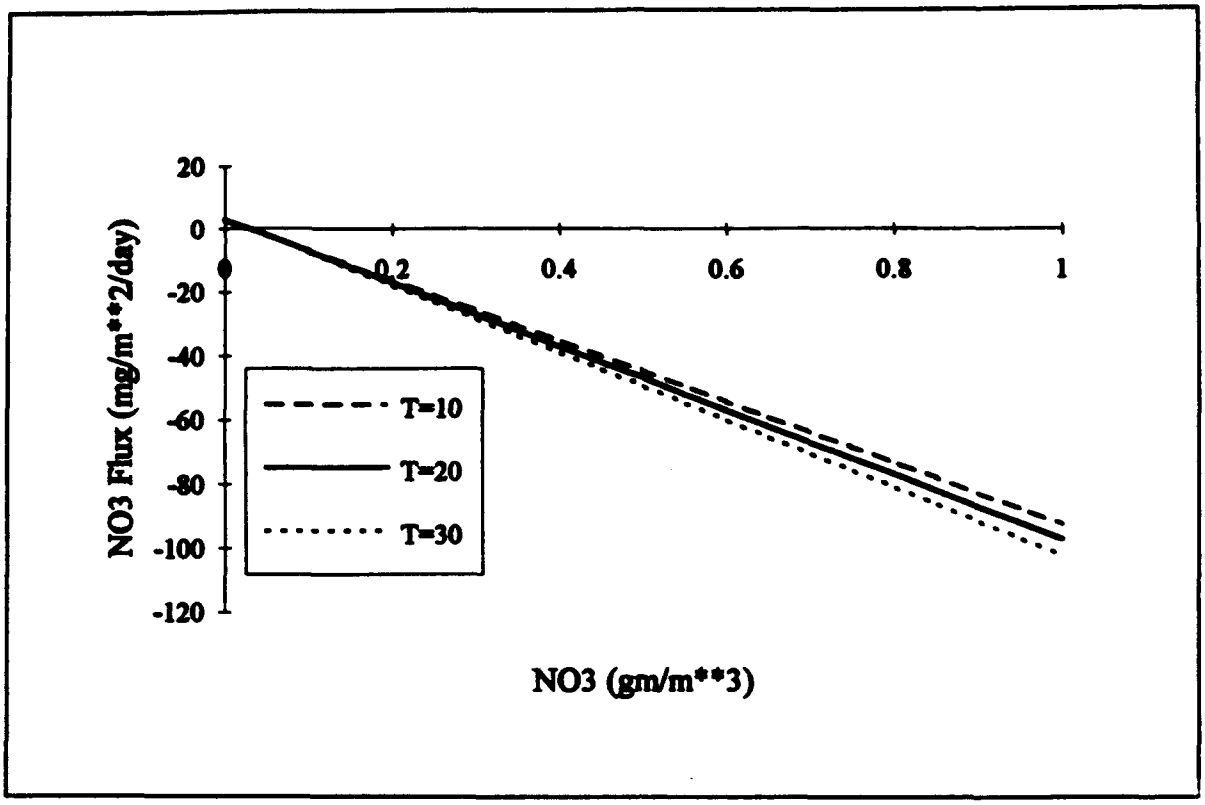

Figure 8-11. Effect of Temperature and Concentration on Sediment-Water Nitrate Flux

$$NO_3flx = s\left(NO_3sed - NO_3wat\right)e^{\alpha(T-20)} - (1 - PN)\,Nlim\,b\,Light \qquad (8\text{-}14)$$

NO_3flx = nitrate flux (gm m^2 day^{-1})

s = sediment-water mass transfer coefficient (m day^{-1})

NO_3sed = sediment nitrate concentration at sediment-water interface (gm m^{-3})

NO_3wat = water-column nitrate concentration at sediment-water interface (gm m^{-3})

Definitions of remaining terms are the same as for SOD (Equation 8-12) and ammonium (Equation 8-13).

No influence of benthic algae on nitrate flux could be discerned in the limited data base. Potential influence of benthic algae was included in the empirical model, however. The influence of benthic algae on nitrate is

identical to the influence on ammonium except that ammonium in the water must be first exhausted before nitrate is consumed. The effect of benthic algae is to increase removal of nitrate from the water column beyond the amount consumed in denitrification (Figure 8-12). The enhanced removal occurs only when light is available, however, and increases in proportion to light availability.

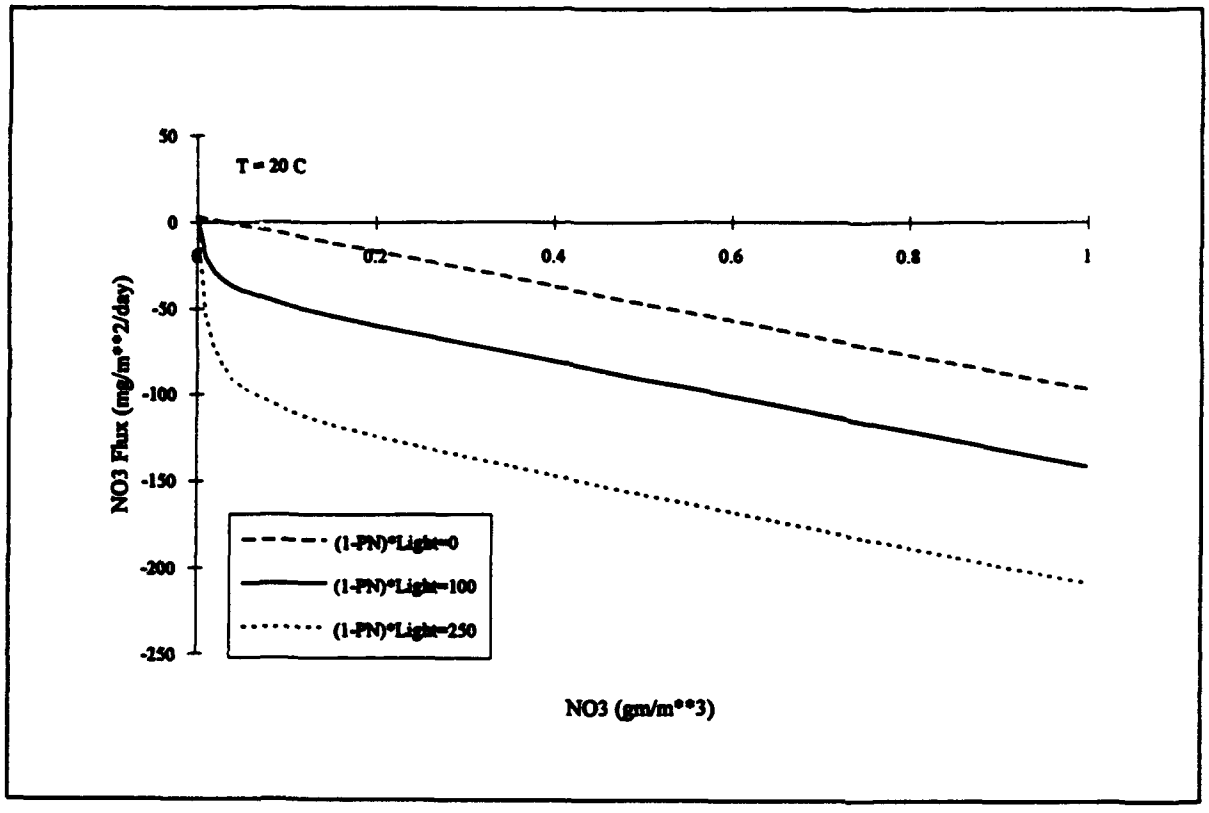

Figure 8-12. Effect of Concentration and Light on Sediment-Water Nitrate Flux

The phosphate flux model was identical in form to the ammonium flux model:

$$PO_4flx = PO_4flx_b \, e^{\alpha (T - 20)} - b \, Plim \, Light \qquad (8\text{-}15)$$

PO_4flx = phosphate flux (gm m^{-2} day^{-1})

PO_4flx_b = phosphate flux at 20 C^0 in a darkened water column

Plim = phosphorous nutrient limitation for algae

Definitions of remaining terms are the same as for SOD (Equation 8-12) and ammonium (Equation 8-13).

Phosphorus flux is positive, from sediment to water, when no light is available at the bottom (Figure 8-13). Sediment phosphate release increases as an exponential function of temperature. When light is available at the bottom, phosphate release is diminished. Under strong illumination at low temperature, sediments take up phosphate. The nutrient limitation term is identical to the term specified for phytoplankton (Equations 6-4). This term prevents sediment phosphate uptake when none is available in the water column.

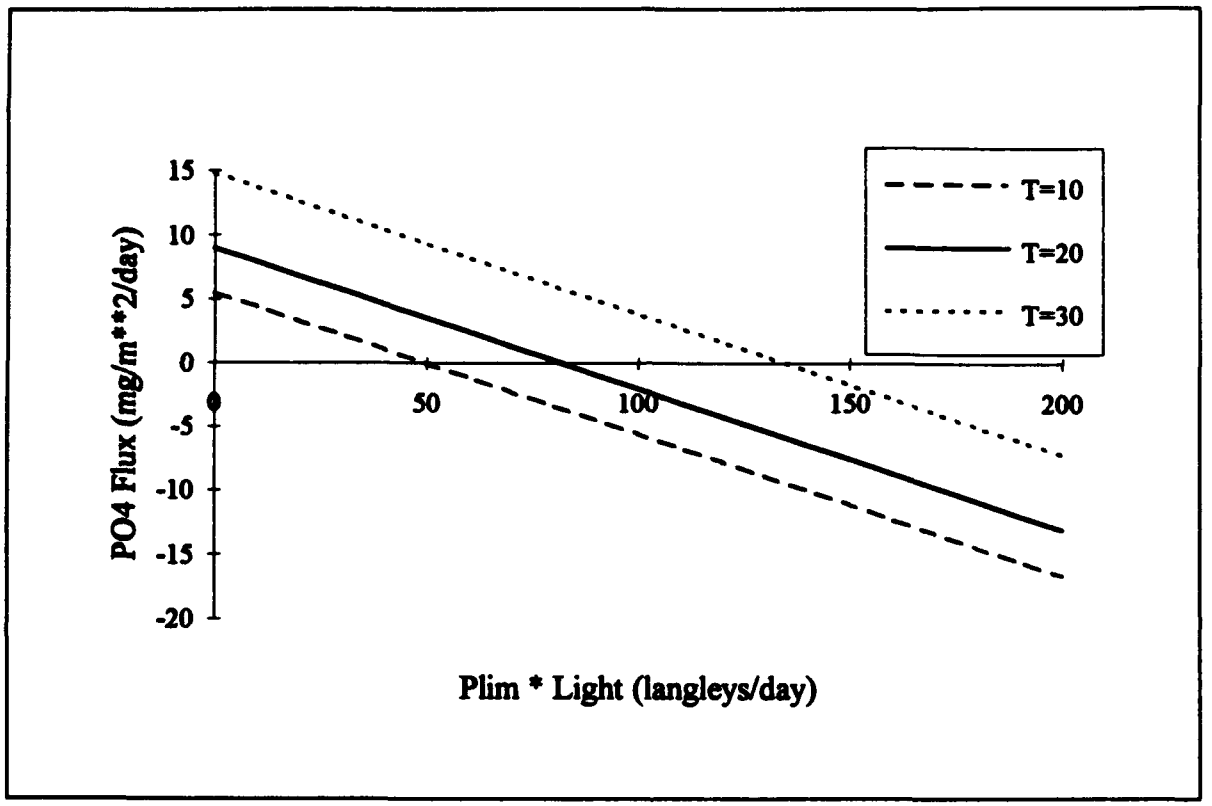

Figure 8-13. Effect of Temperature and Light on Sediment-Water Phosphate Flux

Parameters in the empirical models were initially evaluated through nonlinear regression. Initial values were refined for uniformity and to optimize model calibration. Final values are presented in Table 8-6. Sediment-water fluxes determined by the functions are compared to observations in Figure 8-14.

Computation of BOD

The biochemical oxygen demand (BOD) analysis combines measures of the concentration of oxygen-demanding material and the oxidation rate. BOD is not a model state variable but the BOD of quantities computed by the model

Table 8-6
Parameters in Empirical Flux Models

	Base Flux, gm m^{-2} day^{-1}	α, C^{θ}	b, gm m^{-2} $langley^{-1}$	s, m day^{-1}	NO_3sed, gm N m^{-3}
Sediment Oxygen Demand	−1.45	0.05	0.011		
Ammonium	0.07	0.05	$4.5x10^{-4}$		
Nitrate		0.05	$4.5x10^{-4}$	0.1	0.03
Phosphate	0.009	0.05	$1.1x10^{-4}$		

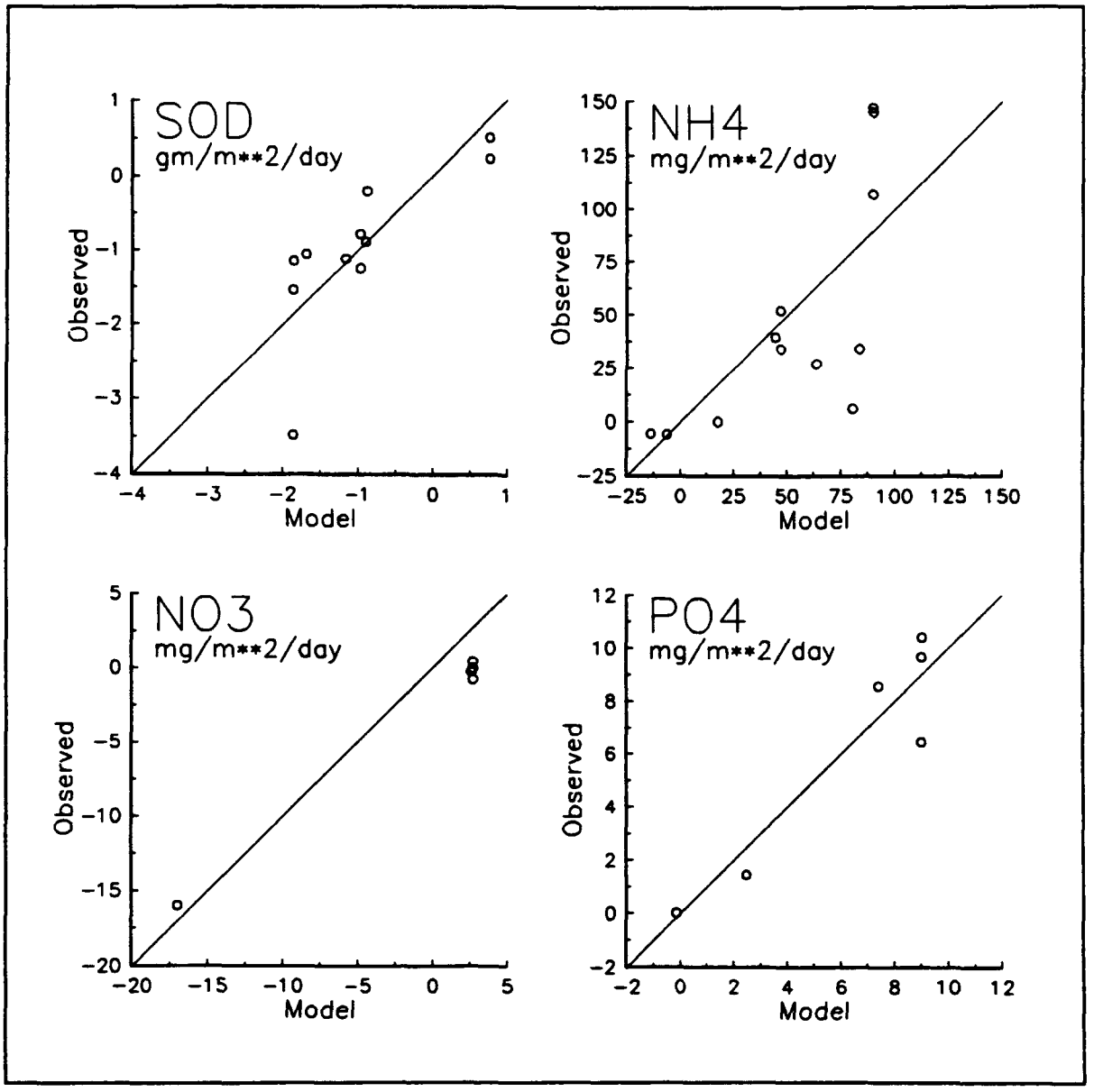

Figure 8-14. Observed and Modeled Sediment-Water Fluxes

can be calculated for comparison to five-day BOD observations. Model BOD_5 was computed:

$$BOD_5 = AOCR\,B\,(1 - e^{-5\,BM}) + AOCR\,DOC\,(1 - e^{-5\,Kdoc}) + AONT\,NH_4\,(1 - e^{-5\,\frac{NTm}{KHnnt}}) \quad (8\text{-}16)$$

BOD_5 = five-day biochemical oxygen demand (gm m^{-3})

AOCR = dissolved oxygen-to-carbon ratio in respiration (2.67 gm O_2 gm C^{-1})

B = algal biomass (gm C m^{-3})

BM = basal metabolism (day^{-1})

DOC = dissolved organic carbon (gm m^{-3})

Kdoc = respiration rate of dissolved organic carbon (day^{-1})

AONT = mass dissolved oxygen consumed per mass ammonium nitrogen nitrified (4.33 gm O_2 gm^{-1} N)

NTm = maximum nitrification rate (gm N m^{-3} day^{-1})

KHnnt = half-saturation concentration of NH_4 required for nitrification (gm N m^{-3})

The relationship is an adaptation of the formulae for oxygen consumption expressed in Chapter 6. In the computation of BOD, oxygen is considered to be available in excess and ammonium is considered to be much less than the half-saturation concentration, KHnnt. Since the BOD analysis is conducted in darkness, algal respiration is considered but not photosynthesis.

Diurnal Dissolved Oxygen Fluctuations

Algal physiological functions that create diurnal dissolved oxygen fluctuations are not well-represented by the conventional photosynthesis and respiration relations employed in eutrophication modeling. Additional influences on diurnal fluctuations, particularly macrophytes, are not represented at all in the model. Consequently, the preferred means of computing daily-minimum dissolved oxygen is through a relationship to predicted daily-mean dissolved oxygen. The relationship was developed by fitting a sinusoidal function (Figure 8-15) to each diurnal dissolved oxygen measure:

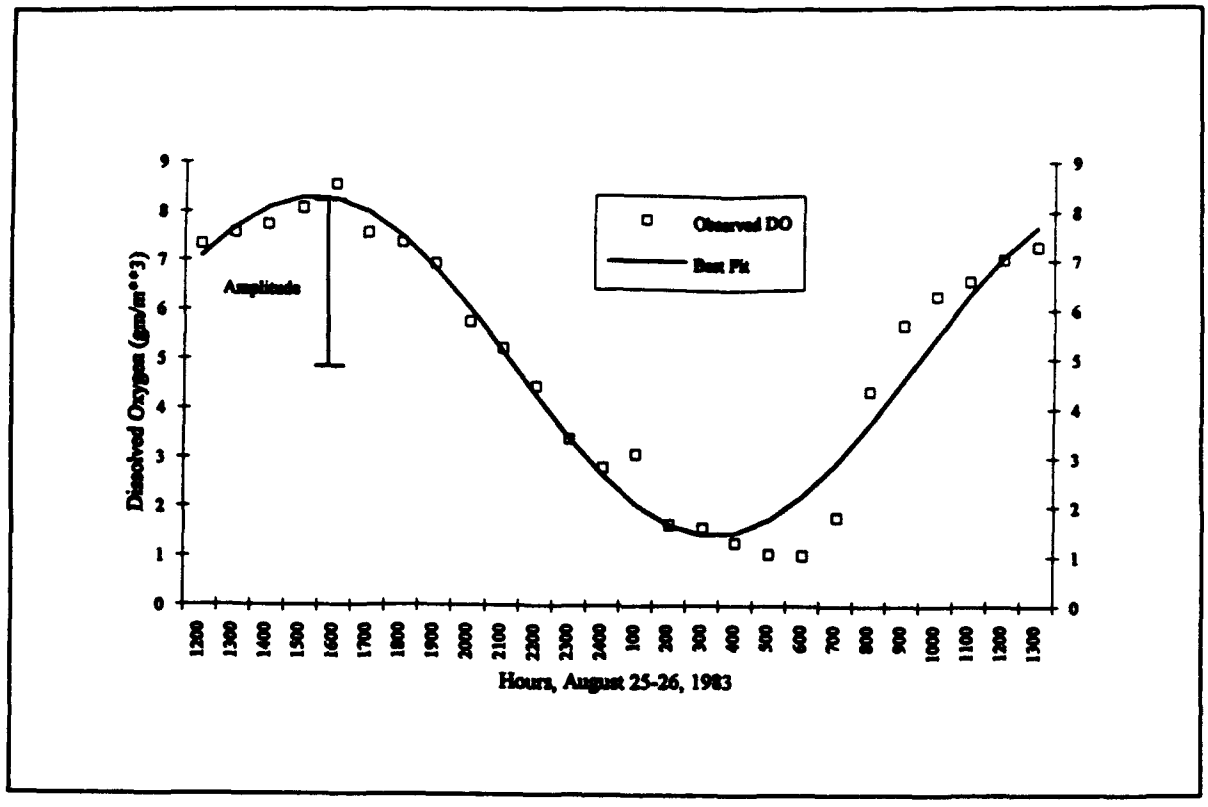

Figure 8-15. Sinusoidal Fit to Diurnal Dissolved Oxygen Data

$$DO = a + b\sin\left(\frac{2\pi}{24}T\right) + c\cos\left(\frac{2\pi}{24}T\right) \qquad (8\text{-}17)$$

DO = observed dissolved oxygen concentration (gm O_2 m^{-3})

a = mean dissolved oxygen concentration (gm O_2 m^{-3})

b, c = parameters that determine amplitude and phase of diurnal DO fluctuation (gm O_2 m^{-3})

Parameters a, b, and c were determined by regression. Amplitude was computed:

$$A = \sqrt{b^2 + c^2} \qquad (8\text{-}18)$$

A = amplitude of diurnal DO fluctuation (gm O_2 m^{-3})

Next, regression was used to relate amplitude to chlorophyll concentration. The resulting relationship was:

$$A = 1.51 + 0.033\,Chl \qquad (8\text{-}19)$$

Chl = chlorophyll 'a' concentration (mg m^{-3})

R^2 for the regression was 0.76. Worth noting is that a diurnal fluctuation of 1.5 gm O_2 m^{-3} exists in the absence of algae (Figure 8-16) and is presumably caused by aquatic vegetation.

To compute daily-minimum DO, daily-average predicted chlorophyll is substituted in Equation 8-19 to obtain amplitude. Amplitude is subtracted from daily-average predicted dissolved oxygen to yield daily minimum.

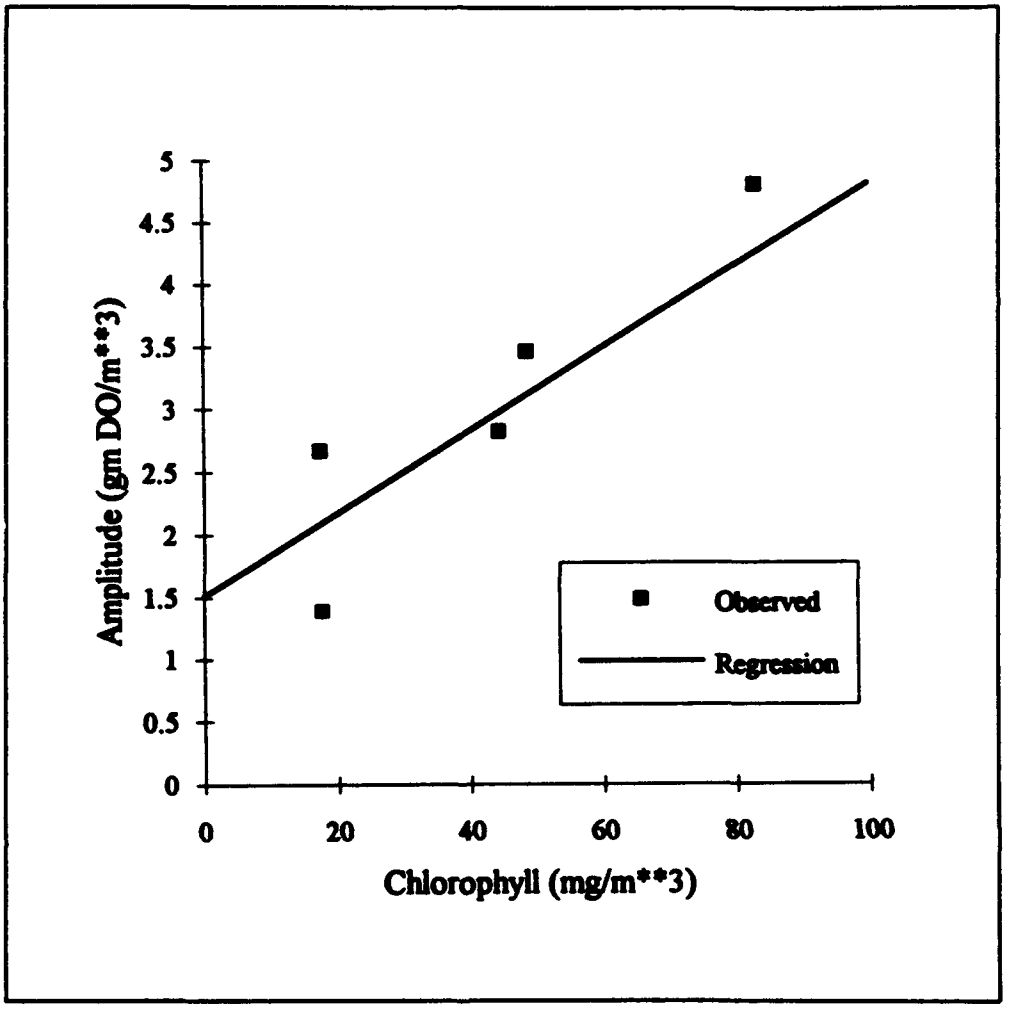

Figure 8-16. Effect of Chlorophyll on Amplitude of Diurnal Dissolved Oxygen Fluctuation

Chapter IX: Water Quality Model Application and Analysis

Water Quality Time Series

The primary means of calibrating the water quality model was through comparison of modeled and observed time series of water quality constituents. Time series were compared in eight model cells (Figure 9-1) selected to provide spatial coverage and a sufficient number of observations. Calibration was an iterative process in which kinetics coefficients (Table 6-2), sediment model parameters (Table 8-6), and load fractions (Table 8-2) were adjusted to improve model-data agreement. Calibration ceased when no additional improvement was possible. The final calibration time series are shown as Figures 9-2 through 9-9. Observations are grab samples collected within a model cell. Symbols indicate the source of the observations. Model results are daily average values for the cell. The temporal origin (Year 0) is January 1, 1988. Time series cease (Year 3) on December 31, 1990.

Longitudinal Transect

Additional insight into the calibration status was gained through comparison of observations and model results along a longitudinal transect that extended from the Millsboro spillway to the mouth of the Indian River inlet. Transects were plotted for the summer of each calibration year (Figures 9-10 through 9-12). The spatial origin (Km. 0) was at the spillway. Data collection along the transect was not synoptic. Neither were observations collected at uniform intervals throughout the summer. Consequently, no attempt was made to produce a summer-average from the data. Grab samples collected in the months of June, July, or August were plotted at the location of the observation. These were compared to summer-average model results. Point-by-point agreement between the model average and grab samples was not expected. Rather, the plots were used to assess observed and predicted spatial trends and approximate agreement in concentration.

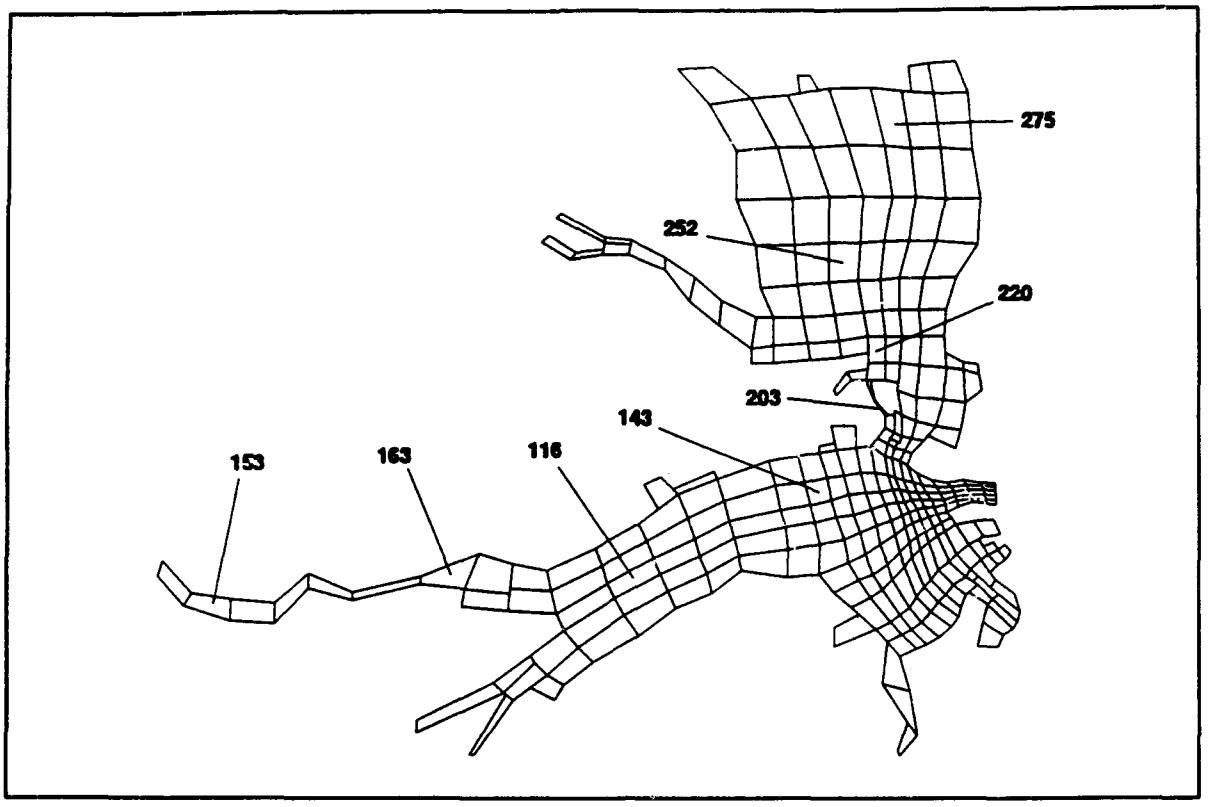

Figure 9-1. Grid Cells Selected for Time Series Presentation

Sediment-Water Fluxes

Time series of modeled sediment-water fluxes (Figures 9-13 through 9-20) were produced at the same locations as the calibration time series (Figure 9-1). By convention, fluxes from water to sediments were shown as negative values. Positive values indicated sediment release to the water column. The "Carbon - Oxygen Flux" time series included carbon deposition to the sediments and sediment oxygen demand. The "Nitrogen Flux" time series included particulate nitrogen deposition to the sediments, sediment-water ammonium flux, and sediment-water nitrate flux. The "Phosphorus Flux" time series indicated particulate phosphorus deposition to the sediments and sediment-water phosphate flux.

Interpretive Information

Time series of interpretive information available from the model (Figures 9-21 through 9-28) were produced at the same locations as the calibration time series (Figure 9-1). One time series indicated the computed nutrient and light limitations on algal growth (Equations 6-4, 6-6). Potential limitation ranged from zero (complete limitation on growth) to unity (no limit on growth). A

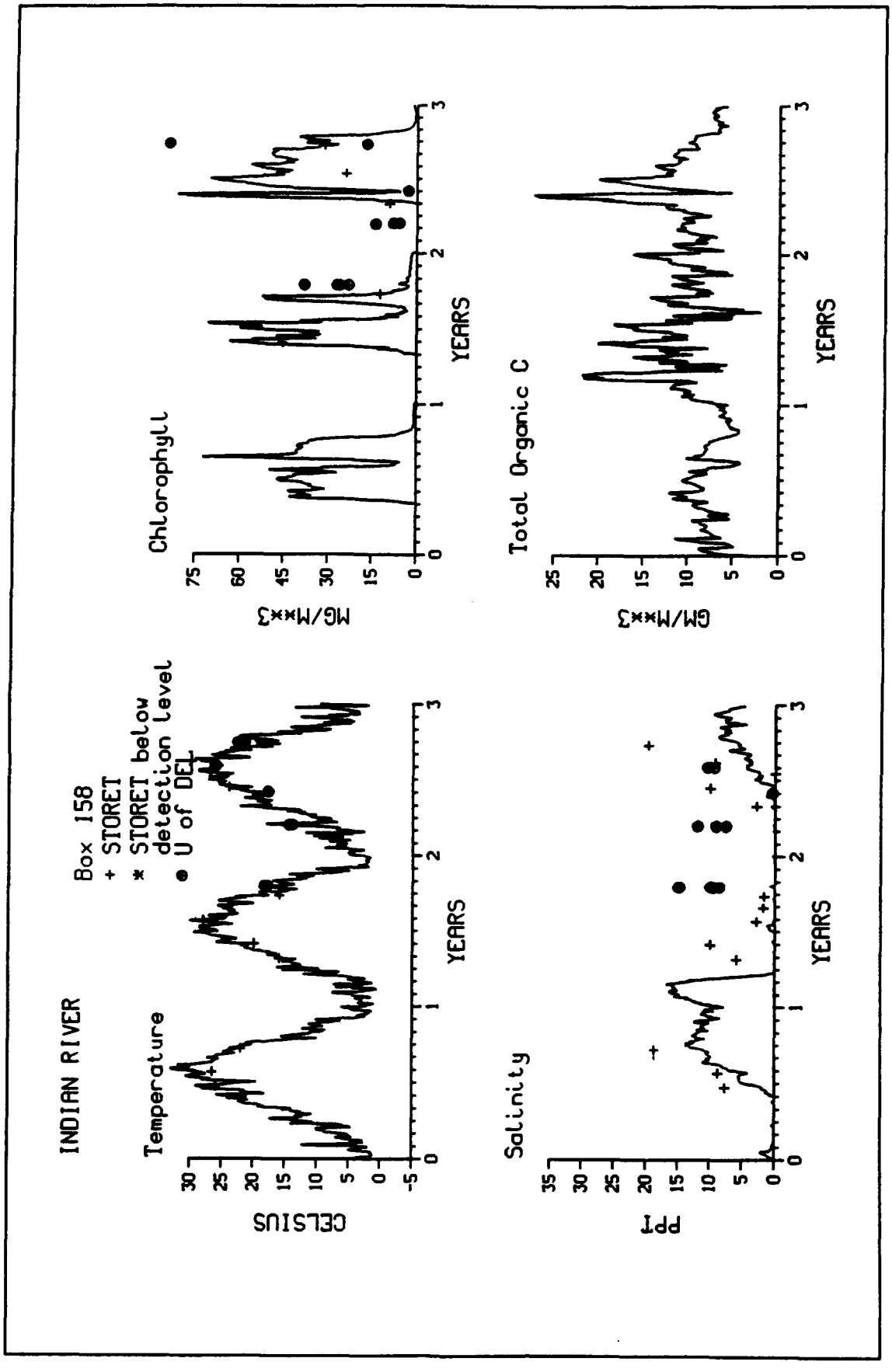

Figure 9-2. Time Series of Observed and Modeled Water-Column Concentrations, Grid Cell 158 (Sheet 1 of 3)

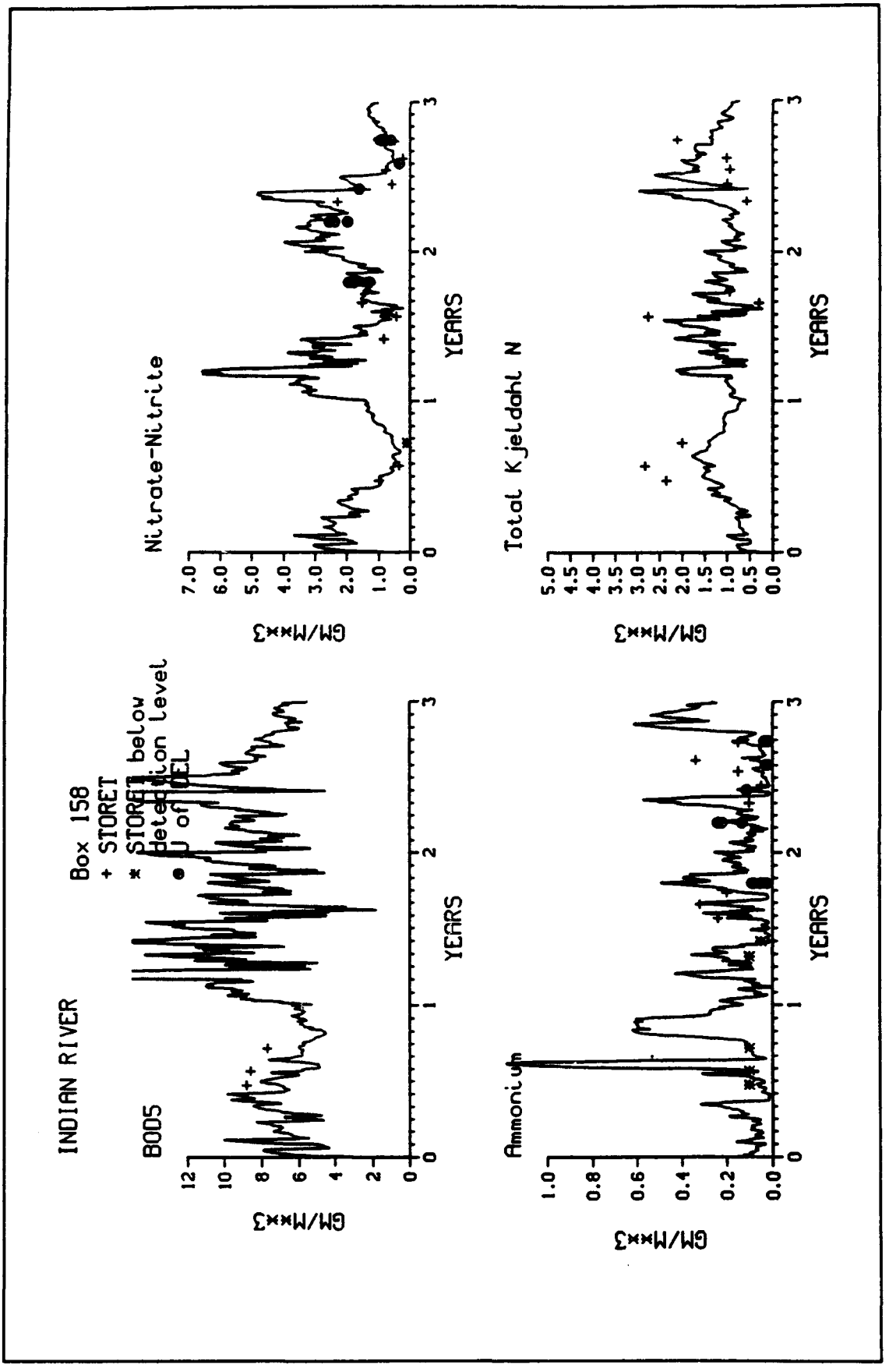

Figure 9-2. (Sheet 2 of 3)

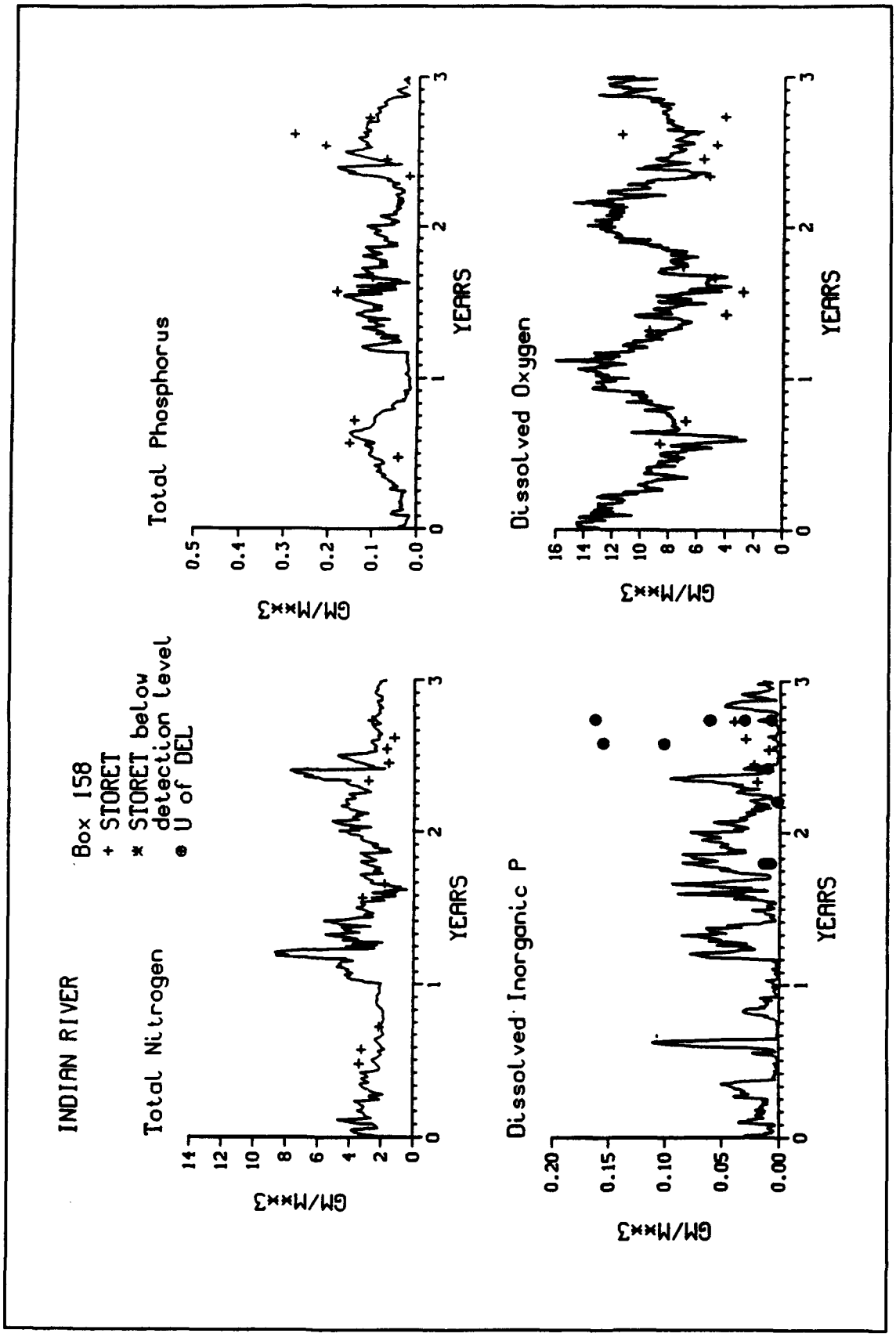

Figure 9-2. (Sheet 3 of 3)

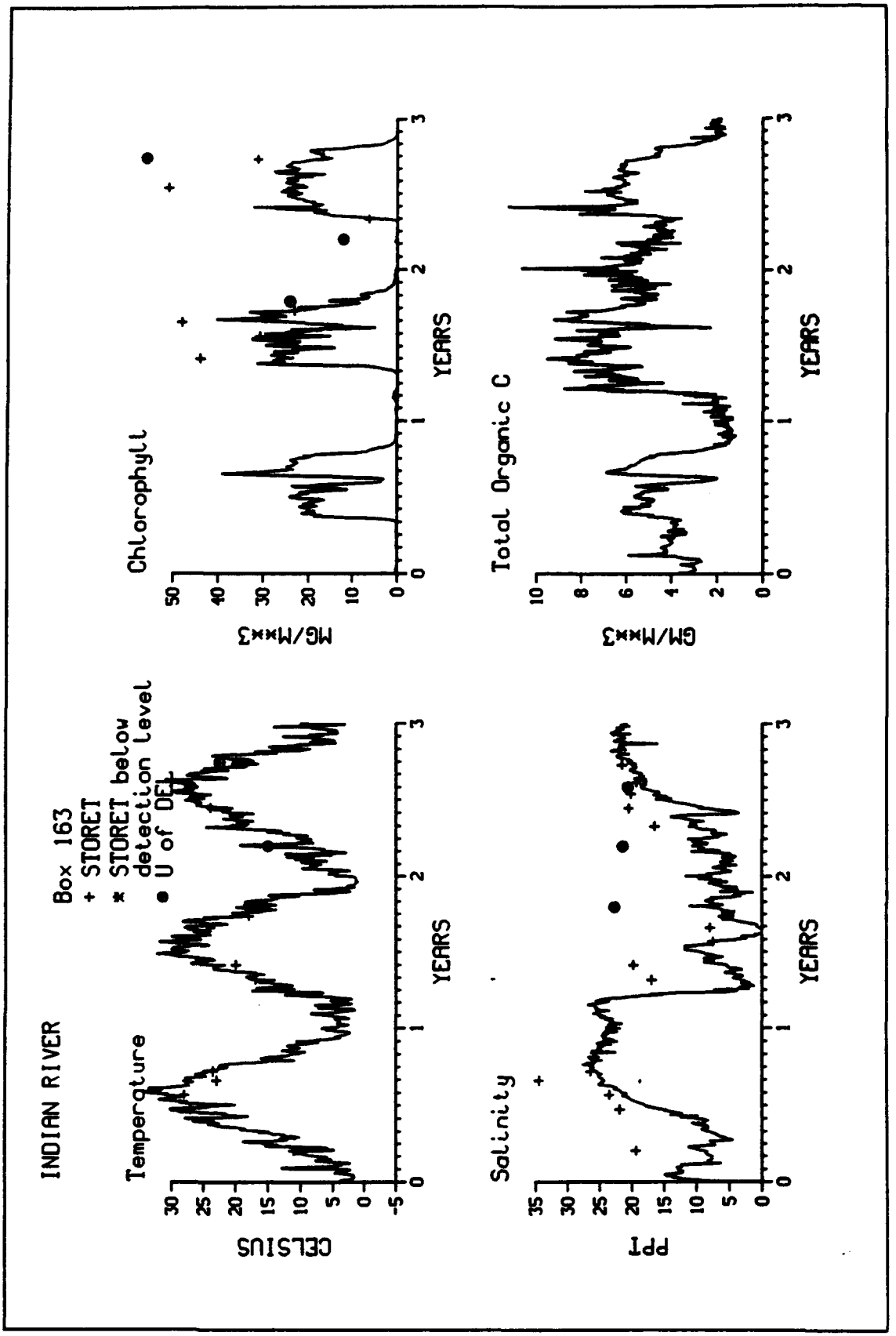

Figure 9-3. Time Series of Observed and Modeled Water-Column Concentrations, Grid Cell 163 (Sheet 1 of 3)

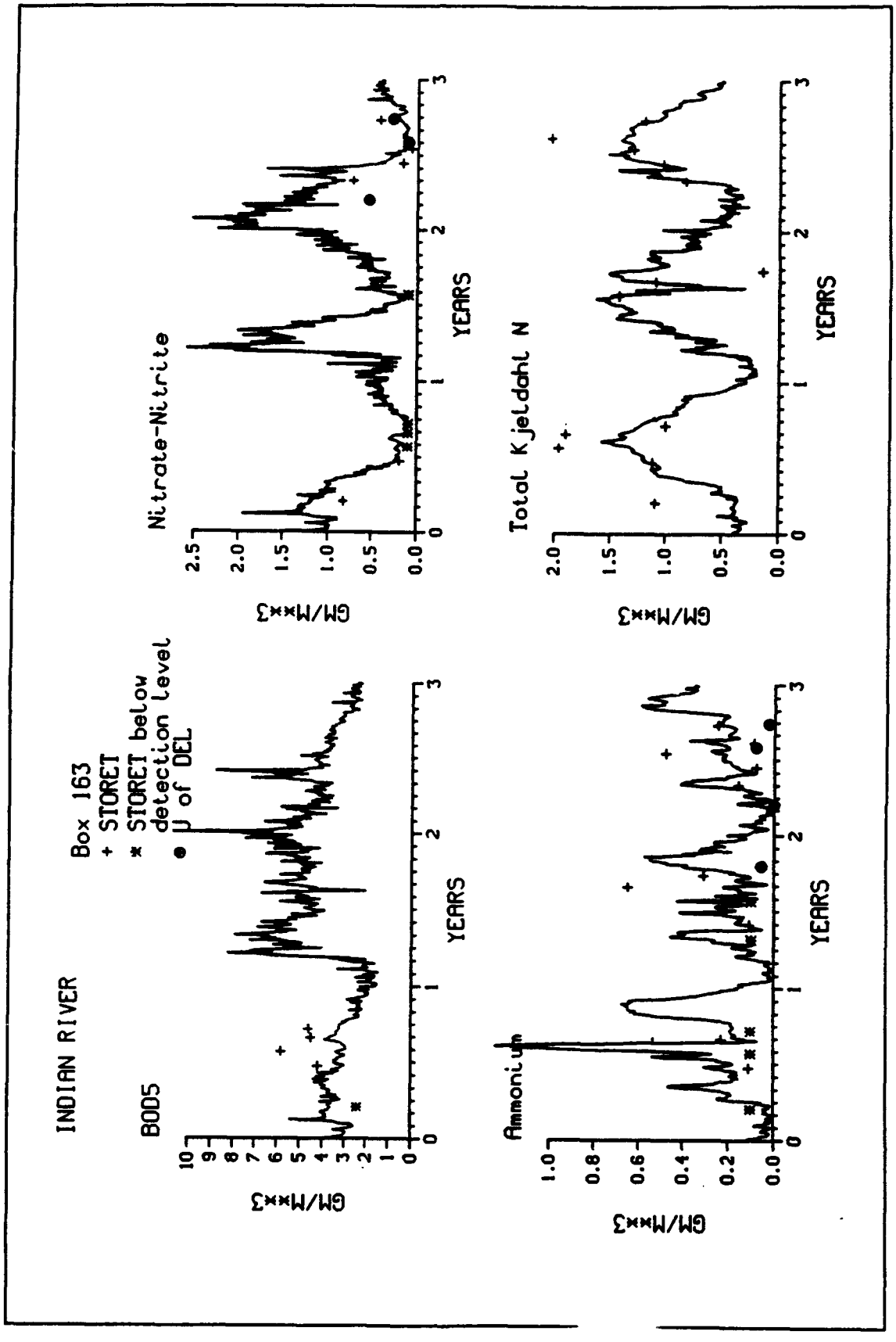

Figure 9-3. (Sheet 2 of 3)

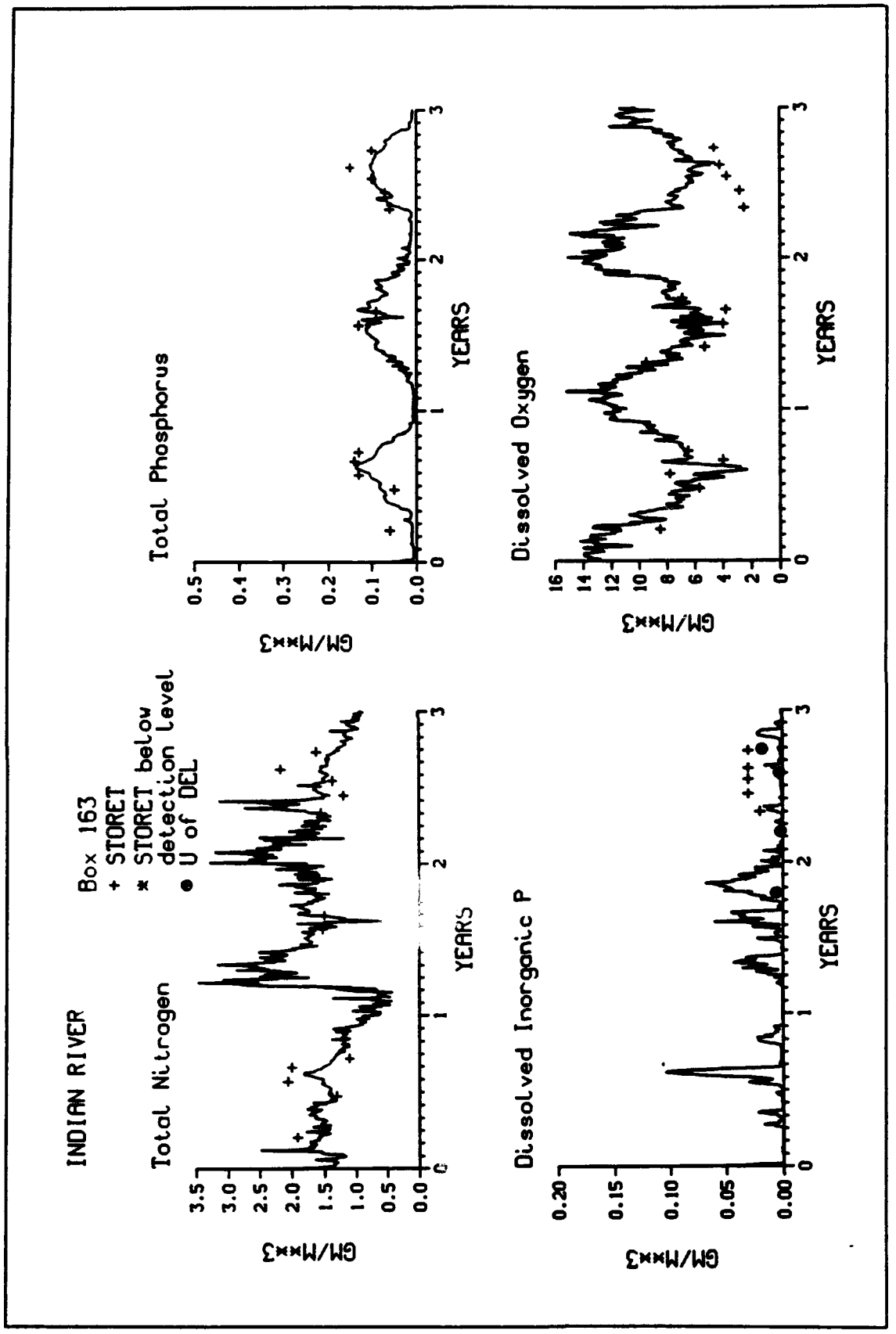

Figure 9-3. (Sheet 3 of 3)

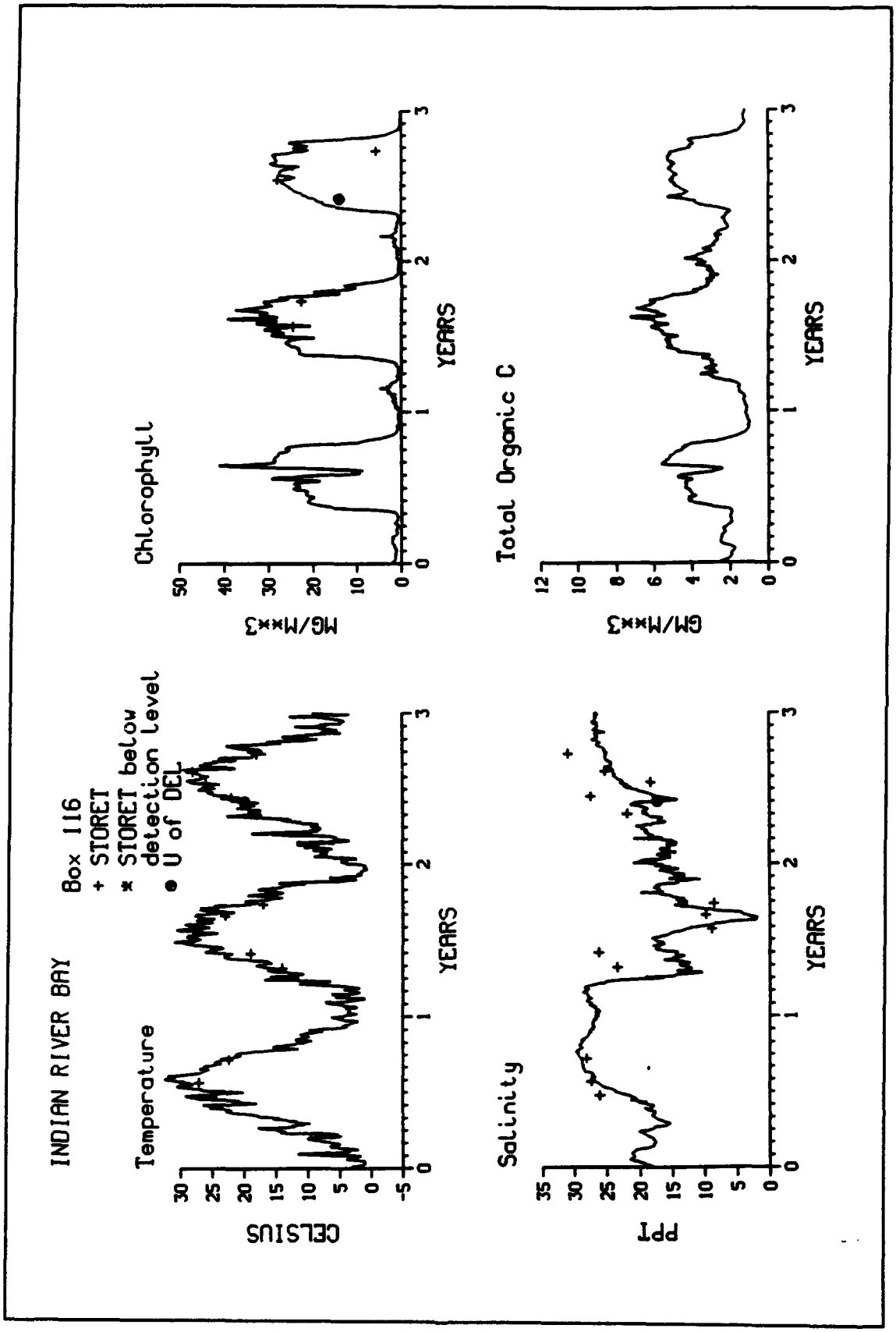

Figure 9-4. Time Series of Observed and Modeled Water-Column Concentrations, Grid Cell 116 (Sheet 1 of 3)

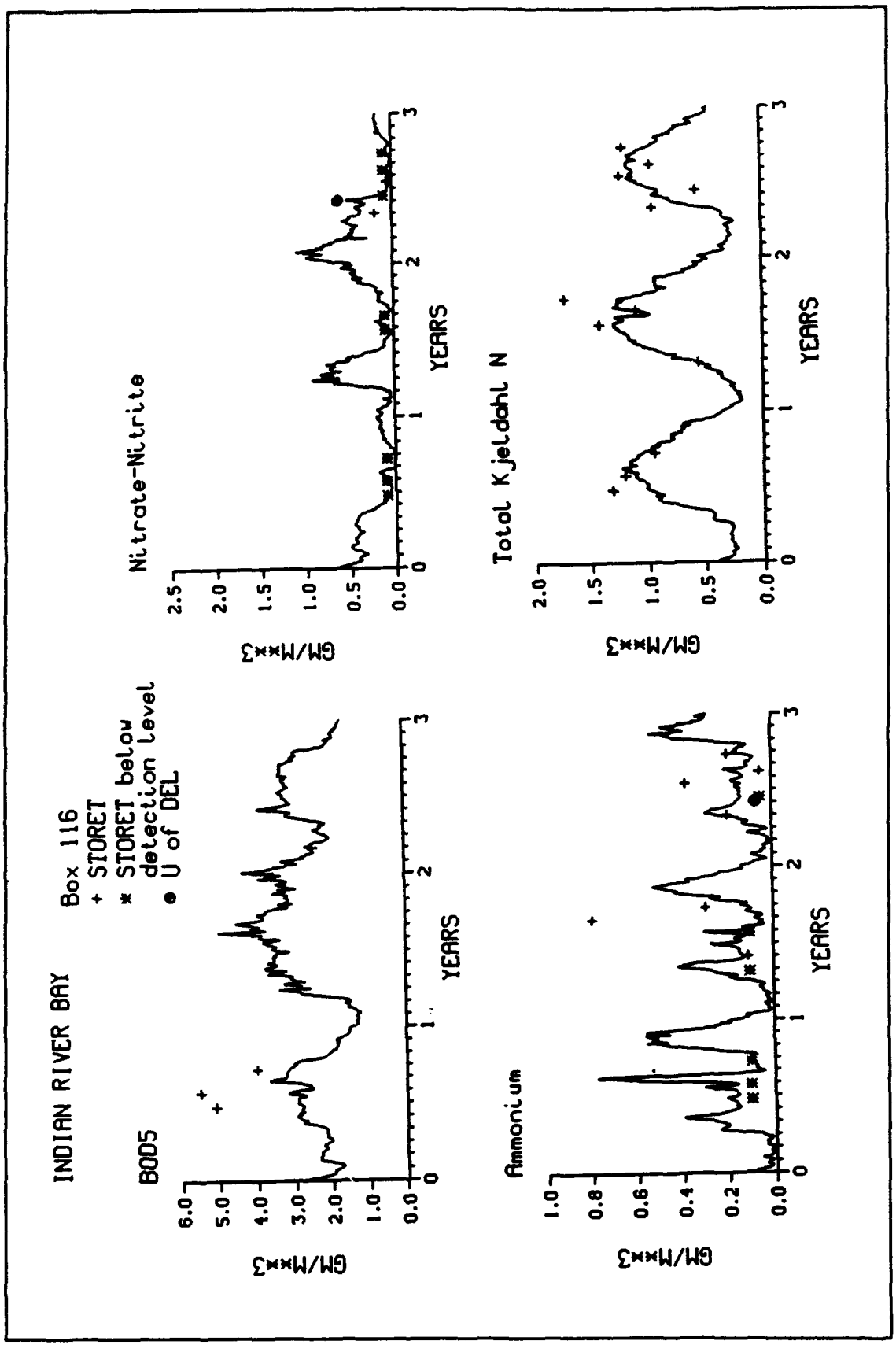

Figure 9-4. (Sheet 2 of 3)

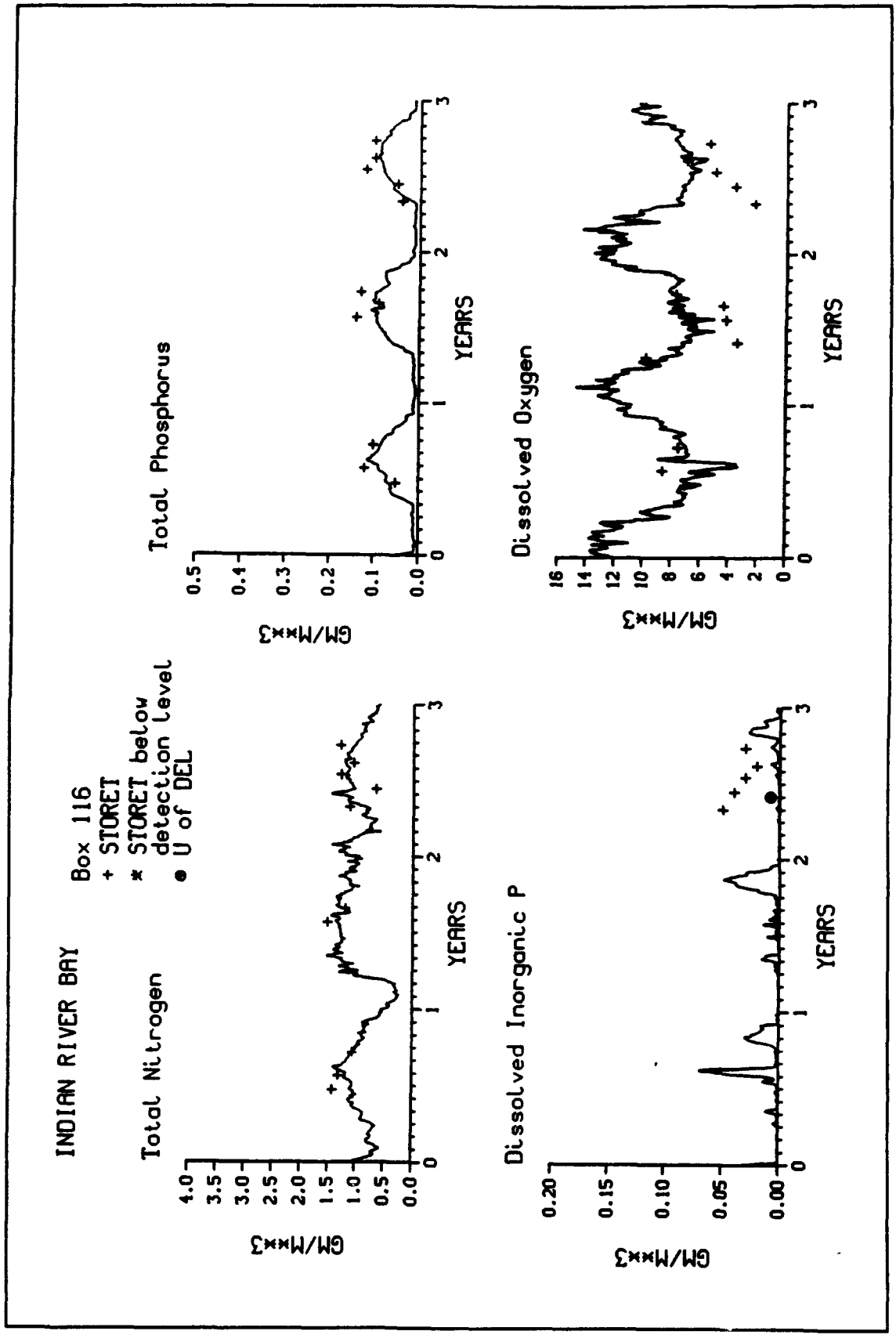

Figure 9-4. (Sheet 3 of 3)

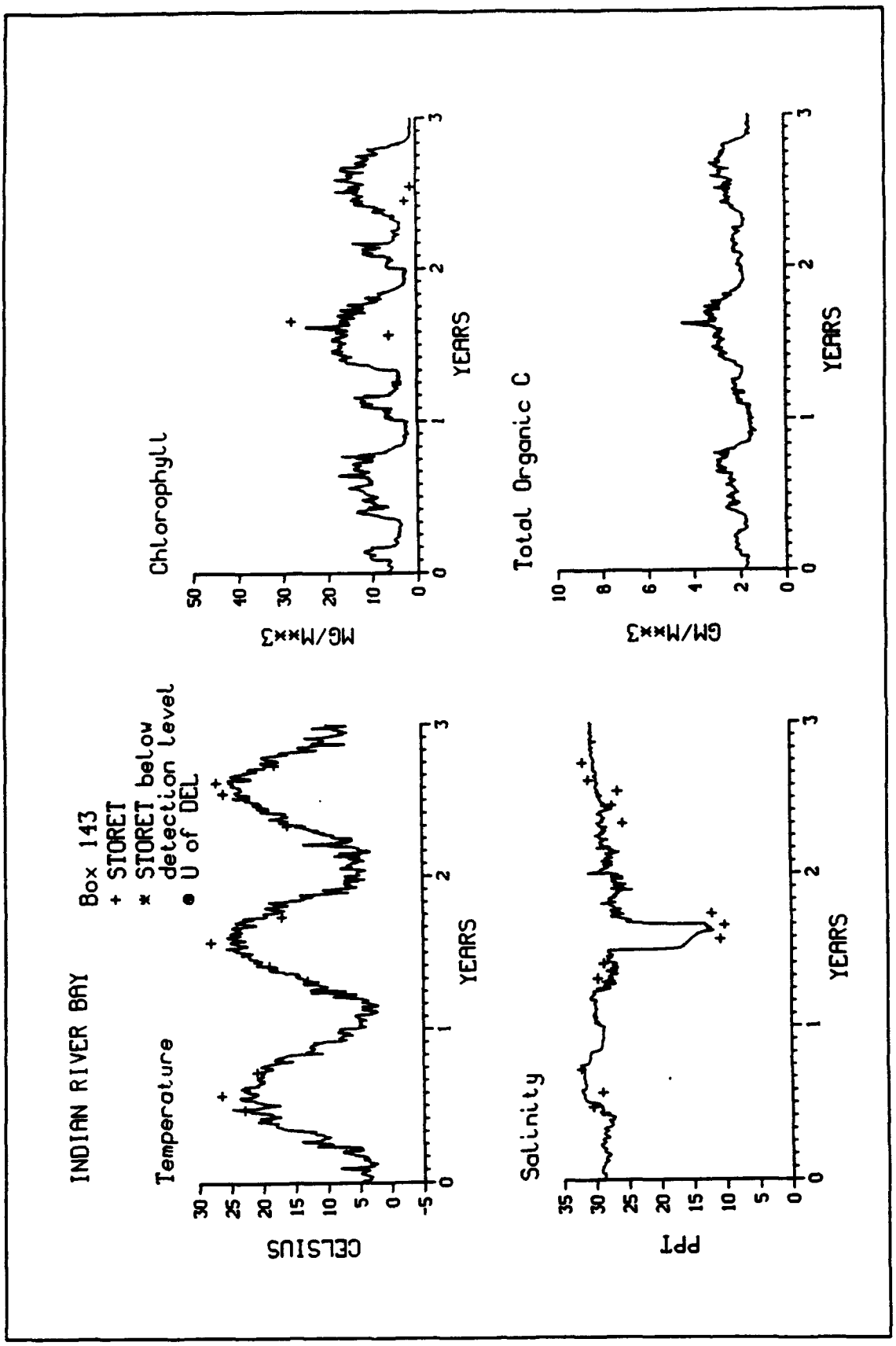

Figure 9-5. Time Series of Observed and Modeled Water-Column Concentrations, Grid Cell 143 (Sheet 1 of 3)

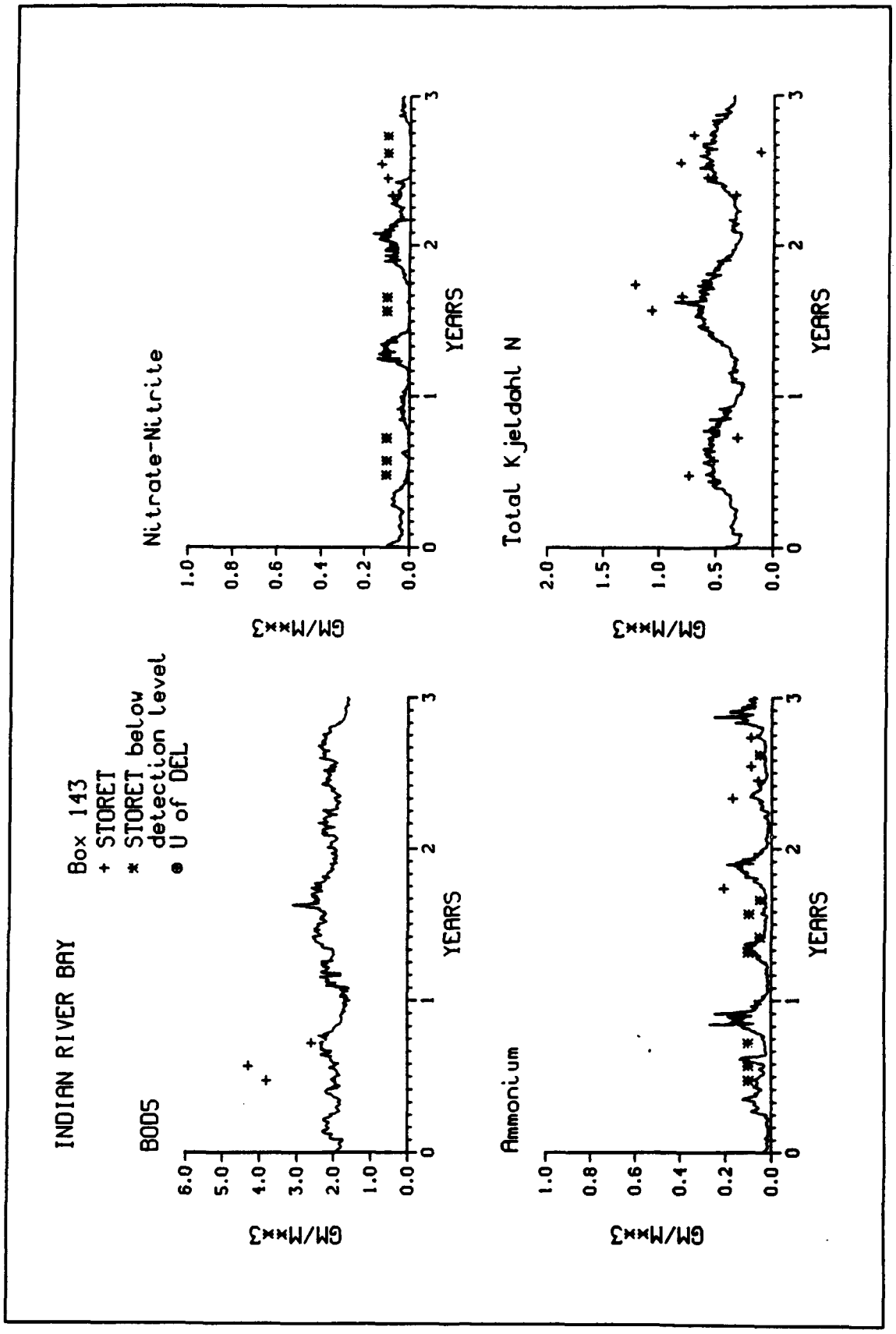

Figure 9-5. (Sheet 2 of 3)

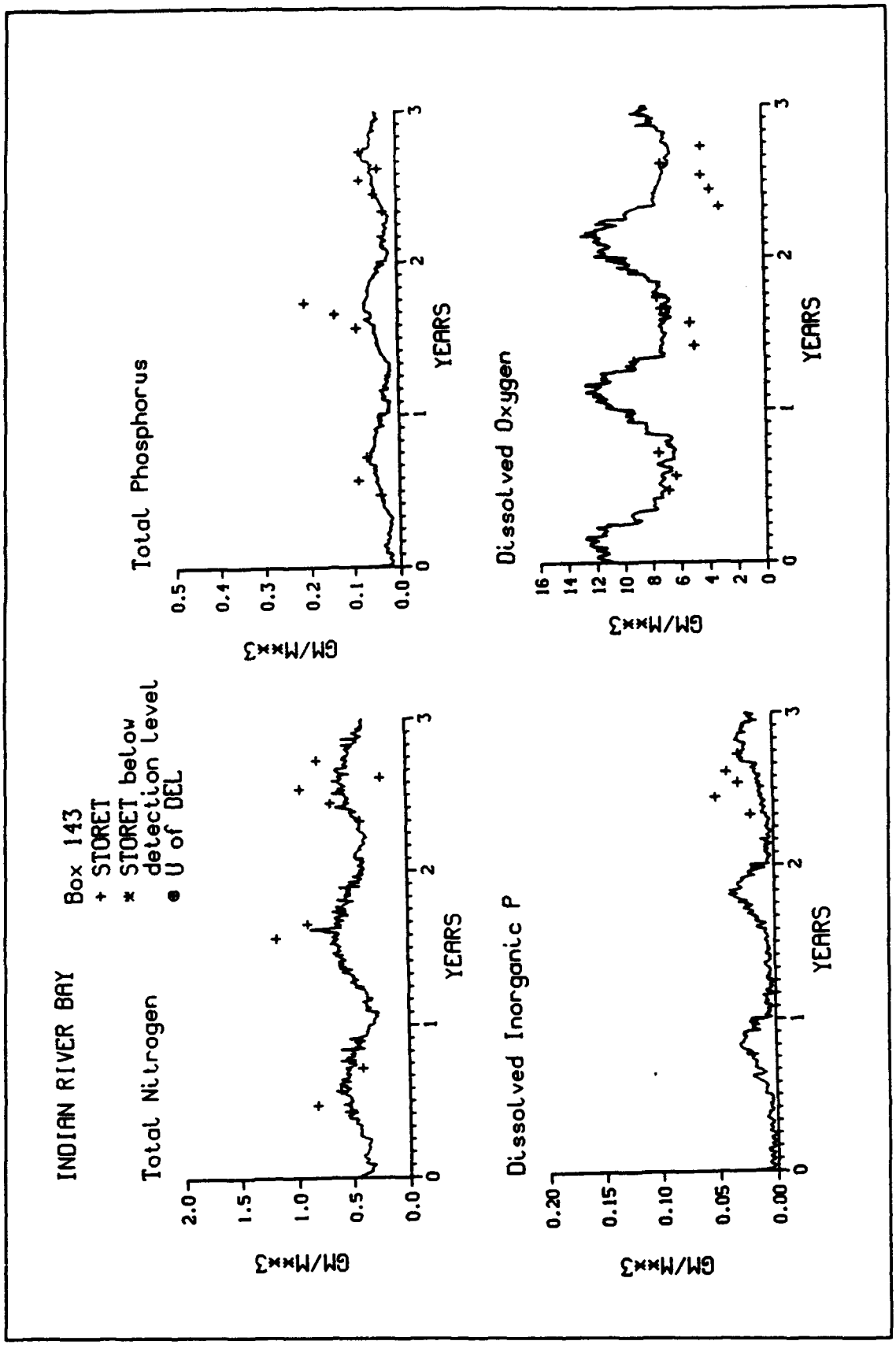

Figure 9-5. (Sheet 3 of 3)

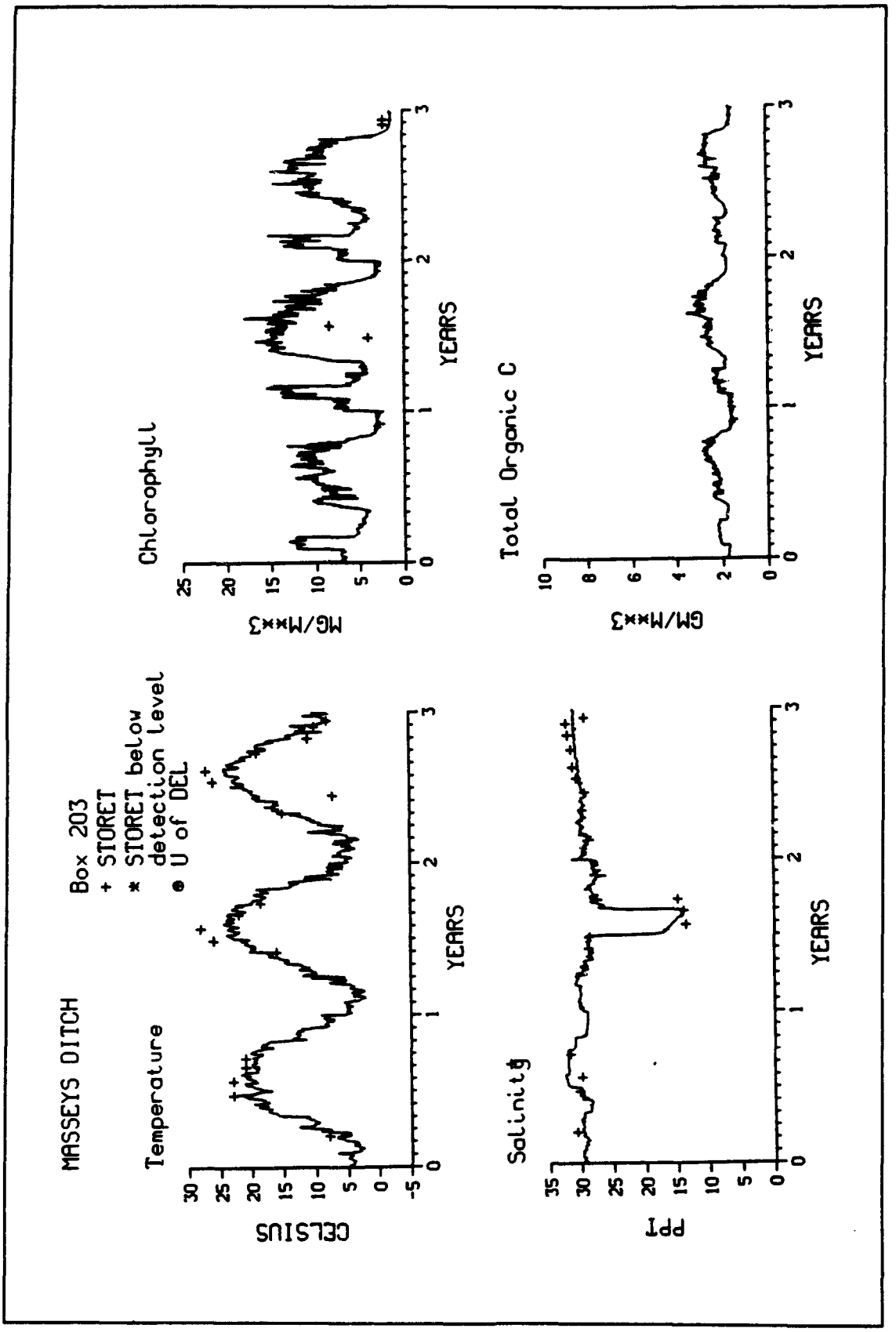

Figure 9-6. Time Series of Observed and Modeled Water-Column Concentrations, Grid Cell 203 (Sheet 1 of 3)

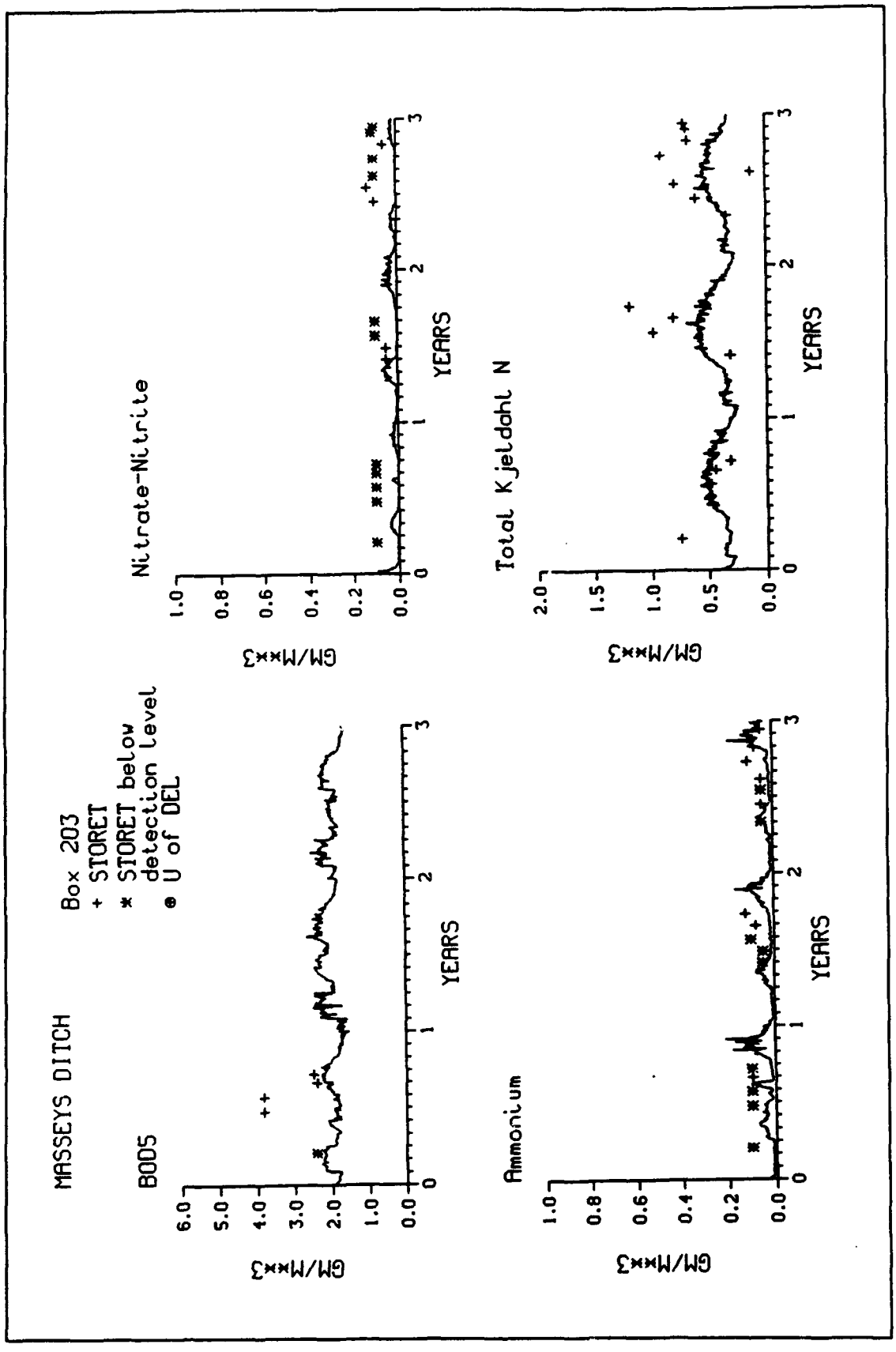

Figure 9-6. (Sheet 2 of 3)

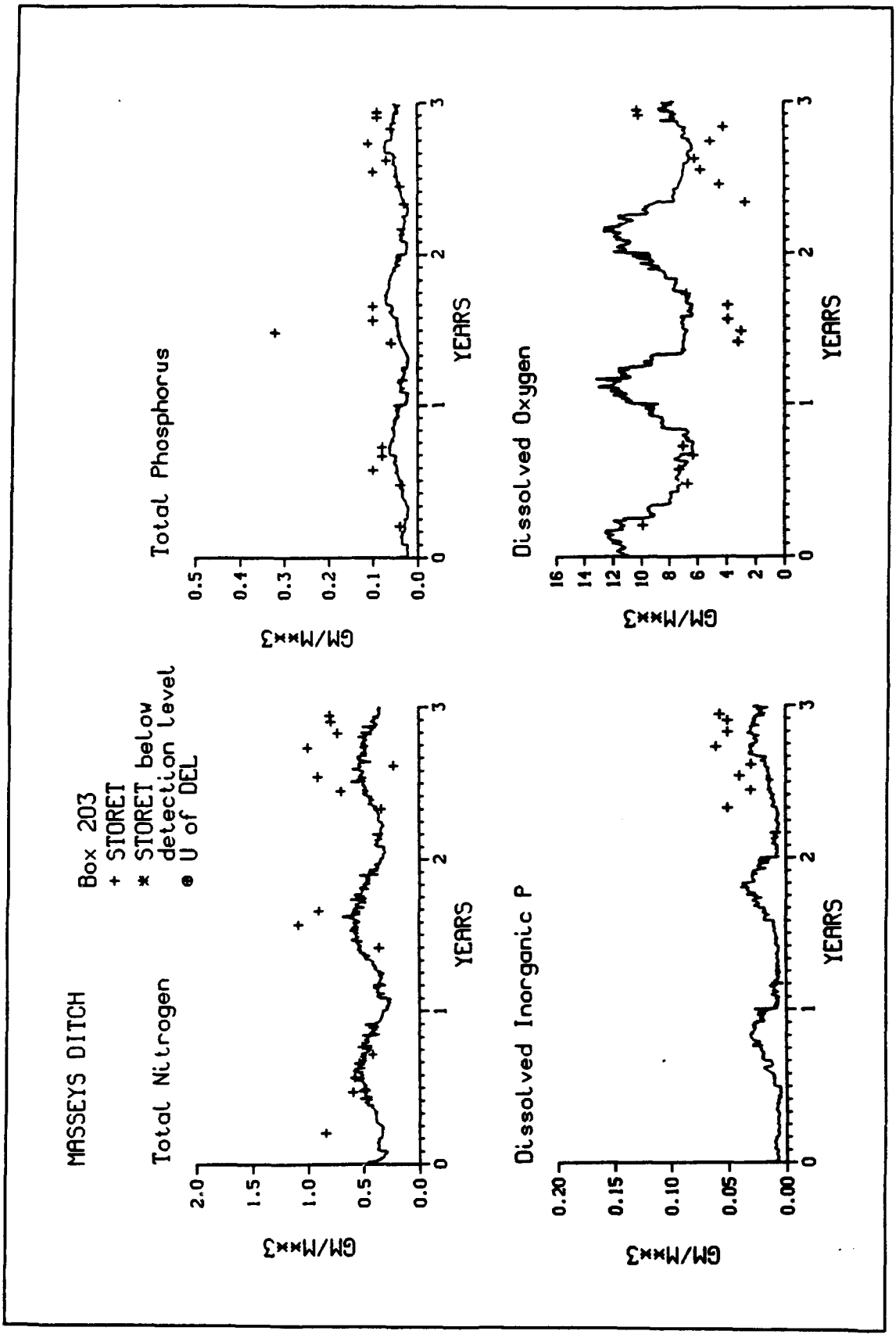

Figure 9-6. (Sheet 3 of 3)

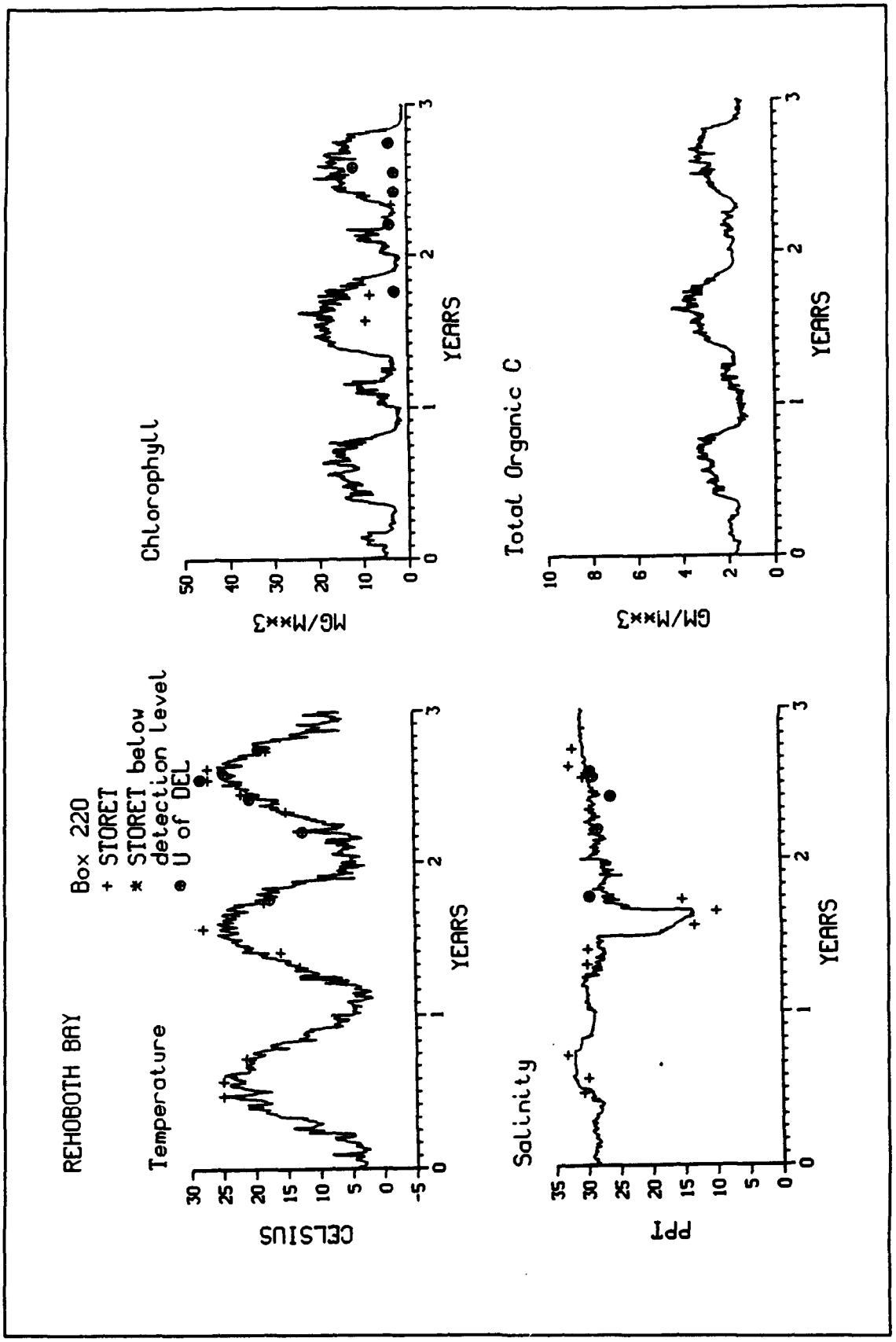

Figure 9-7. Time Series of Observed and Modeled Water-Column Concentrations, Grid Cell 220 (Sheet 1 of 3)

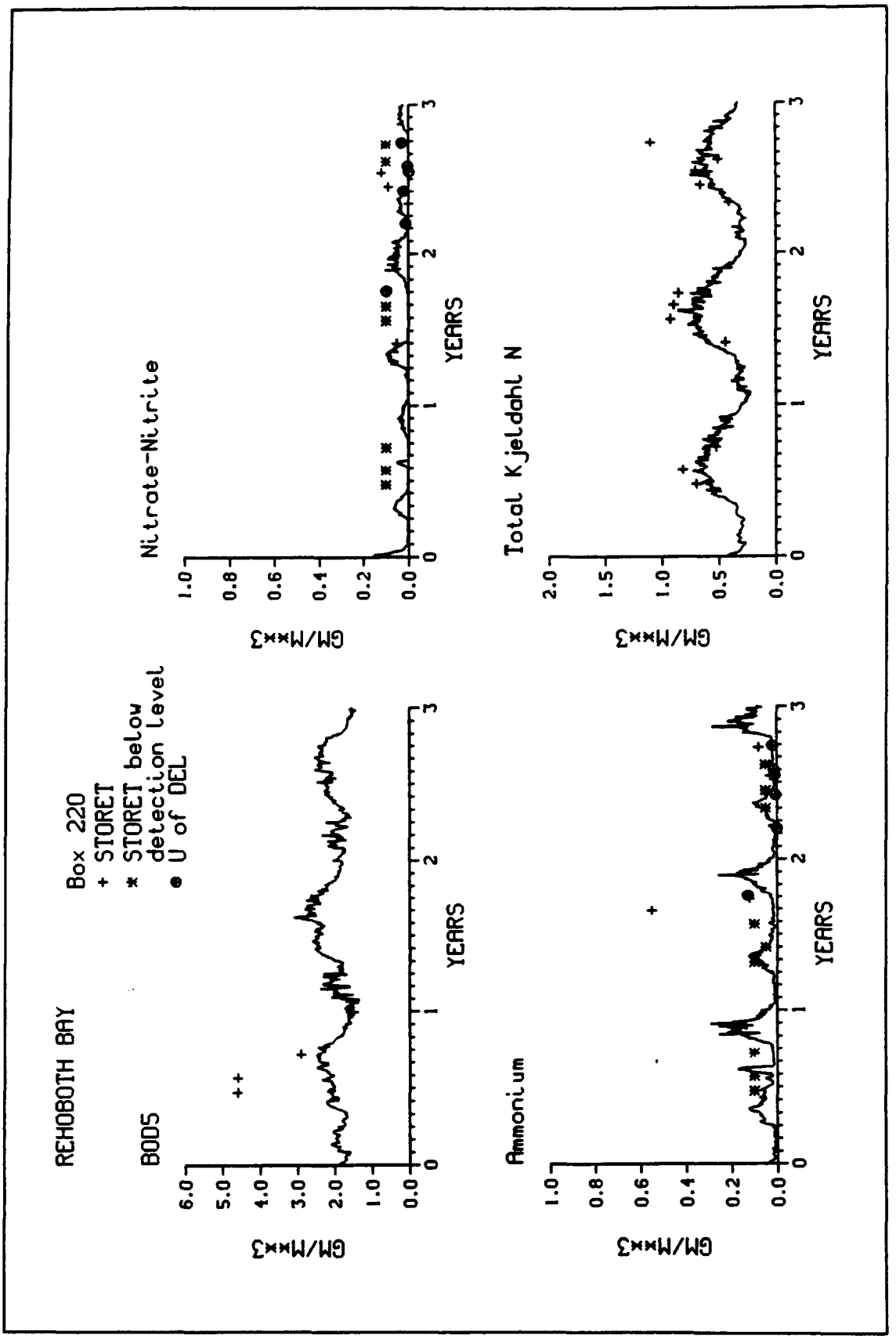

Figure 9-7. (Sheet 2 of 3)

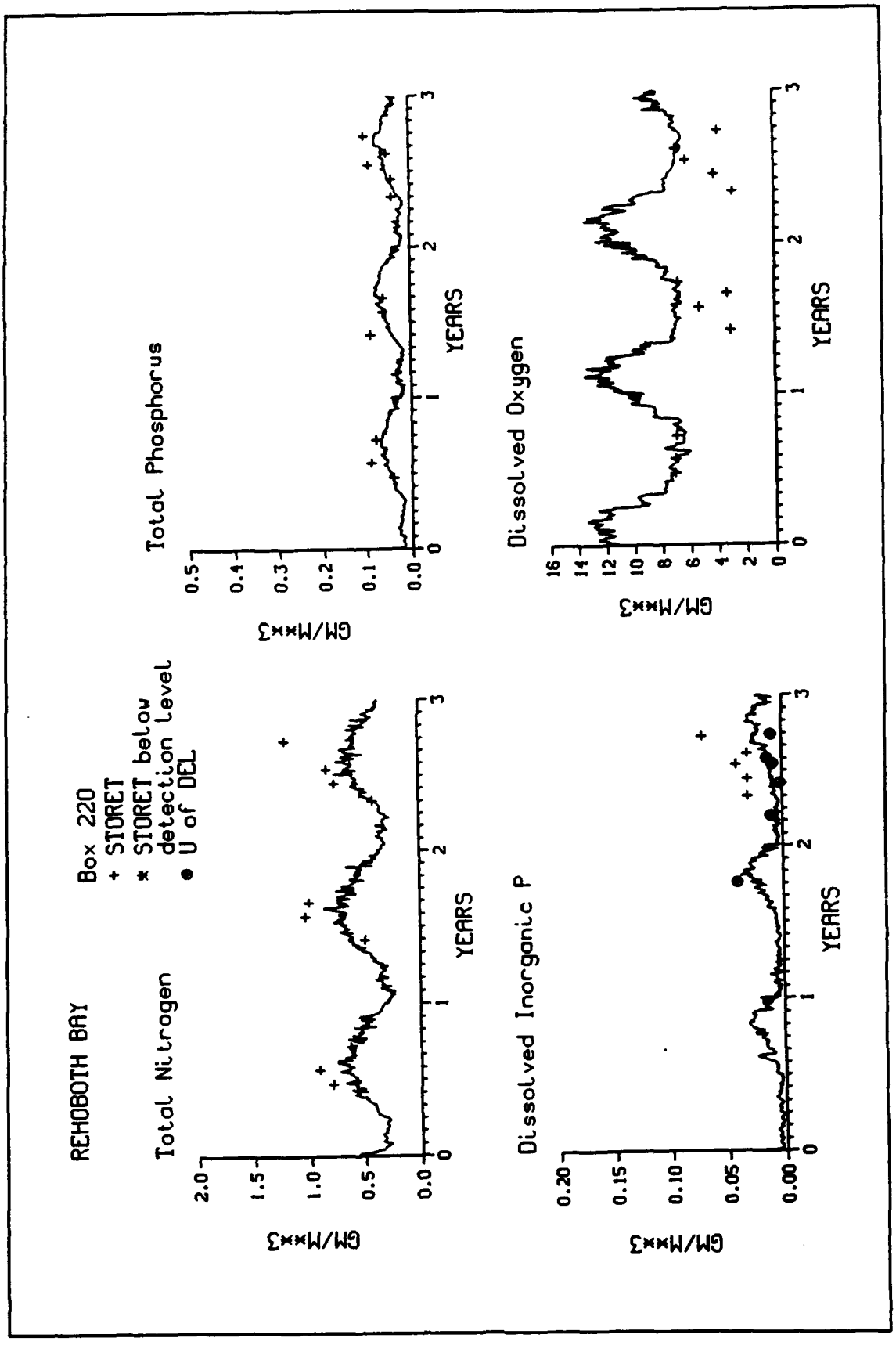

Figure 9-7. (Sheet 3 of 3)

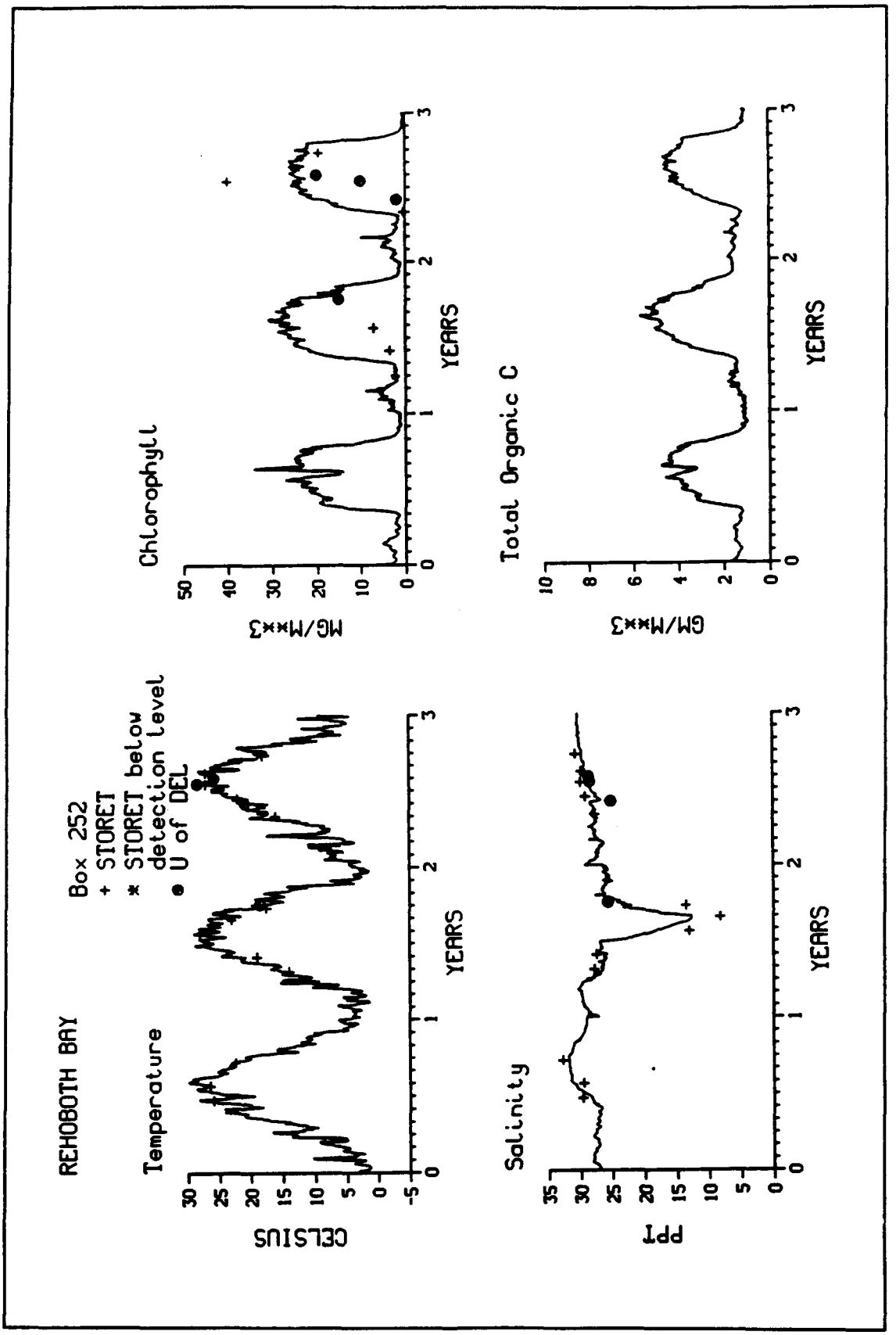

Figure 9-8. Time Series of Observed and Modeled Water-Column Concentrations, Grid Cell 252 (Sheet 1 of 3)

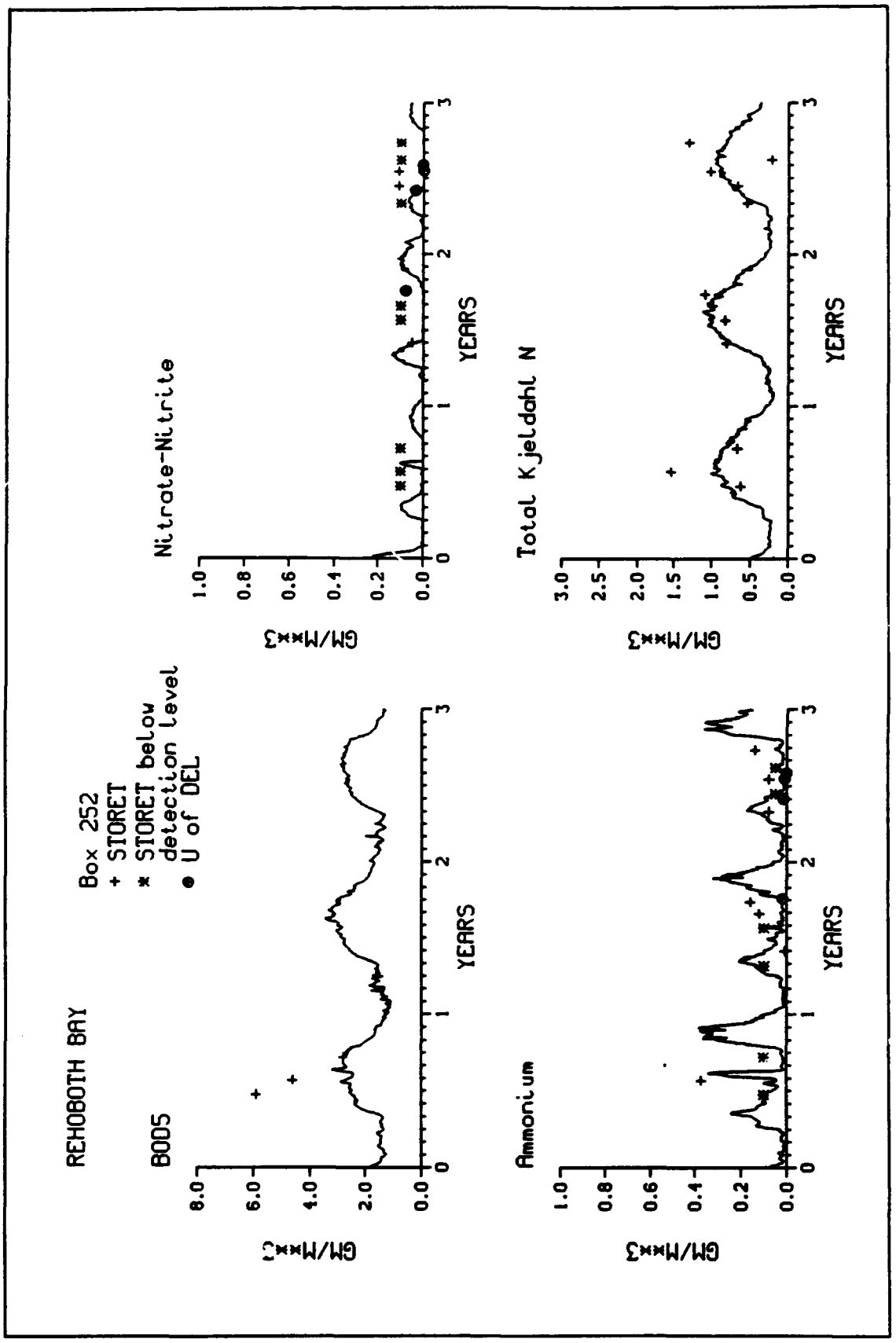

Figure 9-8. (Sheet 2 of 3)

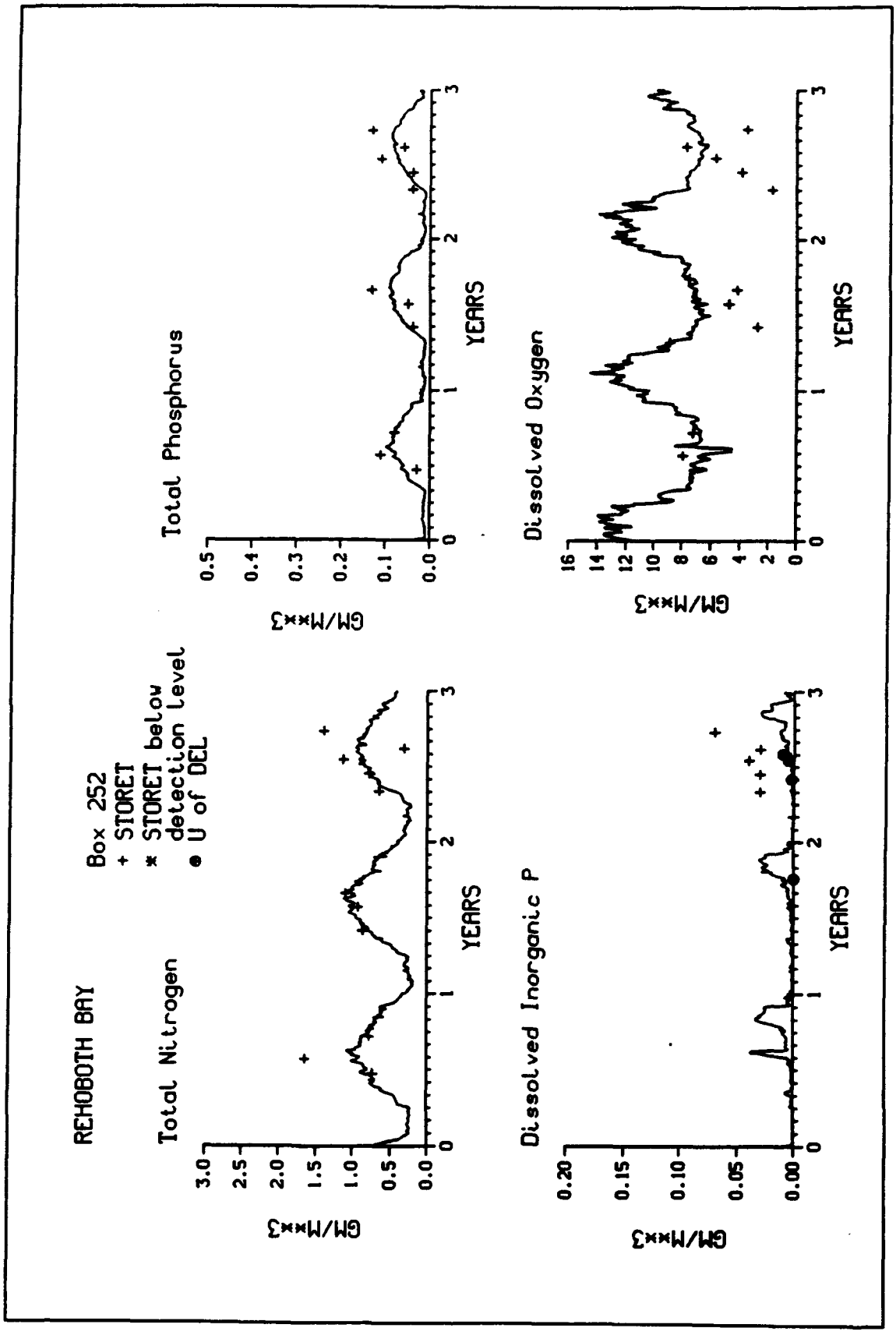

Figure 9-8. (Sheet 3 of 3)

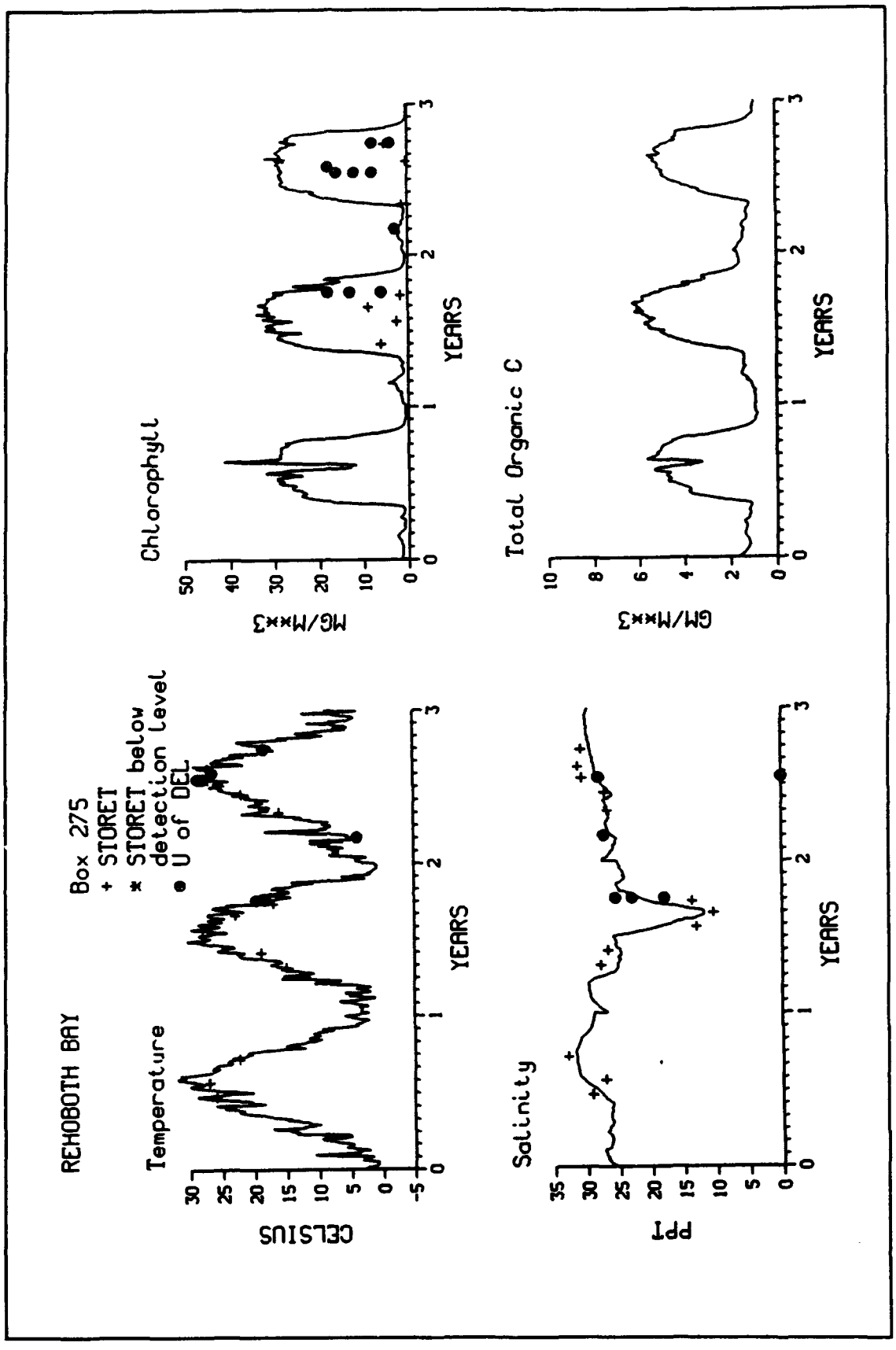

Figure 9-9. Time Series of Observed and Modeled Water-Column Concentrations, Grid Cell 275 (Sheet 1 of 3)

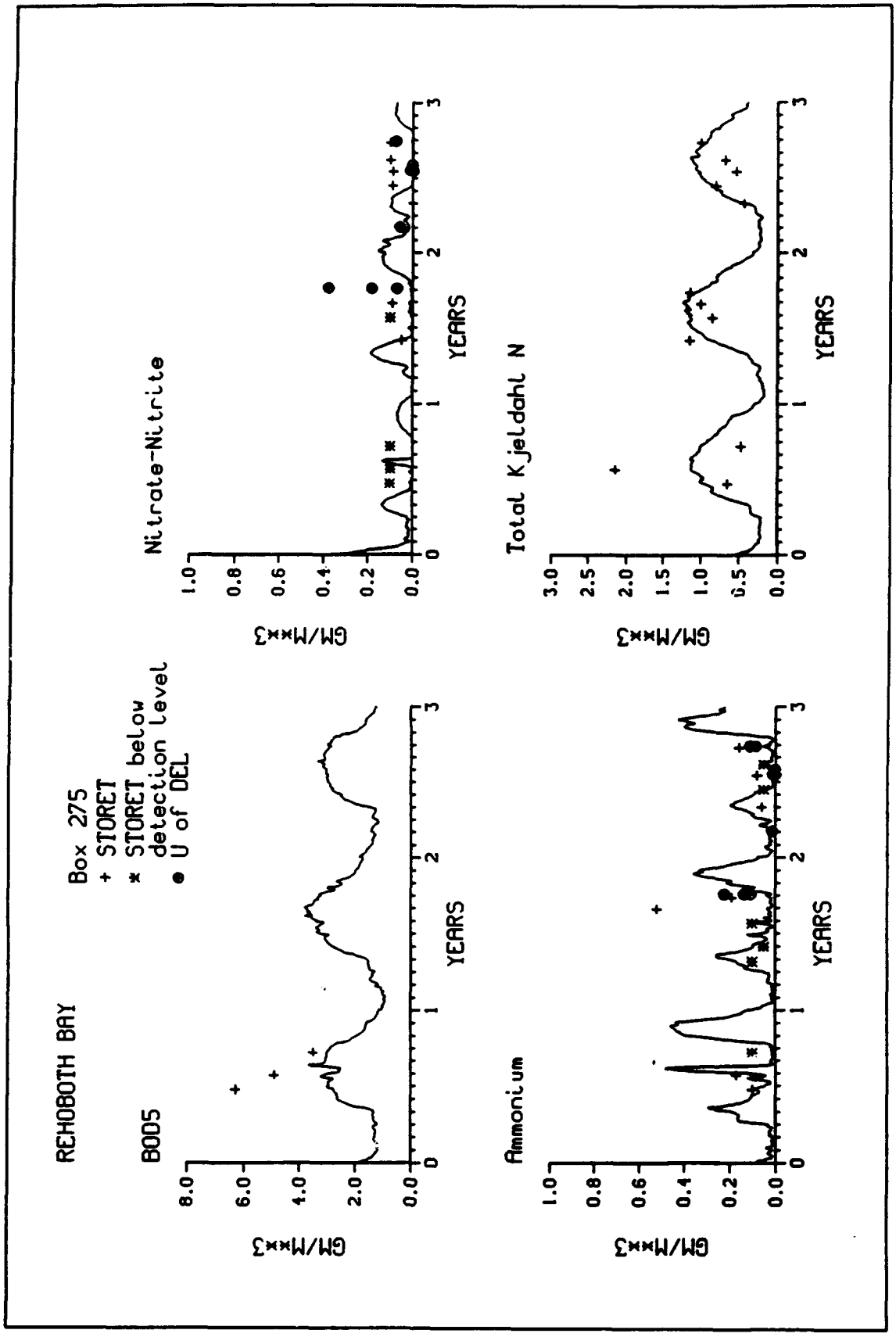

Figure 9-9. (Sheet 2 of 3)

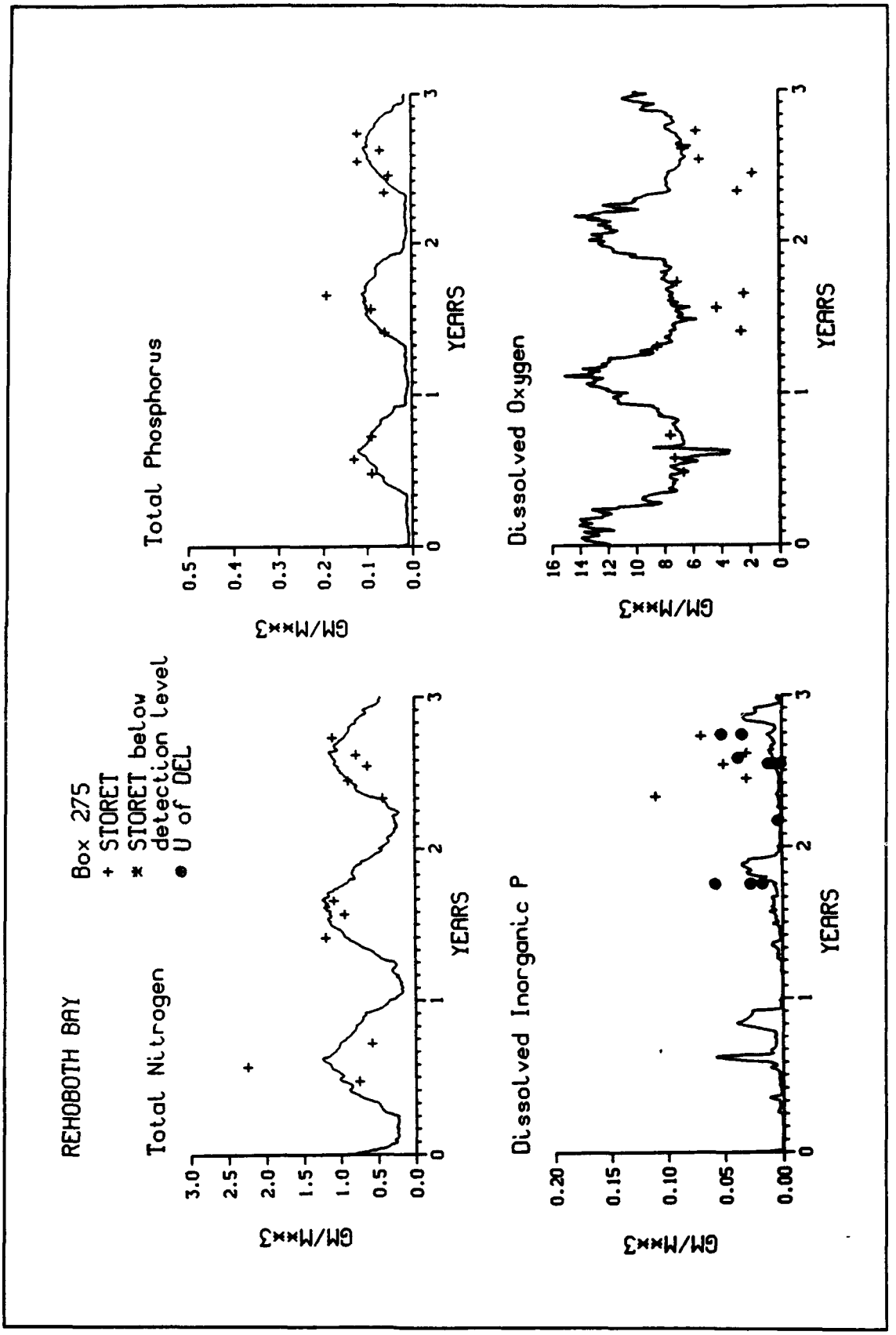

Figure 9-9. (Sheet 3 of 3)

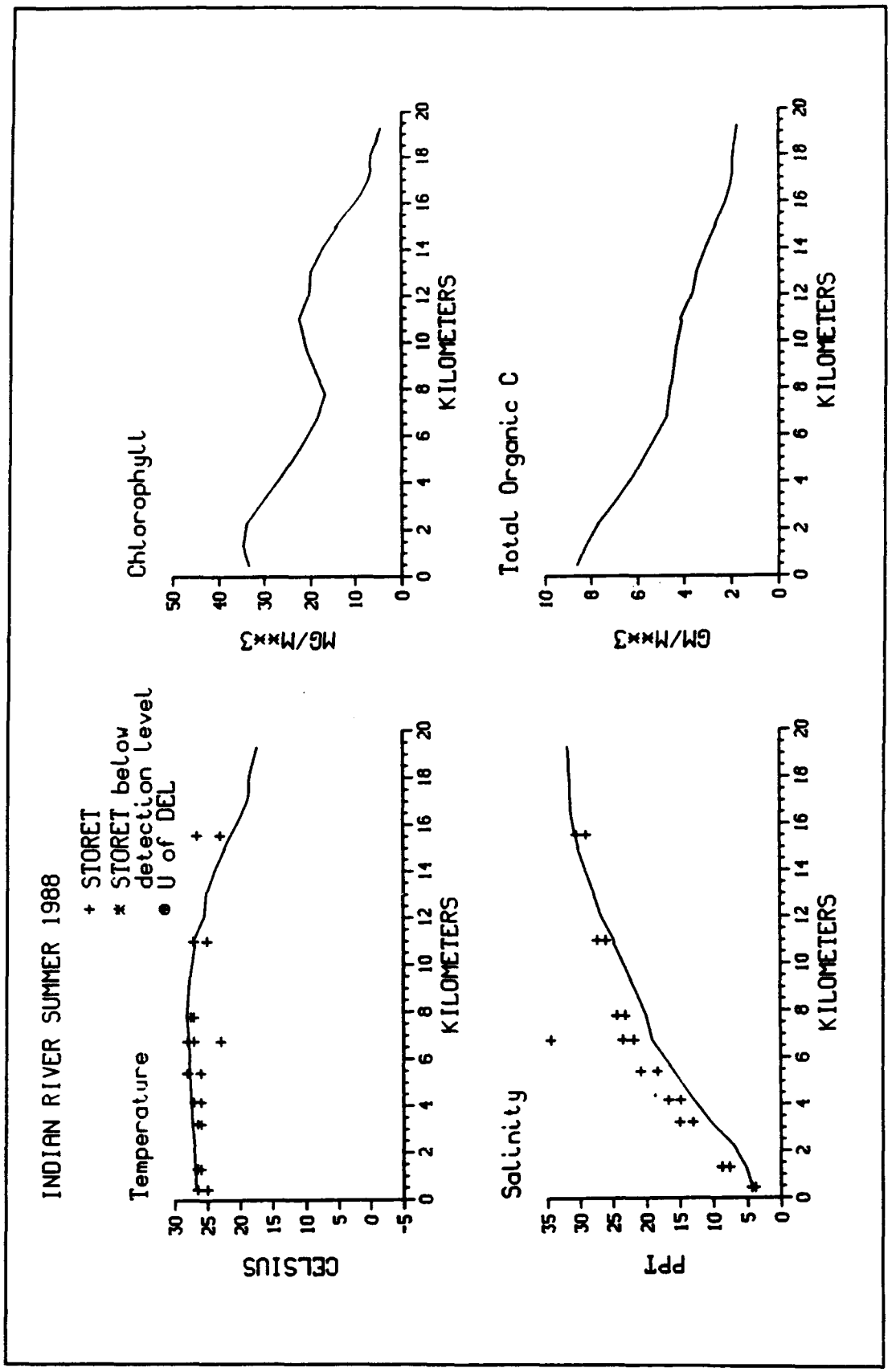

Figure 9-10. Observed and Modeled Water-Column Concentrations Along Transect From Millsboro to Indian River Inlet, Summer 1988 (Sheet 1 of 3)

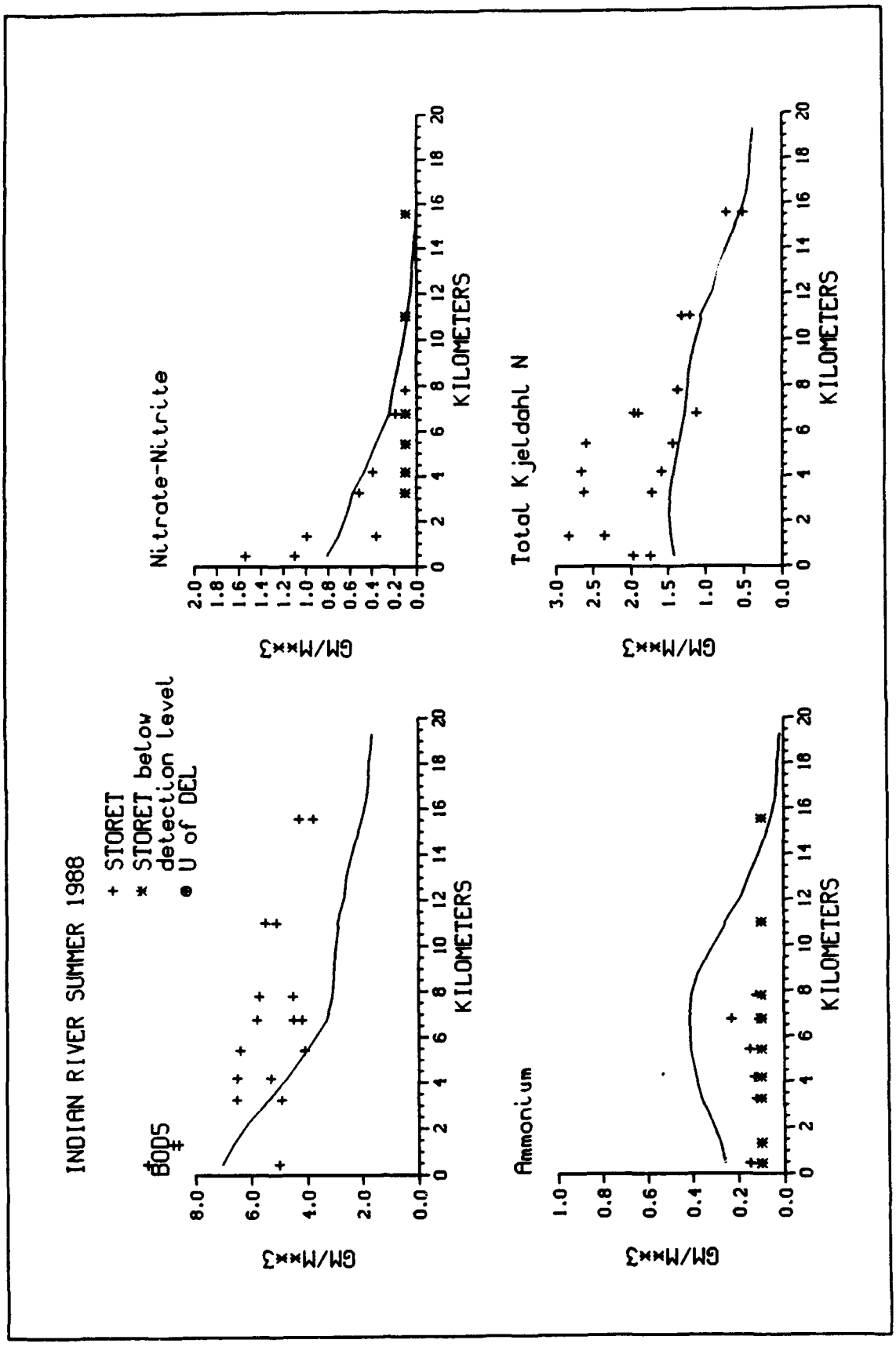

Figure 9-10. (Sheet 2 of 3)

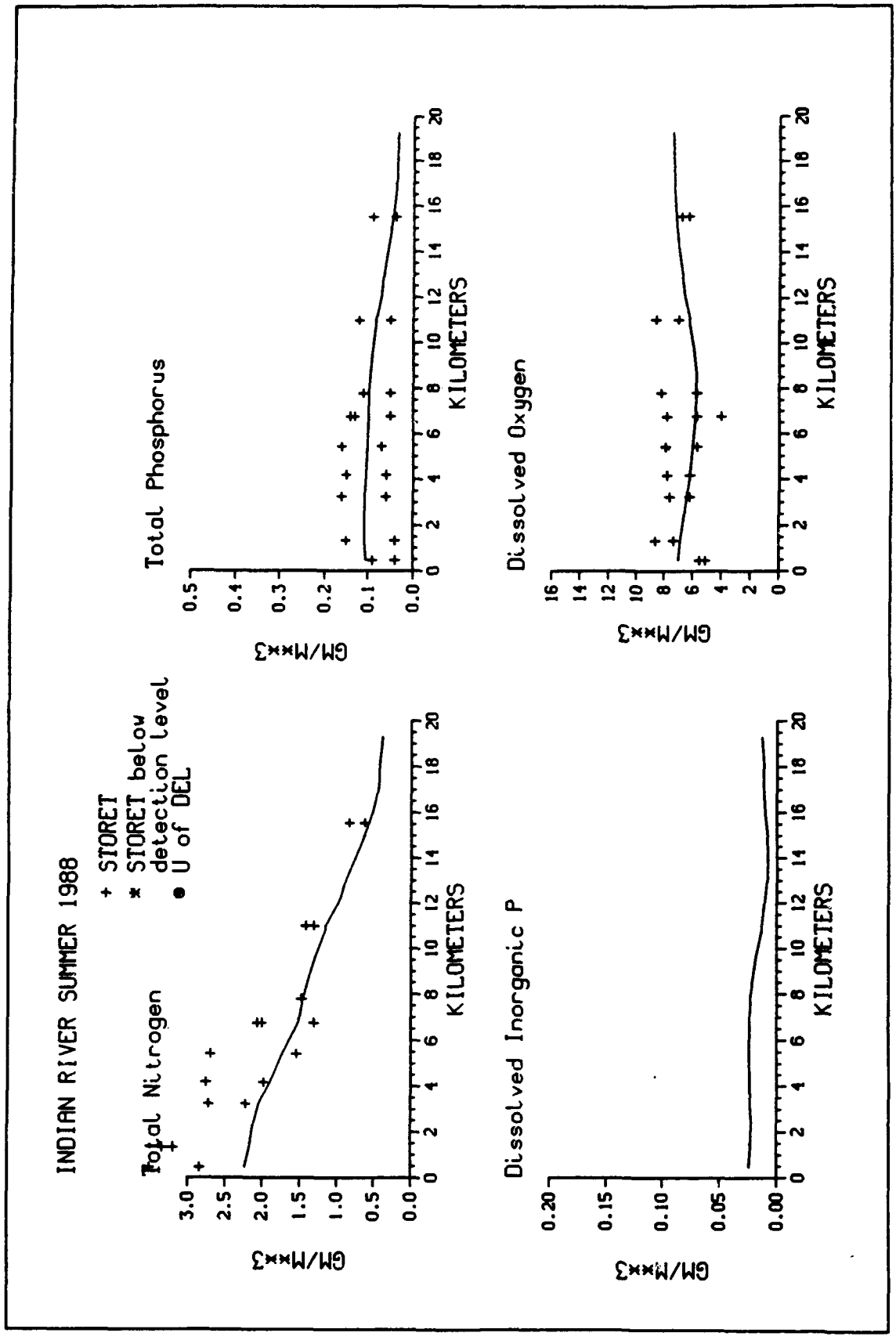

Figure 9-10. (Sheet 3 of 3)

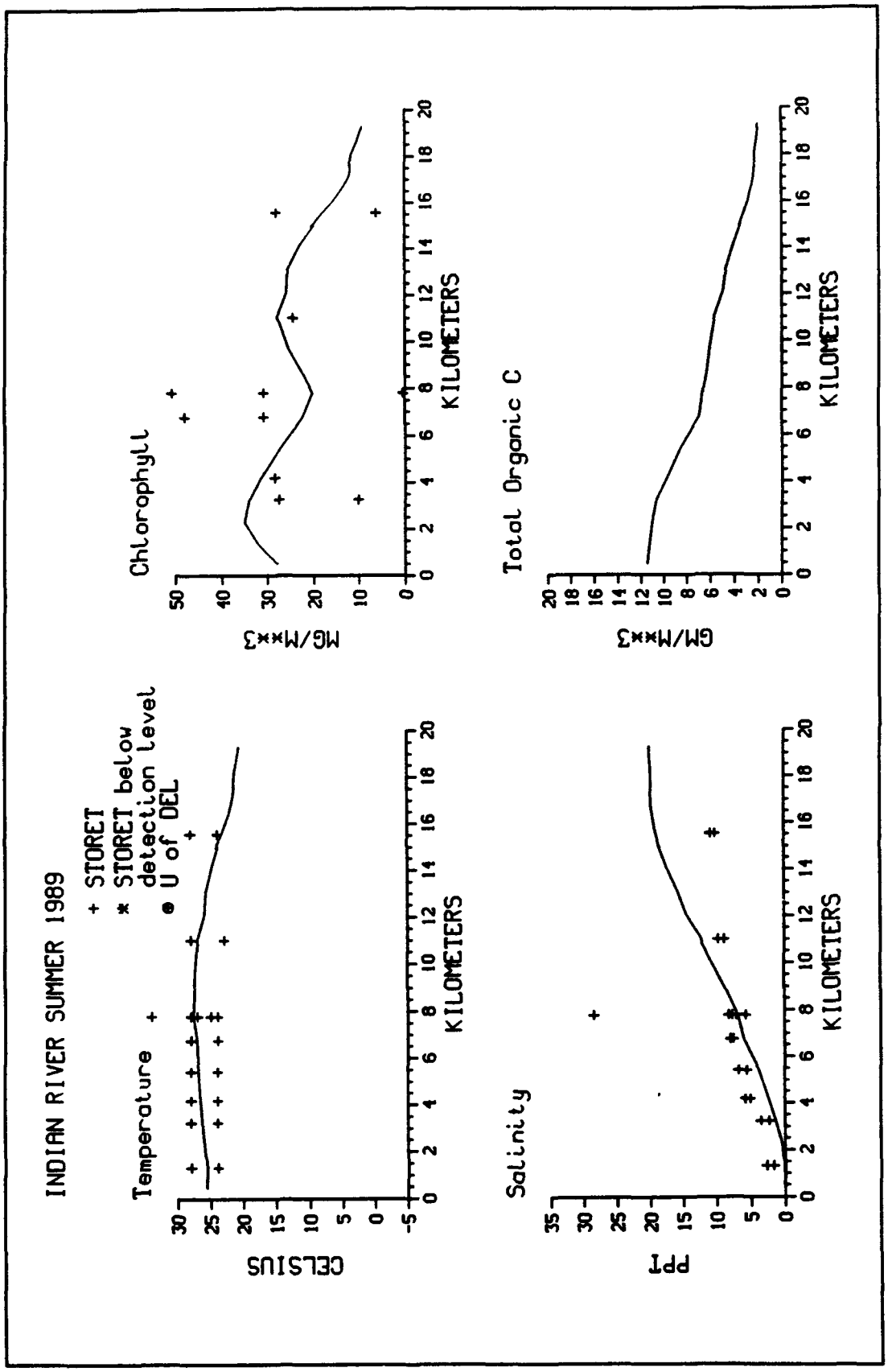

Figure 9-11. Observed and Modeled Water-Column Concentrations Along Transect From Millsboro to Indian River Inlet, Summer 1989 (Sheet 1 of 3)

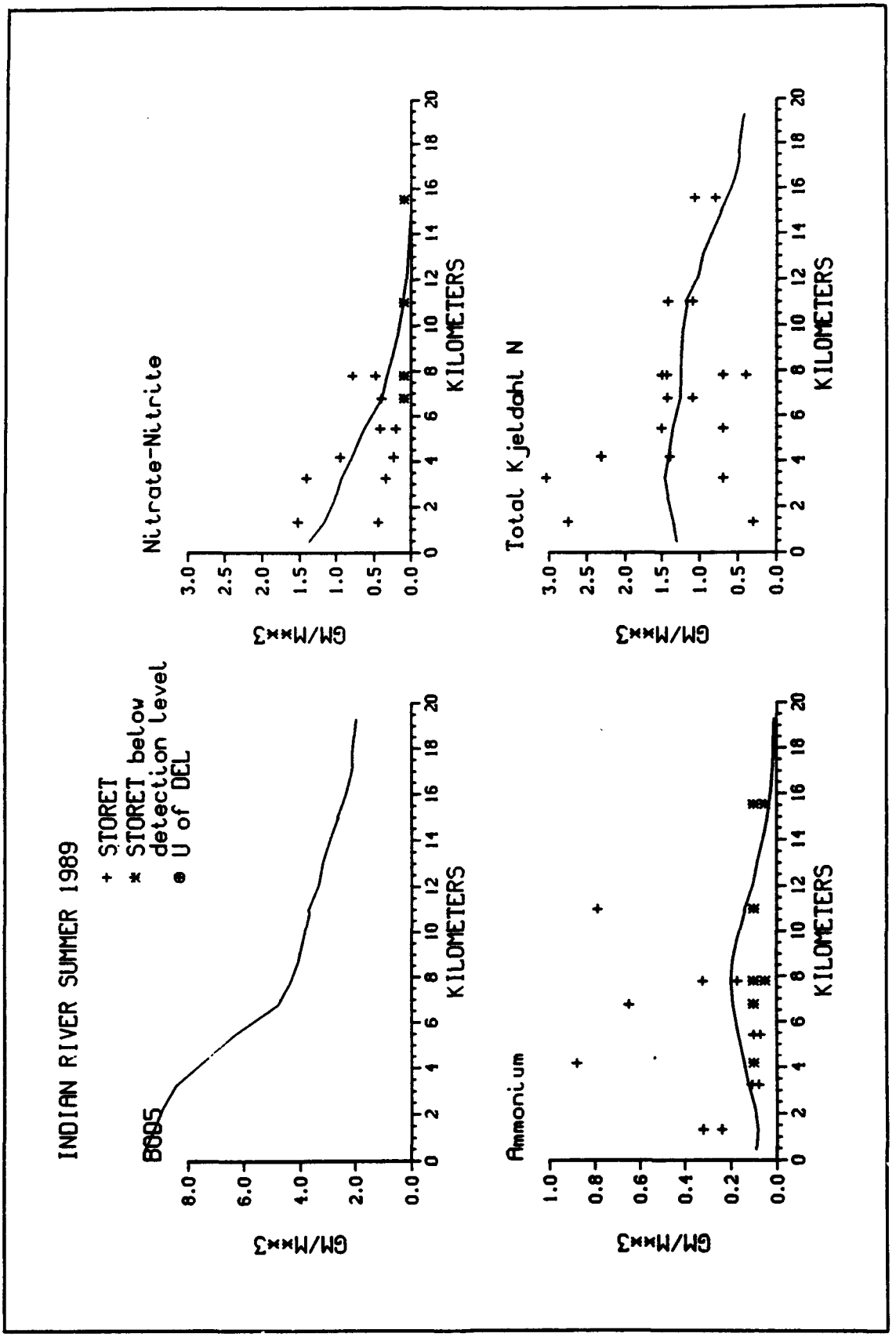

Figure 9-11. (Sheet 2 of 3)

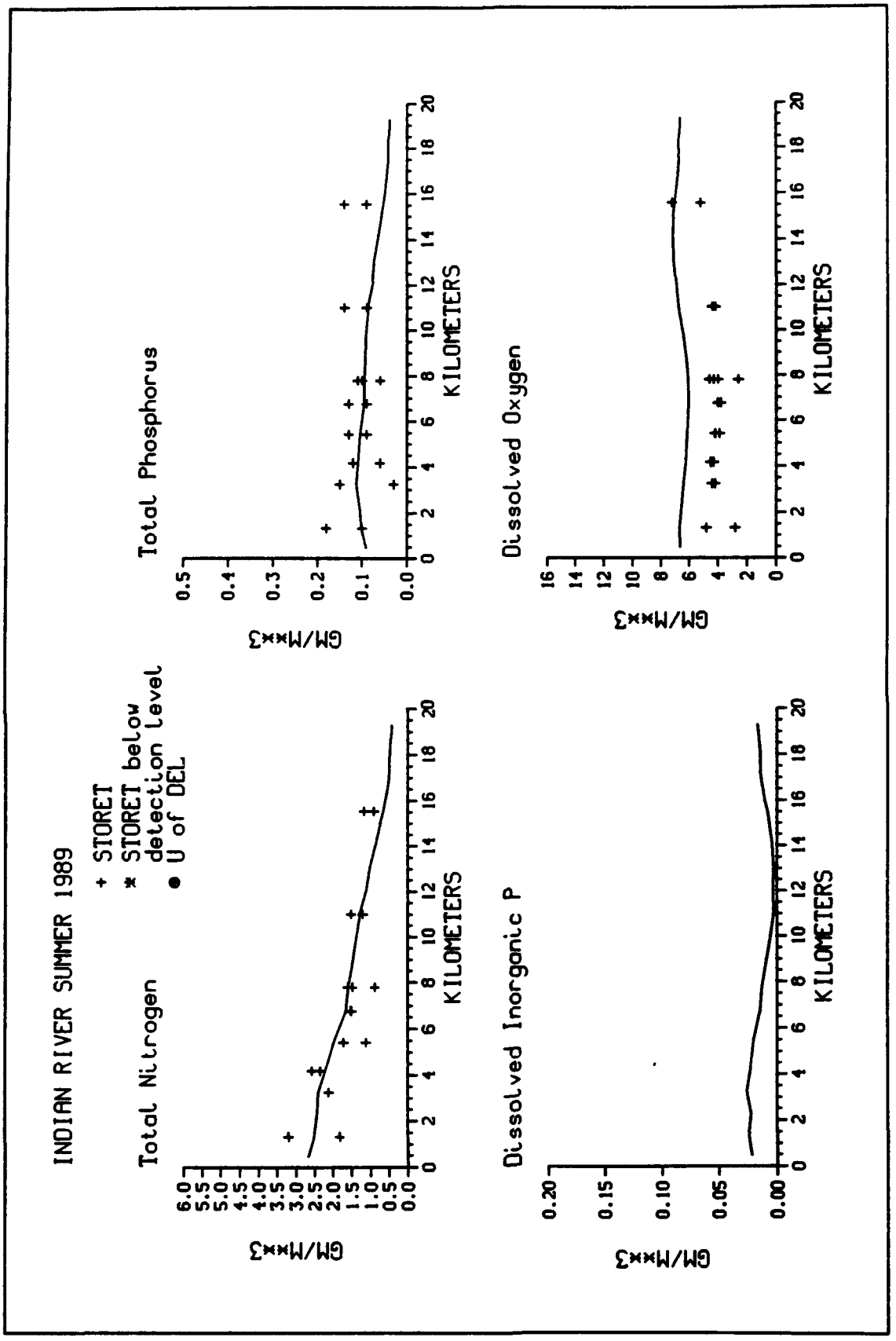

Figure 9-11. (Sheet 3 of 3)

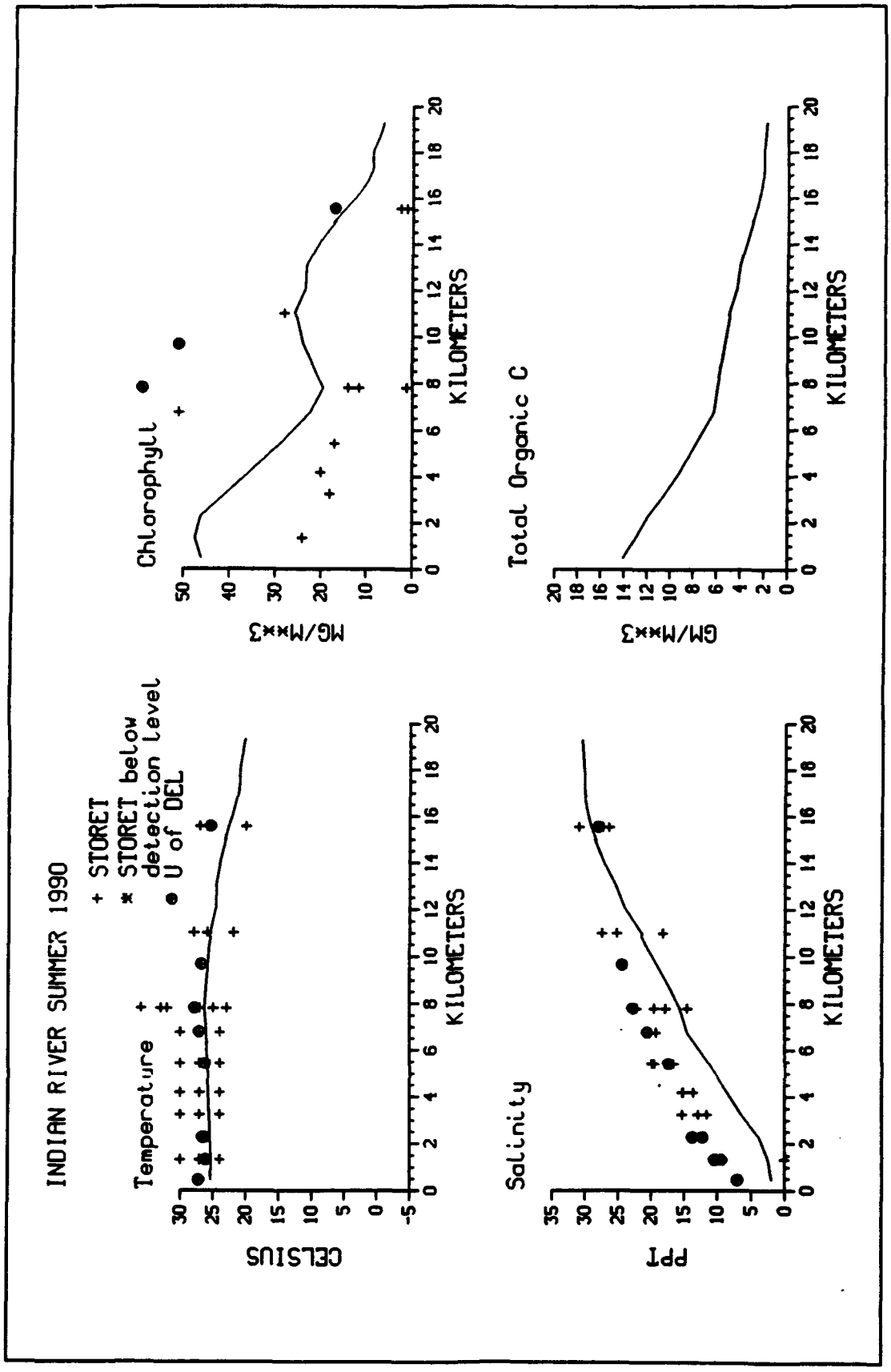

Figure 9-12. Observed and Modeled Water-Column Concentrations Along Transect From Millsboro to Indian River Inlet, Summer 1990 (Sheet 1 of 3)

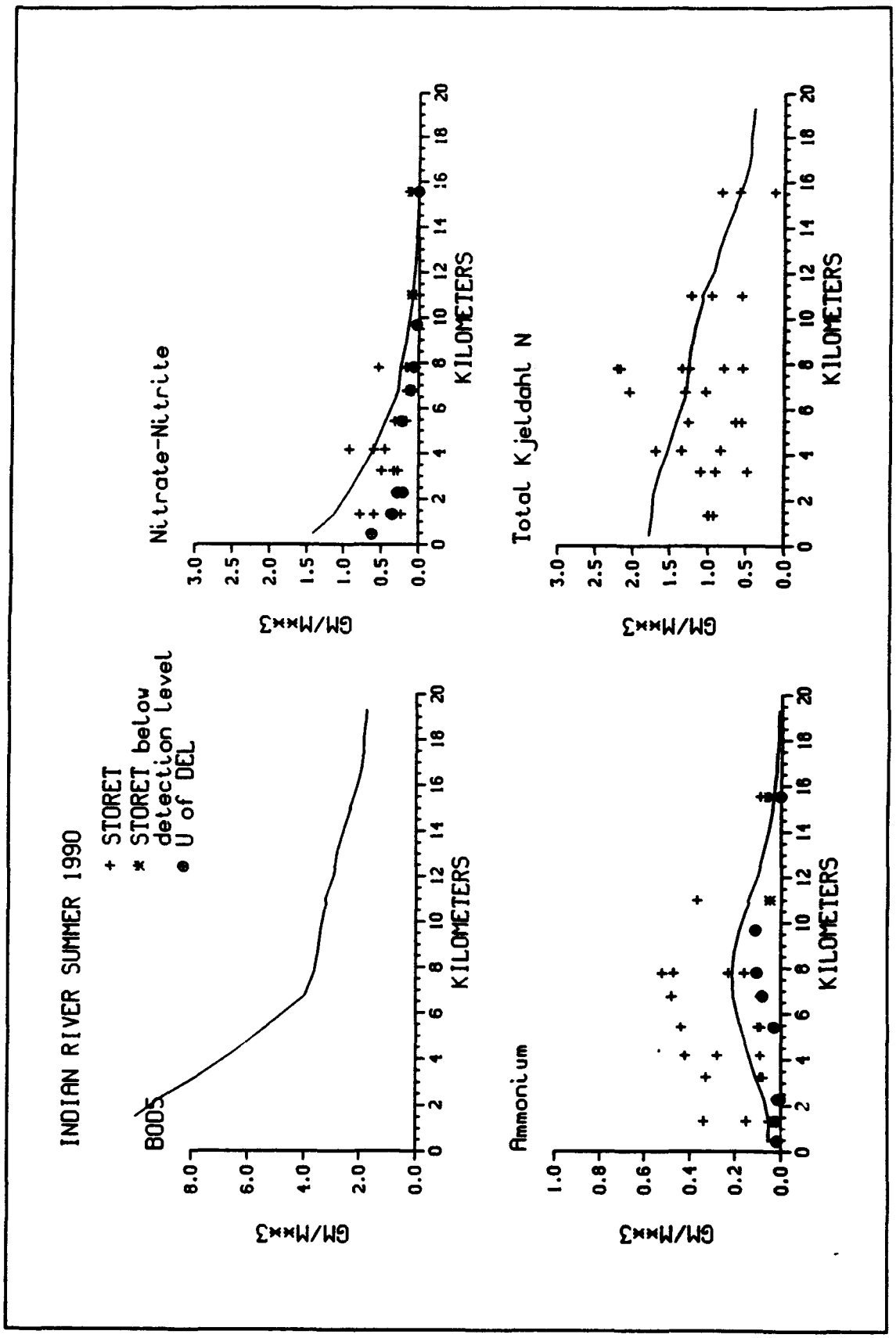

Figure 9-12. (Sheet 2 of 3)

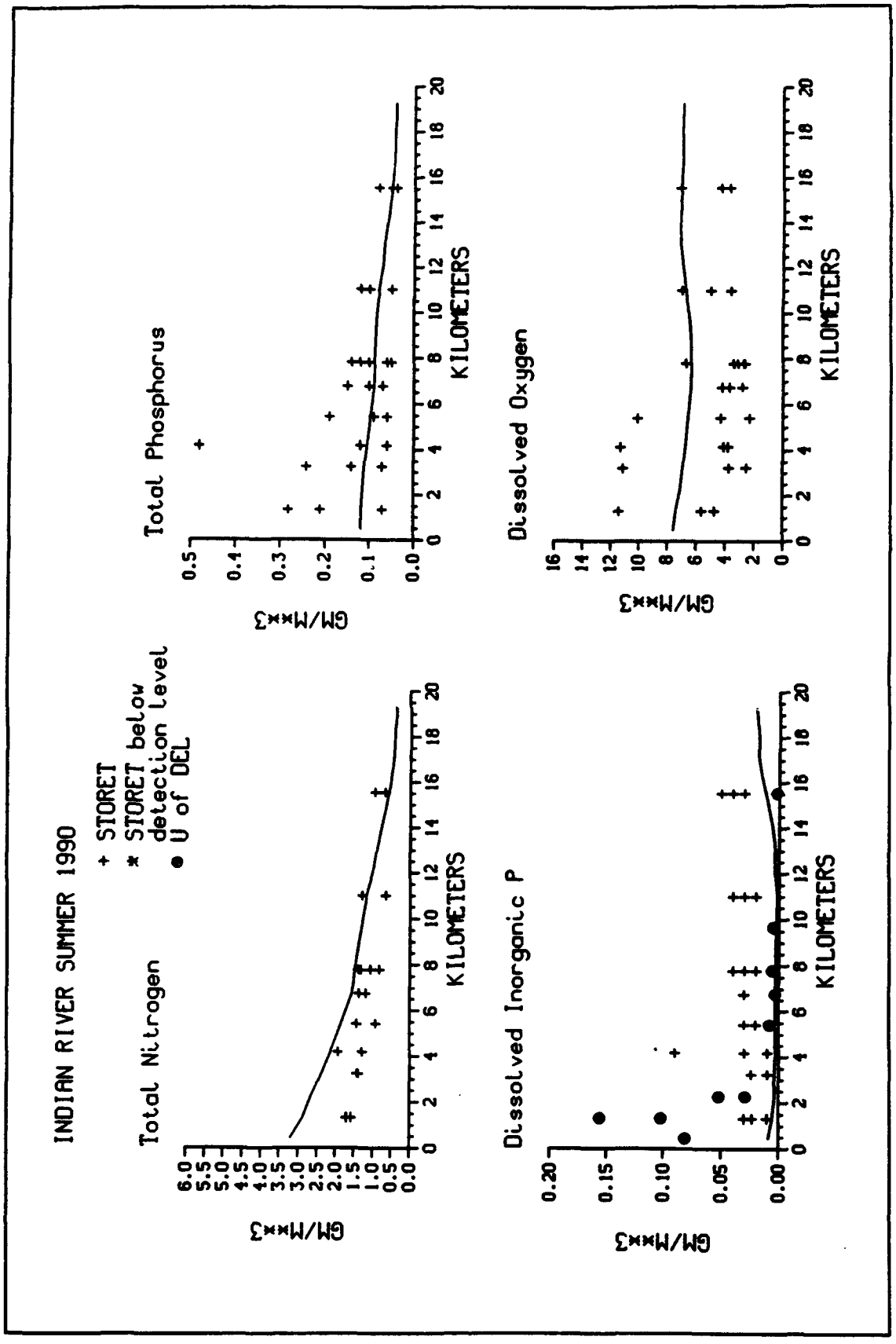

Figure 9-12. (Sheet 3 of 3)

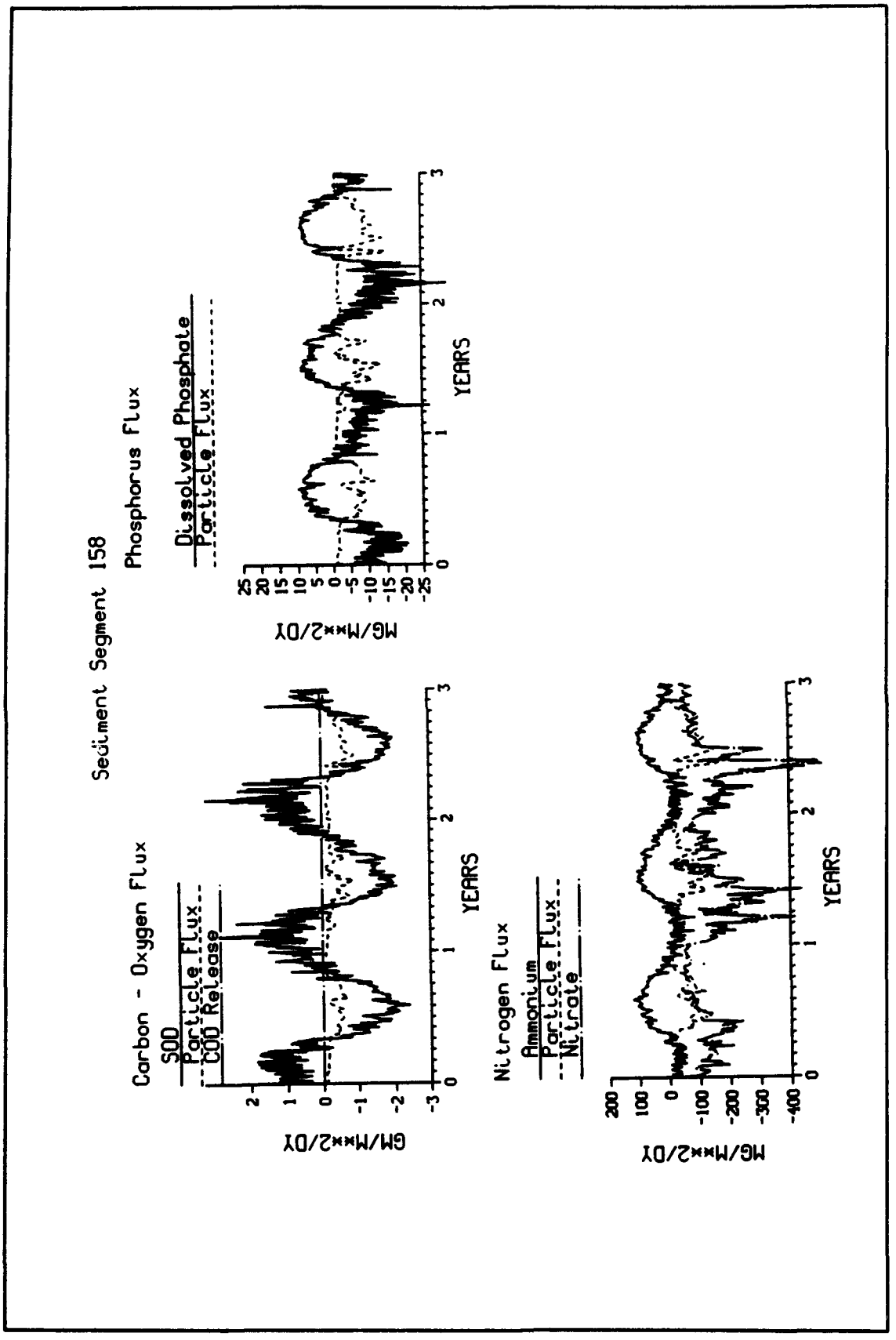

Figure 9-13. Time Series of Modeled Sediment-Water Fluxes, Grid Cell 158

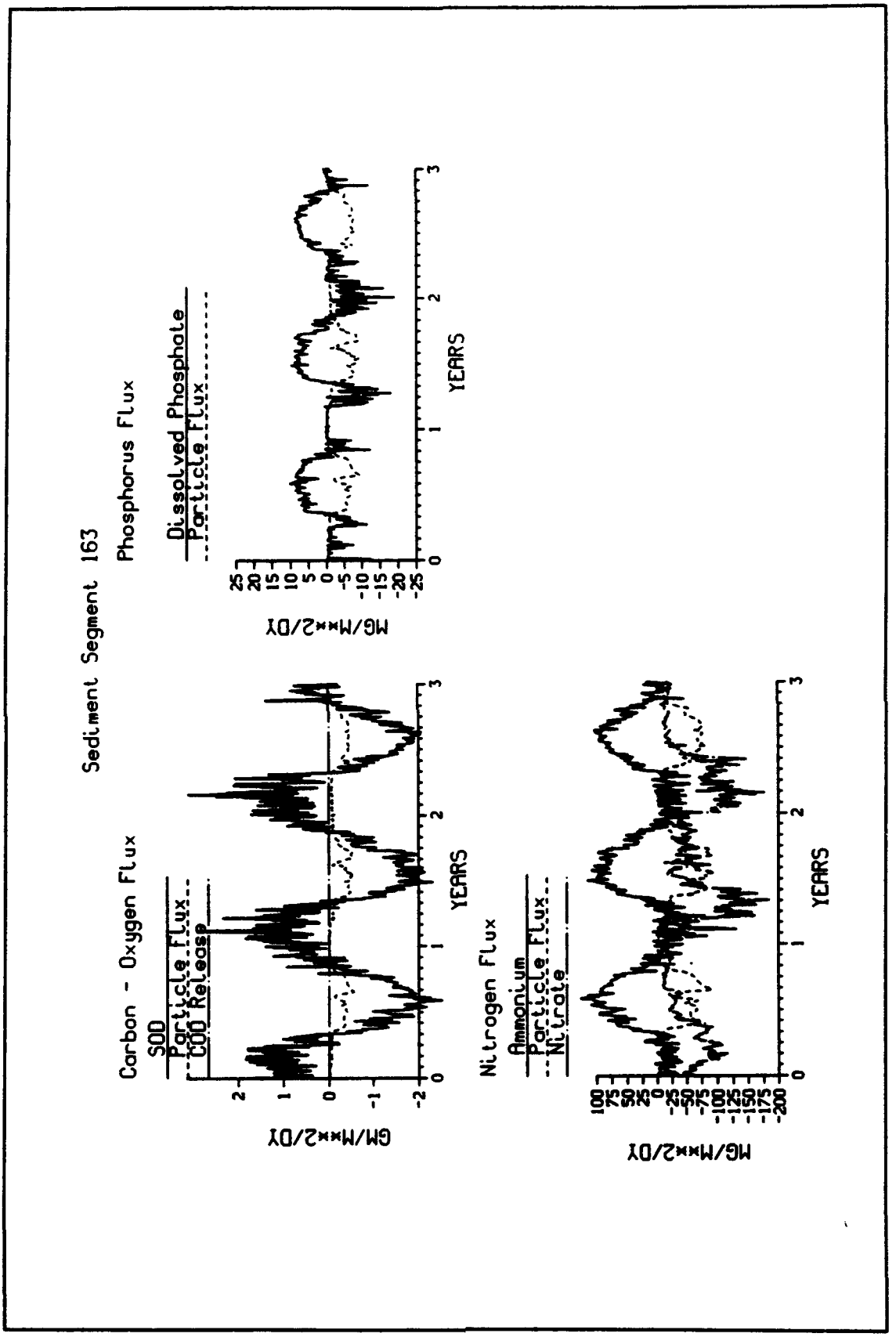

Figure 9-14. Time Series of Modeled Sediment-Water Fluxes, Grid Cell 163

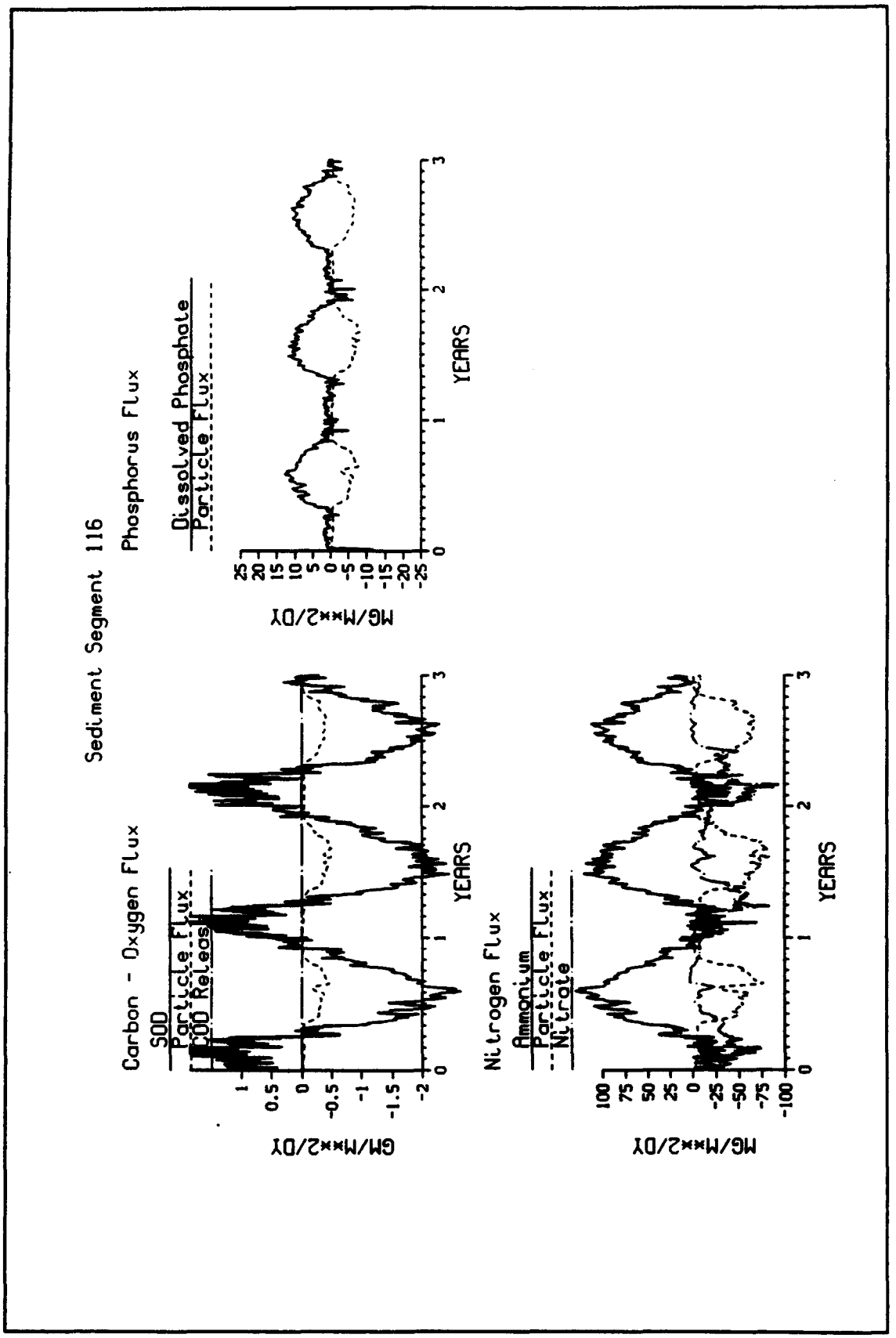

Figure 9-15. Time Series of Modeled Sediment-Water Fluxes, Grid Cell 116

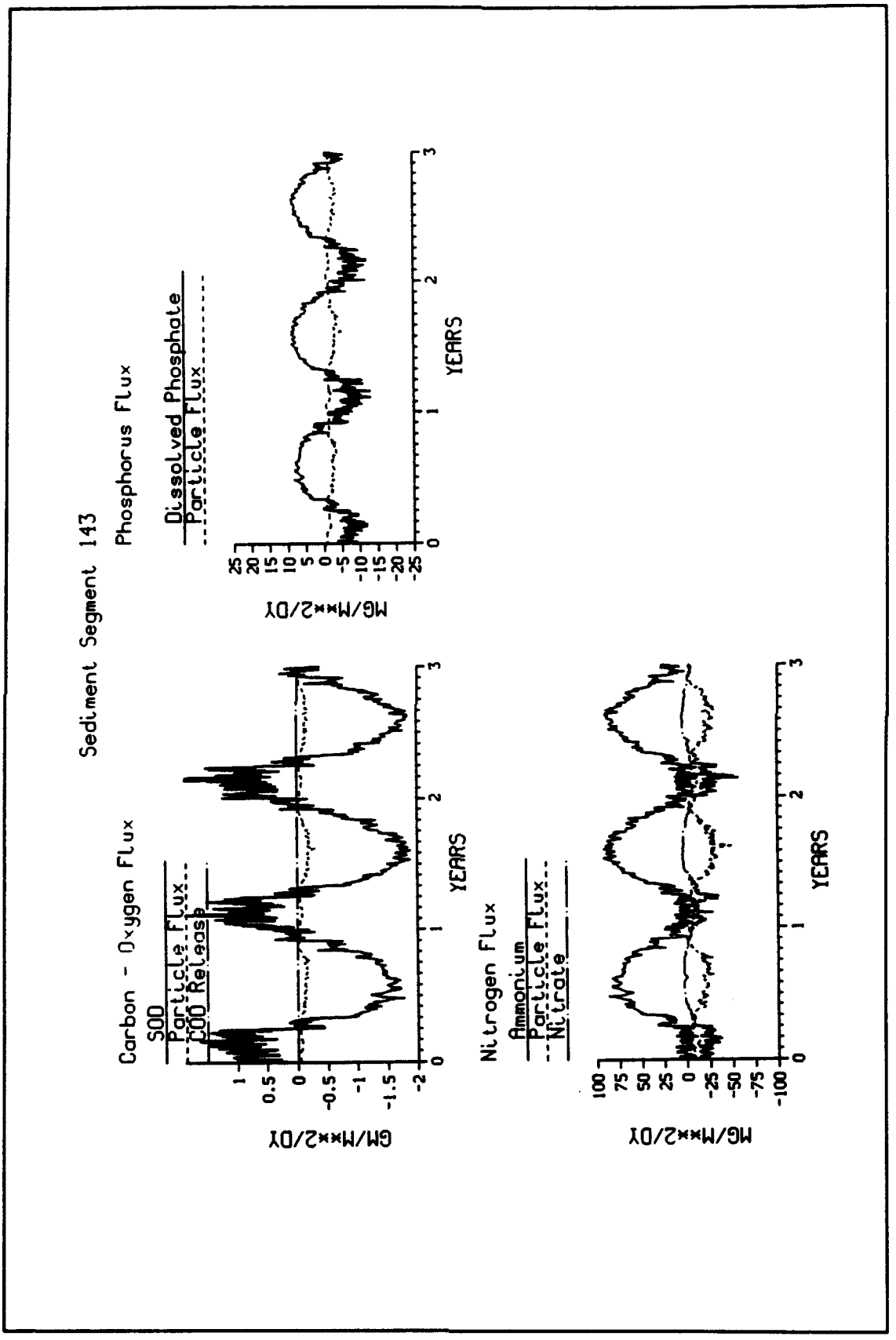

Figure 9-16. Time Series of Modeled Sediment-Water Fluxes, Grid Cell 143

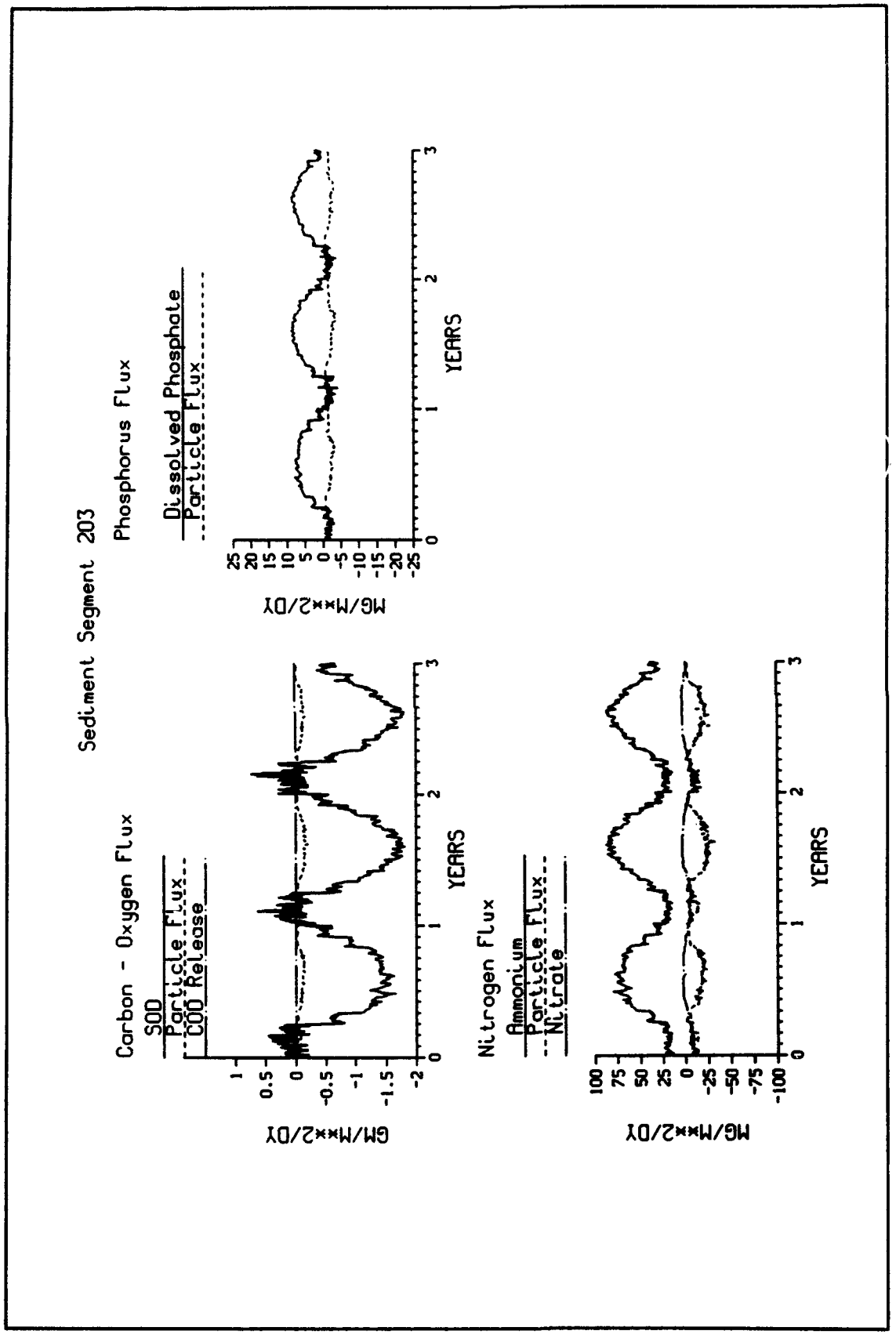

Figure 9-17. Time Series of Modeled Sediment-Water Fluxes, Grid Cell 203

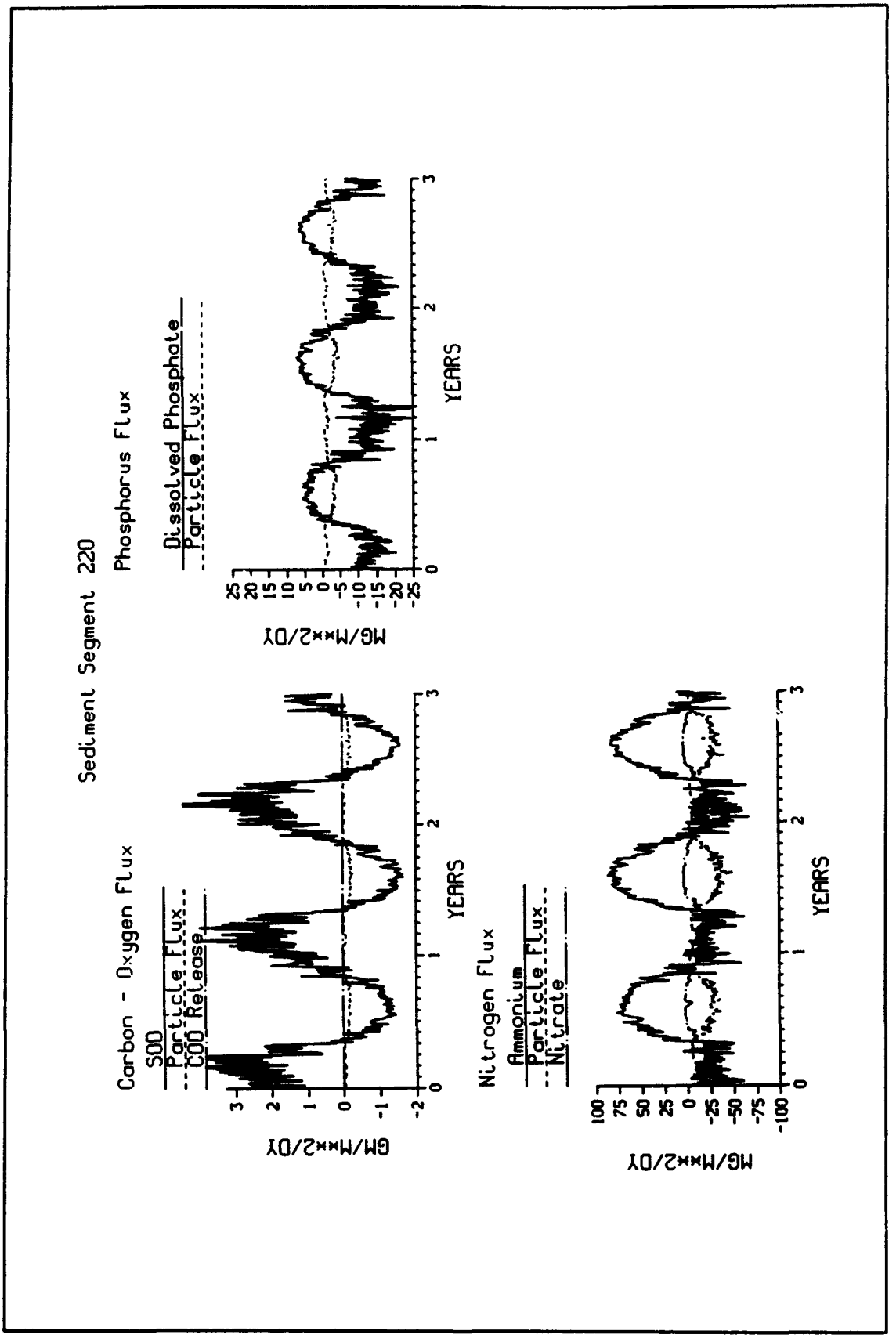

Figure 9-18. Time Series of Modeled Sediment-Water Fluxes, Grid Cell 220

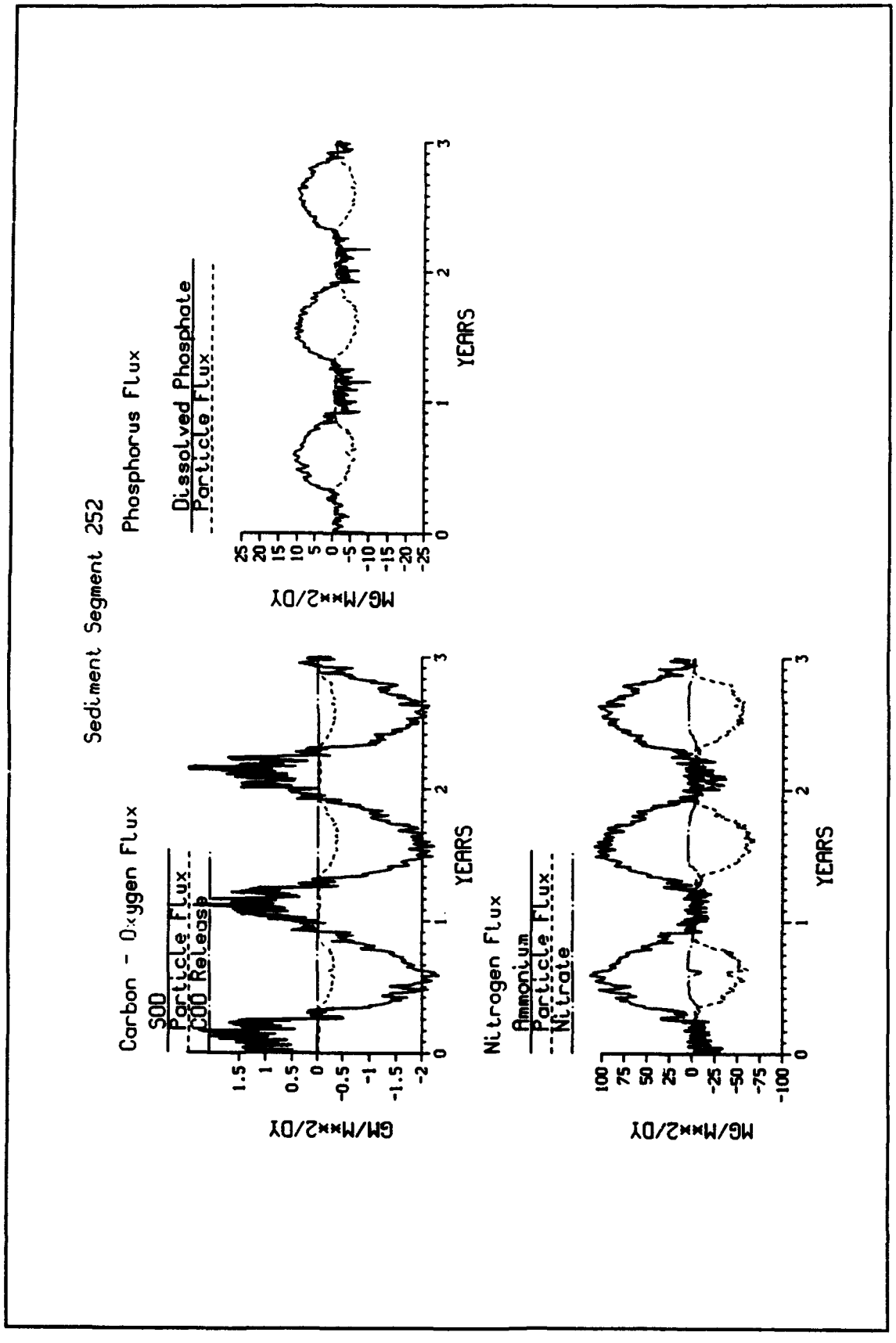

Figure 9-19. Time Series of Modeled Sediment-Water Fluxes, Grid Cell 252

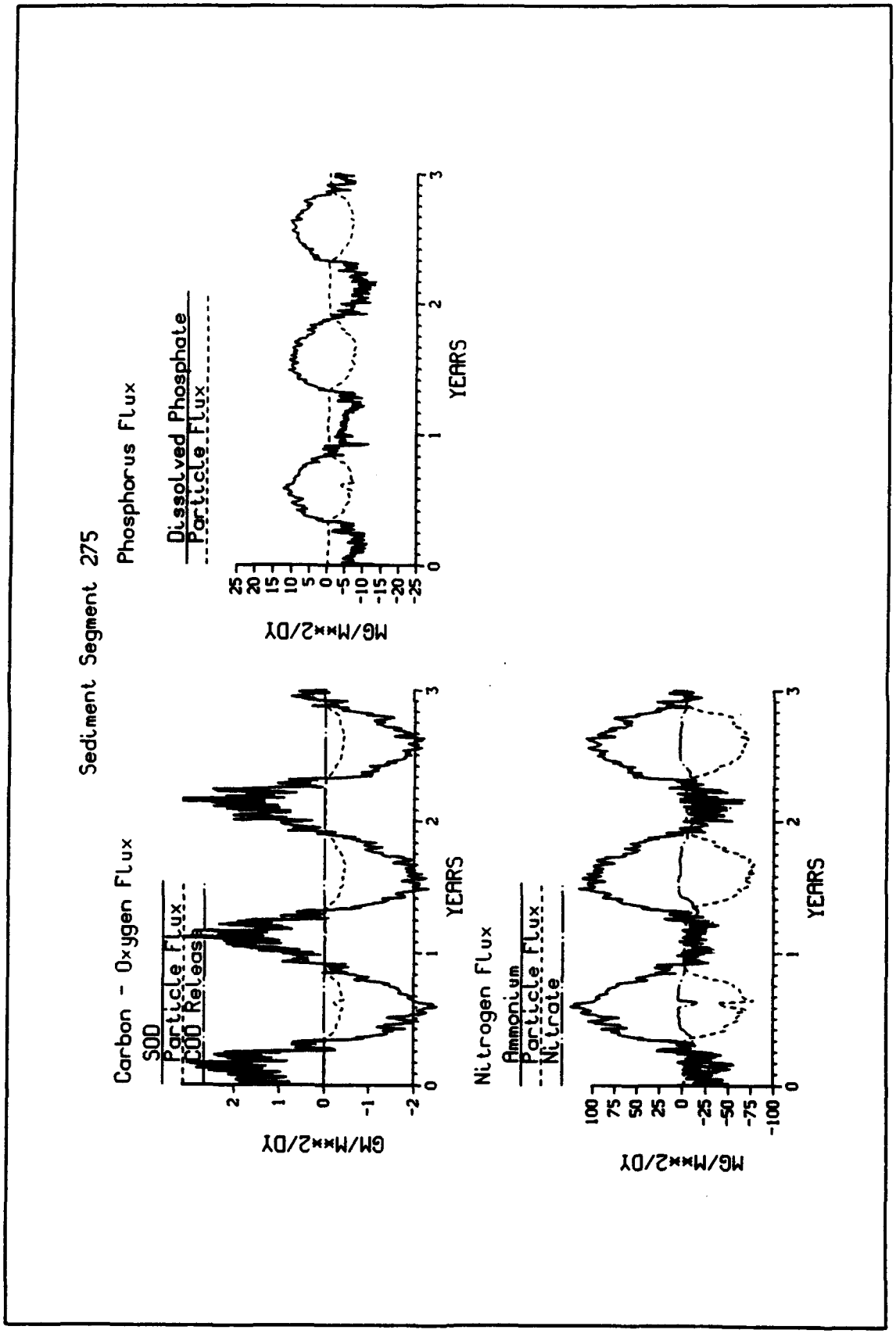

Figure 9-20. Time Series of Modeled Sediment-Water Fluxes, Grid Cell 275

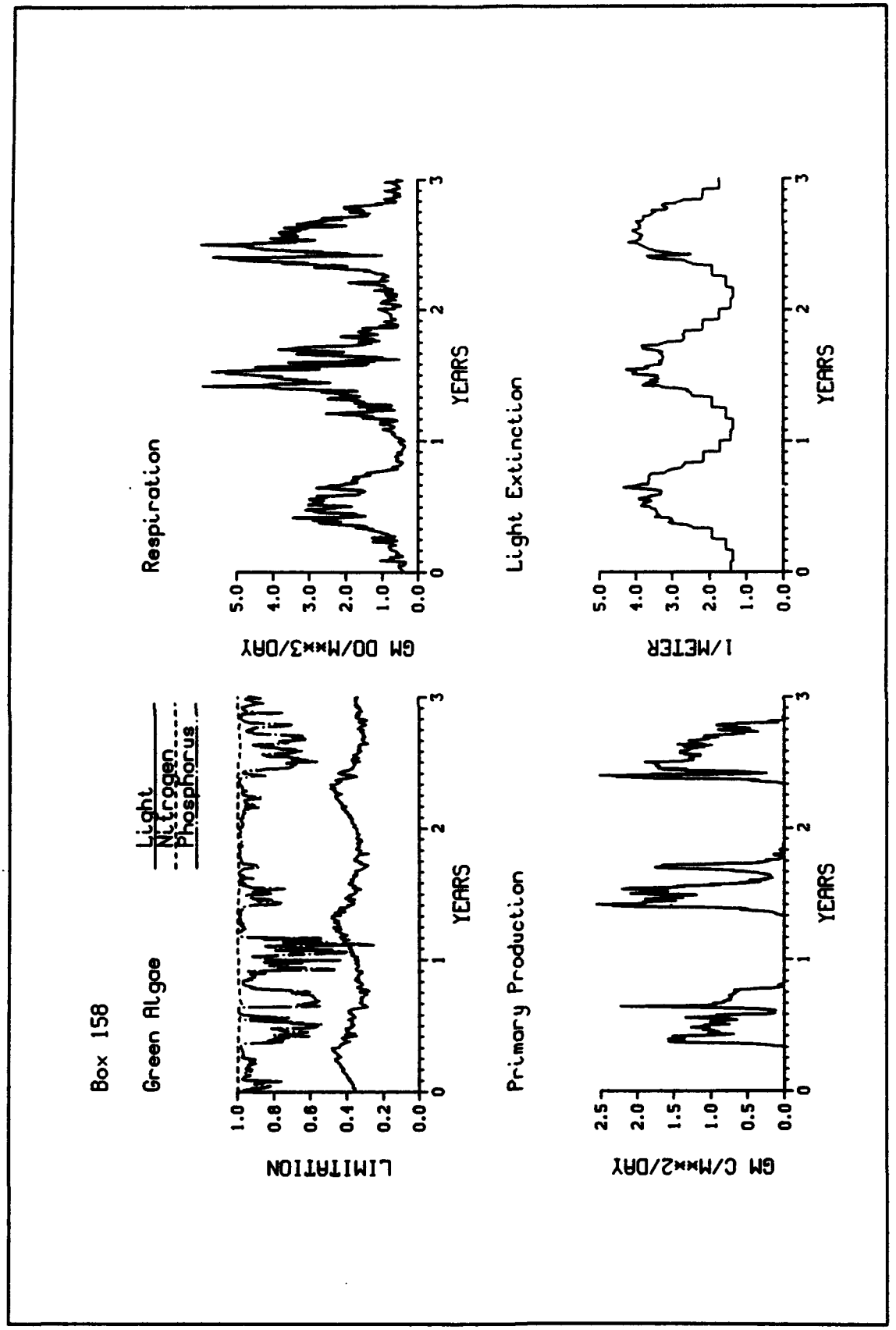

Figure 9-21. Time Series of Interpretive Information, Grid Cell 158

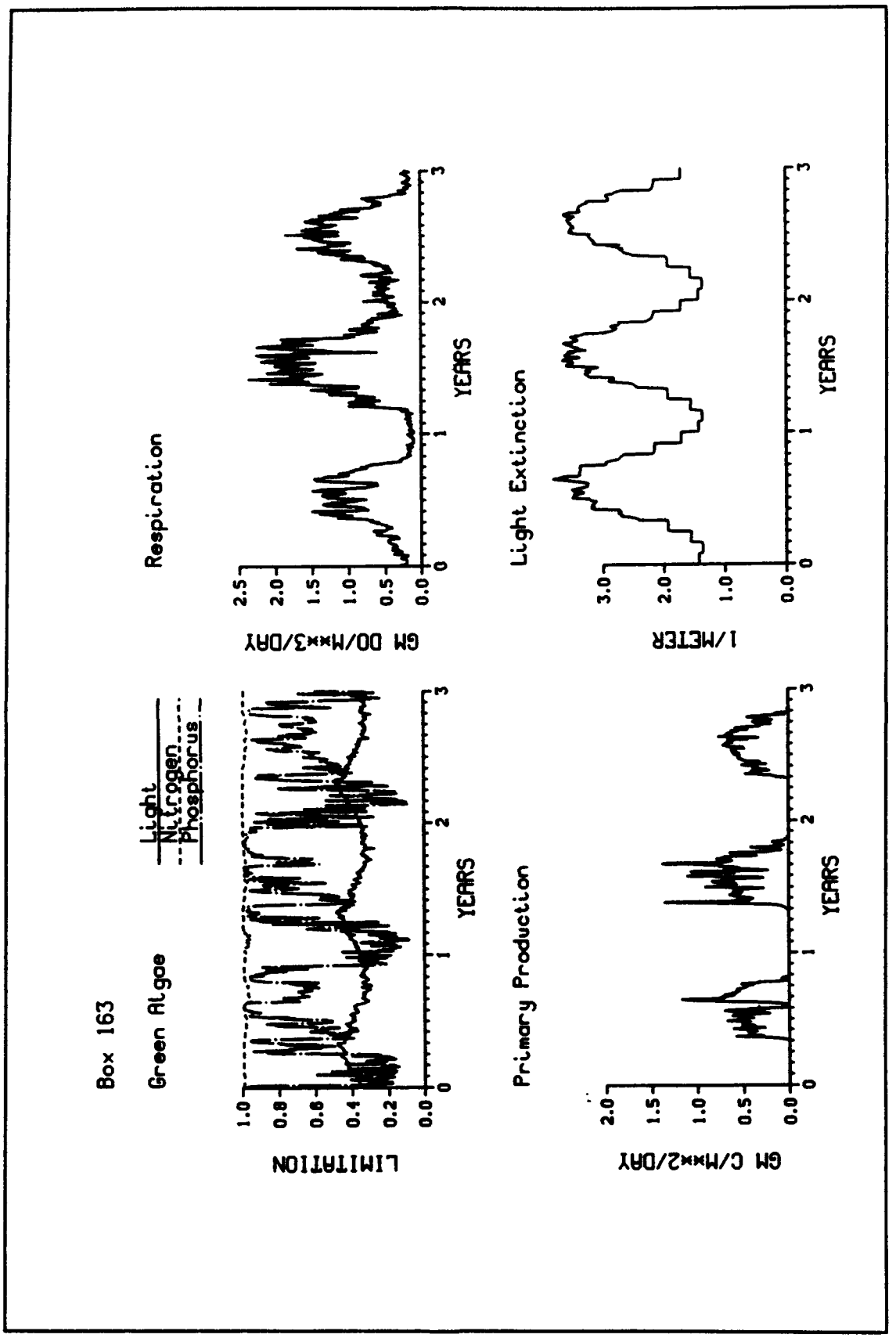

Figure 9-22. Time Series of Interpretive Information, Grid Cell 163

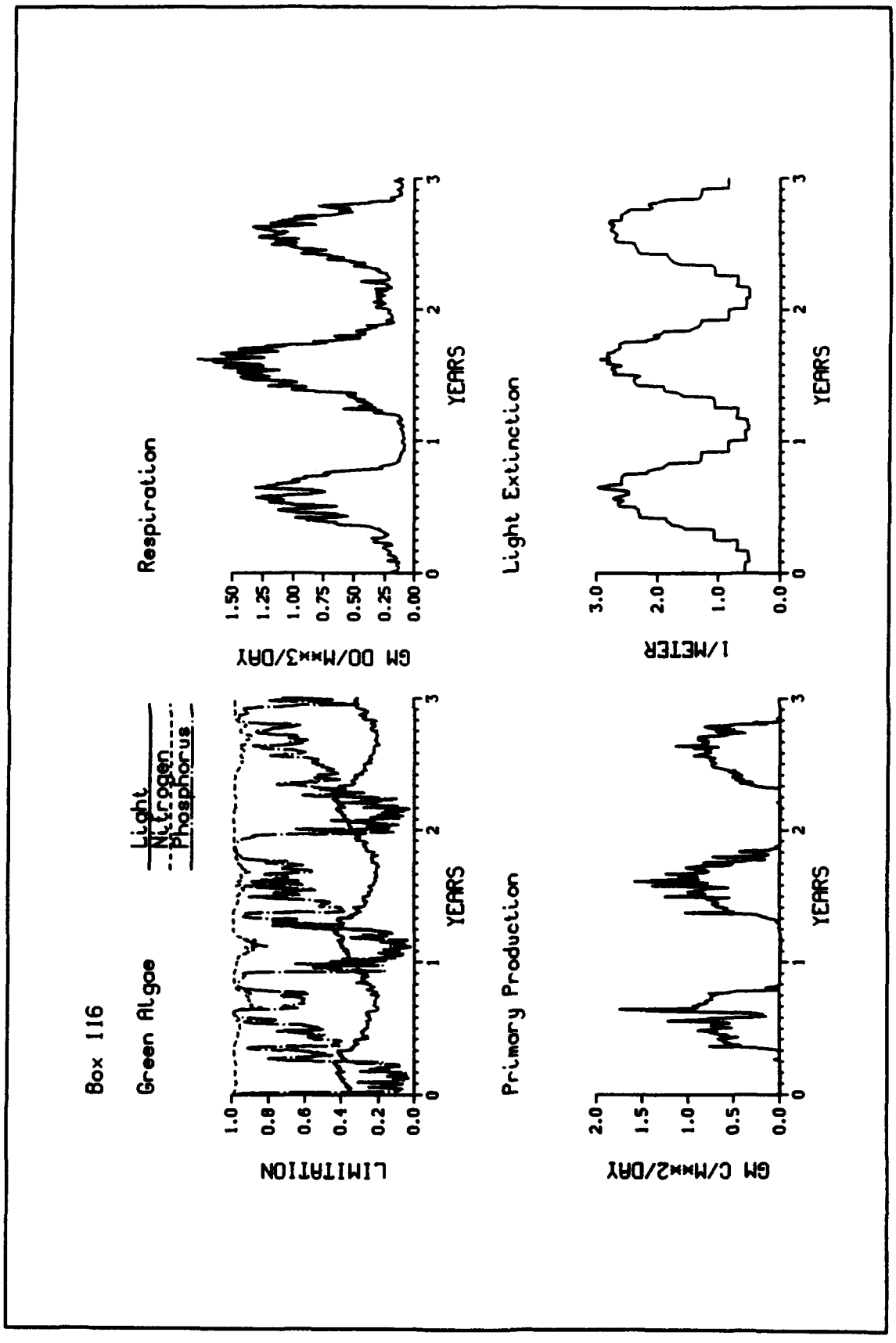

Figure 9-23. Time Series of Interpretive Information, Grid Cell 116

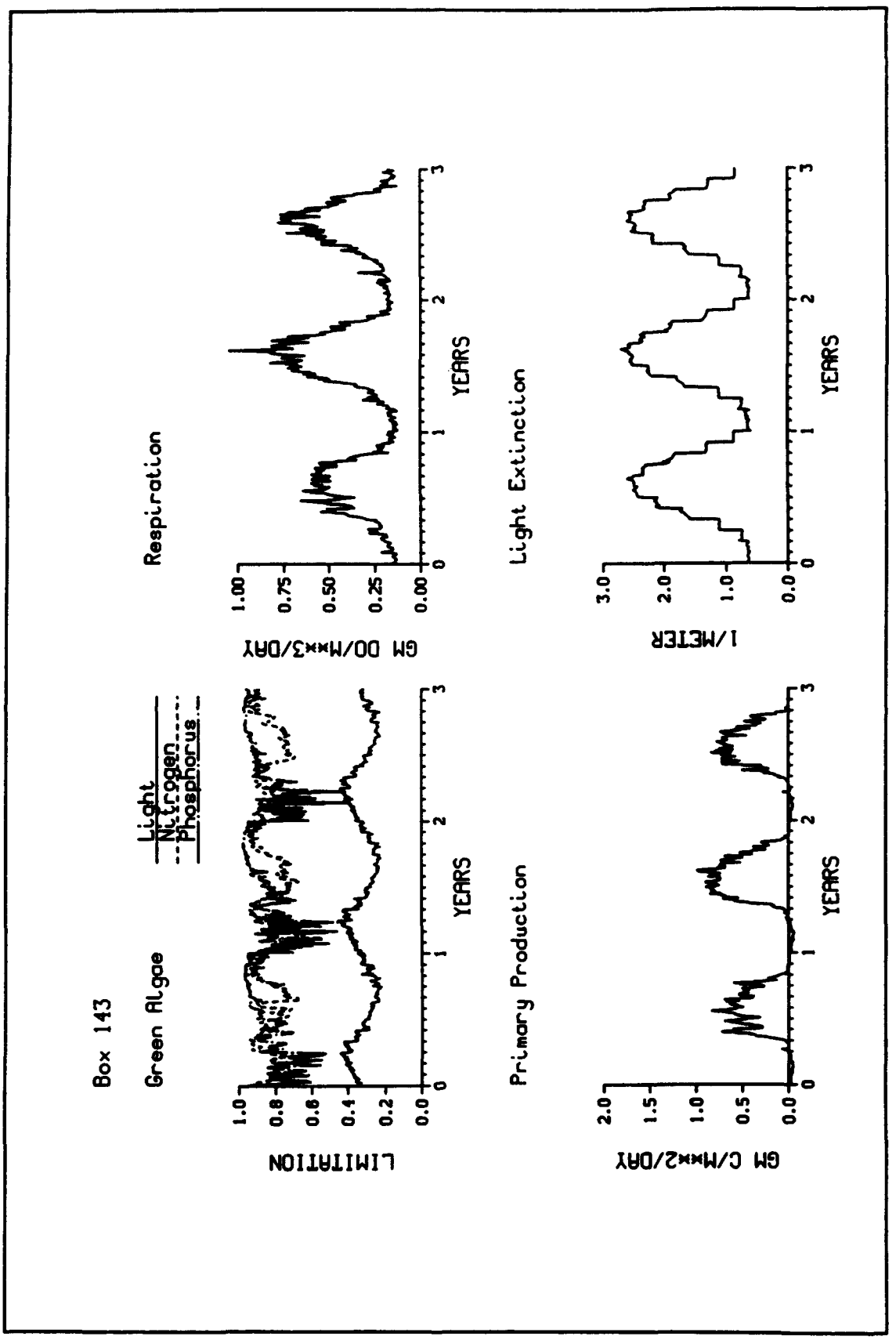

Figure 9-24. Time Series of Interpretive Information, Grid Cell 143

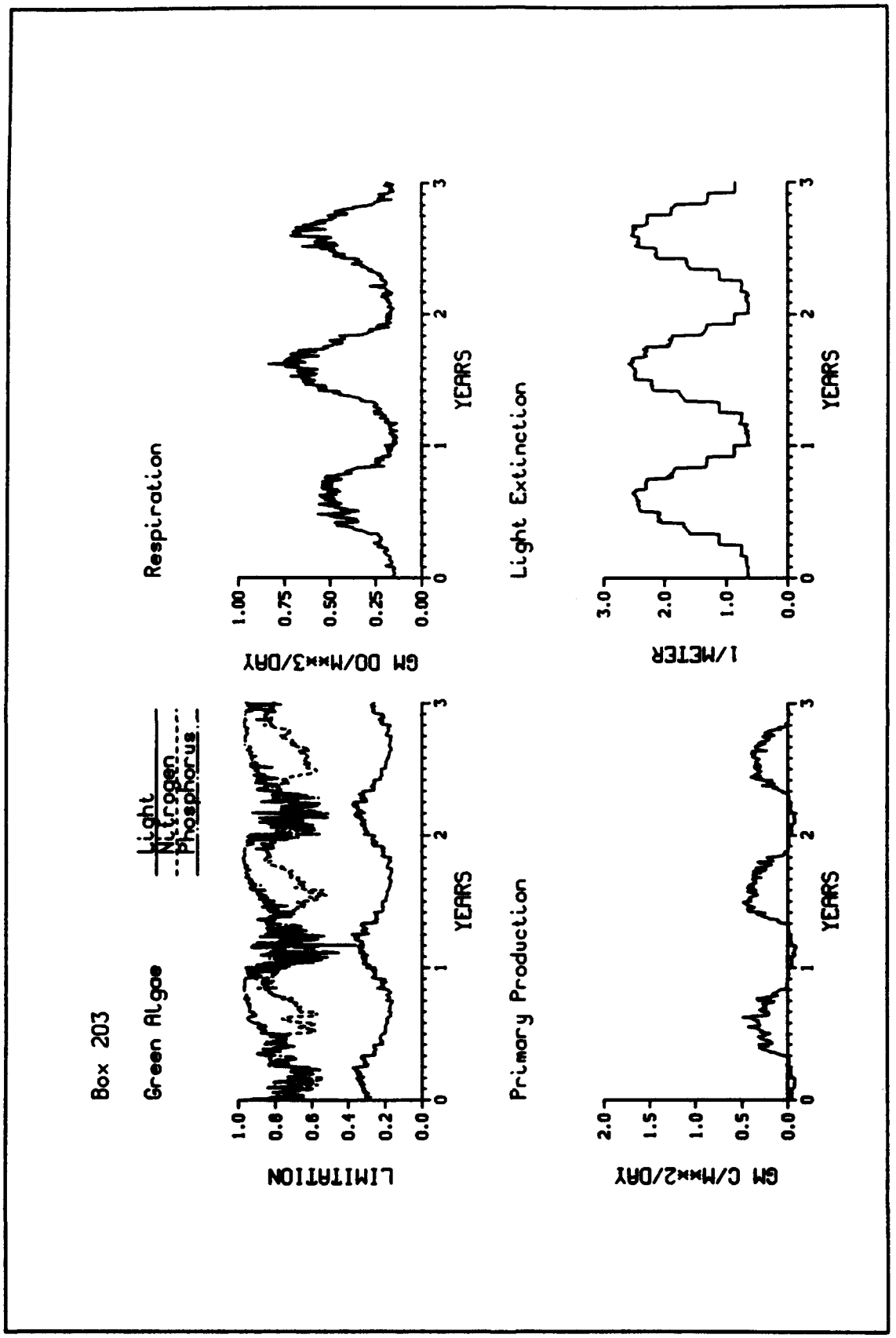

Figure 9-25. Time Series of Interpretive Information, Grid Cell 203

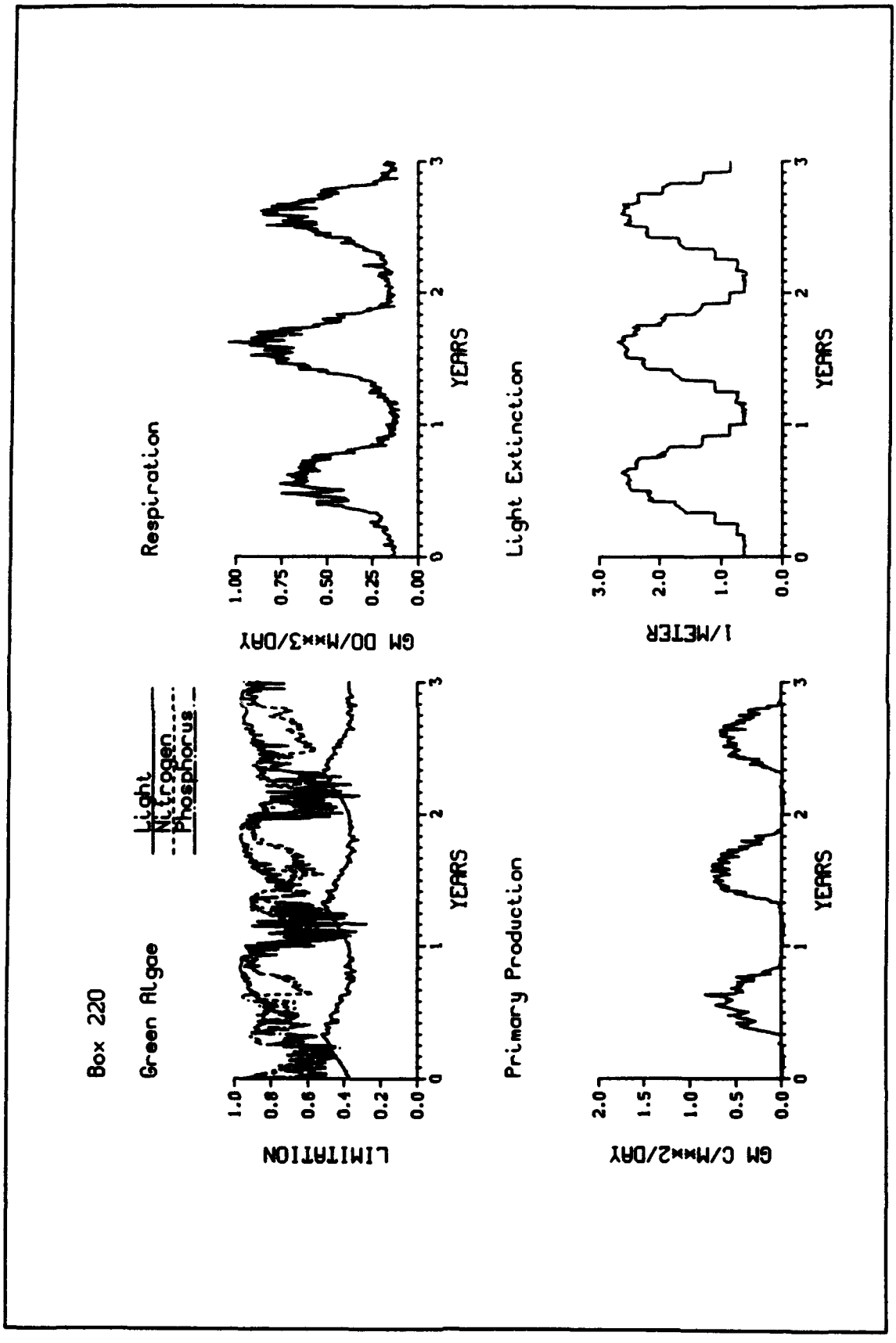

Figure 9-26. Time Series of Interpretive Information, Grid Cell 220

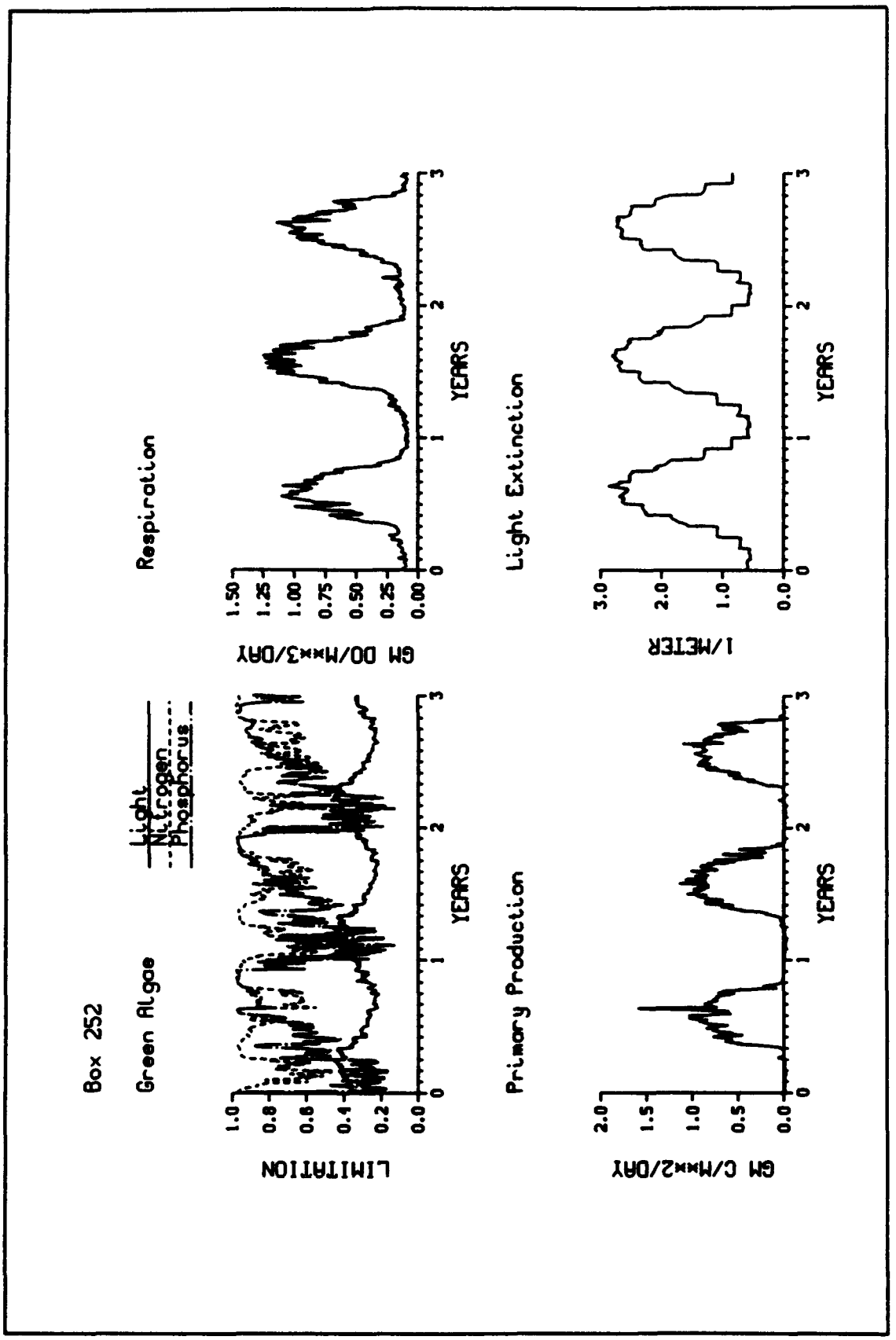

Figure 9-27. Time Series of Interpretive Information, Grid Cell 252

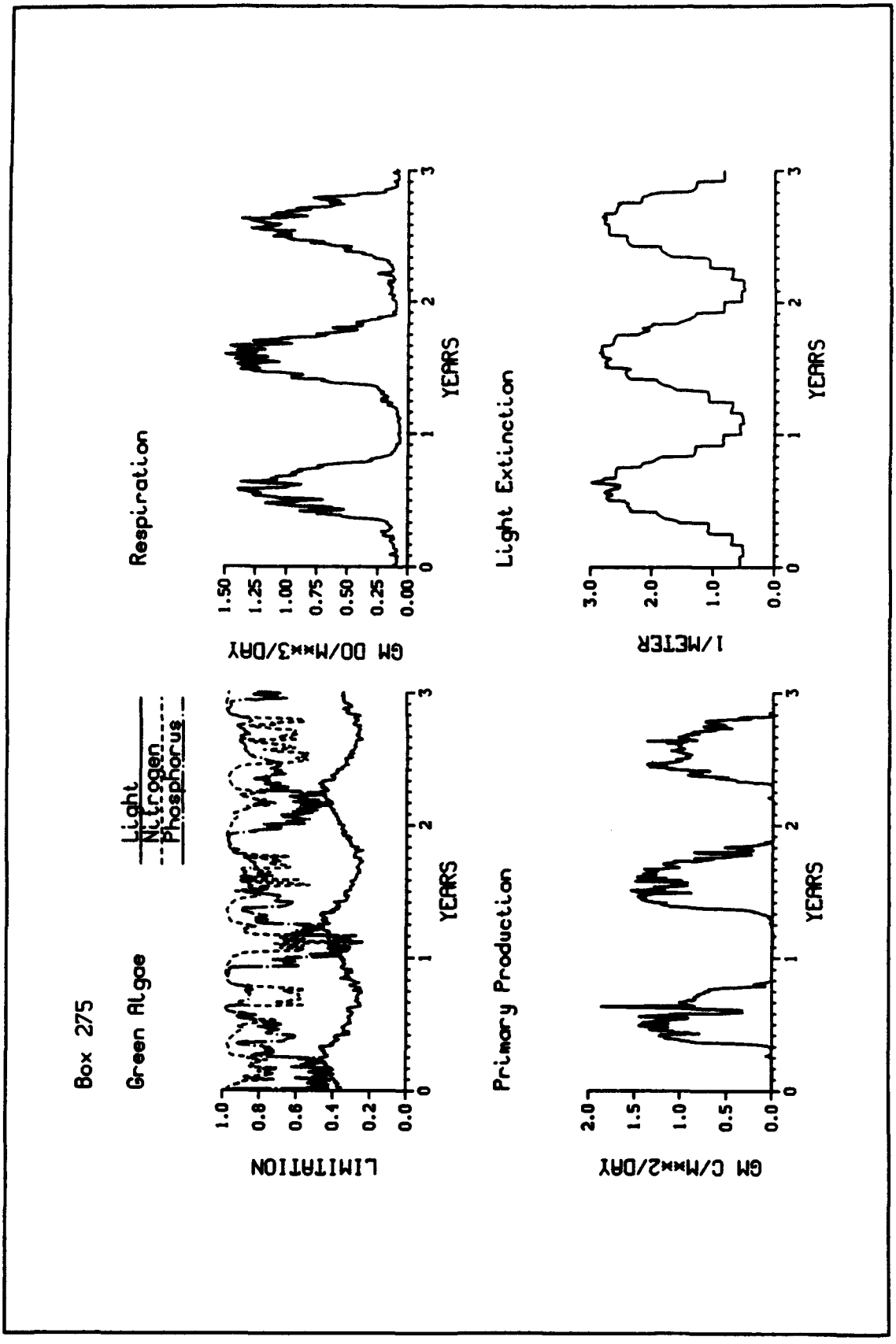

Figure 9-28. Time Series of Interpretive Information, Grid Cell 275

second plot indicated net areal primary production, computed as algal carbon production minus total water column carbon consumption. A third plot indicated instantaneous water-column respiration, on a volumetric basis. Computation of respiration was analogous to computation of BOD (Equation 8-16) except no five-day integration was performed. Together, the primary production and respiration plots indicated biological activity. Regions with high production and respiration are more eutrophic than regions with lesser production and respiration. The final time series was modeled light extinction, the sum of background light extinction input to the model and attenuation due to computed chlorophyll concentration.

Evaluation of Model Performance

Graphical Evaluation

Evaluation of model performance from a large number of time series is difficult. To aid in evaluation, graphical and statistical summaries were performed. For major water quality constituents, scatterplots of observed versus modeled concentrations were produced (Figure 9-29). The summary included each observation in the data base, not only observations in the time series. As with the time series, grab samples were plotted against daily averages in model cells. A solid line indicating one-to-one correspondence was shown on each plot. Cumulative-difference plots were also produced. These indicated the percentage of observations which differed from modeled concentrations by less than an indicated value.

The temperature scatterplot indicated ideal model-data agreement. Discrepancies between predictions and observations were small. Observations and modeled temperatures fell nearly on a one-to-one line throughout the observed range.

Salinity correspondence was also excellent, especially in the upper salinity range. Below ≈20 ppt, the model showed a tendency to underestimate salinity, however.

The chlorophyll scatterplot was typical for this substance. Observations and model agreed well in lower chlorophyll ranges. Extreme observations, above 50 mg m^{-3}, existed which could not be modelled, however. In Indian River/ Rehoboth Bay, most of these observations were collected near Millsboro. The observations were near-surface samples and resulted from algal mat formation and concentration of the mats by wind and physical features. The model, which computes depth-average concentrations, is not suited for prediction of chlorophyll on the scale of these observations.

The BOD scatterplot indicated correct model representation of the processes which produce the range of observed BOD. Observed and modeled maxima

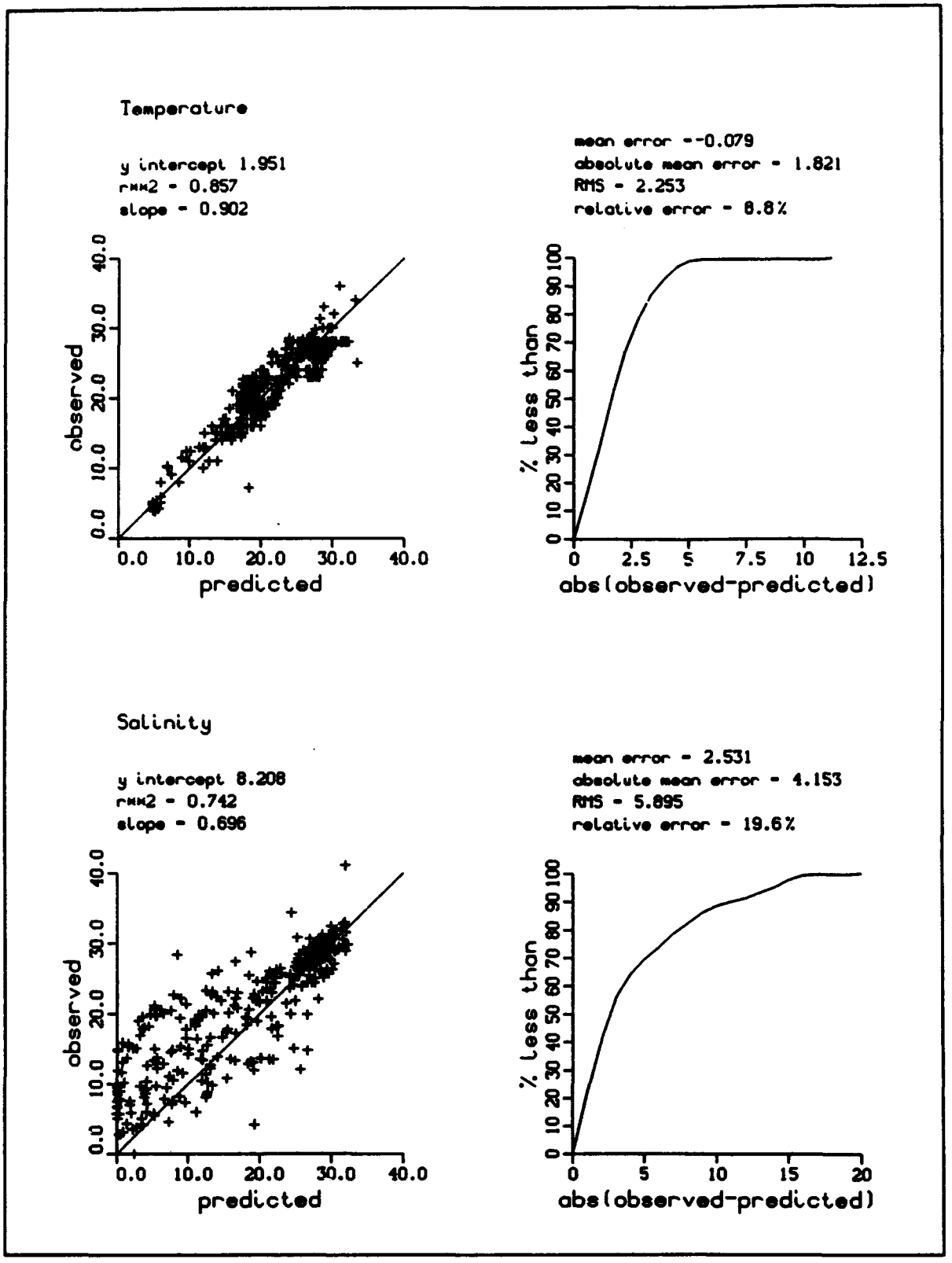

Figure 9-29. Graphical and Statistical Comparison of Individual Observations Versus Model Results (Sheet 1 of 6)

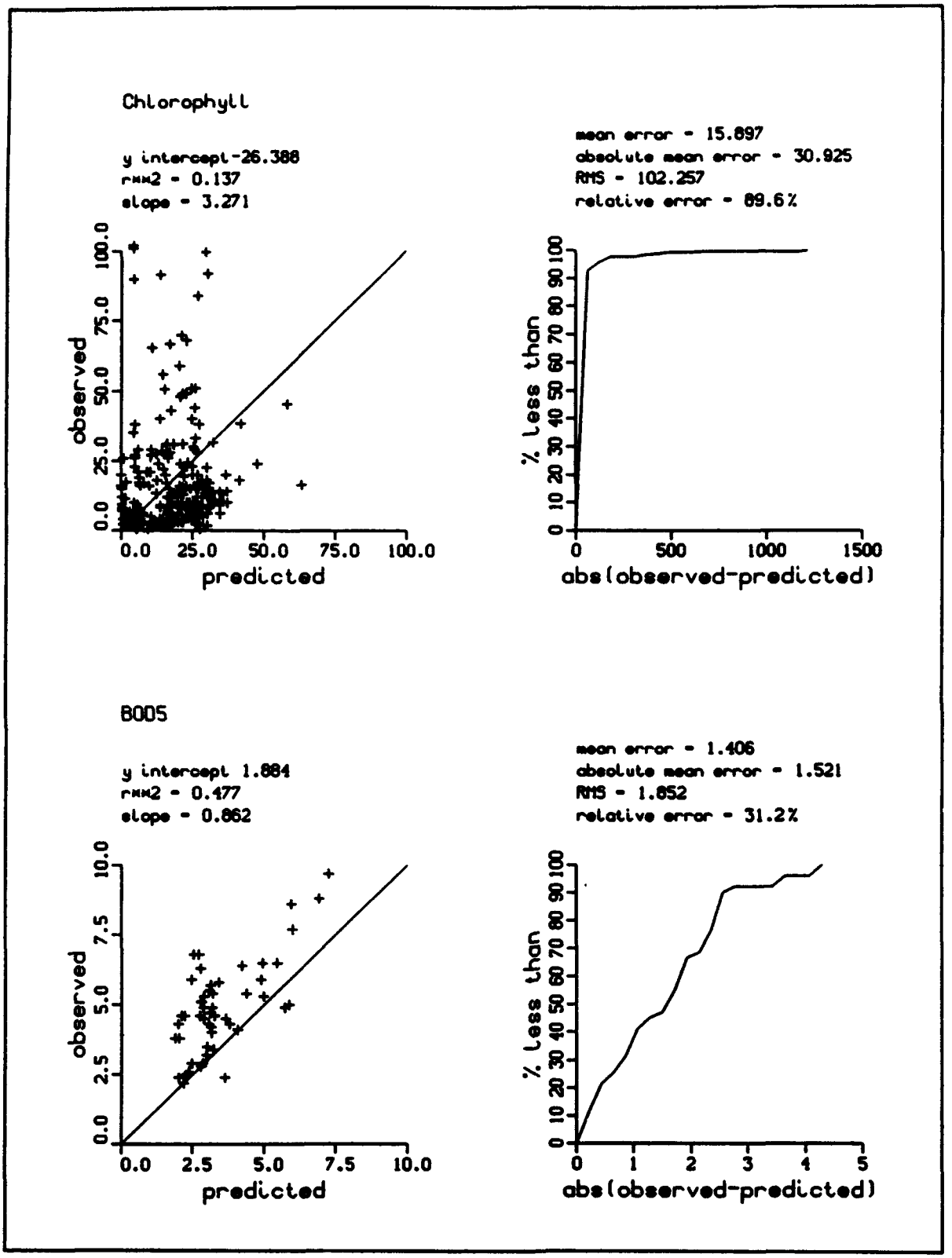

Figure 9-29. (Sheet 2 of 6)

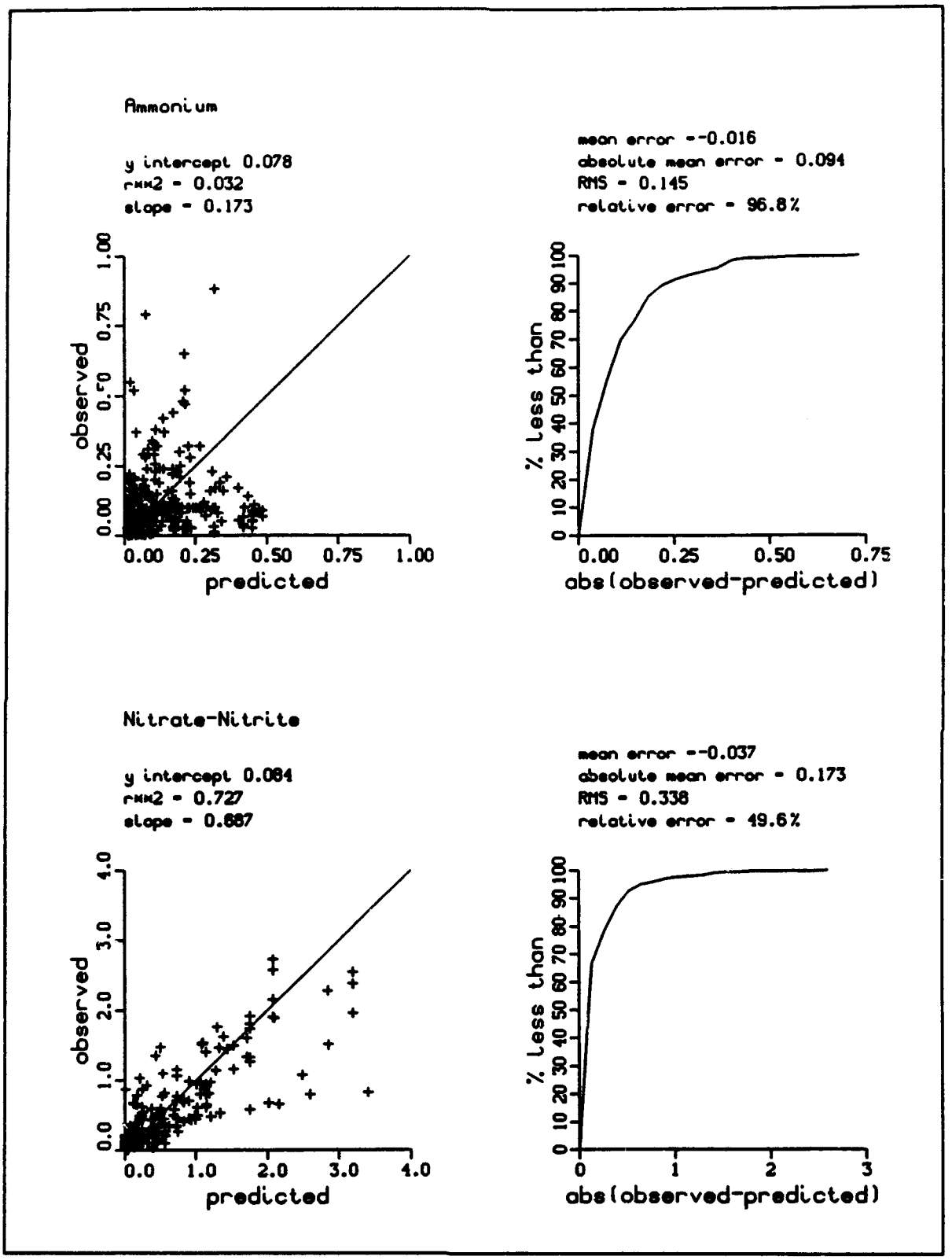

Figure 9-29. (Sheet 3 of 6)

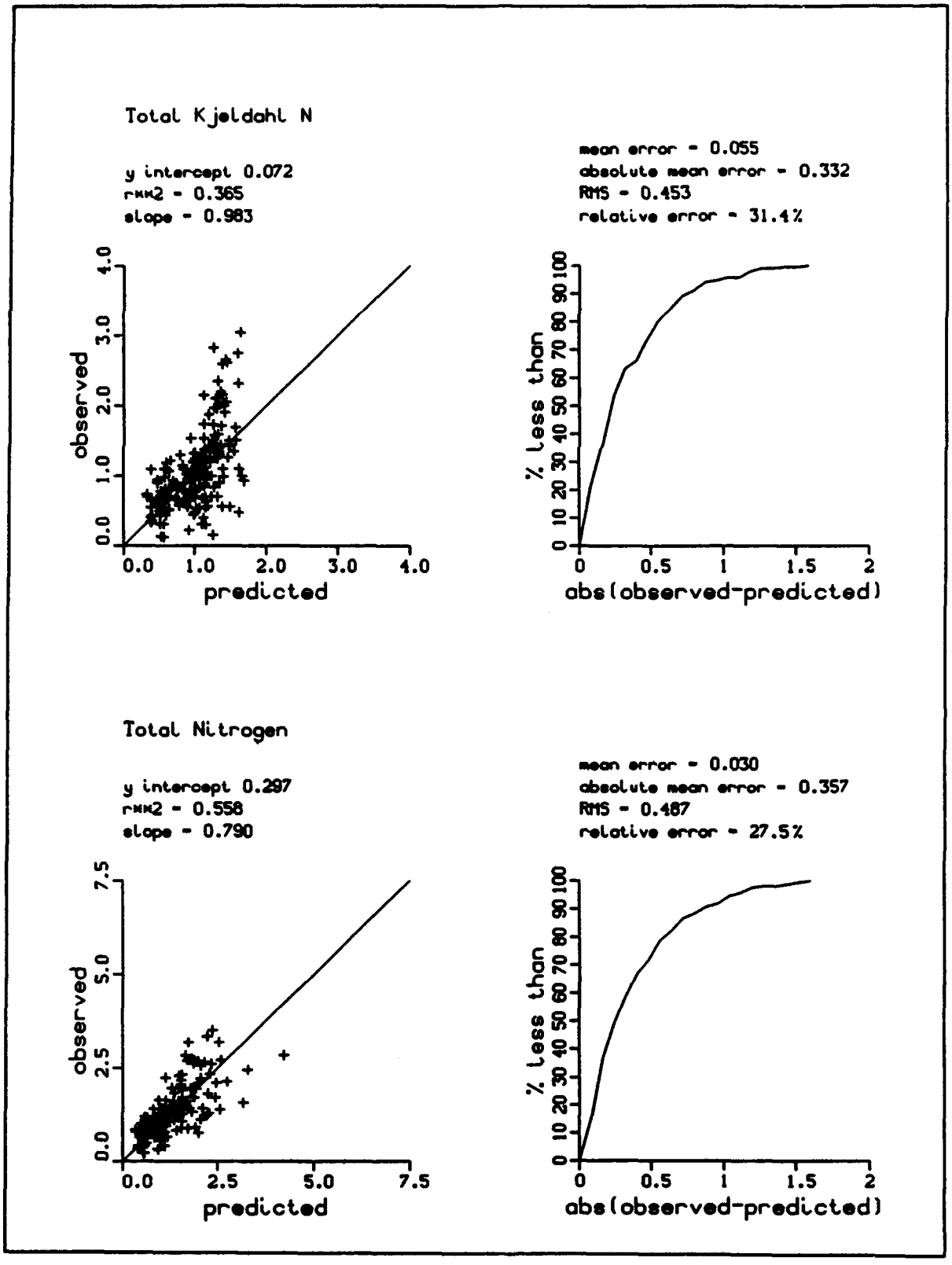

Figure 9-29. (Sheet 4 of 6)

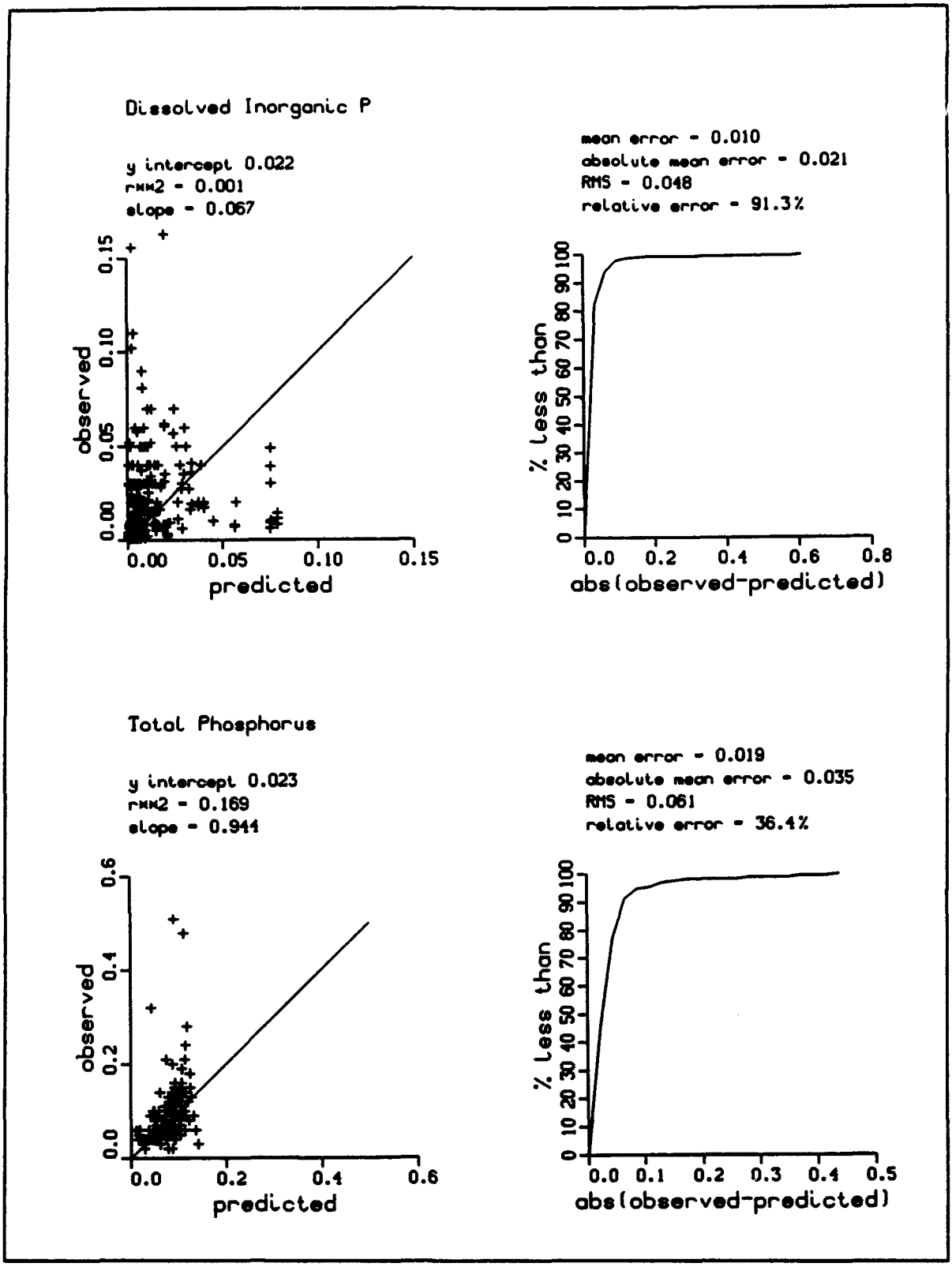

Figure 9-29. (Sheet 5 of 6)

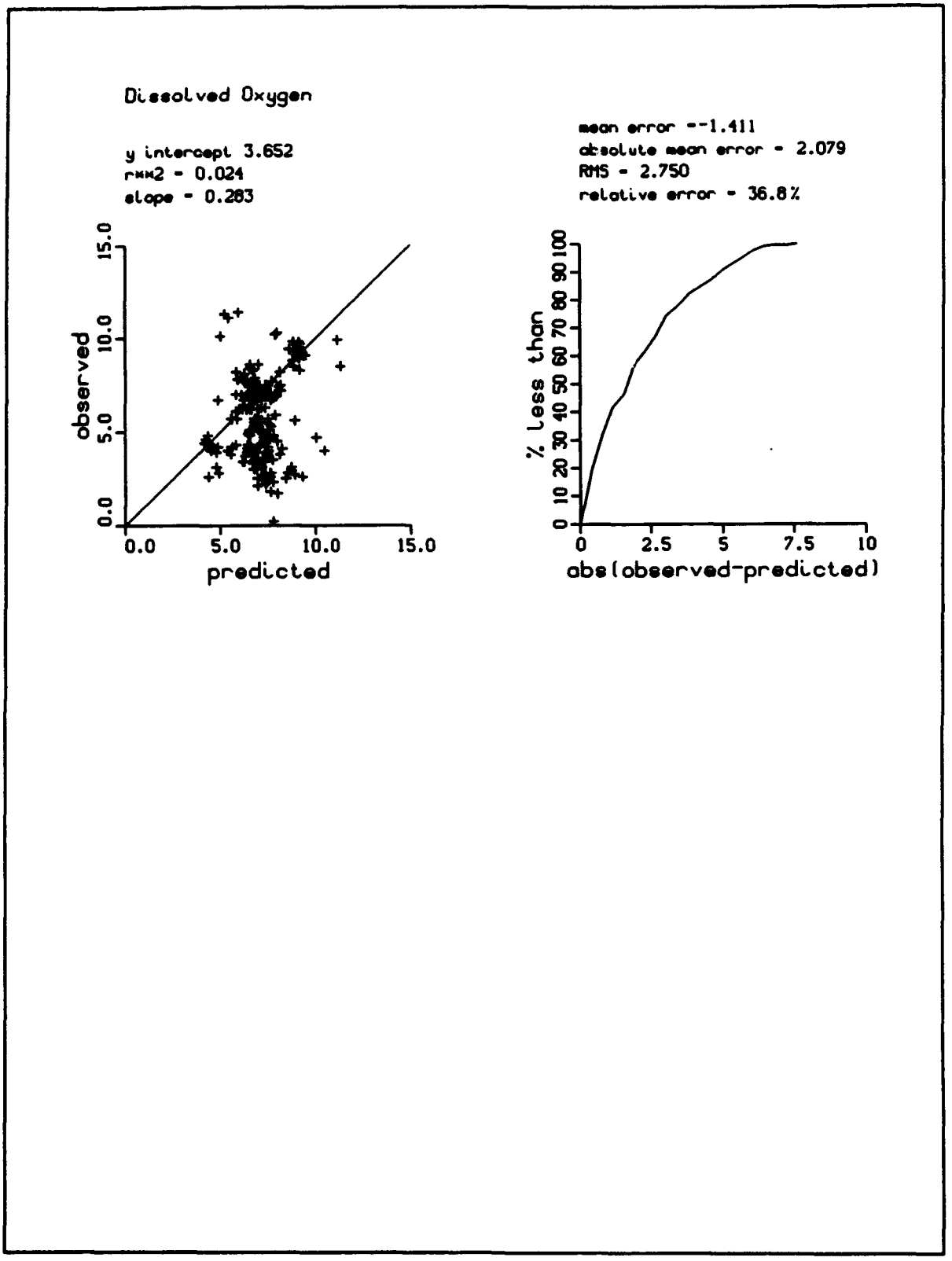

Figure 9-29. (Sheet 6 of 6)

and minima coincided. Modeled BOD was usually less than observed, however.

The ammonium scatterplot was typical for this substance. The range of modeled ammonium agreed with the observed range but little one-to-one correspondence between model and observations existed. The nitrate scatterplot indicated good correspondence between model and observations throughout the observed range. Good model-data correspondence also existed for total Kjeldahl nitrogen and total nitrogen although extreme total Kjeldahl measures were not replicated by the model.

The phosphate scatterplot was similar to ammonium. The range of modeled phosphate agreed with the observed range but little one-to-one correspondence existed, especially for the extreme values. Correspondence between modeled and observed total phosphorus was better than for phosphate. Only a few extreme observations were not replicated.

The dissolved oxygen scatterplot indicated behavior similar to ammonium and phosphate. Observed and modeled range were reasonable but point-by-point comparisons showed large discrepancies. The lowest observations were not well-replicated. One reason for the discrepancies is the comparison of daily-average model values with instantaneous observations. Since the observations are subject to diurnal fluctuations, direct correspondence cannot be expected. The minimum values in the observations are better represented by application of the diurnal curve technique described in Chapter 8 than by direct utilization of model output.

The large number of observations partially obscures interpretation of the scatterplots. The comparison of individual observations also implies temporal and spatial resolution that are not available in the model. The grab samples are point observations influenced by physical processes that occur on time scales less than a tidal cycle. The smallest spatial scale resolved by the model is the cell length, roughly 500 m. While the model time step, roughly five minutes, is consistent with the temporal scale of processes that influence the observations, forcing functions such as loads and light extinction are known only on a monthly basis. Improved, more reliable views of model performance are obtained by temporal and spatial aggregation of observations and model output so that small-scale, essentially random, variations are removed from the observation set.

Aggregation was performed by regional averaging of all data collected in the months of June, July, and August. These months were selected since they contained most data and since summer is the season of critical water quality. Regions were the same as defined for analysis of light extinction (Figure 8-7). An average was computed for each region for summer of 1988, 1989, and 1990. (For some season-region combinations, no observations existed, however.) The averaged observations were compared to model results averaged over identical regions and seasons (Figure 9-30). The analysis also permitted evaluation of model performance on a regional basis.

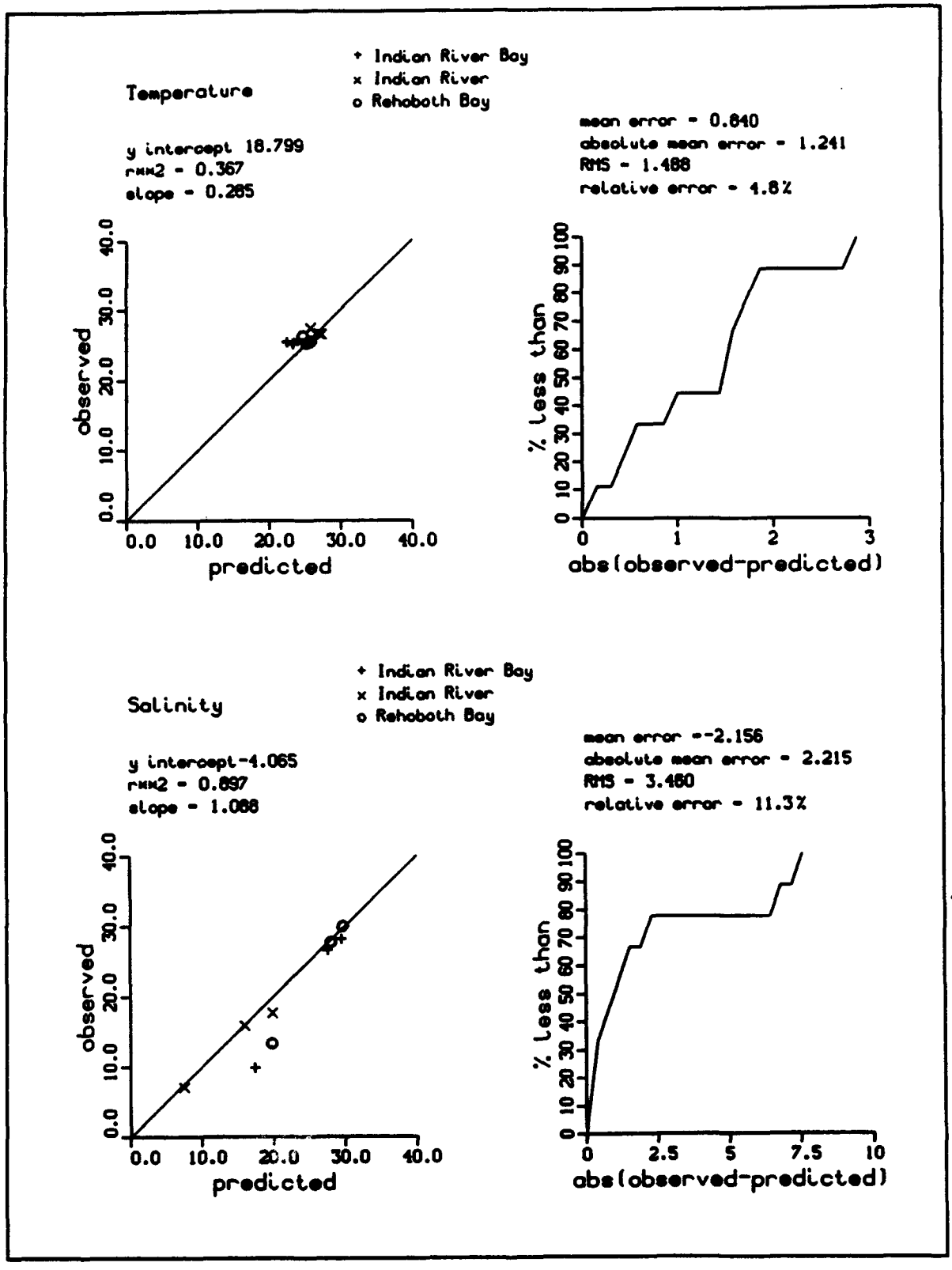

Figure 9-30. Graphical and Statistical Comparison of Summer-Average Observations Versus Model Results (Sheet 1 of 6)

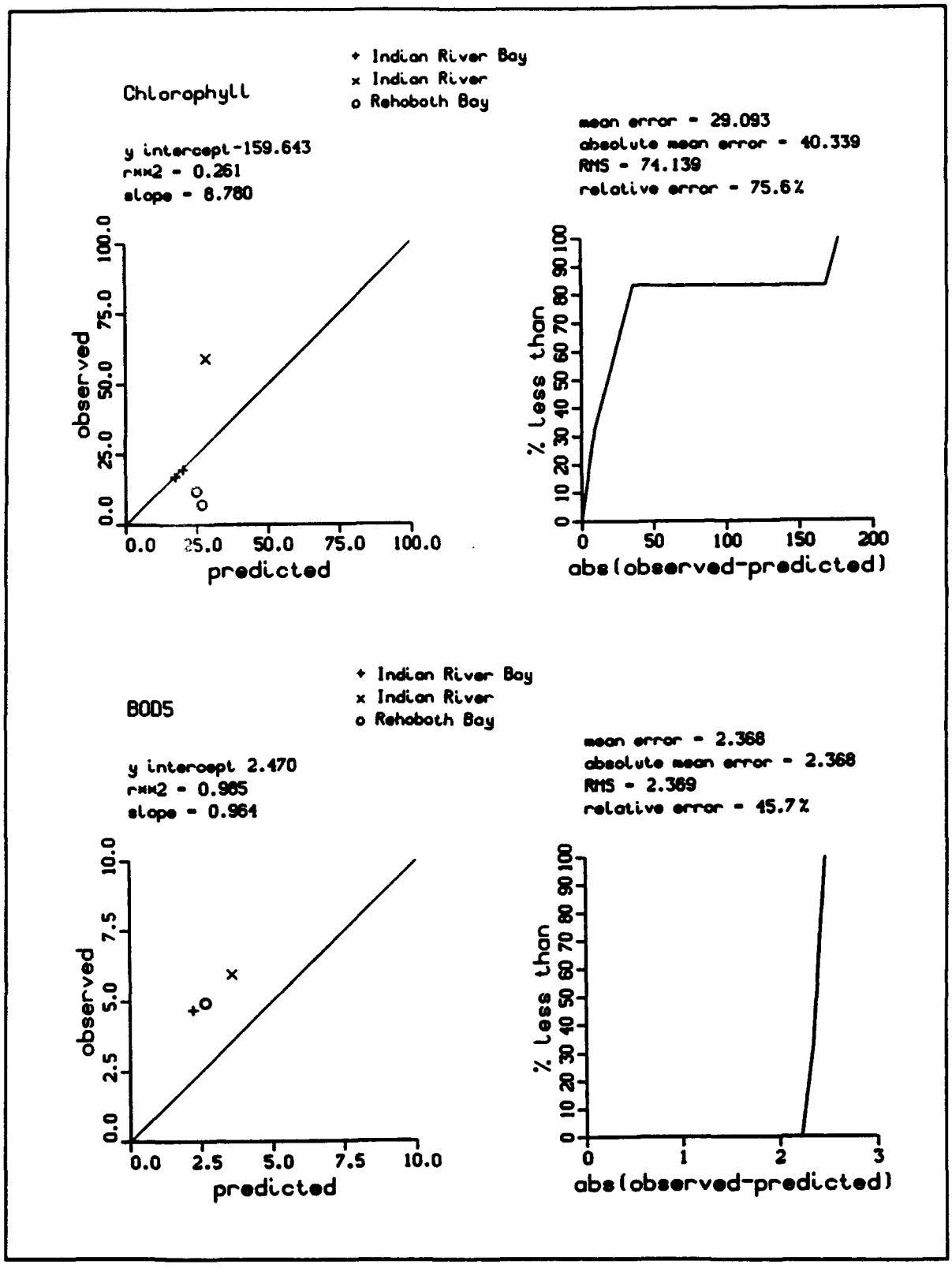

Figure 9-30. (Sheet 2 of 6)

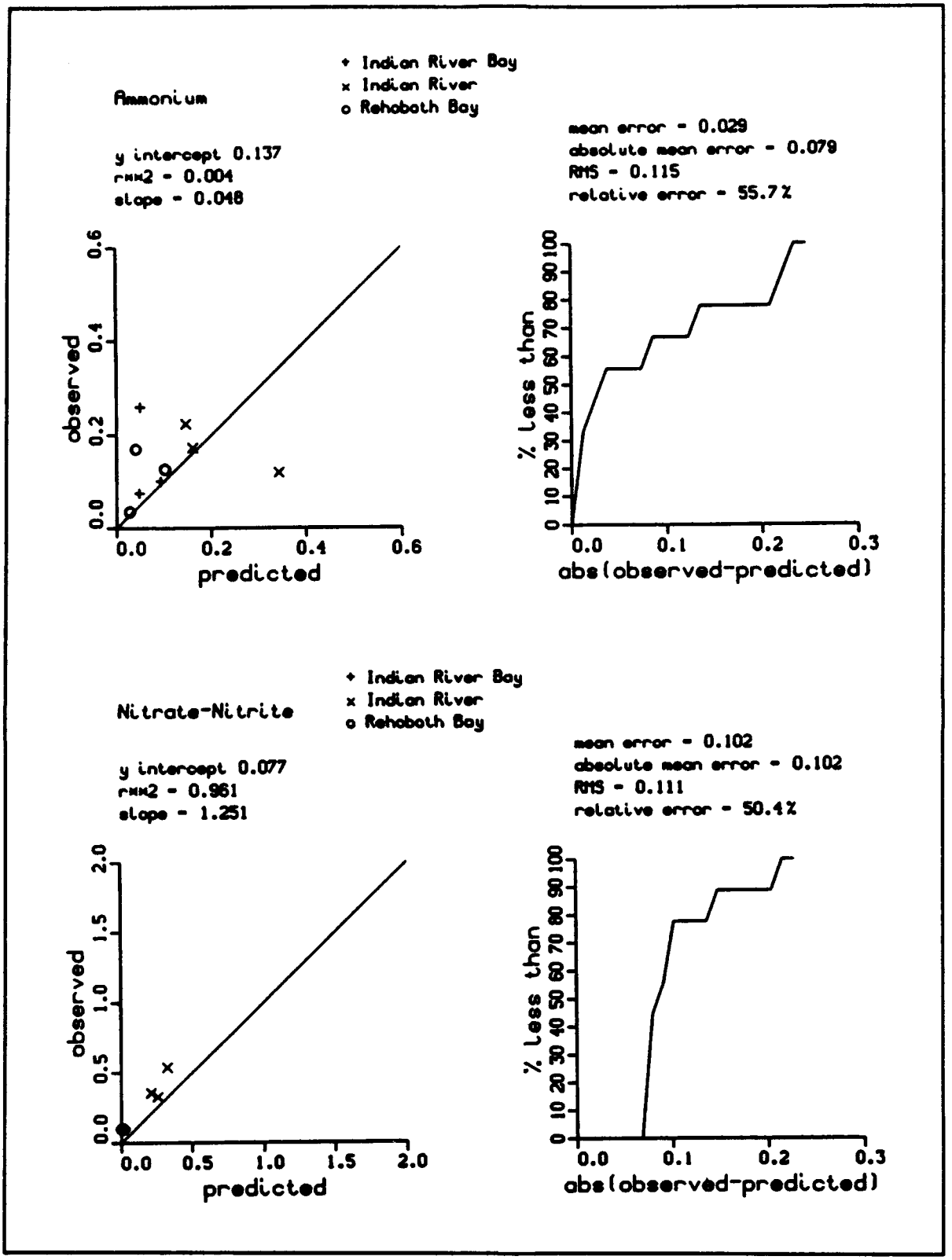

Figure 9-30. (Sheet 3 of 6)

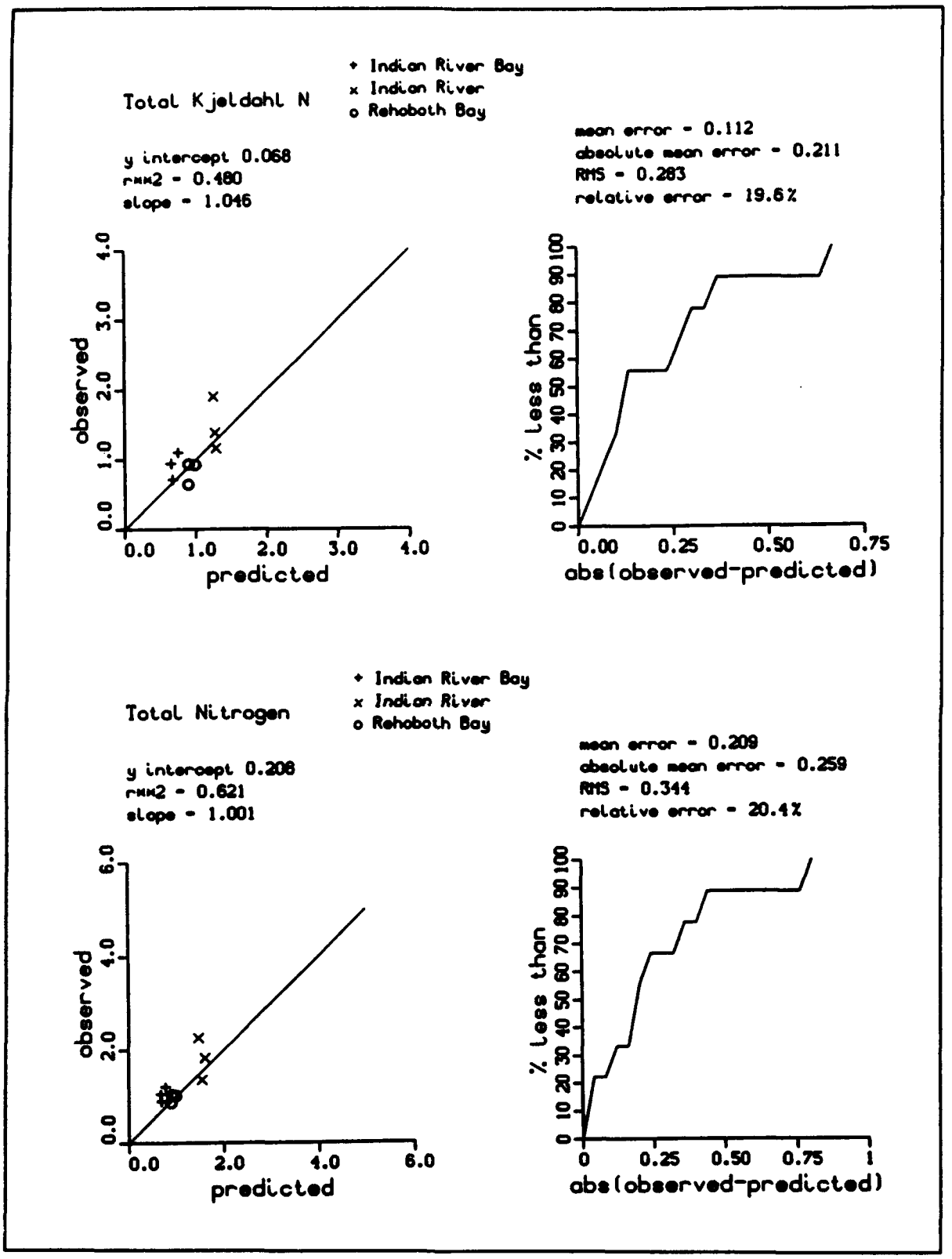

Figure 9-30. (Sheet 4 of 6)

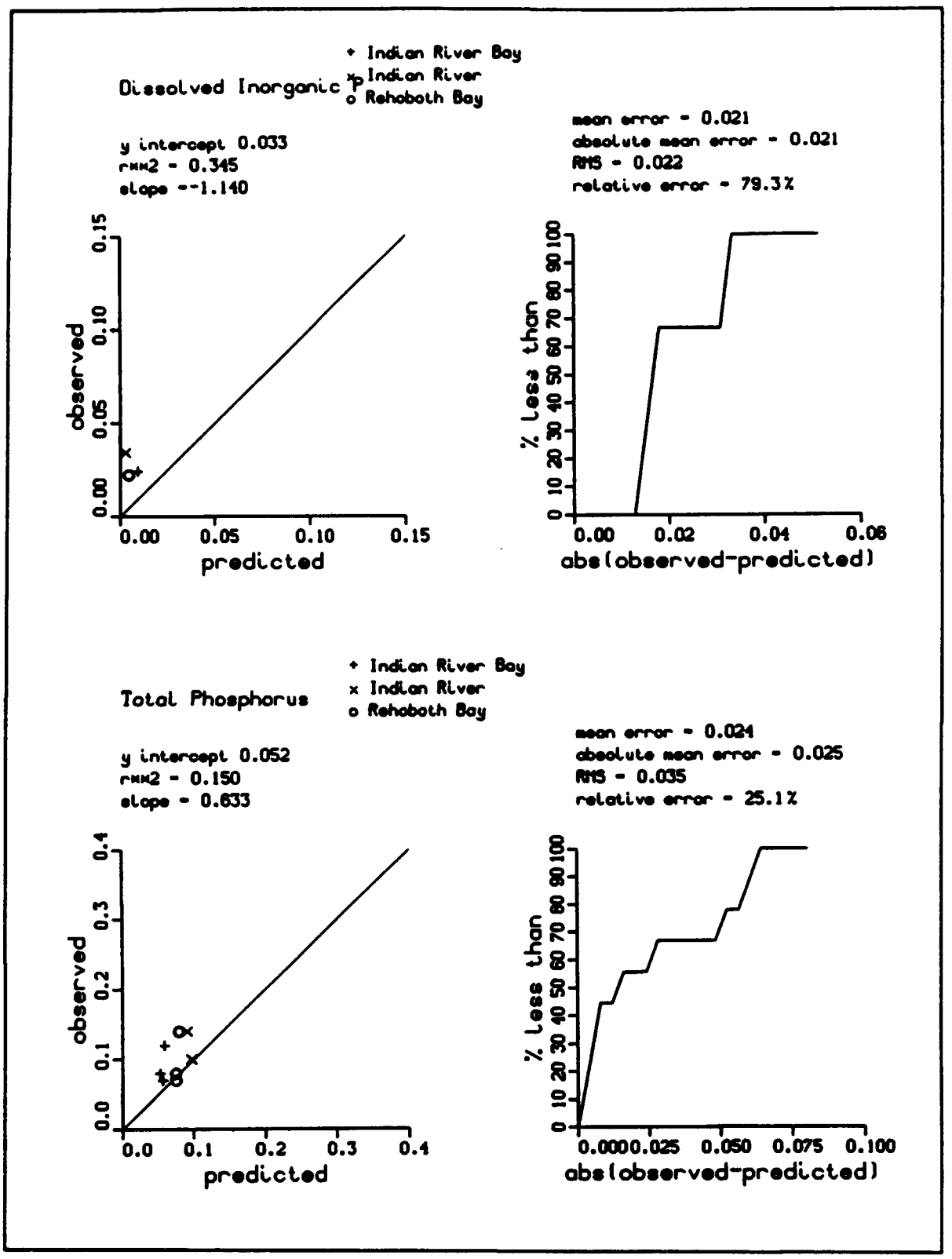

Figure 9-30. (Sheet 5 of 6)

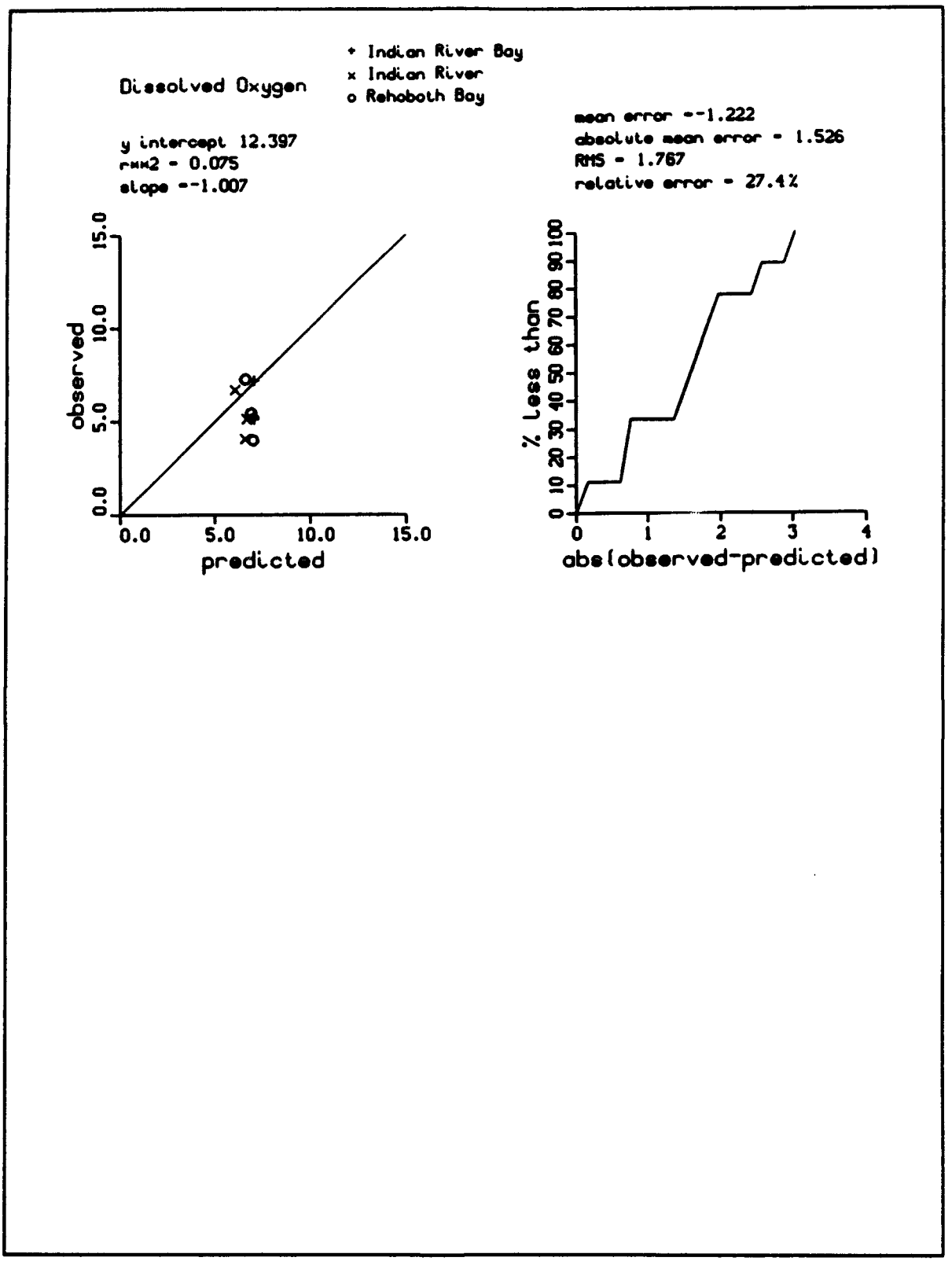

Figure 9-30. (Sheet 6 of 6)

Modeled temperature was ideal on a point-by-point basis so little additional information was gained by examination of aggregated values. Aggregation of salinity, however, indicated nearly perfect model-data agreement for six of nine seasonal-regional averages. Model chlorophyll results were perfect in Indian River Bay. The model overestimated chlorophyll in Rehoboth Bay, however. Chlorophyll in upper Indian River was underestimated for reasons previously explained. The behavior of aggregated BOD was the same as for individual comparisons. The model indicated the correct trend in BOD but underestimated concentration. Large portions of the erratic ammonium comparisons were removed by seasonal-regional averaging. Model-data ammonium comparisons were ideal for five of nine seasonal-regional combinations. Erratic predictions and observations still existed for some seasons and regions, however. Nitrate, total Kjeldahl nitrogen, and total nitrogen comparisons on the seasonal-regional basis mirrored the favorable performance of individual comparisons. Phosphate demonstrated a clear trend of underprediction by the model in all regions. Total phosphorus demonstrated ideal agreement of predictions and observations in most regions and seasons although the model underestimated in some comparisons. Comparisons indicated the model overestimated dissolved oxygen in most season-region combinations but correspondence in several was near-perfect.

Statistical Evaluation

The scatterplots are useful, qualitative summaries of model performance. Quantitative measures are preferred by some analysts, however. No consensus exists on a standard suite of quantitative performance measures. As a result, we compute a large suite, reported on the same figures as the scatterplots (Figures 9-29, 9-30).

Regression Analysis - One popular form of model-data comparison treats model results as independent variables and observations as dependent variables in linear regression analysis. A high degree of correspondence between model and observations is indicated by a correlation coefficient near unity, an intercept near zero, and a slope near unity.

Mean Error - The mean error statistic is defined:

$$ME = \frac{\sum (O - P)}{n} \qquad (9\text{-}1)$$

ME = mean error

O = observation

P = model result

n = number of observations

The mean error is a summary of the model tendency to overestimate or underestimate the data. The mean error can be zero even though large discrepancies exist in individual model-data comparisons. The mean error is especially useful to indicate potential errors in loads, sediment-water fluxes, and other sources and sinks to the water column.

Absolute Mean Error - The absolute mean error statistic is defined:

$$AME = \frac{\sum |O - P|}{n} \qquad (9\text{-}2)$$

AME = absolute mean error

The absolute mean error is a measure of the average discrepancy between observations and model results. The absolute mean error does not differentiate between overestimates and underestimates by the model.

Root Mean Square Error - The root mean square error statistic is defined:

$$RMS = \sqrt{\frac{\sum (O - P)^2}{n}} \qquad (9\text{-}3)$$

RMS = root mean square error

The root mean square error is an alternate quantification of the average discrepancy between observations and model results.

Relative Error - The relative error is defined:

$$RE = \frac{\sum |O - P|}{\sum O} \qquad (9\text{-}4)$$

RE = relative error

The relative error statistic normalizes absolute mean error by the magnitude of the observations. The relative error statistic is especially useful in comparing performance between variables of different magnitude or performance of models of different systems.

The mean error and root mean square error for major water quality constituents are summarized in Table 9-1. Summaries are for instantaneous and seasonal-regional comparisons.

Table 9-1
Summary of Mean and Root Mean Square Error

	mean error	mean error	RMS error	RMS error
Substance	Indian River, Individual Data Points	Indian River, Summer-Regional Average	Indian River, Individual Data Points	Indian River, Summer-Regional Average
Temperature, C^o	–0.08	0.84	2.25	1.49
Salinity, ppt	2.53	–2.16	5.9	3.46
Chlorophyll, mg m^{-3}	15.9	29.1	102.3	74.1
BOD5, gm m^{-3}	1.41	2.37	1.85	2.37
Ammonium, gm m^{-3}	–0.016	0.029	0.145	0.115
Nitrate, gm m^{-3}	–0.037	0.102	0.338	0.111
Total Kjeldahl N, gm m^{-3}	0.055	0.112	0.453	0.283
Total N, gm m^{-3}	0.03	0.209	0.487	0.344
Phosphate, gm m^{-3}	0.01	0.021	0.048	0.022
Total P, gm m^{-3}	0.019	0.024	0.061	0.035
Dissolved Oxygen, gm m^{-3}	–1.41	–1.22	2.75	1.77

The summary indicates mean error is generally larger in magnitude for the summer average than for individual observations. One interpretation of this phenomenon is that sources and sinks for summer only are quantified to a lesser degree of accuracy than for the time period encompassed by the entire data base (April through September). The RMS error for the seasonal-regional average is about half the error for instantaneous comparisons. The implication of this statistic is that the model is more accurate in reproducing spatial and temporal aggregations than individual observations.

Interpretation of performance statistics is facilitated when some basis for comparison is present. We compared the relative error statistics with results of the Chesapeake Bay model study (Cerco and Cole 1993). Individual and seasonal-regional averages from Indian River were compared to seasonal-regional averages from the Bay (Figure 9-31). The Chesapeake Bay study made use of an extensive, high-quality data base and employed highly accurate measures of loads and boundary conditions. Calibration of the model consumed several years and was subject to extensive review. We regard the performance statistics of the Bay study as current state of the art for long-term applications of comprehensive eutrophication models.

Relative error for seasonal-regional averages in the Indian River model application was generally greater than in Chesapeake Bay but comparable for all but two substances. Relative error for chlorophyll in Indian River was double the Chesapeake Bay value. The chlorophyll statistic in Indian River reflected the extreme concentrations observed at the surface near the Millsboro spillway. Concentrations in excess of 1000 mg m^{-3} were in the data base. Discrepancies between these observations and model results added enormous bias to the performance statistics. Relative error for phosphate was also double the Chesapeake Bay value. We were informed by DNREC that the phosphate data in STORET is dubious. We noted the STORET phosphate data frequently disagreed with the observations collected by the College of Marine Studies (Figures 9-3, 9-4, 9-7, 9-8). Most often, when conflicts in the data were noted, model results conformed to the College of Marine Studies rather than the STORET data. We concluded the large phosphate relative error was due to faulty data rather than a shortcoming in the model calibration.

The Annual Cycle of Water Quality

The time series of conditions in the water column, sediment-water interactions, and interpretive quantities, together with other information available from the model permit a description of the annual cycle of water quality in Indian River/Rehoboth Bay.

During the first four months of the year, chlorophyll is virtually absent from the water column (Figures 9-2 through 9-9). Nitrogen, in the form of nitrate, and light to support algal growth are readily available (Figures 9-21 through 9-28). A slight phosphorus limitation to growth is present but the primary influence on algal abundance is temperature. The water is too cold to support substantial primary production by phytoplankton. In May, the water warms sufficiently to support algal production so that chlorophyll concentration rapidly rises to its summer maximum value. Limitations to algal growth during summer vary. Light extinction, due to background extinction and algal-self shading, is at its annual peak (Figures 9-21 through 9-28). In upper Indian River, phosphorus is the limiting nutrient (Figures 9-21 through 9-23). In Lower Indian River and in Rehoboth Bay, however, nitrogen is the dominant nutrient limit on algal growth (Figures 9-24 through 9-28). Chlorophyll concentration fluctuates, in response to flow and loading events, until

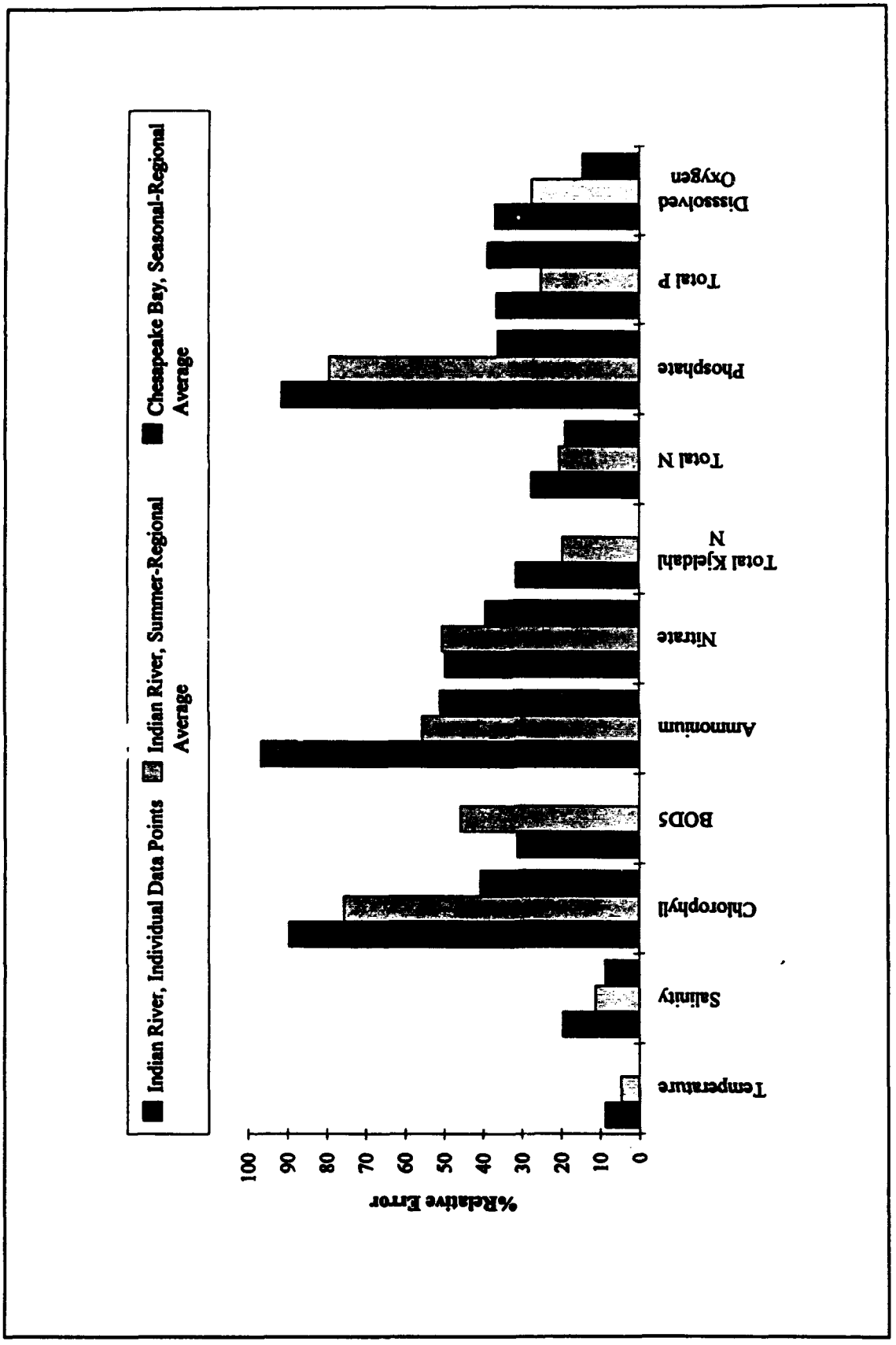

Figure 9-31. Relative Error in Indian River/Rehoboth Bay and Chesapeake Bay Model Applications

mid-October. In October, temperature falls below the level needed to support substantial algal growth and chlorophyll declines to its winter minimum concentration.

During the first four months of the year, background light extinction is near its minimum value and light attenuation by chlorophyll is negligible (Figures 9-21 through 9-28). Light is available to support production by benthic algae. As a consequence, dissolved oxygen is produced at the sediment-water interface and released to the water column (Figures 9-13 through 9-20). Ammonium and phosphate are removed from the water column and consumed at the sediment-water interface. Nitrate transport is into the sediments, driven by the high concentrations in the overlying water. Two phenomenon accompany the warming of the water column in May. First, oxygen consumption and nutrient production in the subsurface sediments increase. Second, light extinction increases due to the seasonal variation in background extinction and chlorophyll attenuation. As a consequence of temperature-enhanced sediment processes and shading of the benthic algae, the sediments consume oxygen removed from the water column. The sediments become sources of ammonium and phosphate to the water. Sediment-water nitrate flux is negligible due to diminished concentration in the overlying water. Sediment consumption of oxygen and production of ammonium and phosphate continue until autumn cooling of the water column. Cooling diminishes diagenetic processes in the sediments and is accompanied by diminished light extinction. Benthic algae become active so that, by the end of the year, dissolved oxygen is again produced at the sediment-water interface. Ammonium and phosphate enter a transition from sediment release to consumption at the sediment-water interface.

The annual nitrogen cycle varies according to location. In lower Indian River and Rehoboth Bay (Figures 9-5 through 9-9), total nitrogen concentration demonstrates a sinusoidal behavior with maximum concentration in late summer. The phase of the total nitrogen function corresponds to the phase of annual temperature variation. The correspondence occurs because temperature drives sediment ammonium release (Figures 9-13 through 9-20), a primary source of nitrogen to the lower Bays. In upper Indian River, total nitrogen is more closely related to runoff events so that maximum concentrations typically occur in late winter or early spring (Figures 9-2 through 9-4). Since nitrate is a major constituent of runoff nitrogen, nitrate maxima occur in winter and spring throughout the system. The magnitude of the maximum diminishes away from the runoff entry points, however. In the lower Bays, in summer, nitrate is virtually absent due to algal uptake and negligible local runoff. The ammonium cycle is complex, influenced by external loading, sediment production/consumption, and algal uptake. In much of the system, a summer maximum, coincident with sediment release would be expected. As rapidly as ammonium is released from the sediment, however, it is consumed by algae. In lower Indian River and Rehoboth Bay (Figures 9-5 through 9-9) maximum ammonium concentrations are evident in October through December. In these months, phytoplankton uptake is diminished but uptake by benthic algae is not sufficient to remove the ammonium from the water column. Upper Indian

River also demonstrates the autumn peak but high concentrations, due to sediment release, occur in summer as well. In this portion of the system, summer algae populations tend to be limited by phosphorus availability so that not all ammonium is removed by algal activity.

The annual cycle of total phosphorus also coincides with the temperature cycle. As with nitrogen, the coincidence is due to temperature-enhanced nutrient release from the sediment. The influence of runoff in the annual phosphorus cycle is not as evident as for nitrogen however (Figures 9-2 through 9-4). Annual cycling in phosphate is similar to ammonium. Lower Indian River and Rehoboth Bay demonstrate an autumn peak (Figures 9-5 through 9-9) that presumably is due to diminished phytoplankton uptake coupled with minimal activity by benthic algae. Near the Millsboro spillway, however, phosphate exhibits erratic behavior due to loading from runoff events, consumption and release in sediments, and algal uptake.

As with most estuarine systems, minimum dissolved oxygen in Indian River/Rehoboth Bay occurs during late summer when water temperature is highest. The coincidence of high temperature and low dissolved oxygen is due to temperature-enhanced respiration in the water and sediments and due to diminished saturation dissolved oxygen concentration. Conversely, annual peaks in dissolved oxygen occur in winter when low temperature diminishes respiration in the water column, light stimulates benthic algal production, and saturation concentration is maximum. Our model indicates minimum daily-average dissolved oxygen concentrations of 2 to 3 gm m^{-3} occur in upper Indian River (Figures 9-2, 9-3). In lower Indian River and Rehoboth Bay, we typically indicate minimum daily-average dissolved oxygen concentrations of 6 gm m^{-3} (Figures 9-5 to 9-9). Observations indicate virtually no dissolved oxygen concentrations below 2 gm m^{-3}. In lower Indian River and Rehoboth Bay, however, a substantial proportion of observations fall below our 6 gm m^{-3} minimum. A portion of the discrepancy lies in the problem of comparing grab samples with daily average model output, as previously described. Several aspects of the comparisons remain problematic, however. Observations at most stations indicate dissolved oxygen was lower in 1989 and 1990 than in 1988 (Figures 9-4 through 9-9). We cannot explain this phenomenon; our model indicates dissolved oxygen is equivalent in the three summers. Our model also agrees well with the summer 1988 observations. Observations at most stations indicate minimum dissolved oxygen in 1990 occurred at the beginning of May, at a water column temperature less than 10 C^0, rather than later in the year. We believe the data base merits careful examination before conclusions are drawn regarding the ability of the model to reproduce the annual cycle of dissolved oxygen.

A mass-balance feature of the model allows computation of internal material sources and sinks. These are compared with the external loads quantified earlier (Chapter 3). On an annual basis, nonpoint sources are the largest nitrogen loads to the Indian River/Rehoboth Bay system (Figures 9-32 through 9-34). Atmospheric loads are the second largest source while point sources are the least of the sources quantified. Most of the nitrogen load to the system is

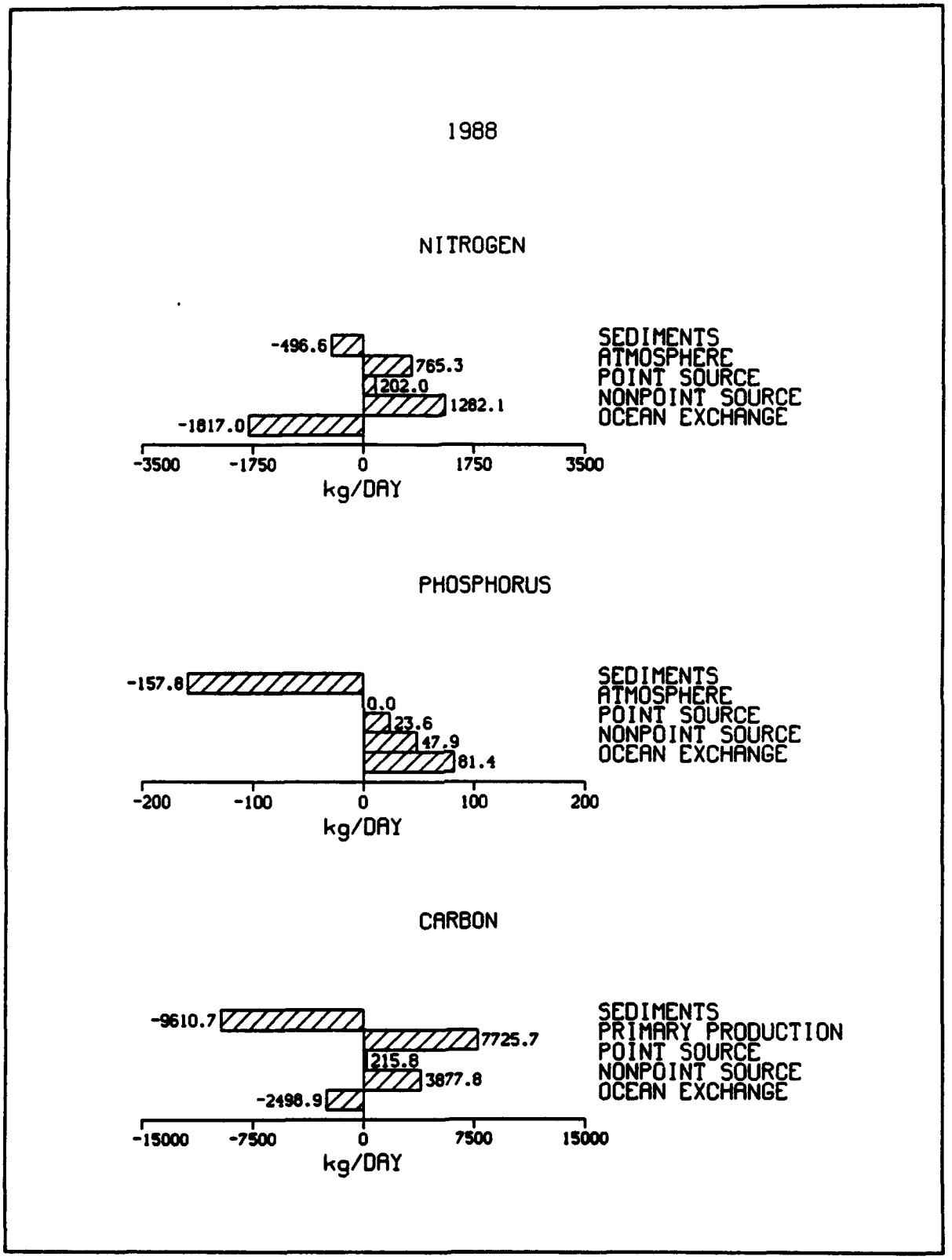

Figure 9-32. Annual Mass Balance, 1988

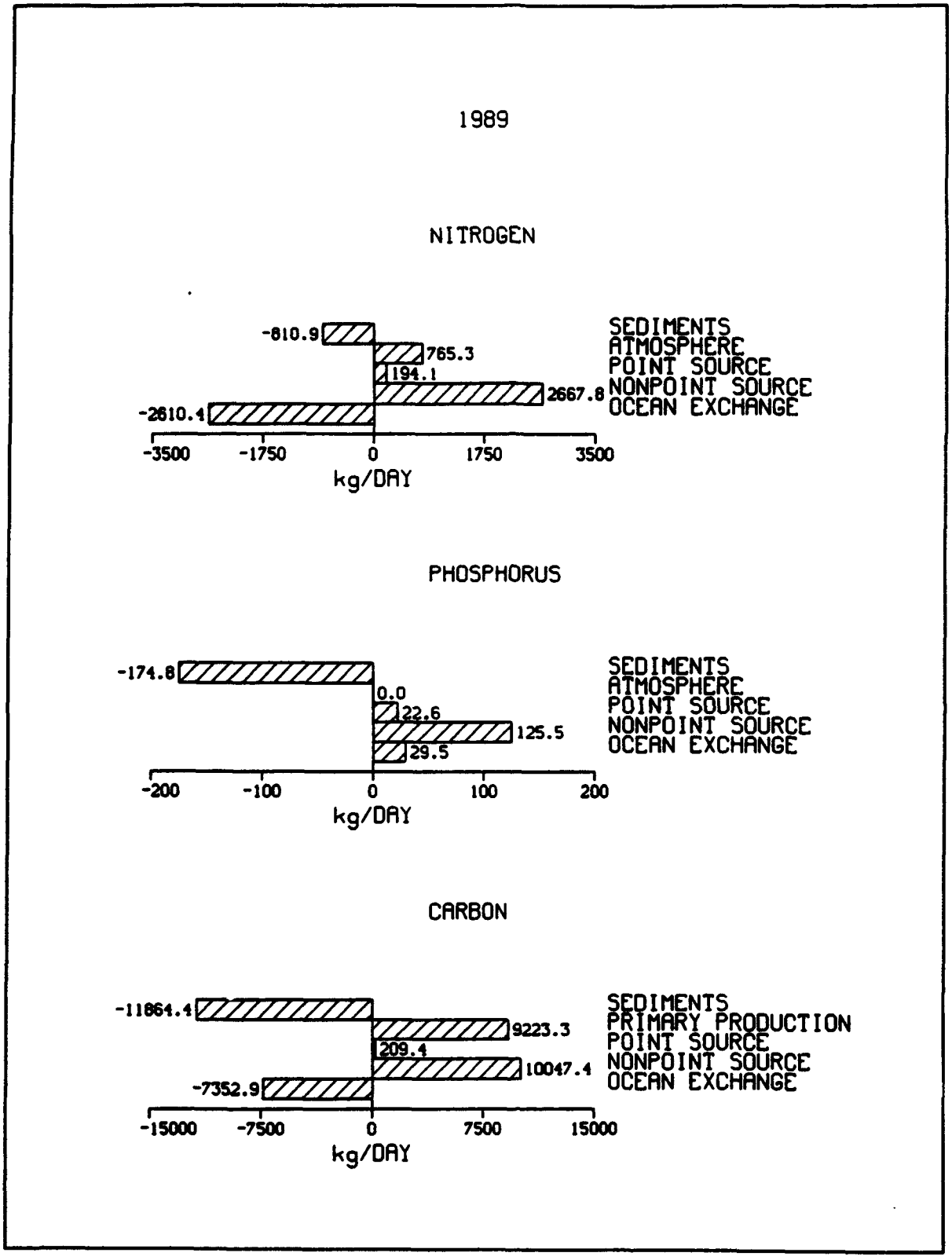

Figure 9-33. Annual Mass Balance, 1989

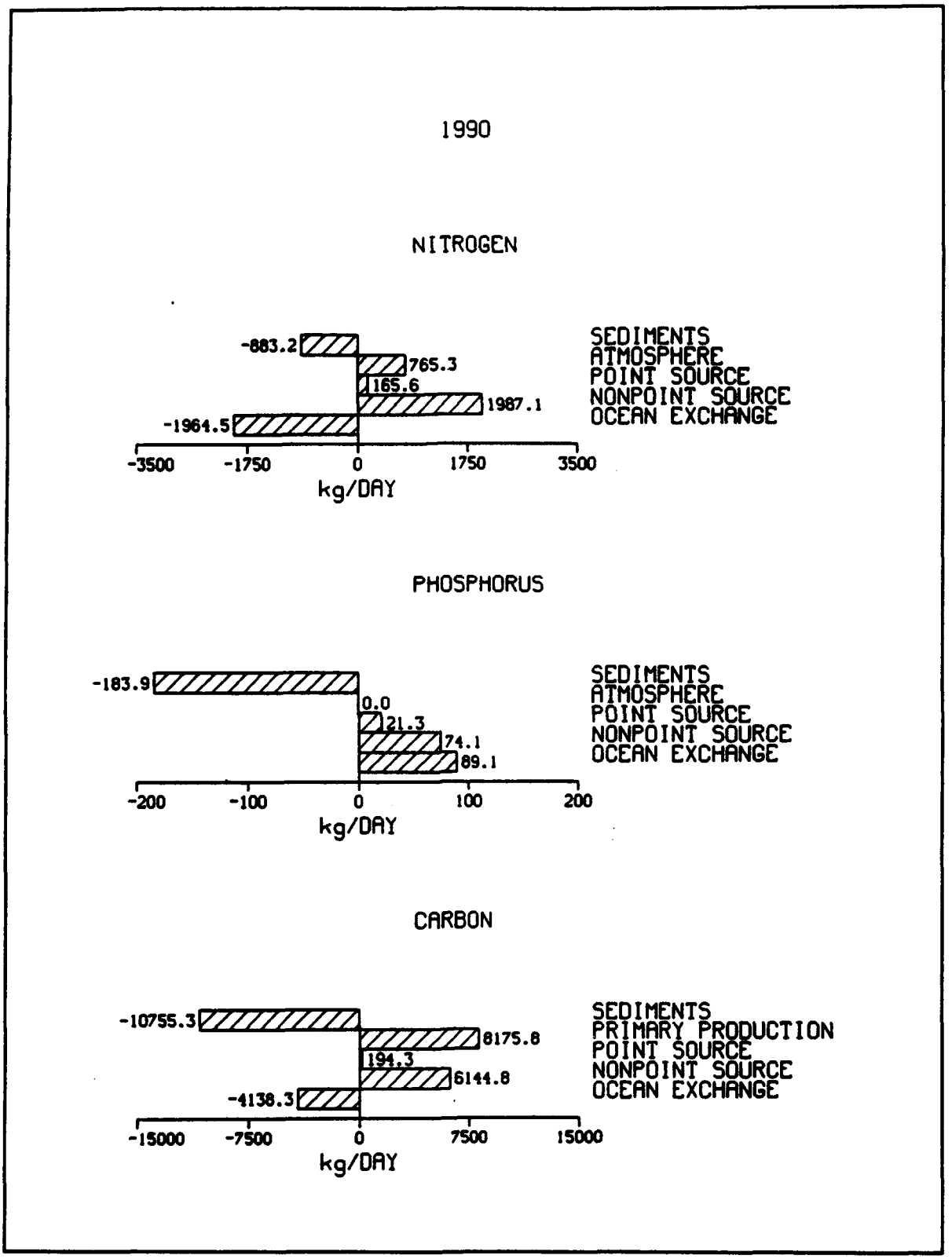

Figure 9-34. Annual Mass Balance, 1990

lost through the mouth to the ocean. The remainder is lost to the sediments where it is buried or denitrified to gaseous form.

During years of dry and normal hydrology, the largest source of phosphorus to Indian River/Rehoboth Bay is import through the inlet from the ocean (Figures 9-32, 9-34). In extremely wet years, however, nonpoint- source loads exceed import from the ocean (Figure 9-33). Point source loads are less than the oceanic import or nonpoint sources. No atmospheric load is thought to exist. The sediments represent the only phosphorus sink. Since no process analogous to denitrification exists for phosphorus, the ultimate sink is burial to deep, inactive sediments.

During years of dry and normal hydrology, the largest source of carbon to Indian River/Rehoboth Bay is primary production by algae (Figures 9-32, 9-34). The carbon produced by algae is oxidized in the water column, as BOD, or in the sediments, as sediment oxygen demand. In a wet year, however, a surprisingly large amount of carbon enters from nonpoint sources so that nonpoint-sources comprise the largest fraction of oxygen demand (Figure 9-33). Point-source carbon loads are negligibly small. Most of the carbon load to the system settles to the sediments where it is oxidized, producing sediment oxygen demand, or buried to deep, inactive sediments. A lesser fraction of the carbon load is exported through the mouth to the ocean.

Summer-Average Water Quality

Spatial representations of water quality (Figures 9-35 through 9-44) were obtained by averaging model results for June, July, and August 1990, an average hydrologic year. Summer was selected for spatial representation since it is the season in which water quality problems most often occur.

The model indicates chlorophyll (Figure 9-36) is maximum near the Millsboro spillway. High chlorophyll concentrations also occur in the headwaters of other major branches. Chlorophyll generally declines away from runoff sources and is least near the Indian River inlet. The chlorophyll distribution is governed by the distributions of ammonium (Figure 9-38), nitrate (Figure 9-39), and dissolved phosphate (Figure 9-42). Nitrate and ammonium are abundant, relative to the half-saturation concentration for nitrogen uptake (Table 6-2), throughout most of Indian River. In Rehoboth Bay and Indian River Bay, however, nitrate and ammonium are nearly depleted. The spatial distribution of nitrate reflects the source in runoff and wasteloading and the sink in the ocean. The ammonium distribution indicates a major source is sediment release. Dissolved phosphate is maximum in the inlet, indicating concentration in this region is strongly influenced by the ocean boundary condition. Phosphate is also high near Millsboro and the Rehoboth Beach outfall. Minimum phosphate concentrations occur midway between the inlet and Millsboro and in portions of Rehoboth Bay. The high chlorophyll levels in upper

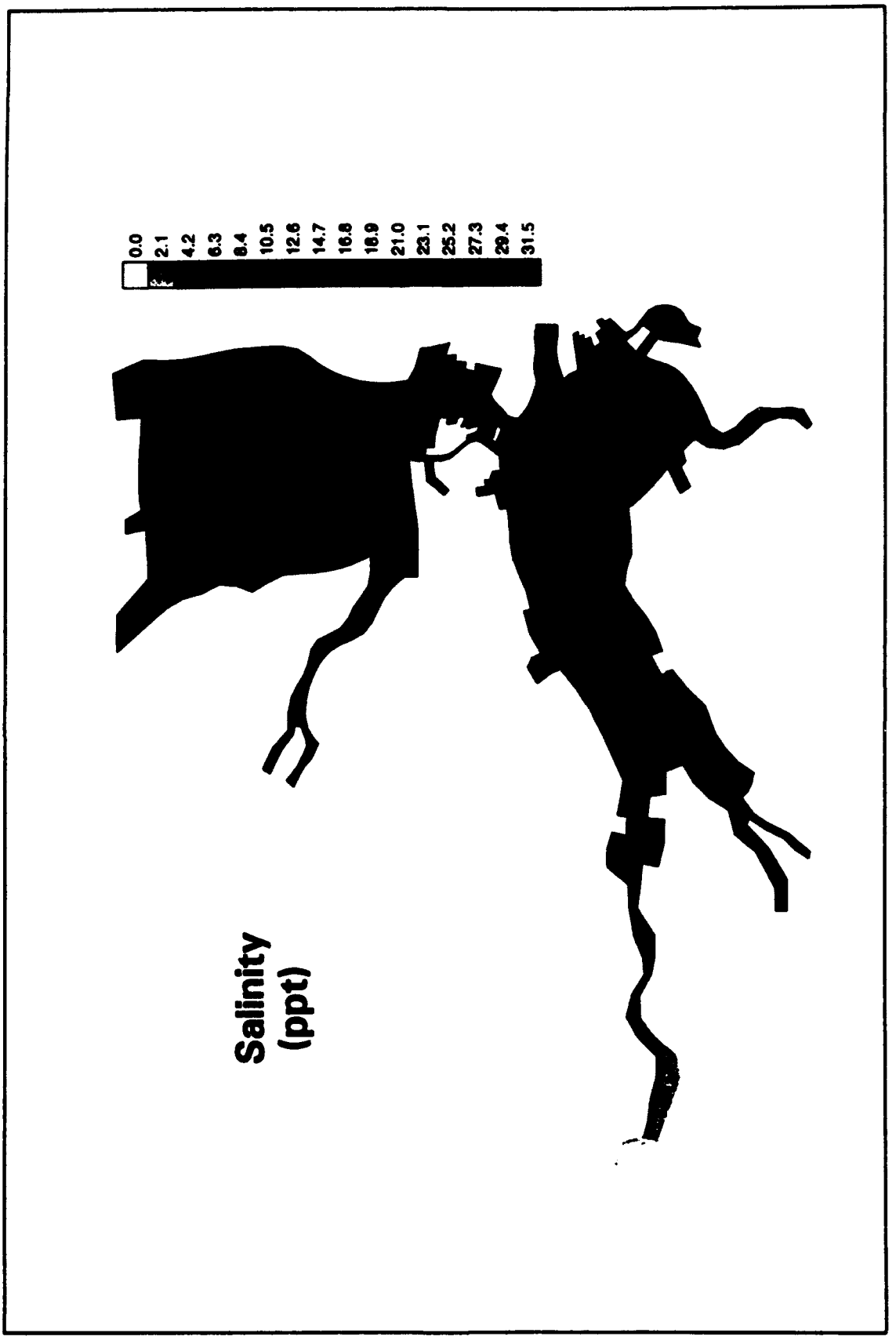

Figure 9-35. Modeled Salinity, 1990 Summer Average

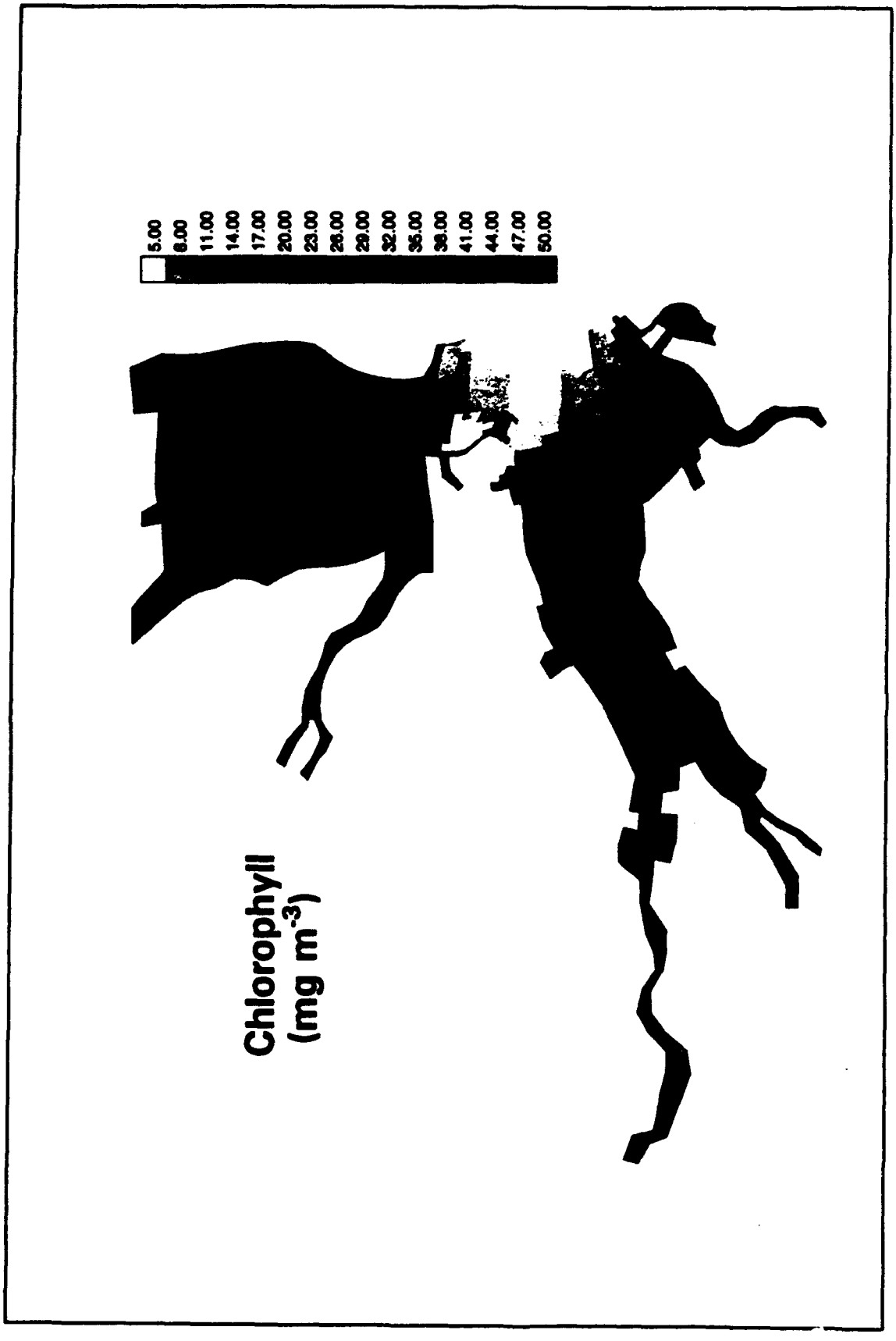

Figure 9-36. Modeled Chlorophyll, 1990 Summer Average

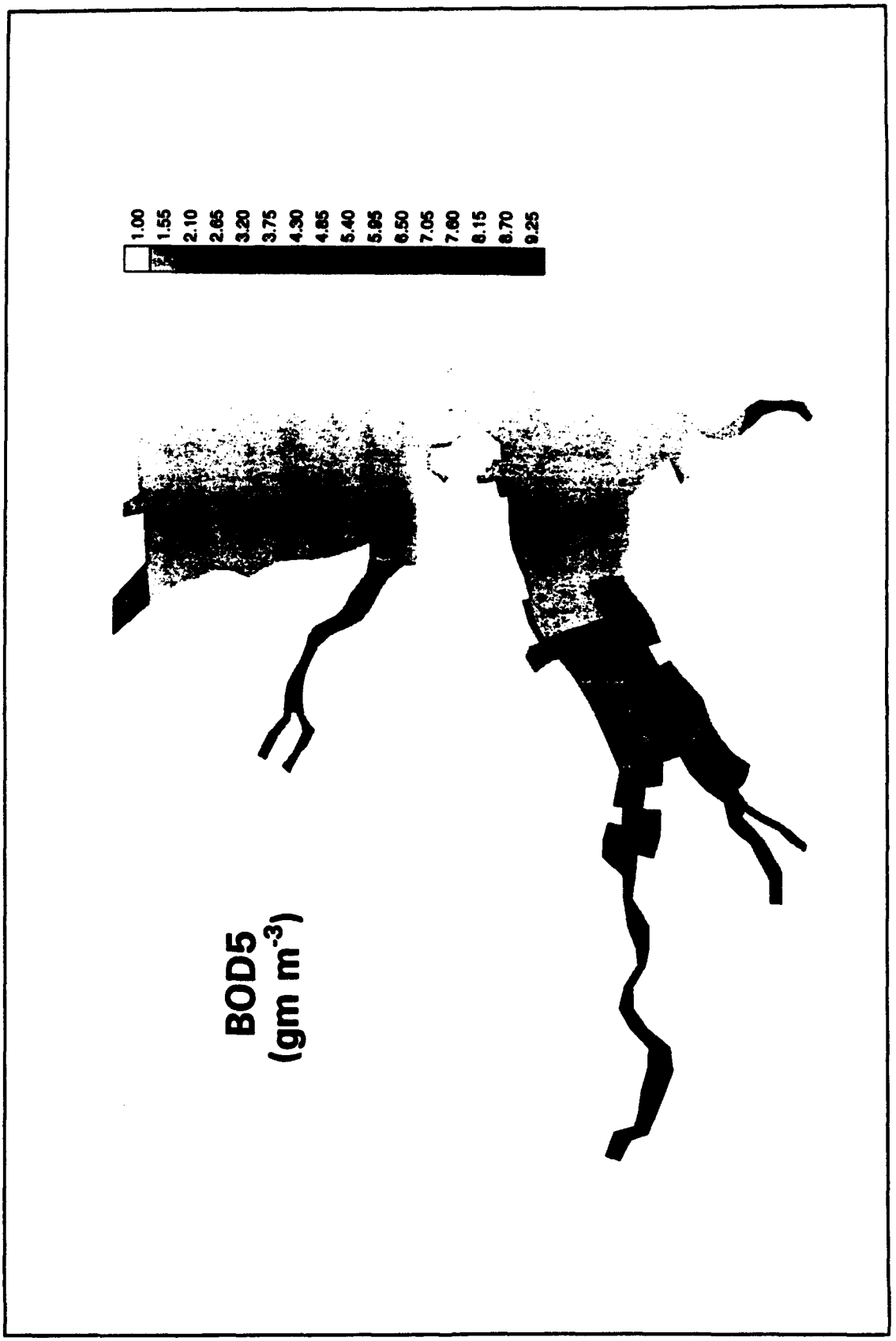

Figure 9-37. Modeled Biochemical Oxygen Demand, 1990 Summer Average

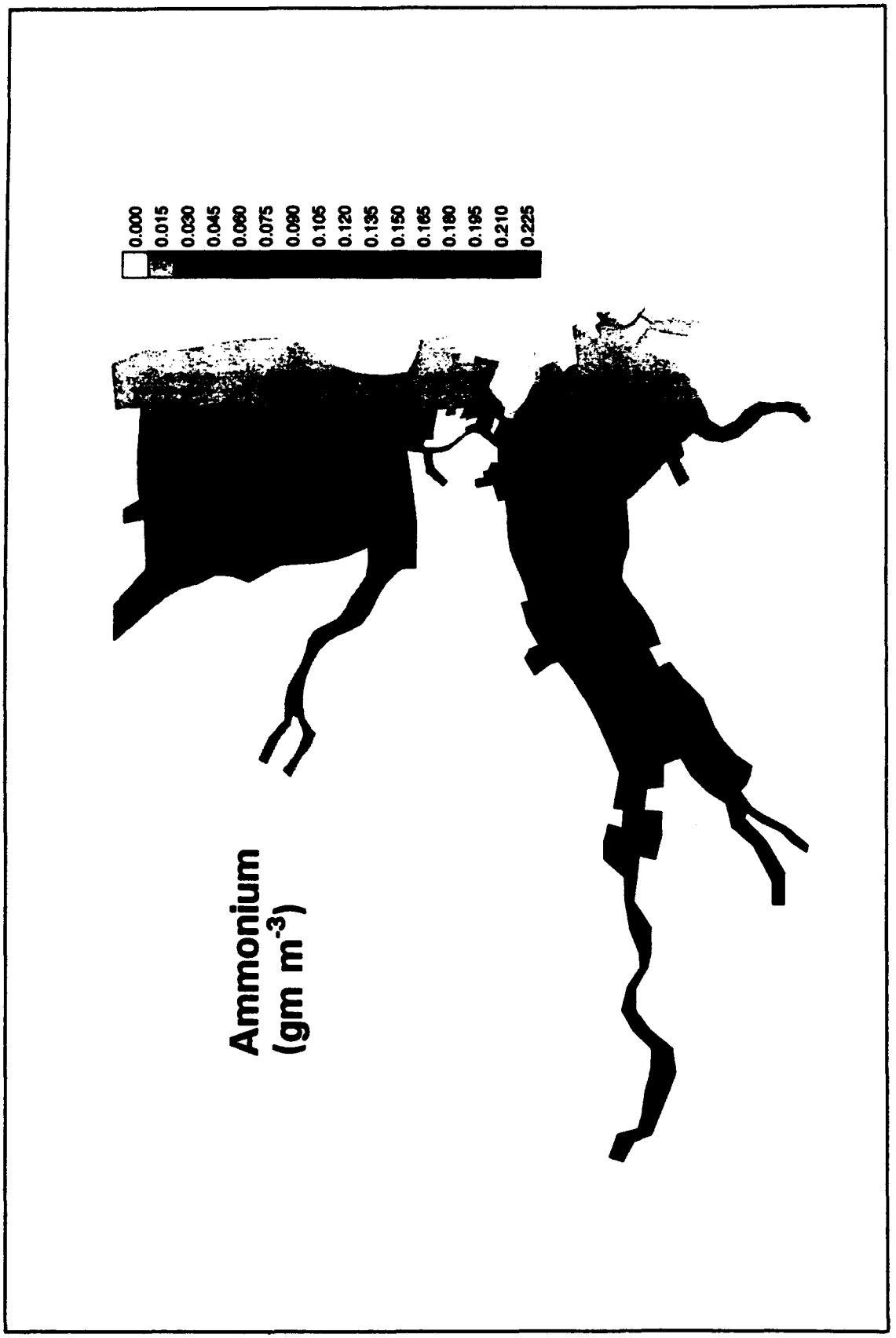

Figure 9-38. Modeled Ammonium, 1990 Summer Average

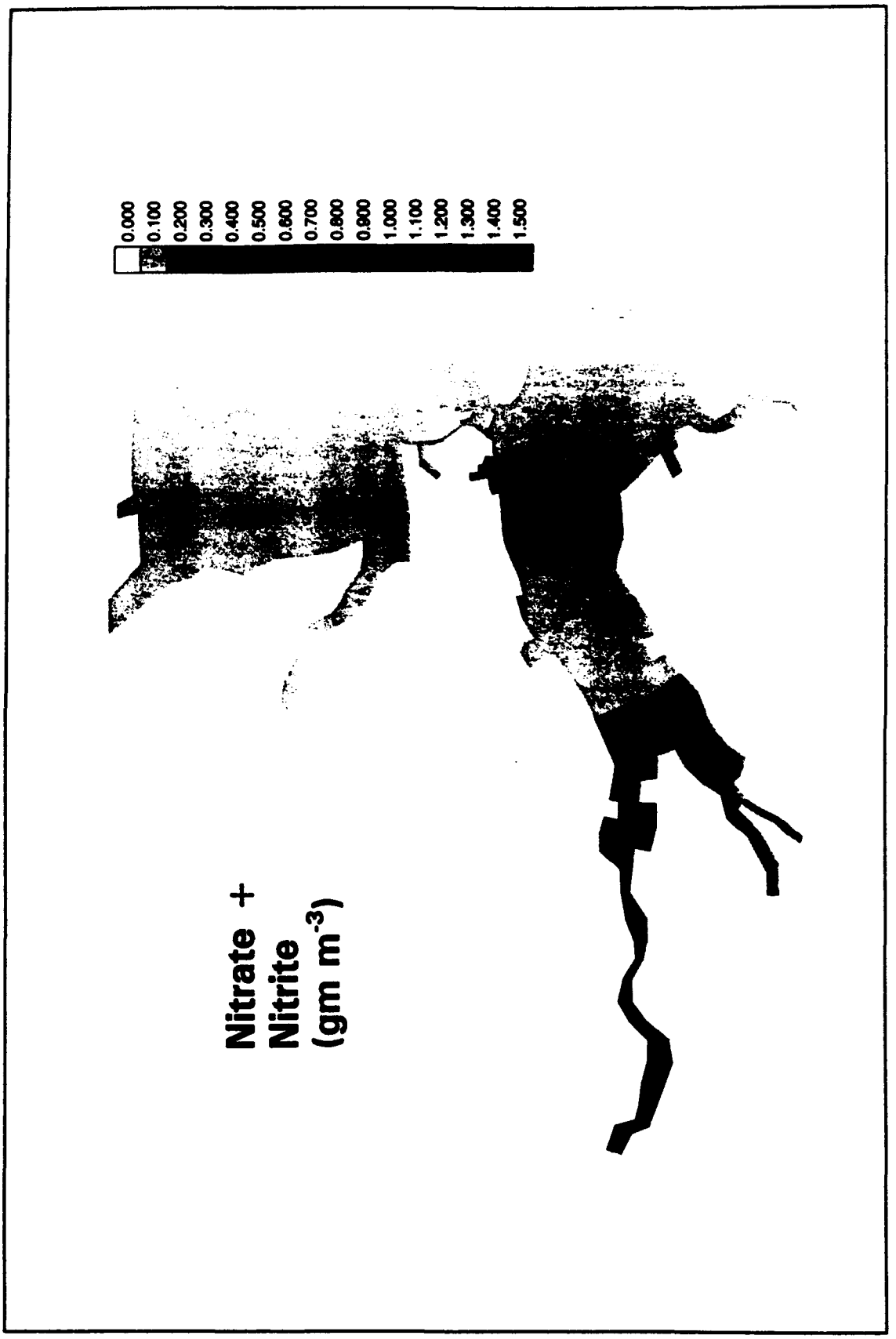

Figure 9-39. Modeled Nitrate, 1990 Summer Average

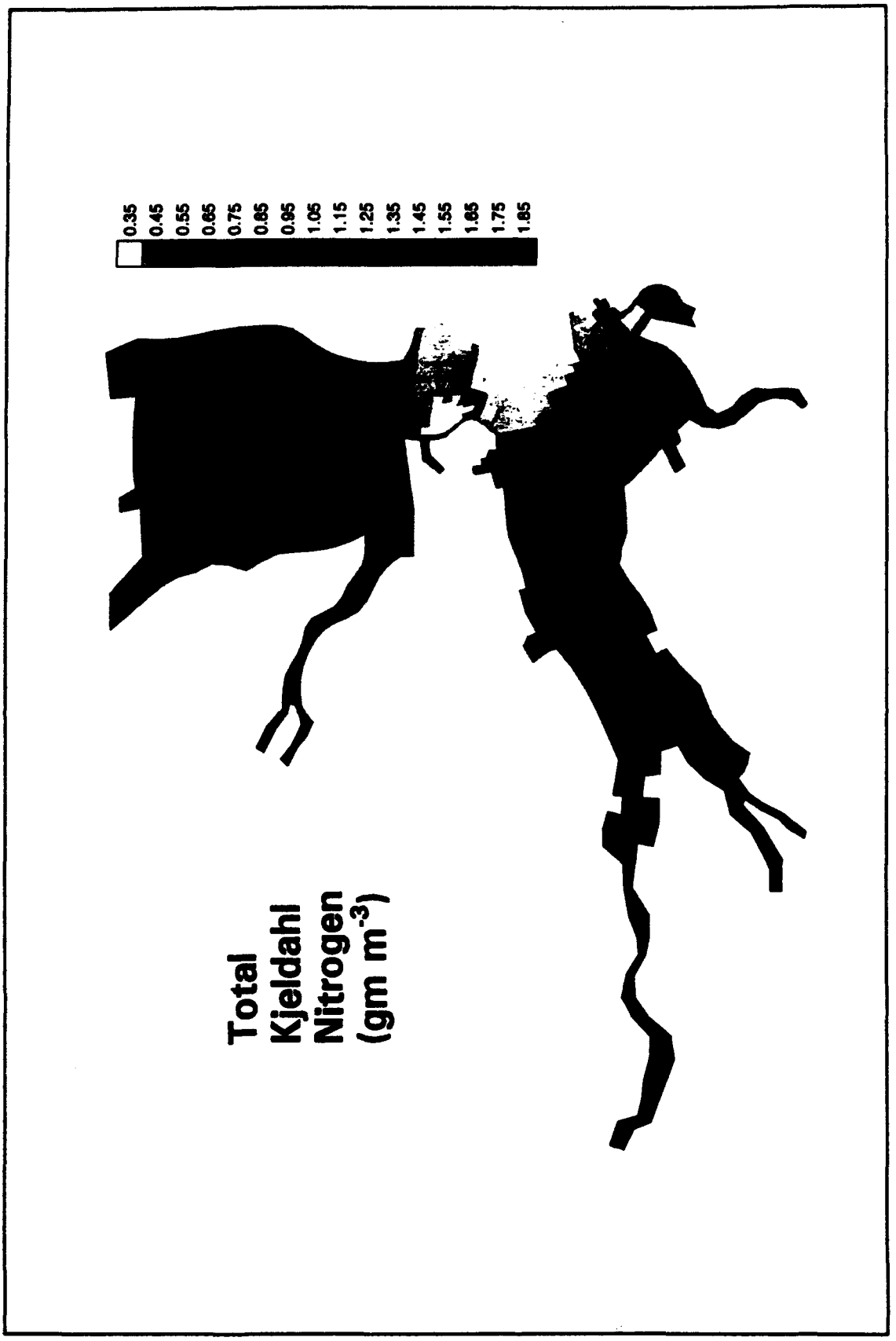

Figure 9-40. Modeled Total Kjeldahl Nitrogen, 1990 Summer Average

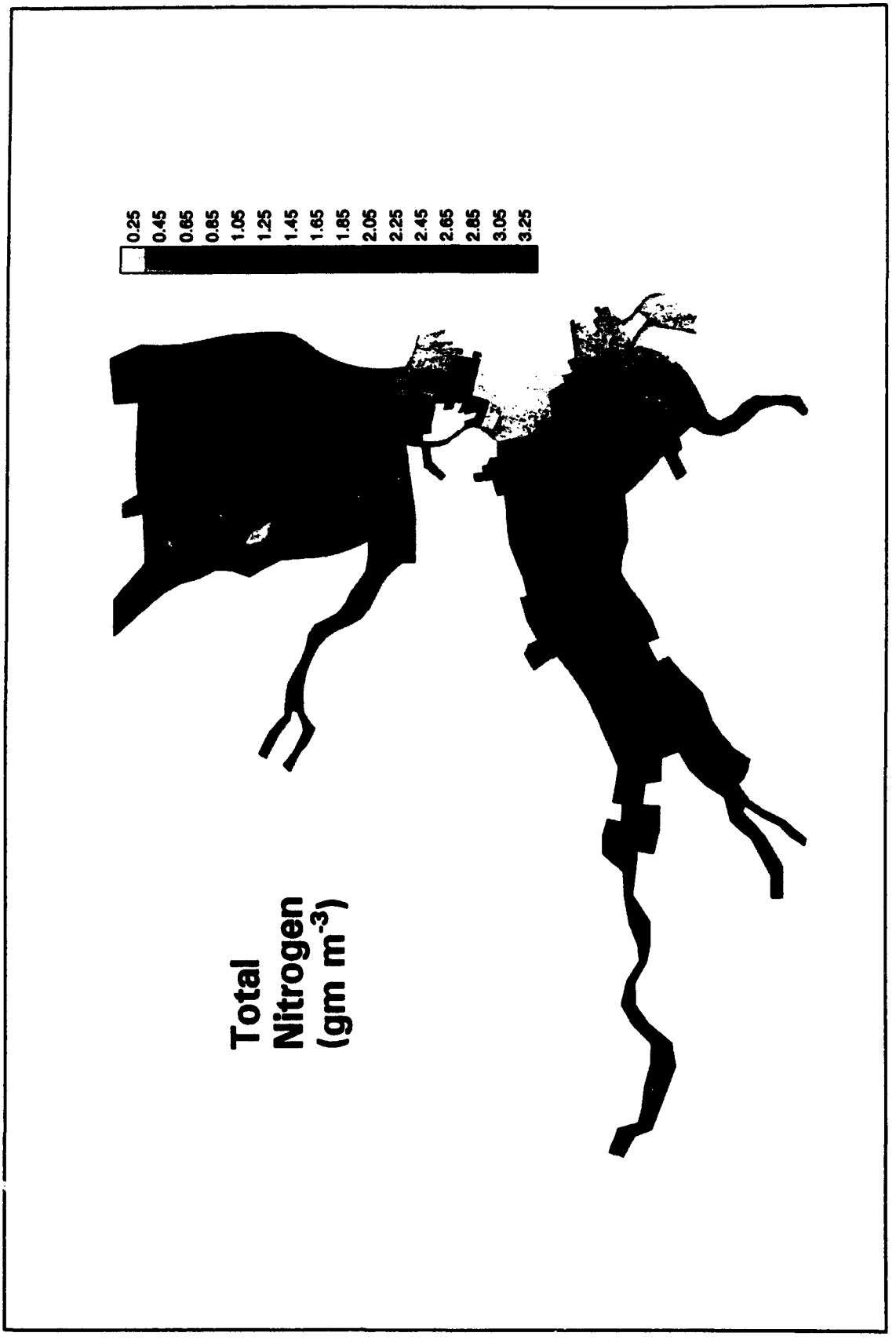

Figure 9-41. Modeled Total Nitrogen, 1990 Summer Average

Figure 9-42. Modeled Dissolved Inorganic Phosphorus, 1990 Summer Average

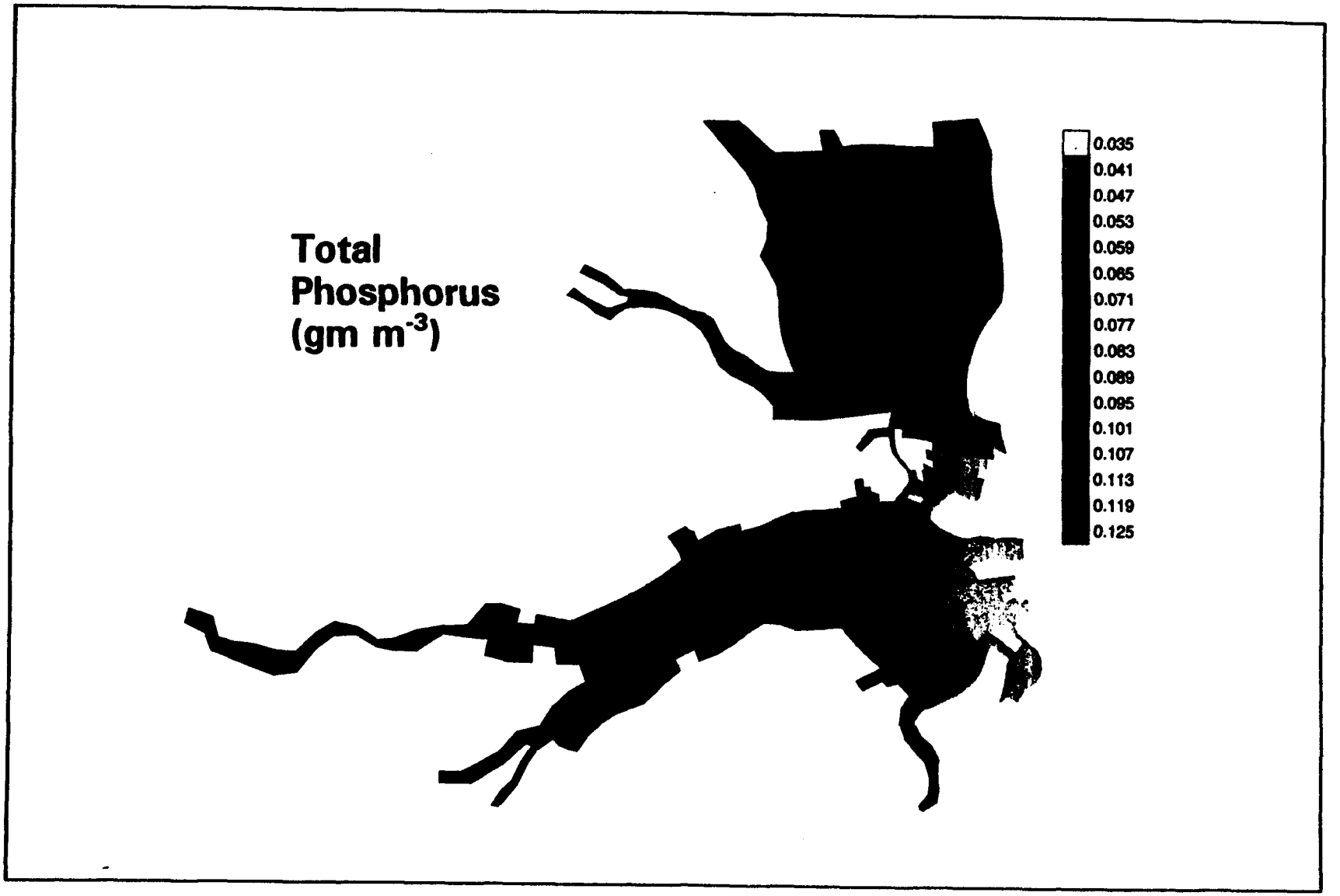

Figure 9-43. Modeled Total Phosphorus, 1990 Summer Average

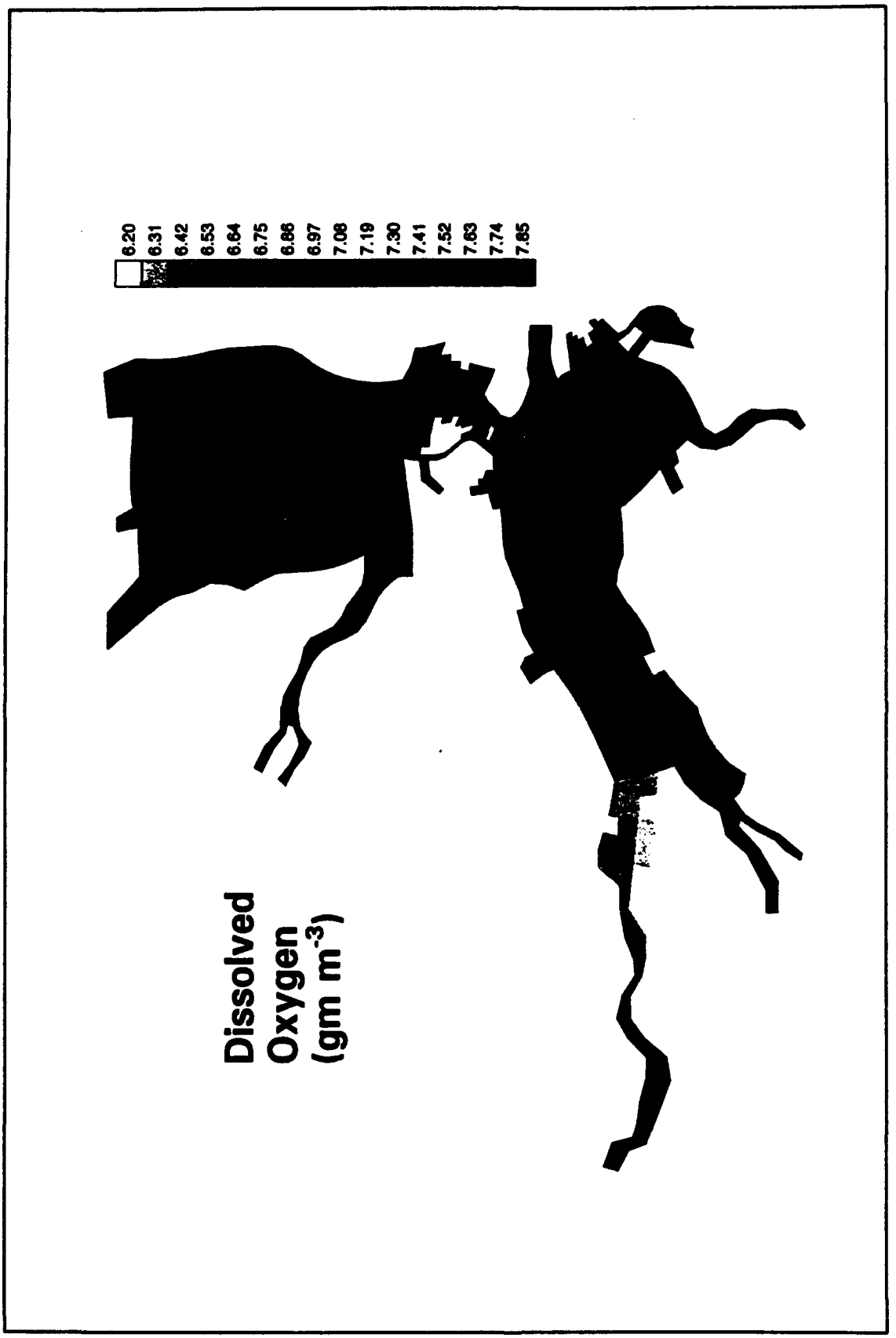

Figure 9-44. Modeled Dissolved Oxygen, 1990 Summer Average

Indian River reflect the availability of nitrogen and phosphorus for algal growth. Phosphorus is the limiting nutrient in this region (Figures 9-21 through 9-23). In lower Indian River and Rehoboth Bay, phosphorus is available to support algal growth but nitrogen is limiting (Figures 9-24 through 9-28). The transition from phosphorus limitation in headwaters to nitrogen limitation near the ocean interface is a typical estuarine characteristic.

The distribution of total nitrogen (Figure 9-41) shows clearly the transition from sources along the shore to the sink in the ocean. Total phosphorus exhibits the same trend (Figure 9-43).

Results of the model indicate anoxia is not a permanent feature anywhere in the system (Figure 9-44). Summer-average dissolved oxygen exceeds 6 gm m^{-3} everywhere. Observations and the model indicate, however, that concentrations as low as 2 gm m^{-3} occur. Excursions below average occur on a diurnal basis due to algal respiration, and on the time scale of days due to flow events and similar phenomenon. Highest dissolved oxygen concentrations coincide with highest chlorophyll concentrations indicating the role of algal production in dissolved oxygen production. Minimum dissolved oxygen occurs about halfway between Millsboro and Indian River inlet. The origin of the minimum is not apparent but chlorophyll is also low in this region suggesting the minimum is due to limited algal production.

A substantial and significant difference exists between annual mass balances (Figures 9-32 through 9-34) and summer-average mass balances (Figures 9-45 through 9-47). During summers of dry and normal hydrology (Figures 9-45, 9-47) sediments are the largest nitrogen source to the system, through the mechanism of ammonium release. Even in an extremely wet summer, sediments rival nonpoint sources of nitrogen (Figure 9-46). The summer mass balance contrasts with the annual balance in which sediments are a net nitrogen sink. A similar balance exists for phosphorus. The sediment release of phosphorus is sufficient to convert the system into a net exporter of total phosphorus during the summer. By contrast, on an annual basis, the sediments are a phosphorus sink and the system imports phosphorus from the ocean. The role of sediments in summer in Indian River/Rehoboth Bay is consistent with the role of sediments in larger, deeper estuaries. The net nutrient release in summer is due to two factors. High temperature which enhances diagenetic (decay) processes in the sediments and seasonal turbidity increase which shades out benthic algae.

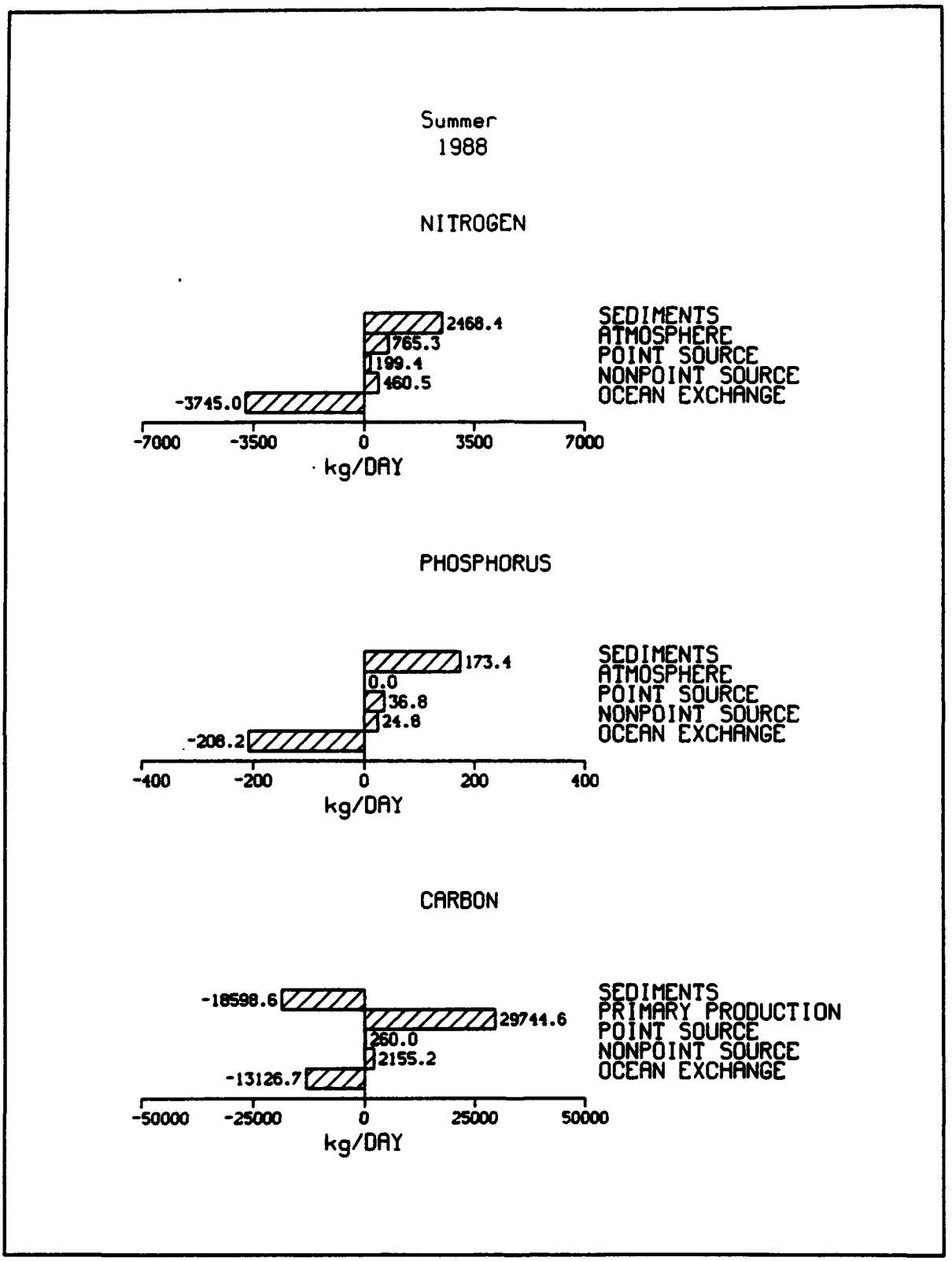

Figure 9-45. Summer Mass Balance, 1988

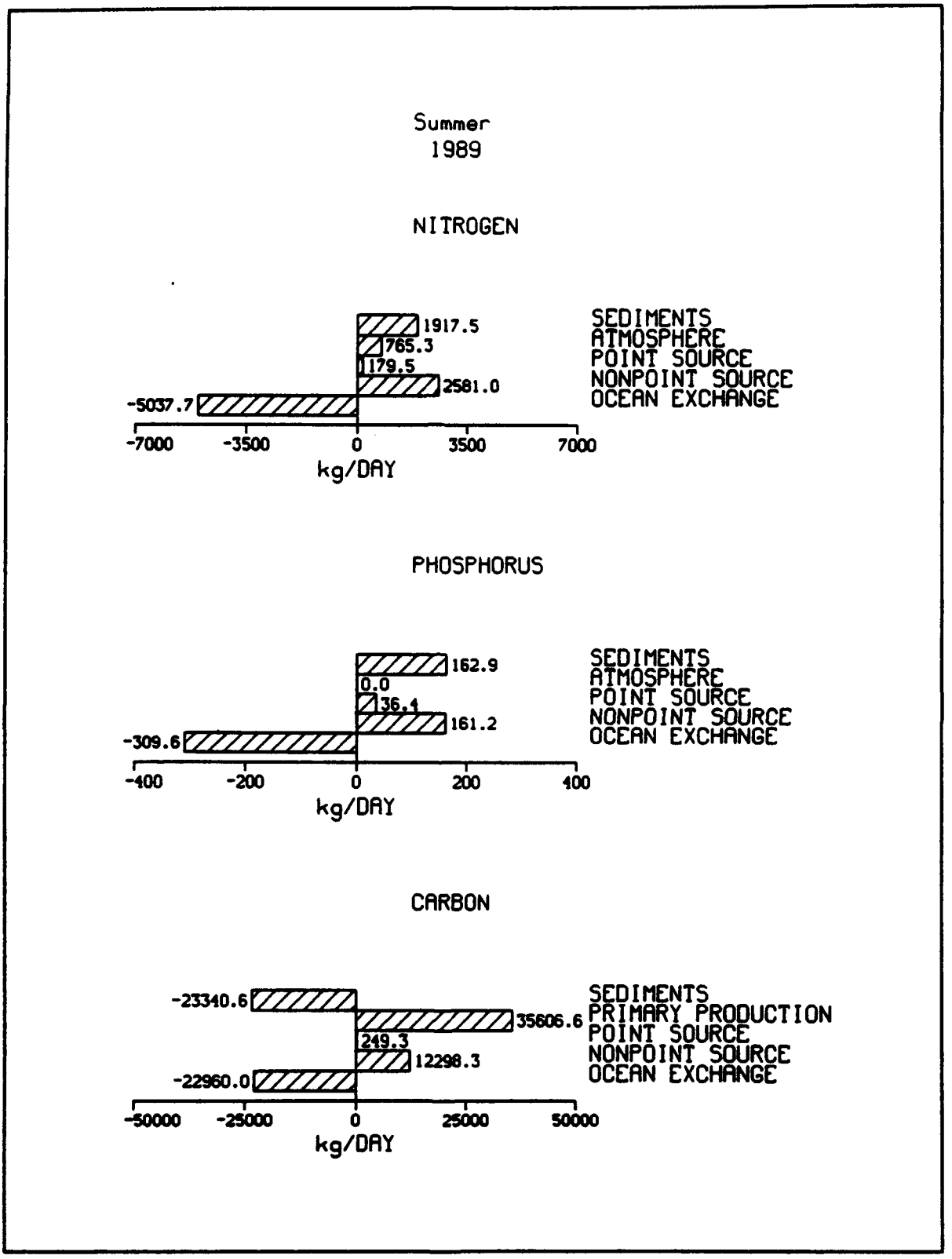

Figure 9-46. Summer Mass Balance, 1989

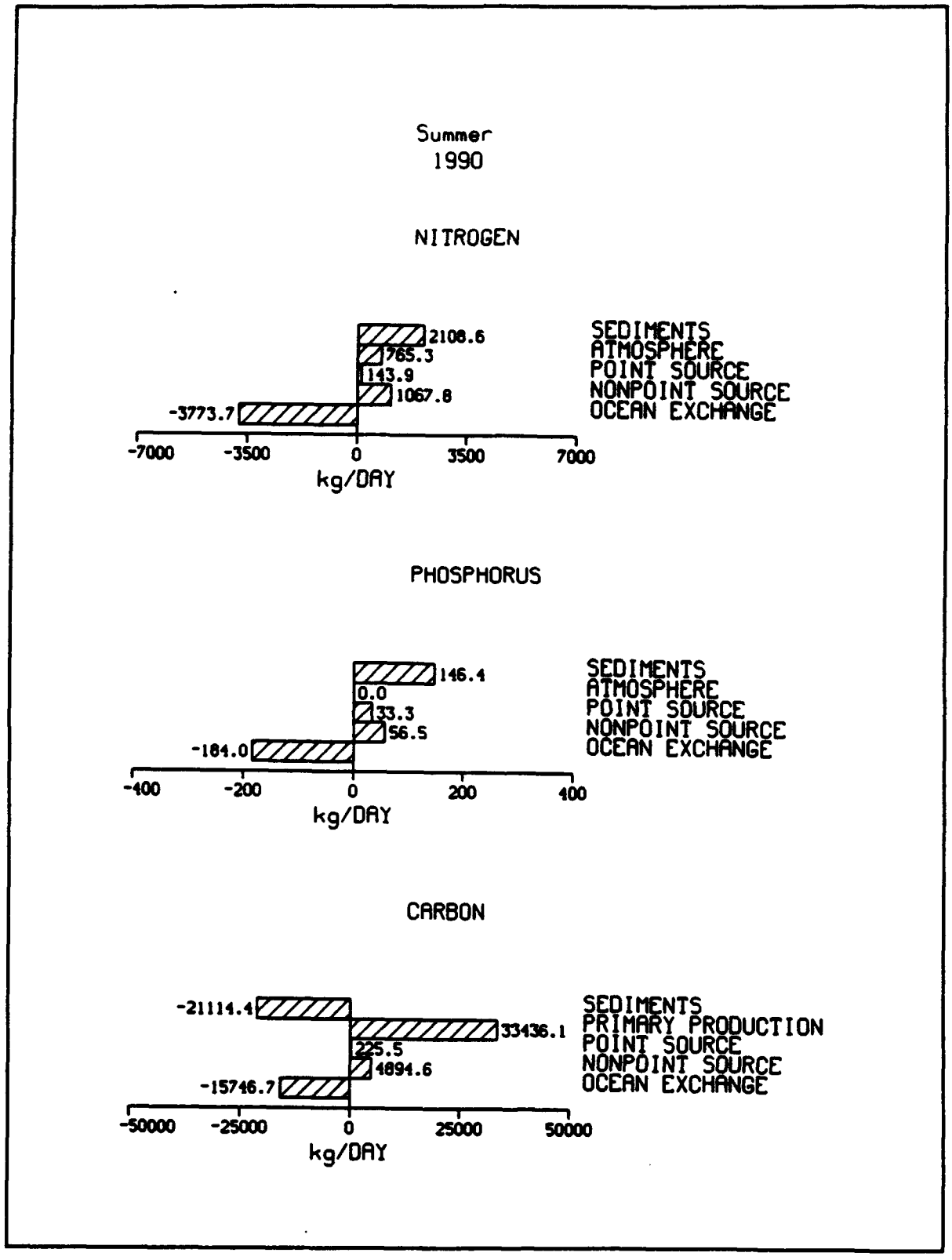

Figure 9-47. Summer Mass Balance, 1990

Chapter X: Conclusions and Recommendations

Conclusions

Hydrodynamic Model Application

The CH3D hydrodynamic model simulated transport in Indian River/ Rehoboth Bay for three years: 1988, 1989, and 1990. Two-dimensional depth-average transport was calculated on a grid containing over 2000 cells roughly 50 m by 100 m in lateral and longitudinal extent. Integration time step was 30 seconds.

Performance of the model was verified by comparison to observed tide records, current measurements, and salinity data. The model reproduced observed surface levels throughout the system with an accuracy of a few centimeters. Current measures, concentrated in the passage between Rehoboth Bay and lower Indian River, were also well-represented by the model. The predicted spatial salinity distribution compared well with observations collected in three independent surveys.

Computation of transport in Indian River/Rehoboth Bay represents the current state of the art in this field. The transport computations are entirely suited for use in a eutrophication model of the system.

Water Quality Model Application

The water quality model was applied in a continuous mode to simulate conditions in Indian River/Rehoboth Bay for the years 1988-1990. Transport for water quality simulation was provided by the CH3D hydrodynamic model. Other water-quality forcing functions included nonpoint-source loading of nutrients and organic matter, point-source loading of nutrients and organic matter, atmospheric nutrient loading, sediment-water nutrient and oxygen exchanges, oceanic material exchanges, and seasonal light attenuation. Quantification of loads and other forcing functions was performed specifically for this study and employed the most recent available information. The model

provided a consistent representation of water quality throughout the system throughout the year.

The water quality model operated on a temporal scale of ≈300 seconds and a spatial scale of ≈500 m. Forcing functions were not resolved on these scales, however. Consequently, comparisons of model results with observations were more favorable when model and observations were temporally and spatially aggregated. Performance statistics for the Indian River/Rehoboth Bay model application were nearly at the state of the art for most substances simulated. Unfavorable statistics noted for two substances were attributed to unique, highly-localized conditions and to dubious observations.

The model package is entirely suitable for employment to meet the objectives stated at the initiation of the project. Existing point-source and nonpoint-source loads are quantified and located throughout the system. These can be adjusted to develop total maximum daily loads for nutrients and organic matter. Diurnal dissolved oxygen variations are obtained by a process that quantifies diurnal range as a function of predicted daily-average dissolved oxygen and chlorophyll concentrations.

Recommendations

Application to the existing model package to the existing data base is optimal. No improvement of model-data agreement is possible without collection of additional data. Representation of the system cannot be improved without revisions to the model formulations. Suggested improvements to the data base and the model follow.

Data Collection

Water-column observations should be collected at consistent locations in Indian River/Rehoboth Bay and at consistent depths. The collection of surface samples only should be replaced with a procedure that provides samples representative of the entire water column. A recommended protocol is to collect samples at mid-depth when depth is less than 1 m. Collect surface and bottom samples in water of depth between 1 and 2 m. Collect surface, mid-depth, and bottom samples in water of depth greater than 2 m. Salinity, temperature, and dissolved oxygen are low-cost measures, often observed in situ. These can be measured at multiple depths easily. If resources for analysis are limited, samples of nutrients and organic matter can be composited into one depth-average sample prior to analysis.

The existing data base is highly biased towards the months April through September. While these are the months in which water quality problems are most severe, lack of observations in the remaining months limits analyses that might relate summer water quality conditions to phenomenon that occur in

colder months, for example load events or winter diatom blooms. Regular sampling throughout the calendar year is recommended.

The BOD5 observations currently collected are no longer favored as a component of long-term estuarine data bases. Neither is BOD a state variable in state-of-the-art eutrophication models. The BOD observation should be replaced or supplemented with observations of total organic carbon. The total organic carbon analyses are necessary in observations of point-source and nonpoint-source loads as well as the water-column. Direct analysis of particulate and dissolved organic carbon fractions will greatly facilitate future model applications.

The detection levels of ammonium, nitrate, and phosphate in the STORET data base, 1988-1990, are unsuited for the levels of these nutrients often found in Indian River/Rehoboth Bay. A large fraction of the observations are below detection level. Much improved detection levels are possible, as demonstrated in the College of Marine Studies data base.

Light extinction greatly affects water quality in Indian River/Rehoboth Bay. The existing data base, however is assembled from observations of disk visibility (secchi depth). The conversion of disk visibility to extinction relies on an approximate conversion. Moreover, we found the disk visibility observations in the STORET data base to be so unreliable we could not use them. Direct, in-situ, measurement of extinction with a photometer or similar instrument is recommended.

The present program of sediment-water nutrient and oxygen flux measures should be continued. Measures should be collected at several times throughout the year. Concurrent with the flux measures, water-column light extinction and light intensity at the sediment-water interface should be recorded. In view of the role of benthic algae, chlorophyll measurements in surficial sediments should be added to the sampling program.

Mechanistic Sediment Model

One component of the Chesapeake Bay model package applied to Indian River/Rehoboth Bay was a mechanistic, predictive model of sediment-water nutrient and oxygen exchanges. Employment of the benthic sediment model was discontinued, however, since it did not account for activity of benthic algae noted in Indian River. The mechanistic model was replaced with empirical models calibrated to available observations. The empirical models performed well in relating existing fluxes to existing conditions, primarily temperature and light. Inherent in the empirical models, however, was the assumption that basic fluxes will not be altered as a result of management activities. The empirical models also related sediment-water fluxes to ambient conditions only. The models did not relate summer nutrient fluxes to loads or benthic algal blooms that occurred the previous winter. Reactivation of the mechanistic sediment model is recommended. In order to employ the model,

however, it must be modified to account for the effects of benthic algae. A reasonable starting point for the modifications is adaptation to benthic algae of existing kinetics formulations that represent water-column phytoplankton.

Multi-Layer Hydrodynamic Model

The data base for Indian River/Rehoboth Bay provided little information on vertical variations in water quality. Most observations were surface only. Examination of limited available observations, collected in Indian River (Tyler 1989), indicated vertical variations in temperature, salinity, and dissolved oxygen were small, typically less than 1 C^0 for temperature, 1.5 ppt for salinity, and 0.15 gm m^{-3} for dissolved oxygen. No distinct pyncnocline was evident and bottom-water anoxia was absent. Representation of water quality conditions in Indian River/Rehoboth Bay did not require a multi-layer model.

The slight salinity stratification suggests, however, that classic density-driven circulation exists, to some extent, in the reach from Millsboro spillway to the Indian River inlet. The density-driven circulation is superimposed on the twice-daily flow reversals induced by tides and is characterized by net motion downstream near the surface and upstream near the bottom. The strength of the circulation depends on runoff volume and salinity at the inlet. The density-driven circulation is subject to alteration by local wind conditions. At present, effects of multi-layer circulation, to the extent that they exist, are represented by a dispersion term in the mass-transport equation. This representation is adequate, as evidenced by agreement in modeled and observed salinity at most locations and times. Still, some improvement in modeled circulation may be expected by employment of a multi-layer model. In view of the shallow depth in Indian River/Rehoboth Bay, two layers would suffice. No multi-layer modeling can be conducted, however, until an extensive data base of vertical salinity and temperature observations is assembled. Long-term current measures at several locations in the vertical are also desirable.

References

Academy of Natural Sciences. (1988). "Phytoplankton, nutrients, macroalgae and submerged aquatic vegetation in Delaware's Inland Bays," Benedict Estuarine Research Laboratory, Benedict, MD.

American Society of Civil Engineers. (1961). "Effect of water temperature on stream reaeration," *Journal of the Sanitary Engineering Division*, 87(SA6), 59-71.

Ammerman, J., and Azam, F. (1985). "Bacterial 5'-nucleodase in aquatic ecosystems: a novel mechanism of phosphorus regeneration," *Science*, 227, 1338-1340.

Anders, F. J., Lillycrop, W. J., and Gebert, J. (1990). "Effects of natural and man-made changes at Indian River Inlet, Delaware," Proceedings of the Third Annual National Beach Preservation Technology Conference, St. Petersburg, FL pp 280-294.

Andres, A. S. (1992). "Estimate of nitrate flux to Rehoboth and Indian River Bays, Delaware, through direct discharge of groundwater," Open File Report No. 35, Delaware Geological Survey, University of Delaware, Newark, DE.

Biggs, R. B. (1984). "Ambient dissolved oxygen concentrations in Delaware Inland Bays," College of Marine Studies, University of Delaware, Newark, DE.

Bird, D., and Kalff, J. (1984). "Empirical relationships between bacterial abundance and chlorophyll concentration in fresh and marine waters," *Canadian Journal of Fisheries and Aquatic Science*, 41, 1015-1023.

Boni, L., Carpene, E., Wynne, D., and Reti, M. (1989). "Alkaline phosphatase activity in Protogonyaulax Tamarensis," *Journal of Plankton Research*, 11, 879-885.

Cerco, C. F., and Cole, T. (1993). "Application of the three-dimensional eutrophication model CE-QUAL-ICM to Chesapeake Bay," draft report in revision, U.S. Army Engineer Waterways Experiment Station, Vicksburg, MS.

Chrost, R., and Overbeck, J. (1987). "Kinetics of alkaline phosphatase activity and phosphorus availability for phytoplankton and bacterioplankton in Lake Plubsee (North German eutrophic lake)," *Microbial Ecology*, 13, 229-248.

Cole, J., Findlay, S., and Pace, M. (1988). "Bacterial production in fresh and saltwater ecosystems: a cross-system overview," *Marine Ecology Progress Series*, 43, 1-10.

DiToro, D. (1980). "Applicability of cellular equilibrium and Monod theory to phytoplankton growth kinetics," *Ecological Modelling*, 8, 201-218.

DiToro, D., O'Connor, D., and Thomann, R. (1971). "A dynamic model of the phytoplankton population in the Sacramento-San Joaquin Delta." *Non-equilibrium Systems in Water Chemistry*. American Chemical Society, Washington, DC, 131-180.

Droop, M. R. (1973). "Some thoughts on nutrient limitation in algae," *Journal of Phycology*, 9, 264-272.

Edinger, J., Brady, D., and Geyer, J. (1974). "Heat exchange and transport in the environment," Report 14, Department of Geography and Environmental Engineering, Johns Hopkins University, Baltimore, MD.

Galperin, B., and Mellor, G. L. (1990). "A time-dependent, three-dimensional model of the Delaware Bay and River system. Part 1: Three-dimensional flow fields and residual circulation," *Estuarine, Coastal, and Shelf Science*, Vol 31, pp 255-281.

Galperin, B., and Mellor, G. L. (1990). "A time-dependent, three-dimensional model of the Delaware Bay and River system. Part 2: Three-dimensional flow fields and residual circulation," *Estuarine, Coastal, and Shelf Science*, Vol 31, pp 255-281.

Garratt, J. R. (1977). "Review of drag coefficients over oceans and continents," *Monthly Weather Review*, Vol 105, pp 915-929.

Genet, L., Smith, D., and Sonnen, M. (1974). "Computer Program Documentation for the Dynamic Estuary Model," U.S. Environmental Protection Agency, Systems Development Branch, Washington, DC.

Johnson, B. H., Heath, R. E., Hsieh, B. B., Kim, K. W., and Butler, H. L. (1991). "User's guide for a three-dimensional numerical hydrodynamic, salinity, and temperature model of Chesapeake Bay." Technical Report HL-91-20, U.S. Army Engineer Waterways Experiment Station, Hydraulics Laboratory, Vicksburg, MS.

Johnston, R. H. (1976). "Relation of ground water to surface water in four small basins of the Delaware coastal plain," Report of Investigations No. 24, Delaware Geological Survey, University of Delaware, Newark, DE.

Karpas, R. M. (1978). "The hydrography of Indian River and Rehoboth -- Delaware's small bays," Master's thesis, University of Delaware, Newark, DE.

Kremer, J., and Nixon, S. (1978). "Light acclimation and the selection of Iopt." *A Coastal Marine Ecosystem Simulation and Analysis.* Springer Verlag, New York, NY.

Leonard, B. (1979). "A stable and accurate convection modeling procedure based on quadratic upstream interpolation," *Computer Methods in Applied Mechanics and Engineering* 19, 59-98.

Lillycrop, W. J., Anders, F. J., McGehee, D. D., Raney, D. C., Gebert, J., Chasten, M. A., and Welp, T. L. (1991). "Indian River Inlet, Delaware, scour study," Technical Report CERC 91- , U.S. Army Engineer Waterways Experiment Station, Coastal Engineering Research Center, Vicksburg, MS.

Mark, D. J., Scheffner, N. W., Butler, H. L., Bunch, B. W., and Dortch, M. S. (1993). "Hydrodynamic and water quality modeling of Lower Green Bay, Wisconsin," Technical Report CERC 93-16 , U.S. Army Engineer Waterways Experiment Station, Coastal Engineering Research Center, Vicksburg, MS.

Matavulj, M., and Flint, K. (1987). "A model for acid and alkaline phosphatase activity in a small pond," *Microbial Ecology*, 13, 141-158.

Monod, J. (1949). "The growth of bacterial cultures," *Annual Review of Microbiology*, 3, 371-394.

Morel, F. (1983). "Effects of biological processes on pH and alkalinity." *Principles of Aquatic Chemistry.* John Wiley and Sons, New York, NY, 149-151.

Nielsen, P. (1990). "Tidal dynamics of the water table in beaches," *Water Resources Research,* Vol 26, No 9, pp 2127-2134.

O'Connor, D. (1983). "Wind effects on gas-liquid transfer coefficients," *Journal of the Environmental Engineering Division*, 190, 731-752.

O'Connor, D., and Dobbins, W. (1958). "Mechanisms of reaeration in natural streams," *Transactions of the American Society of Civil Engineers*, 123, 641-666.

Odum, E. (1971). "Principles pertaining to limiting factors." *Fundamentals of Ecology*. W. B. Saunders, Philadelphia, PA, 106-107.

Parsons, T., Takahashi, M., and Hargrave, B. (1984). *Biological oceanographic processes*. Pergamon Press, Oxford.

Putrevu, U., and Trowbridge, J. (1987). "Numerical simulation of hydrodynamic circulation in Indian River and Rehoboth Bays," Report to Delaware DNREC by University of Delaware, Newark, DE.

Raney, D. C., Doughty, J. O., and Livings, J. (1990). "Tidal prism numerical model investigation and risk analysis of the Indian River Inlet scour study," Bureau of Engineering Research, Report No. 500-183, Tuscaloosa, AL.

Redfield, A., Ketchum, B., and Richards, F. (1966). "The influence of organisms on the composition of sea-water." *The sea vol. II*. Interscience Publishers, New York, NY, 26-48.

Ritter, W. F. (1986). "Nutrient budgets for the Inland Bays", FPR-86-001, Agricultural Engineering Department, University of Delaware, Newark, DE.

Roache, P. J. (1976). *Computational Fluid Dynamics*, Hermosa Publishers, Albuerque, NM.

Sheng, Y. P. (1986). "A three-dimensional mathematical model of coastal, estuarine and lake currents using boundary fitted grid." Report No. 585, A.R.A.P. Group Titan Systems, New Jersey, Princeton, NJ.

Smith, R. 1976). "Longitudinal dispersion of a buoyant contaminant in a shallow channel," *Journal of Fluid Mechanics*, Part 4, 677-688.

Smullen, J. (1992). "Water quality of Inland Bays," Roy F. Weston Inc., West Chester, PA.

Steele, J. (1962). "Environmental control of photosynthesis in the sea," *Limnology and Oceanography*, 7, 137-150.

Stumm, W., and Morgan, J. J. (1981). "Oxidation and reduction." *Aquatic chemistry*. John Wiley & Sons, New York.

Talley, J. H., and Simmons, R. H. (1988). "Inland bays low-flow monitoring July 1985 - September 1988," Prepared for Delaware DNREC by Delaware Geological Survey and U. S. Geological Survey.

Thomann, R., and Fitzpatrick, J. (1982). "Calibration and verification of a mathematical model of the eutrophication of the Potomac Estuary," Hydro-Qual Inc., Mahwah, NJ.

Thompson, J. F., Warsi, Z. U. A., Mastin, C. W. (1985). *Numerical Grid Generation Foundations and Applications*, Elsevier Science, New York.

Tchobanoglous, G., and Schroeder, E. D. (1985). "Chemical characteristics of water: organic matter." *Water quality*. Addison-Wesley, Reading, MA, 120-121.

Tuffey, T., Hunter, J., and Matulewich, V. (1974). "Zones of nitrification," *Water Resources Bulletin*, 10, 555-564.

Tyler, M. (1989). "Inland Bays phytoplankton monitoring study 8 May through September 1988: phytoplankton taxonomy and bloom scenarios final report," Versar Inc., Columbia, MD.

Wezernak, C., and Gannon, J. (1968). "Evaluation of nitrification in streams," *Journal of the Sanitary Engineering Division*, 94(SA5), 883-895.

Wen, C., Kao, J., Wang, L., and Liaw, C. (1984). "Effect of salinity on reaeration coefficient of receiving waters," *Water Science and Technology*, 16, 139-154.

Wong, K-C. (1987). "Tidal and subtidal variation in Delaware's inland bays," *Journal of Geophysical Research*, Vol 17, pp 413-422.

Wong, K-C., and DiLorenzo, J. (1988). "The response of Delaware's inland bays to ocean forcing," *Journal of Geophysical Research*, Vol 93, C10, pp 12525-12535.

REPORT DOCUMENTATION PAGE

Form Approved
OMB No. 0704-0188

1. AGENCY USE ONLY (Leave blank)	2. REPORT DATE	3 REPORT TYPE AND DATES COVERED
	May 1994	Final report

4. TITLE AND SUBTITLE
Hydrodynamic and Eutrophication Model Study of Indian River and Rehoboth Bay, Delaware

5. FUNDING NUMBERS

6. AUTHOR(S)
Carl F. Cerco, Barry Bunch
Mary A. Cialone, Harry Wang

7. PERFORMING ORGANIZATION NAME(S) AND ADDRESS(ES)
U.S. Army Engineer Waterways Experiment Station
3909 Halls Ferry Road
Vicksburg, MS 39180-6199

8. PERFORMING ORGANIZATION REPORT NUMBER
Technical Report
EL-94-5

9. SPONSORING/MONITORING AGENCY NAME(S) AND ADDRESS(ES)
U.S. Environmental Protection Agency, Region III, Philadelphia, PA 19107; Delaware Department of Natural Resources and Environmental Control, Dover, DE 19903; U.S. Army Engineer District, Philadelphia, Philadelphia, PA 19106-2991

10. SPONSORING/MONITORING AGENCY REPORT NUMBER

11. SUPPLEMENTARY NOTES
Available from National Technical Information Service, 5285 Port Royal Road, Springfield, VA 22161.

12a. DISTRIBUTION/AVAILABILITY STATEMENT
Approved for public release; distribution is unlimited.

12b. DISTRIBUTION CODE

13. ABSTRACT *(Maximum 200 words)*

Indian River and Rehoboth Bay are two shallow bodies that form part of the Delaware Inland Bays system. The Bays are subject to eutrophication problems that accompany agricultural, commercial, and recreational development in the coastal zone. A hydrodynamic/water quality model package was applied to provide a management tool to address eutrophication issues in the two Inland Bays.

The CH3D hydrodynamic model simulated transport in Indian River/Rehoboth Bay for 3 years: 1988, 1989, and 1990. Two-dimensional depth-average transport was calculated on a grid containing over 2,000 cells roughly 50 by 100 m in lateral and longitudinal extent. Integration time step was 30 sec. Performance of the model was verified by comparison to observed tide records, current measurements, and salinity data.

The water quality model was applied in a continuous mode to simulate conditions in Indian River/Rehoboth Bay for the years 1988-1990. Transport for water quality simulation was provided by the CH3D hydrodynamic model. Other water-quality forcing functions included nonpoint-source loading of nutrients and organic matter, point-source loading of nutrients and organic matter, atmospheric nutrient loading, sediment-water nutrient and oxygen exchanges, oceanic material exchanges, and seasonal light attenuation.

(Continued)

14. SUBJECT TERMS

Delaware	Eutrophication	Models	Rehoboth Bay
Dissolved oxygen	Indian River	Nitrogen	
Estuaries	Inland bays	Phosphorus	

15. NUMBER OF PAGES
262

16. PRICE CODE

17. SECURITY CLASSIFICATION OF REPORT	18. SECURITY CLASSIFICATION OF THIS PAGE	19. SECURITY CLASSIFICATION OF ABSTRACT	20. LIMITATION OF ABSTRACT
UNCLASSIFIED	UNCLASSIFIED		

13. Concluded

Project objectives required a model package suitable for development of total maximum daily loads, point-source waste load allocations, and nonpoint-source load allocations of nutrients and organic substances. Additional requirements were that the model package operate in a continuous multiyear mode and provide information on diurnal dissolved oxygen variations. The model package was also to provide an organized framework for collection and employment of additional observations in the study system. The model package described in this report is entirely suitable for employment to meet these objectives.